Improving the performance of Drilling Fluids by Using Nanoparticles

Mortatha Saadoon Mohammed Al-Yasiri

Submitted in accordance with the requirements for the degree of
Doctor of Philosophy

The University of Leeds
School of Chemical and Process Engineering

Leeds, UK

January 2019

The candidate confirms that the work submitted is his own and that appropriate credit has been given where reference has been made to the work of others.

This copy has been supplied on the understanding that it is copyright material and that no quotation from the thesis may be published without proper acknowledgement.

Acknowledgements

All glory and thanks to God for grace, strength and motivation for the successful completion of this research.

First and foremost, I would like to express my profound gratitude to Professor Dongsheng Wen for his thorough supervision, guidance, encouragement and support. I am also would like to extend my appreciation to Dr Joseph Antony, who has been very helpful and supportive throughout this project. Their motivation, insight, passion, encouragement and assistance throughout this project were the driving force for the success of this work. Thanks to Professor Chris Greenwell for his support in experiment facilities, papers correction and useful suggestion. Thanks to my colleague Shahid Pervaiz contributed to sample characterization and advices. Also, special thanks to my Iraqi friends. Talking with them has broadened my horizon, laughing and sometimes even singing together are good times and sweet memories during the PhD journey. Also, special thanks to MSc student, Amthal Al-Gailani, for helping with set up and conduct some of the Computer Simulation. Thanks to my friend Waleed Al-Sallami for his motivation, encouragement and support.

I wish to express my gratitude to the Higher Committee for Education Development in Iraq (HCED) for their financial support. Special thanks and appreciation to my parents, brothers, sisters and every member of my family for the strong foundation and pillars upon which this success is built. Their prayers, the bond, the constant encouragement, support and love really made it possible.

My deepest appreciation to ***my lovely wife*** Rafal Khafaji, for her perseverance, support and encouragement throughout this research.

Abstract

The development of new oil production techniques such as extracting via long deviated wells and drilling in ultra-deep water, requires improvements in the performance of conventional drilling fluids. It is essential to design new recipes of drilling fluids that possess improved properties both at rest and in dynamic. Seeding nanoparticles into a drilling fluid is a recent development aiming to improve the drilling fluid's performance. However, it is still in its infancy, and many inconsistent results have been reported. Understanding the influences and the mechanisms of nanoparticles with regards to different drilling fluid functions could provide the information required for designing novel receipts. This project aims to explore and assess the influence of various nanoparticles and their mixtures on the performance of water-based muds (WBM), including rheological, filtration, swelling, lubrication properties, and corrosion inhibition, as well as lifting capacity improvement.

A number of nanoparticles (SiO_2, CNT, CB, Gr and Al_2O_3) and their mixtures were employed in two WBMs, both with and without biopolymers. The particles and nanofluids were characterized by scanning electron microscope (SEM), dynamic light scatting (DLS), X-ray diffraction (XRD), Fourier transform infrared spectroscopy (FTIR) and thermal-gravimetric analysis (TGA). The rheological properties of the formulating drilling fluids were examined by an Anton Parr rheometer and Fann 35 Viscometer. The filtration and lubrication properties of different hybrid nanoparticle and nanofluid based WBMs were conducted by using a differential sticking tester. A novel simple method to simulate pipe erosion-corrosion in a reservoir-like environment under both static and dynamic conditions was developed, and the influence of wellbore temperature, pressure and salinity of WBMs on the corrosion behaviour of the drill pipe was examined. The lifting capacity of the drilling fluid flow was simulated by a four-way coupling scheme to take into consideration particle-particle interactions.

The results show that the addition of nanoparticles generally increased the performance of WBMs both under stationary and dynamic conditions, due to the formation of an appropriate gel structure and easy break under low shear stress. In addition, these nanoparticles increased the degree and the speed of the structural recovery by reducing the relaxation time, which is desirable to prevent the sedimentation of the cuttings and weighting materials. In particular, using appropriate hybrid nanoparticles allowed for enhancements in rheology, filtration, lubrication and

thermal features, leading to an overall performance improvement. For WBM with biopolymers, the addition of nanoparticles was found to increase the thermal and mechanical stability of the biopolymer, leading to less filtrate loss and improved performance.

The addition of SiO_2/Xanthan nanoparticles was found to inhibit the erosion-corrosion rates of the drill pipe, which is also affected by the cuttings morphology and concentration. The simulation results showed that the cutting's transport process and fluid viscosity were significantly enhanced by adding nanomaterials.

The present work suggests that using appropriate nanoparticles mixtures could improve the overall performance of conventional drilling fluids, leading to improved rheology, filtration, and transport properties.

Table of Contents

List of Tables

List of Figures

Nomenclature

API	American Petroleum Institute
(LVE)	Linear viscoelastic range
CS	Croscarmellose sodium
Ag	Arabic gum
XG	Xanthan gum
CMC	Carboxymethyl Cellulose Sodium
AV	Apparent viscosity
PV	Plastic viscosity
YP	Yield point
XRD	X-ray diffraction
TGA	Thermal gravimetric analysis
RPM	Rotation per minute
FTIR	Fourier transform infrared spectroscopy
SEM	Scanning electron microscope
TEM	Transmission Electron Microscope
DLS	Dynamic light scatting
CNT	Carbon nanotube
NPs	Nanoparticles
G’	Storage modulus
G’’	Loss modulus
G*	Complex modulus
CFD	Computational Fluid Dynamics
DDPM	Dense Discrete Phase Model
DEM	Discrete element method
HTHP	High Temperature and High Pressure
WBM	Water based mud
PL	Power law

OBM	Oil based mud
GBM	Gas based mud
EDX	Energy-dispersive X-ray spectroscopy
RANS	Reynolds-averaged Navier–Stokes
V_q	The volume of phase
q &q	Phases
V	Velocity
m_{qp}	Mass transfer from the q^{th} to p^{th} phase
P	Pressure
G	Acceleration gravity constant
Sq	Phase source term
R_{pq}	Interaction force between phases
$\overrightarrow{\mathbf{F_q}}$	External body force
$\overrightarrow{\mathbf{F_{lift,q}}}$	Lift force
$\overrightarrow{\mathbf{F_{vm,q}}}$	Virtual mass force
$\overrightarrow{\mathbf{F_{td,q}}}$	Turbulent dispersion force
Qq	Specific enthalpy of the q^{th} phase
Qpq	Intensity of heat exchange between phases
Hpq	The interphase enthalpy
K	Turbulence kinetic energy
T	Temperature
$\mathbf{F_D}$	Drag force
N	Power law index
K	Consistency Index

1 Introduction

1.1 Research Background

Every drilling process involves three structures that operate simultaneously when boring the wellbore: a rotation system that rotates the drill pipe, a hydraulic system that raises and turns down the drill string into the wellbore, and a circulatory system that executes the duty of a fluid movement (Figure 1-1), which is, called the drilling fluid [1]. Drilling fluids are essential for drilling completion as they surge oil recovery and reduce the time required to attain primary production [2]. The drilling fluid in the drilling process is similar to blood in the human circulatory system. The drilling fluid pump is the heart, the cuttings that are carried from the borehole by the drilling mud are the rejected constituents that are eliminated from the body, and the solid separation equipment operates as the kidney and lungs.

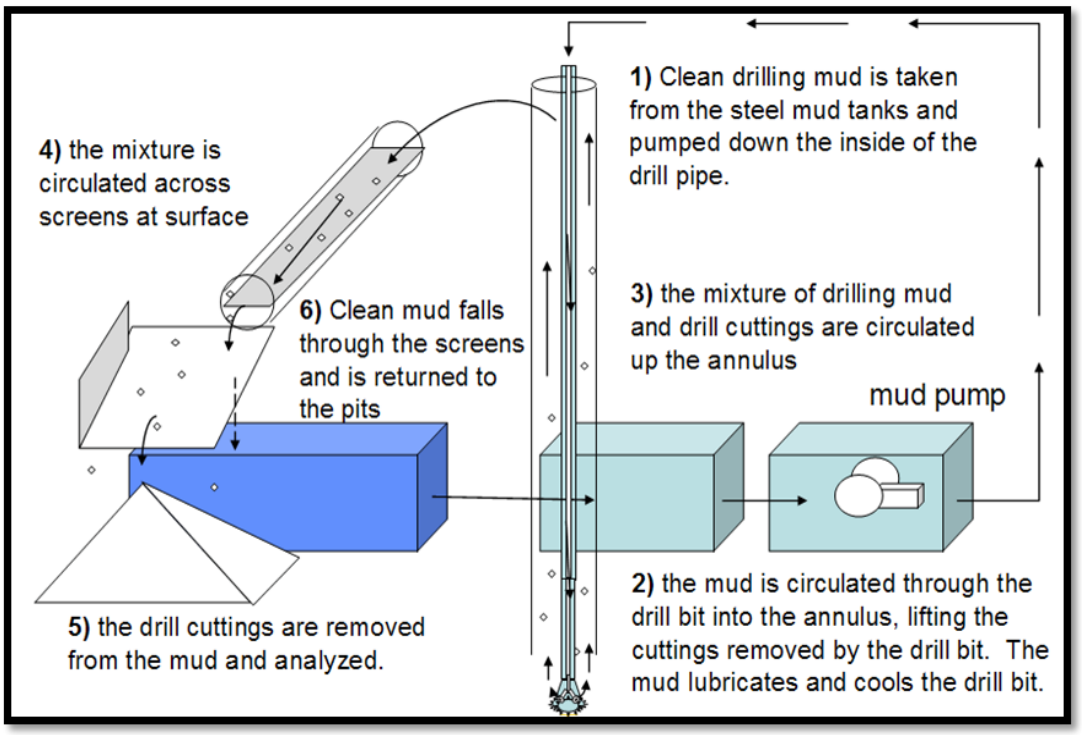

Figure 1-1 Schematic diagram of drilling fluid cycle

Difficulties during drilling operations in the petroleum industry have led to the preparation of diverse types of drilling muds. Nonetheless, the main

constituents of these muds are water, oil and gas, besides other chemicals. The drilling muds are categorized as water-based mud, oil-based mud and gas-based mud depending on base fluid. The most widespread drilling fluid is water-based mud (WBM), whereas oil-based mud (OBM) is frequently utilized in swelling shale formation [3]. OBM is employed in swelling shale formation, since as with water-based mud, the shale will absorb the water, and as a result of this, it enlarges. This enlargement may then cause a sticking pipe problem [3]. Nevertheless, there are particular situations where the liquid drilling fluid is not an appropriate circulating medium. Consequently, air, foam and gases are used as circulating fluid (Ibid). In this state, the drilling fluid is defined as a gas-based mud (GBM).

In drilling operations, the drilling muds are used to serve a number of purposes. The drilling fluid's function is to:

1- Cool and lubricate the drilling assembly: During drilling, a large portion of energy spread out as heat. The drilling fluid is used to absorb this heat from the drilling assembly which is then dispersed on the surface by radiation. The drilling fluid is also used to lubricate the drilling assembly to reduce friction at the drill bit and between the drill string and the wellbore wall.

2- Remove the cutting from the wellbore: the drilling fluid circulation causes the cuttings to lift from the bottom of the wellbore to the outside. Effective cuttings removal demands sufficient circulating rates to exceed the force of gravity acting upon the cuttings. There are other factors affecting the cuttings removal, which include drilling mud density and rheology, hole angle, annular velocity and cuttings-slip velocity.

3- Control the sub-surface pressures: the drilling fluid pressure should be more eminent than the formation pressure in order to preclude the formation fluid flow into the well. Nonetheless, the pressure difference should not be too high to avoid fluid loss, formation damage and a stuck pipe.

4- Suspend solids: When a drilling fluid's pumps are shut off, the drilling fluid will take on a gel-like state. This state helps retain cuttings and

weighting materials suspended in the drilling fluid. Otherwise, they will fall to the bottom of the wellbore. The suspension of particles in the drilling fluid depends on the particle density and size, as well as the drilling fluid density, viscosity, and the thixotropic (gel-strength). It is appropriate that the drilling fluid quickly develops high gel strength to resist the settling of heavy particles out of suspension.

5- Stabilize the wellbore: the density of the drilling fluid should be within the required range to stabilize the mechanical forces on the wellbore. An additional reason behind borehole instability is a chemical reaction that can happen between the drilling fluid and the formations. In many cases, the borehole instability is a result of water absorption by the shale. The most important factor is the generation of a superiority filter cake (thin with low permeability) on the walls to minimize the fluid invasion.

6- Secure the formation information: mud loggers analyse the returned mud and drilled cuttings for signs of oil and gas. They inspect the drilled cuttings to detect visual signs of hydrocarbons, mineral composition, porosity, formation pressure, etc.

7- Seal permeable formations: The differential pressure mean that the base liquid of the drilling mud filters into the formation while particles form a relatively impervious cake on the wellbore wall. The characteristics of this cake rule the amount of filtrate loss to the permeable formation. Drilling fluids should produce a thin, low permeability filter cake on the formation wall to limit the invasion of mud filtrate. This increases wellbore stability and inhibits a number of drilling problems.

8- Transmit hydraulic horsepower to the bit: the rate of mud flow should be adjusted to provide the optimal quantity of hydraulic energy to clean wellbore.

Various materials are employed in drilling muds to increase its strength by adapting the properties and composition, mostly when conditions call for drilling fluid with specific powers to increase the oil production operation [4]. The type and quantity of the additives depend on the drilling technique and

the formation type of wellbore [3].The traditional ingredients and chemical additives are:

1- Weighting agents to increase the density of the drilling fluid, which are used to control subsurface pressures.
2- Viscosifier agents to thicken the drilling fluid and increase hole-cleaning ability
3- Dispersants or deflocculates to thin the mud.
4- pH control to adjust the acidity and alkalinity of the drilling fluids.
5- Bactericides to overcome bacterial growth.
6- Corrosion inhibitors to inhibit corrosion and to avoid scales in the drilling fluids.
7- Defoamers to remove a foaming action.
8- Emulsifier agents to build a mixture of two immiscible liquids
9- Filtrate loss to cut water loss to the formation.
10- Flocculants to settle out the solids
11- Lubricants to decrease the friction coefficient

1.2 Limitations in Using Traditional Drilling Fluids

There are still restrictions during the use of the conventional drilling fluids, despite the chemicals that are added to amend the drilling mud efficiency. The foremost restriction of water-based muds is their capability to dissolve salts that may cause an undesirable leap in density. In addition, the WBM has the ability to interfere with gas and oil flow through the permeable formation. Another restriction is the capability of WBM to increase clay degradation and division, along with the failure of WBM in order to work in water sensitive formations. This is in addition to the strength of WBM to corrode the drill bits and drill pipes [5].

As with water-based mud, oil-based drilling mud has some restrictions. Oil-based mud is expensive, since the components of this mud are very costly and the treatment and disposal of the cuttings are also expensive [6]. Additionally, oil-based mud is not friendly to the environment owing to the fact that their disposal may cause contamination of water bearing aquifers and

lands. Furthermore, this kind of mud is restricted to usage in dry gas reservoirs [7].

Furthermore, gas-based mud (GBM) also has several constraints. The most common constraint is the high risk of explosion, due to high pressure that may be produced since GBM is a gas or foam. Furthermore, GBM also causes corrosion and cannot be utilized in water-bearing formations because the drilled cuttings will aggregate with each other [7].

Moreover, drilling techniques have evolved from vertical and horizontal to deviant and deep-sea wells. These modern methods require specialized drilling fluids [3], while the traditional muds are compatible with low to medium pressure and low to medium temperature conditions. Even though oil-based mud is used in high pressure and temperature environments, this mud probably experiences certain impairments, such as the degradation of weighting materials, gelation, and the breakdown of polymeric additives under HTHP conditions [8]. This debasement of traditional fluids in harsh conditions causes deceleration of penetration rates, which lead to insurmountable problems and this causes the survival of most the unrecovered oil [2].

1.3 Aims

This project aims to explore and assess the influence of various nanoparticles and their mixtures on the performance of water-based muds (WBM), including rheological, filtration, swelling, lubrication properties, and corrosion inhibition, as well as lifting capacity improvement.

1.4 Objectives

The above aims will be attained by satisfying the following research objectives:

1- Formulate different recipes of nano-drilling fluids and investigate the physico-chemical properties of these fluids using XRD, SEM, DLS, FTIR and TGA.

2- Investigate the rheological properties, including the viscosity, viscoelasticity and thixotropy characteristics, of the formed drilling fluids in rotational and oscillation modes.
3- Examine the filtration loss and the swelling behaviour of formed drilling fluids.
4- Examine the influences of environment parameters, including temperature, pressure and salinity of water-based drilling fluids, on the corrosion behaviour of the drill pipe, and the erosion-corrosion rate.
5- Simulate numerically the drilling process of a number of nano drilling fluids that we are developed, especially the flow in the annulus, and cuttings transportation.

1.5 Thesis Outlines

Chapter one introduces the industry-related background information and a brief review of the limitations of traditional drilling fluids.

Chapter two includes a review of some previous work and various nanoparticles for enhanced drilling fluid properties and the proposed solutions that can offer by nanoparticles. This chapter was divided to 5 sections. In the first section, the possible role of nanoparticles to solve most common drilling fluids problems was presented. The rest part of the chapter deals with literature review on:

- Nanoparticles to enhance drilling fluids
- Erosion-corrosion and corrosion control
- NPs-polymer to enhance drilling fluids
- Drilling fluid system simulation

Chapter three is the methodology chapter and is divided into three main parts: i) the preparation of nano-based drilling fluids and their characterization, ii) the corrosion and the erosion-corrosion experiments of drill pipes that caused by drilling fluids, and iii) the methodology of numerical simulation on cuttings transport.

Chapter four investigates the influence of nanoparticles on WBM without biopolymer. The rheological properties are experimental studied for three types of fluids, i) the base drilling fluid ii) WBM with single nanoparticle dispersed, and iii) WBM with mixture nanoparticle dispersed. The characteristics of the prepared fluids were evaluated by measuring viscosity, gel strength, viscoelasticity, thixotropy, filtrate loss and lubricity, and compared. The performance of CB-SiO_2, Al_2O_3-CNT, and SiO_2-Al_2O_3 based drilling fluids are presented in this Chapter sequentially.

Chapter five investigates the influence of nanoparticles on WBM with biopolymer. Firstly, silica nanoparticles are dispersed into various WBM with different biopolymers and the enhancement in viscosity, filtration and lubrication properties were analysed. Then, different types of nanoparticles (SiO_2, CNT, CB, Gr and Al_2O_3) with xanthan gum are conducted and the outcomes regarding the performance of Al_2O_3-XG, SiO_2-XG, CB-XG, Gr-XG and CNT-XG based drilling fluids are presented.

Chapter six presents the experimental results of the corrosion and erosion-corrosion rate of carbon steel API X-95 drill pipe specimens in a drill cuttings/ water-based-drilling fluid system. The corrosion rate in a reservoir-like environment under both static and dynamic conditions and investigated the influence of wellbore conditions, including temperature, pressure, and salinity of water-based drilling fluids was discussed. The erosion-corrosion rate in cuttings/water systems at different sizes and different concentrations of actual drill cuttings was presented. Finally, the erosion-corrosion rate at different nanofluids (NPs with xanthan) was discussed to prove the applicability of nanofluids in control erosion-corrosion.

Chapter seven studies the effects of various parameters on the cuttings transport through a concentric, rotating drill pipe by ANSYS-FLUENT CFD code, based on Power Law and Herschel–Bulkley rheological models. The influence of fluid flow rate, cuttings density, shape, and concentration are studied, as well as the fluid-particle coupling regime influence.

Chapter Eight provides summary, conclusion and suggestions for future work.

2 Literature Review

2.1 Nanoparticles Solutions for Drilling Fluids

2.1.1 Wellbore Instability

Before drilling, rock strength is in balance with the in-situ rock stresses, but when a wellbore is being penetrated, the equilibrium is broken. Drilling fluids are injected that cause an interaction between the formation and borehole fluids, which causes the wellbore instability problem. The reasons behind this can be mechanical failure caused by in-situ stresses, erosion caused by fluid circulation, or chemical interaction caused by the interaction between the borehole fluids with the formation [9]. On that point, are four patterns of wellbore instability:

- Hole closure
- Hole enlargement
- Fracturing
- Collapse

The related problems related with these patterns of wellbore instability are:

- ❖ Pipe sticking
- ❖ Lost circulation
- ❖ Bad hole cleaning

Hole closure and collapse can cause pipe sticking, and hole enlargement could cause bad hole cleaning, while fracturing causes lost circulation (Ibid).

It is acknowledged that every year, millions are lost owing to wellbore instability occurring during contact between the shale and the mud [10]. The drilling muds that involve nanoparticles have the capability to minimize wellbore instability by isolating the interaction between the drilling fluid and the formation, plugging the pore throats, [11], building an internal mud cake and thereby reducing the fluid invasion into the [12].

2.1.2 Lost Circulation

One of the usual known drilling troubles lost circulation [10], which is an incomplete or total deprivation of the drilling mud to the formation. This state takes place through naturally fractured cracks and grooves [13]. Lost circulation leads to increasing the expense and time expected to reach the objective depth [10]. In addition, lost circulation induces a lack of pressure control (Ibid). Thus, a great deal of time and effort has been employed to hold the loss circulation through the production of new additives. However, the employment of micro and macro materials have exhibited limited results [14]. The employment of nanoparticles is oriented towards reducing loss circulation by developing the cake of the structure, and further sufficiently raising the carrying capacity to hold the drilled cuttings and keep the drilling mud weight over a vast range of operational requirements [15].

2.1.3 Pipe Sticking

Differential pipe sticking, and mechanical pipe sticking are two types of drill pipe sticking. The main reason behind the differential pipe sticking problem is a thick filter cake, formerly deposited on a porous formation as shown in Figure 2-1. Differential sticking results from the drill string sticking to the thick filter cake [16], where the required force to make the drill string move surpasses the tensile strength of the drill pipes. Differential sticking can result in breaking part of the drill string or the loss of tools. This problem is costly for the following reasons [17]:

- Loss time: the lost drilling time when freeing the pipe
- Cost of fishing: when trying to pull out the broken part
- Abandon the tool: since it is very difficult or too expensive to remove from the wellbore.

The main causes of the mechanical pipe sticking vary. Mechanical sticking can be induced by an accumulation of drilling cuttings, unstable formation and key seating [17]. The settling of suspended drilled cuttings form a cuttings bed on the low side of the wellbore and this bed can curb the movement of a drilling assembly, which causes pipe sticking (Figure 2-2A).

During drilling a deviated wellbore, with great tenseness and curvature in the drilling string, the drill string presses the surface of the wellbore and cutting grooves, which is called the key seat. Drilling in a soft to medium hard formation has a great propensity to obtain the key seat. Mechanical sticking occurs when pulling out of the hole, where the drill collar gets stuck in the key seat (Figure 2-2B). It's possible to continue drilling when key seating occurs.

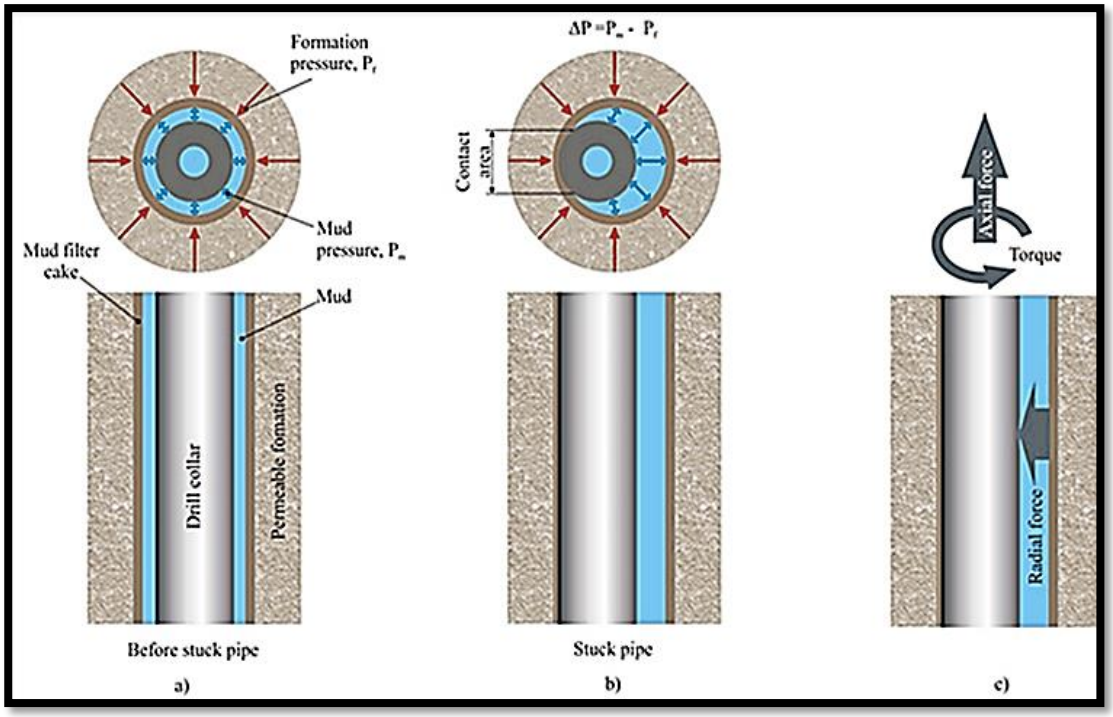

Figure 2-1 Schematic diagram of differential pipe sticking [18].

The most difficult wellbore instability problems happen when drilling shale, since shale can slough in or plastically flow, which causes mechanical pipe sticking. In the same manner, drilling in salt demonstrates plastic behaviour under surcharge pressure, where the salt has the tendency to flow inward if mud density is not sufficiently high. Additionally, mechanical pipe sticking can result from the use of mud that is low in density, since this mud can cause the collapse of the wellbore in any formation (Figure 2-2C). The sticking of the drilling pipe has a critical influence on the drilling operation and its costs. Numerous parameters relate to the sticking of the drill pipe, which are handed out to the drilling fluid and formation. The nanoparticles play a role in preventing and recapturing the sticking pipe.

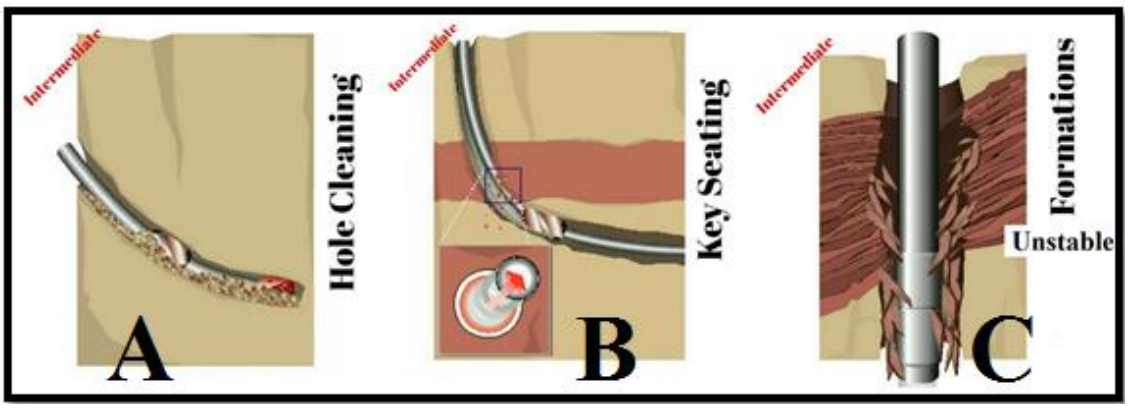

Figure 2-2 Mechanical pipe sticking causes. (A) Accumulation of drilled cuttings. (B) Key seating. (C) Unstable formation [19].

Nanoparticle based drilling fluids have the ability to control the differential pipe's sticking by decreasing mud cake thickness [17] and bringing down the sticking tendency of mud cakes by lessening the friction coefficient between the drill pipe and the wellbore. In addition, nanoparticle based drilling fluids have superior holding capacity, hence controlling the mechanical pipe sticking by efficiently removing the drilled cuttings from the wellbore [10].

2.2 Review of Nanoparticles Application in Drilling Fluids

Nanomaterial-based drilling fluids are drilling fluids with nanomaterials in their recipe. These nanomaterials can be dispersed in the base liquid of the drilling fluids in lower amounts, which are matched to similar additives of larger sizes [20]. Likewise, the nanofluids are ordered into advanced and straightforward depending on the concentricity of the nanomaterials in the drilling muds. The available publications in the field of using nanoparticles in drilling fluid are scant; this area still requires more research. In the following section, a review of the application of nanomaterials in drilling fluids will be described in detail.

Paiaman and Duraya [21] proposed a new method to decrease stuck pipes during drilling wells. Their study focused on the contact area between the drill string and the mud cake, since a greater contact area causes greater friction, and this can produce pipe sticking. They experimentally demonstrated that the

filter cake thickness can be thinned by using carbon black nanomaterials in the drilling fluid recipe. The outcomes of their research indicated that the reduction percentage of filter cake thickness is near 25% when adding 2% of carbon black nanoparticles.

Although Paiaman and Duraya's research showed a reduction in mud cake thickness, their study is vague in other areas. There is no experimental methodology, so we don't know how they obtained the filter cake. Also, nothing is explained about which techniques they used to measure mud cake thickness. Likewise, although they provided the results concerning the mud cake, they disregarded the effects of filtrate loss, where while it is impossible to obtain a filter cake without the filtration process.

Amanullah et al. [22] examined the rheological and filtration properties of three nano-based drilling fluids. Their study showed that the nano-based drilling mud produced rheological properties. In addition, it showed a significant decrease in filtrate loss along with the NPs with a deposition of a thin and compact mud cake, which in turn lead to a reduction in differential pipe sticking in permeable formations.

Jung et al. [23] discussed the formulation of iron oxide (Fe_2O_3) nano-based drilling fluids and the preliminary results of rheological and filtration properties as a function of temperature and pressure. Their results showed that the rheological parameters, such as viscosity, yield stress and gel strength, increased with increase of Fe_2O_3 NPs, while the filtrate loss decreased with an increase of Fe_2O_3 NPs concentrations. In their discussion, they attributed the rheological properties enhancement to the Fe_2O_3 NPs embedded in randomly dispersed pore structures on the surface of clay particle and links between bentonite particles, which promoted the gelation of the bentonite particles. The results of this work regarding Al_2O_3 bear a close resemblance to Fe_2O_3 behaviour, which can be attributed to the fact that both are metal oxide nanoparticles.

Abdo and Danish [24] tested a material called ATR as a new clay. The results demonstrated that the nanoparticles of ATR were found to be suitable for use in drilling fluids. The mud of ATR nanoparticles shown a low viscosity without compromising the density requirement and thus expected to minimize drilling

problems. This mud also shows that high gel strength is important for avoiding many severe drilling problems. Moreover, the combination of ATR nanoparticles and bentonite showed promising properties: high densities of bentonite, low viscosity of ATR nanoparticles, and high gel strength. They also examined the effect of the addition ATR nanoparticles on the filtrate loss and lubrication of bentonite clay. The results showed a reduction in torque and filtrate loss.

Later, Abdo and Danish produced further research [25] where, they tested new nanoparticles as rheology stabilizer. They presented an approach to stabilizing the drilling fluid rheology at a wide range of temperatures and pressures by using nano palyorsikite. They made a stable recipe of Montmorillonite and nano palyorsikite at both high temperature and pressure. They examined the shear thinning, fluid loss, lubrication quality and rheology at both high temperature and high pressure of this drilling fluid recipe. Their results showed stability at a wider range of values of pressure and temperature and a significant reduction in torque and fluid loss.

Riveland [26] investigated the influence of nanoparticles in order to develop the filter cake. Different sizes and types of nanoparticles were examined for oil-based and water-based muds. The main test to examine the influence of nanoparticles to enhance the filter cake was the LTLP API filter press test. At LTLP conditions, both the base case and nanofluid showed a little fluid loss; therefore, the data are not trusted worthy. Based on that, Riveland suggested a high-pressure and a high temperature filter test with a ceramic filter.

Ragab and Noah [27] studied the reduction of fluid loss for water-based mud by using silicon oxide nanoparticles. They investigated the effect of nanoparticles size and concentration alongside fluid loss reduction. Three different size ranges of silica nanoparticles (5-15nm, 10-25nm, and 70-95nm) were used to detect the effect of nanoparticle size on fluid loss. They examined the size ranges of silicon oxide nanoparticles by using Scanning Electron Microscope (SEM) while they verified the nanoparticles composition by using Energy Dispersive X-ray Spectroscopy (EDX). The results indicated that the optimal size range was 5-15 NM and that effective concentration is between 20% and 30%, which leads to a 56% reduction in fluid loss.

William et al. [28] used CuO and ZnO prepared nanofluids to enhance the thermal, electrical and HPHT rheology of water-based mud. The base fluid of nanofluids was xanthan gum and the nanoparticle concentrations are 0.1, 0.3 and 0.5 weight%. They added these nanofluids as additives to WBM (NWBM). The percentage additive of these nanofluids was 1% of the total WBM volume. It was observed that the concentration increase of nanoparticles promotes thermal and electrical features of NWBM. The results showed that NWBM enhanced thermal and electrical characteristics by approximately 35% compared to WBM. It was observed that the drilling fluid based on CuO nanofluids had increased thermal properties and developed resistance to HPHT conditions more than the drilling fluid based on ZnO nanofluids. Additionally, HPHT rheological investigations were conducted for prepared nano-drilling fluids in order to ascertain the impact of nanofluids on the rheological properties at different pressures (0.1Mpa and 10Mpa) and temperatures (25, 70, 90 and 110 °C). The results also indicated that the influence of pressure was more significant at higher temperatures on the rheology of NWBM and shows better rheological stability.

Jabrayilove [29] analysed the improvement of lubrication behavior of OBM drilling fluids by adding nanoparticles. Tribological and rheological analyses were carried out to measure reduced friction and rheology of the drilling fluid by using titania and silica nanoparticles as an additive. According to the laboratory results, titania and silica showed well-reduced friction properties. Notably, the addition of silica nanoparticle with the concentration of 0.25 weight% reduced friction coefficient by 47% of the temperature of 50°C. It is likewise observed that silica nanoparticles are more efficient in overcoming the friction coefficient when matched to silica micro particles.

Jahns [30] also investigated the improvement of lubrication behavior by adding nanoparticles like Jabrayilove [31] but for WBM drilling fluids. The same experimental methodology was applied, where Alumina, titania and silica nanoparticles were used as additives and different concentrations were examined at several temperatures. According to the results, the titania and silica nanoparticles efficiently reduced the friction factor. The alumina particles have a limited friction reduction, which is a consequence of an increased friction factor with the increasing particle concentration in the fluid.

Barry et al. [13] illustrated how modifying the surface charge of clay-based drilling fluids via intercalation and NP addition can alter the rheological properties and fluid filtration characteristics of conventional drilling muds under LTLP and HTHP conditions. The investigated the influence of iron oxide (Fe_2O_3) NP additives, iron oxide clay hybrid (ICH) and aluminosilicate clay hybrid (ASCH) nanoparticles to develop the rheological and filtration properties under Low Pressure/Low Temperature and High Pressure/High Temperature conditions. They noticed that the addition of ICH and ASCH in bentonite solutions reduced both LTLP and HTHP fluid loss as much as 37% and 47%, when compared to the control, under the respective conditions. The pure addition of 0.5 wt% 3 and 30 nm Fe2O3 NP increased the LTLP fluid filtration as much as 14%, compared to the control. However, this addition of Fe_2O_3 NP decreased the HTHP fluid filtrate volumes as much as 28% compared to the control. Barry et al. attributed this decrease in fluid loss to a restructured mode of clay platelet interaction, attributed to a modification in surface charge. The addition of ICH particles into the bentonite solution promoted the attraction of positives charges on the surfaces of the hybrid clay platelet with the negative charges of the bentonite platelets. This attraction was between the edge of the ICH particle and the face of a non-hybrid bentonite clay platelet (E–F), as well as an attraction between the face of the hybrid iron-oxide clay platelet and the face of the non-hybrid clay platelet (face-to-face (F–F) flocculation), resulting in the formation of a rigid 3D clay platelet network, thus low filtration volumes. In contrast, embedded Al_2O_3–SiO_2 nanoparticles promoted negative charges at the edge of the ASCH particle, increasing the negativity of the net charge of the hybrid particle. This resulted in the generation of repulsive forces between the hybrid ASCH and bentonite clay platelets in the fluid system. This strong electrostatic repulsion prevented coagulation and the subsequent formation of a strong clay platelet network. Thus, there were minimal clay platelet network formation and low permeability filter cakes. The above study is considered complementary to them previous research [32], which discussed the same influence of nanoparticles on the rheological properties of the bentonite fluids.

Contreras et al. [33] examined the use of in-house prepared iron-based and calcium-based nanoparticles, with the presence of graphite as a filtrate

reduction agent in oil-based mud to minimise the filtrate loss in a permeable formation. They observed that the samples containing calcium NPs moderately increased their plastic viscosity, while the samples containing iron NPs caused a reduction in the yield point, especially at a high graphite concentration. The results also showed that all the prepared nanofluids were able to reduce the fluid loss compared to the values given by the control sample. More precisely, iron-based NPs gave a higher reduction in fluid loss value, especially at low concentrations under HP/HT conditions, while calcium-based NPs yielded a remarkable decrease at a high level under HP/HT environments.

Vryzas et al. [34] investigated the usage of synthesised magnetite NPs to develop water-based drilling fluids. They used XRD and TEM to characterise the synthesised NPs. The results showed that the addition of 0.5wt% of Fe_3O_4 NPs increases the yield stress by around 27% compared to the base fluid. However, the 10sec and 10min gel strength values were reduced by the addition of NPs. The authors noticed that the NPs are able to reduce the filtrate loss and filter cake thickness compared to base fluid. They justified their results that demonstrated the ability of using NPs to create a rigid microstructure network with bentonite platelets, thus building an impermeable thin filter cake.

Ponmani et al.[35] examined the thermal conductivity enhancement of CuO and ZnO nanofluids at different concentrations in different base fluids (xanthan gum, polyethylene glycol and polyvinylpyrrolidone) compared to their micro-fluids. The authors observed that enhanced thermal conductivity properties were achieved when nanoparticles were added (when compared to the micron-sized materials), and higher concentrations of nanoparticles promoted better thermal conductivity properties.

Halali et al. [36] studied the CNT as a desired additive in this study to fulfil the ongoing severe challenge of HPHT conditions in different polymeric fluids (Tween 80, PMMA, and ACUMER). Their results showed that CNT could boost the viscosity of drilling fluids, especially at low shear rates, which is in accordance with the shear thinning behaviour of fluid in the presence of CNT. Furthermore, CNT boosts the absolute value of zeta potential, which was

under −20 mV for all the nanofluids. In addition to CNT advantages, it could reduce the filtration by over 93.3% at HPHT conditions, enhance the thermal conductivity of fluid by 12%, and increase the shale recovery by 10.5%.

Many researchers have employed nano silica (SiO_2) as a drilling fluid additive for both oil and water-based drilling fluids. Salih et al. [37] identified that the usage of nano silica NPs in a concentration between 0.1–0.3 wt% had the most critical influence on water-based drilling fluid properties than higher levels. Besides, they also demonstrated that water-based drilling fluids with nano silica can substitute oil-based drilling fluids in horizontal, directional, and shale drilling techniques, due to the ability of the nano drilling fluid to reduce drilling and production difficulties.

Ismail et al. [38] examined the applicability of multi-walled carbon nanotube (MWCNT) and nanosilica as drilling fluid additives for improving the rheological and filtration characteristics as well as the lubricity of water-based drilling fluids. Their study revealed that addition of MWCNT and nanosilica improved the rheological properties, such as plastic viscosity and yield point compared to that of the base fluid. Furthermore, the results showed that the coefficient of friction (CoF) for drilling fluid without nanoparticles was 0.238 while, just 0.01 ppb of MWCNT and nanosilica provided 44% and 38% CoF reduction. MWCNT showed 4.5 ml of filtrate volume and 2/32 inch of mud cake thickness. Apparently, the present study's results regarding MWCNT appear to be in contradiction with their results, but this not the truth. In our experiment, we added the nanoparticles to base drilling fluid (just bentonite and water) to discover the role of the nanoparticles, while they used drilling fluid contain polymers (flowzan, PAC and PHPA). Therefore, the results of this study are significant only for a nano-polymer addition, which is what we got for MWCNT-Xanthan.

Li et al. [39] discovered the impact of cellulose nanoparticles (CNPs), including micro fibrillated cellulose (MFC) together with CNCs, in improving the rheological and filtration performance of water-based drilling fluids (WDFs). Their results showed that CNC-WDFs had superior rheological properties, higher temperature stability, less fluid loss volume, and thinner filter cakes than WDFs and MFC-WDFs. Moreover, the presence of polyanionic cellulose

(PAC) further improved the rheological and filtration performances of CNC-WDFs, suggesting a synergistic effect between PAC and CNCs.

Li et al. [40] took advantage of the incorporation of polyanionic cellulose (PAC) and cellulose nanocrystals (CNCs) to develop an environmentally friendly and high-performance water-based drilling fluid. Their results showed that the presence of PAC lead to building low permeable filter cake and subsequently an excellent filtration property, whereas the presence of CNCs had a greater impact on the rheological properties. The combined use of CNCs and PAC yielded better rheological and filtration properties.

Amarfio and Abdulkadir [41] explored the effect of Al_2O_3 NP on the rheological properties of water-based mud. They showed that Al_2O_3 NP provided thermal stabilization for the drilling fluid under high-temperature conditions and that the Al_2O_3 NPs were able to maintain the shear stresses of the fluid as temperature increases. In our view, their work suffers from several weaknesses and shortcomings. Aiming to address these limitations, we examine the effect of Al_2O_3 nanoparticles on water-based mud properties, which will be discussed in detail in the next section.

Javeri et al. [42] took advantage of Silicon NPs to develop drilling fluid filtration and rheological properties to mitigate the loss of circulation and differential sticking. They built the hypothesis that the nano size of silicon nanoparticles can reduce the mud cake thickness and at same time the presence of nanoparticles make the mud cake more continues and will cause lower filtrate volume and less mud cake thickness. Javeri et al. showed that the silicon NPs reduced the mud cake thickness by 34%. However, this study may not be practical. A fundamental limitation of this research is that it does not address the disadvantages of the addition of silicon NPs, they just measured the filter cake thickness without mentioning the volume of filtrate loss. Another major drawback of this approach is decreasing the rheological properties. Therefore, resulting in a drilling fluid with less viscosity and more filtrate loss that is not able to produce less filter cake and these limitations make it impractical.

Parized and Shahbazi [43] explored the impact of Tin oxide (SnO_2) NP on polymeric water-based drilling fluid properties. They found that adding SnO_2

NPs enhanced the characteristics of the drilling fluids such as rheology, thermal and electrical conductivities, thixotropy and filtration characteristics. More specifically, electrical conductivity and thermal conductivity were increased by 30 % and 15 %, and they also noticed a 20% reduction in fluid loss by adding 2.5 g/L SnO_2 NPs.

Saboori et al. [44] and Fereydouni et al. [45] investigated the influence of carboxymethyl cellulose (CMC) and polyanionic cellulose (PAC) polymer nanoparticles on fluid loss, where mud-cake-thickness regular powder CMC and PAC are used as additives for the drilling fluids. CMC and PAC nanoparticles were made in-house. The authors found that adding CMC and PAC nanoparticles resulted in a desirable reduction of the amount of fluid loss and mud cake thickness when compared to conventional polymers of the same type. It was motivating to compare nano CMC and PAC with regular powder CMC and PAC in order to indicate the significance of nanoparticles in improving such performance.

Samsuri and Hamzah [46] examined the ability of MWNTs NPs to improve the lifting capacity of water-based drilling fluids. They aimed to study the effect of different concentrations of MWCNTs used, cutting size and mud annular velocity on the mud lifting capacity. They also noticed that the increase in NPs concentration caused an increase in drilling fluid viscosity. Therefore, the lifting capacity also increased. A rig model, as shown in Figure 2-3 was used in the experimental works with cutting sizes of 2, 2.8 and 4.8 mm. A 10 lb/gal water-based mud was added with various amounts of MWNTs and an annular velocity of 29.2 to 102.1 ft/min.

Altogether the above works have taken place in laboratory scale. Nevertheless, it is essential to evaluate nanofluids in real conditions. The challenge for nanoparticle-based drilling fluids is that in order to gain acceptance, they cannot merely match the industry's conventional chemistries, they must outperform them. Two studies in the literature highlight the successful application of novel nanofluids in the field. Taha and Lee [47] presented the use of a nano drilling fluid containing a blend of proprietary surfactants engineered with nano-graphene to improve the lubricity and thermal stability of the drilling fluids. They tested the developed nano drilling

fluid in the field (HP/HT onshore well) and observed a significant enhancement in the fluids' thermal stability, as well as in its lubricity. They also observed a 30% reduction in fluid loss compared to conventional muds.

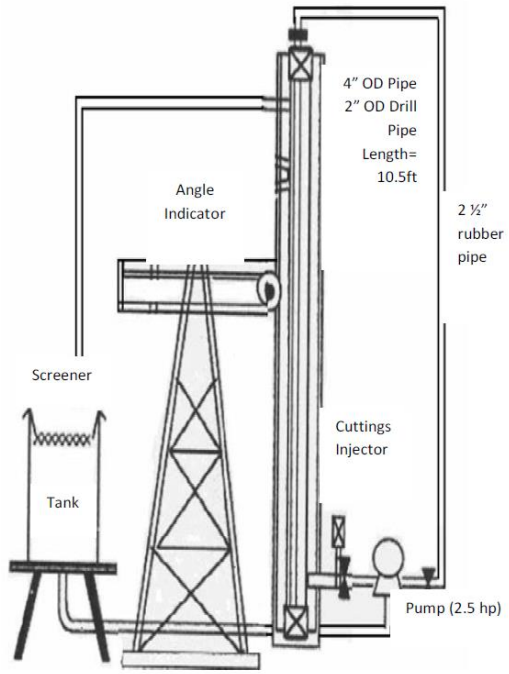

Figure 2-3 Schematic of the rig model [46].

Furthermore, they obtained an improved rate of penetration (ROP) by 125%, actual reaming torque reduction of 20% and more than 75% increase in the bit's lifespan. Borisov et al. [48] presented positive results from a field application of nanoparticle-based invert emulsion drilling fluids (an oil-based drilling fluid). They emphasised that drilling fluids that combine LCM with nanoparticles can significantly reduce fluid loss and create a thinner filter cake, compared to fluids containing LCM alone. Due to their superior properties, NP have the ability to fill the gaps between the micron-sized particles, which leads to lower permeability and decreased filtrate flux. They concluded that their attempt to upscale the NP synthesis was successful. Total mud losses were reduced by 22–34% in the presence of 0.5 wt % calcium NP, which agrees with what was obtained in the lab.

2.3 Corrosion and Erosion-Corrosion Control of Drill pipe

The corrosiveness of water-based drilling fluids is a major problem in drilling operations and still needs to be resolved. Advancements in drilling engineering pose an additional challenge for the use of drilling fluid due to severe environmental conditions. For deep and ultra-deep wells, where the temperature and pressure are high, drilling fluids tend to be more corrosive. According to one of the oil companies of China, drilling fluids consume 4kg of drill pipe per meter depth. The losses by corrosion were estimated from 20%–50% of the total drilling cost [49]. Another study has shown that drilling fluid corrosion losses are approximately 60% of the total drilling cost due to failures caused by the drilling fluids and costs associated with these incidents [50]. Drilling fluids are corrosive due to the presence of dissolved gases, such as O_2, CO_2 and H_2S, and erosion by chemical composition or drilled cuttings during the drilling process.

Corrosion investigation under downhole conditions can provide information regarding the corrosiveness of the drilling fluid and the type of corrosion encountered. It is difficult to effectively simulate the chemistry, harsh conditions and flow components of the drilling process in a laboratory. Moreover, very few studies have investigated the corrosive effects of drilling fluid environments on drill pipes. These studies were limited to specific working conditions and most of these studies were conducted under ambient and static conditions, which were considerably different from the actual corrosive conditions present during an actual drilling operation [49, 51, 52]. Dynamic experiments were mainly performed in simple glass cells comprising a rotating cylinder electrode (RCE), which could exhibit some basic corrosion characteristics but does not capture the downhole conditions or large flow loops under high pressure and temperature, which were used to mimic the complex and expensive downhole conditions [53-55].

In a practical operation, the drilling fluid cycle is often unstable and alternates between static and dynamic states, and usual ambient steady corrosion tests cannot simulate the highly corrosive conditions present in a drilling operation [49]. To control and mitigate corrosion, it is necessary to understand how

drilling fluids under downhole conditions influence the process of corrosion and the factors affecting the values of the corrosion rates.

One of our research goals is to improve our understanding of the corrosion process of drilling fluids. A novel simple method was used to mimic drill-pipe corrosion for both the static and dynamic tests under high-pressure, high-temperature (HPHT) working conditions. An HPHT cell autoclave with a mechanical stirrer driven by a shaft was used to simulate the flow condition and investigate the effect of rotation speed. Instead of using a flat surface, a cylindrical coupon constructed from a typical pipe material, i.e. steel X95, was mounted at the lower end of the shaft, which rotated in the HPHT cell filled with drilling fluids. The coupon simulates the shape of the drill pipe. Factors, including the temperature, pressure and salinity of the drilling mud on the corrosion behaviour of the drill pipe were analysed to investigate their effect on the corrosion rates of the samples. In addition, as Haaland (1976) reported, the particle size and the hardness of the additives could lead to erosion corrosion [56]. Scanning electron microscopy (SEM) imaging and a pure erosion test were conducted to study the surface characteristics.

Drilling fluids are used to carry out a wide range of functions. Perhaps the most crucial role related to this study is to remove the drill rocks cuttings from the bottom of the wellbore to the surface. When drilling is in progress, the drilling fluid is pumped down through the drill string, and out of the nozzles in the bit. Since the diameter of the bit is larger than that of the drill string, an annulus space is left around the drill string as drilling progresses. The drilling fluid returns to the surface through the annulus carrying with it the cuttings from the bottom of the wellbore. Therefore, the presence of drill cuttings rocks, water-based drilling fluids and flow, as well as drill pipe rotation, can cause corrosion and erosion-corrosion to the drill pipe material.

The size and the concentration of the drill cuttings are variable during drilling, depending on drill pit diameter, penetration rate, and formation type and drilling fluid flow. During drilling the first section, the size of the drill bit as well as its teeth are very large, resulting in large rocks cuttings. The size of the drill bit and the teeth gradually decreases when drilling the remaining sections, producing smaller rocks cuttings. On the other hand, the drill cuttings

concentration also changes during drilling depending on penetration rate, formation type and drilling fluid flow rate. In the same way, the drilling fluid type and viscosity is also changeable, which is governed by various parameters. However, most of the previous studies do not take into account the erosion-corrosion of the drill pipe that happens due to the presence of cutting rocks with drilling fluid in the wellbore. The mechanism of the destruction of these materials occurs due to metal removal by the cuttings action of high-speed abrasive particles. Meanwhile, erosion also removes the corrosion products that make corrosion happen faster. No study, to the author's knowledge, has focused on the erosion-corrosion of the drill pipe by drilling fluid/cuttings rock mixture that resulted in oil and gas wells drilling. To fill this research gap, we have examined erosion-corrosion behaviour under different conditions by using actual limestone drill cuttings rocks taken from the Nasiriya oil field from a depth of 1650 m to 1700 m. This research aims to evaluate the influence of real rock cuttings sizes and concentration, as well as investigate the effect of base fluid type on the erosion-corrosion rate. Our research also aims at finding a solution to this challenging problem by supposing SiO_2-nanfluid as the base fluid to control the erosion-corrosion of the drill pipe. This research is complementary to our previous study in which it was examined the effect of drill pipe rotation speed, the salinity of drilling fluids, temperature and pressure on the drill pipe corrosion rate. It has been suggested that there is certain method that can be used to simulate complicated wellbore conditions during drilling [57]. In the present study, these factors were taken into consideration because they are crucial during drilling.

2.4 Review of Nanoparticles and Water-Soluble Polymer Application in Drilling Fluids

In the past few years, few researchers have demonstrated that nanoparticle-polymer could enhance drilling fluid performance. The addition of nanoparticles exhibits a notable enhancement to a polymer's physico-chemical, mechanical and thermal properties, due to the large surface area/volume ratio offered by the nanoparticles. Several researchers have

attempted to incorporate different nanoparticles into different polymers for rheological, filtration control and shale inhibition instead of using just polymers. Jay Karen et al. [28] discussed the formulation and preliminary test results of CuO and ZnO nanofluids in Xanthan gum. They found that the NWBM based on CuO nanofluid are observed to show improved thermal properties, which are more resistant to HPHT conditions than ZnO- based NWBM. High-pressure rheological experiments are conducted on NWBM to understand the effect of nanofluids on the rheological properties at varying temperatures (25, 70, 90 and 110 ^{o}C) and pressures (0.1MPa and 10MPa). They draw author's attention to the rheological stability of NWBM at high pressures and temperatures. They observed that NWBM shows improved thermal and electrical properties by about 35% compared to WBM. Unfortunately, it does neglect to explain why this improvement occurs with nanofluids. The main limitation of this study is ignoring the filtration, shale inhibition and lubrication properties and just focusing on rheology. An additional problem is that there are no morphological and chemical characterisations for nanoparticles and nanofluids.

The first related systematic study was conducted in 2015 by Rajat Jain et al. [58]. They discussed the feasibility of polyacrylamide-grafted-polyethene glycol/SiO_2 nanocomposite as a potential additive for the drilling of troublesome shale formations. They started the research by synthesising the nanocomposite, characterised by Fourier transform infrared spectroscopy (FTIR), Field emission scanning electron microscopy (FESEM), Energy dispersive spectroscopy (EDX), Atomic force microscopy (AFM), and thermogravimetric analysis (TGA). Then, the substance was employed in the preparation of the water-based drilling mud system. The results indicated that the synthesised nanocomposite exhibited superior shale inhibition properties. The nanocomposite acted synergistically with other additives in the developed system and furnished good rheological properties and filtration characteristics. It also showed lower formation damage, higher shale recovery, and higher thermal stability than the partially hydrolysed polyacrylamide (PHPA) polymer.

In same year, Rajat Jain et al. produced another study [59]. Likewise, they synthesized a new nanocomposite polyacrylamide/clay PANC utilising free radical polymerisation technique, which was characterised first by Fourier

transform infrared spectroscopy, field emission scanning electron microscopy, and thermogravimetric analysis. The results showed that the prepared nanocomposite exhibited superior shale recovery than the partially hydrolysed polyacrylamide (PHPA) polymer.

In 2016, Rajat Jain et al. [60] published a third study in this area and this time they synthesised polyacrylamide grafted xanthan gum/multiwalled carbon nanotubes (PA-g-XG/MWCNT) nanocomposite also by utilising the free radical polymerisation technique. They reported in the results that plastic viscosity, apparent viscosity, yield point, and gel strength increased at higher concentrations of the nanocomposite. The research methodology of the three studies was precisely same in its synthesis, characterisation and investigations.

Alizadeh et al. [61] studied the nanocomposite as a rheology modifier. They synthesised Alumina/polyacrylamide nanocomposite utilising the solution polymerization method and they exclusively examined this nanocomposite as a viscosity modifier. The mean issue with their method was that the prepared nanocomposite was tested as a viscosity modifier only, we don't know if it can work with other drilling fluid properties. Research has tended to focus on viscosity, rather than rheology properties. An additional problem is that the concentrations of alumina nanoparticle, polyacrylamide polymer and the volume of water are unknown.

Mao et al. (2015) introduced micro-nano composite material to drilling fluids. They synthesized a polymer based nano-silica (coded as SDFL) by inverse micro emulsion polymerization and sol-gel formulation. They analysed the particle size distribution, the surface area, morphology and structure for producing micro-nanocomposite material. They studied the plugging ability by using micro-model drilling fluid flooding of the core column. The results indicated that micro-nanoparticles could effectively plug the micro-pores since the micro-nanoparticles cross-linked and bridged together under the action of the molecular chain of the polymer matrix. Moreover, the polymer matrix non-polar element of micro-nanoparticle material made it difficult for the polar molecules (like water) to pass over the film, which was formed by non-polar molecules, so, the filtration loss could be reduced.

In the same year, Mehran Sadeghalvaad and Samad Sabbaghi employed the TiO_2/polyacrylamide (PAM) nanocomposite additive towards improving the water-based drilling fluid properties [62]. They synthesised TiO_2/polyacrylamide (PAM) nanocomposite by solution polymerization method. The prepared nanocomposite was characterized by X-ray diffraction (XRD), Fourier transform infrared (FTIR) spectroscopy, Ultraviolet–visible (UV–Vis) spectroscopy, scanning electron microscopy (SEM), and dynamic light scattering (DLS). The results indicated that the additive contributes to an increase in the viscosity and a decrease in the fluid loss and filter cake thickness.

In 2016, Aftab et al. [63] investigated the effect of employing a zinc oxide nanoparticle-acrylamide composite on the rheological properties and shale inhibition characteristics of water based drilling fluids. They synthesised the nanocomposite and used XRD, FTIR, TGA, FESEM and SEM for characterizations. Their study's finding reported that the thermal and chemical stability of drilling fluids improved along with the synthesized composite. The filtrate loss and frication coefficient were reduced. Moreover, the yield point and gel strength improved and shale swelling also improved. Our experimental methodology bears a close resemblance to that of Aftab et al.

In 2017, Weobel and Belayneh investigated the effect of Molybdenum Disulphide-Graphene nanocomposite on the lubricity of drilling fluids. They reported that the addition of 0.2 MoS_2 and 0.1 graphene reduced the friction coefficient by around -44% and -34 respectively. This reduction increased drilling depth by around 26% and 7.7% respectively during simulation by using Landmark/wellplan software.

In 2018, Huang et al. Introduced the synthesis of a nanoscale acrylic resin/nano-SiO_2 composite (AR/SiO_2) with a core-shell structure for water-based drilling fluid (WBM) [64]. The core-shell structure of AR/SiO_2 was characterized by a transmission electron microscope (TEM). Thermal Gravity Analysis (TGA) indicated the thermal resistance of AR/SiO_2 up to 250 °C. The results demonstrated that WBM containing AR/SiO_2 can substantially enhance plugging efficiency and reduce fluid invasion. The characterization

of filter cakes revealed that AR/SiO_2 improved the quality of filter cakes, which resulted in a considerable improvement in filtration properties.

2.5 Drilling Fluid System Simulation

Predications of drilling fluid performance to transport cuttings in the annulus are very complex, due to numerous parameters that affect drilling operations. Besides, seeding nanoparticles into a drilling fluid is a recent development to improve the drilling fluids performance, although it still needs more research, especially in terms of lifting capacity improvement. Understanding the influences and the mechanisms of cuttings transport improvement by nanoparticles will push drilling fluids development forward. Computational Fluid Dynamics (CFD) is widely used as a numerical technique in handling complex multiphase flow problems in different operational conditions. The present work has taken the advancement of CFD to computationally analyse the influence of nanoparticles and the effects of various parameters such as drilling fluid rheology, flow rate, pipe rotation, cuttings density, shape, concentration and drilling fluid-cuttings' particle coupling regimes on the cuttings' transport in a vertical wellbore.

2.5.1 Drilling Fluid -Cuttings Flow Simulation

The drilling fluid cycle rises from the bottom of the wellbore to transport the cuttings to the outside. The circulating speed of the drilling fluid should be rapid enough to overcome cuttings that tend to overwhelm through the rookie fluid due to the gravitational force. Other factors that also affect the cuttings removal involve drilling mud density, rheology, hole angle, annular velocity, fluid viscoelastic properties, drilled cuttings size and their shape [65]. Based on these, a loss of drilling fluid or filtrate loss can take place because of the flow through the permeable formations. The cutting-drilling fluid flow can be simulated as solid-liquid flow, the cutting stimulated as solid particles, while the drilling fluid can be stimulated as non-Newtown fluid.

There are two techniques of modelling solid-liquid flow. These methods can simulate the cutting-drilling fluid flow within the wellbore:

- Eulerian-Eulerian approach
- Eulerian-Lagrangian approach

Both are accurate and have various strengths and weaknesses. In the next sections, both strategies will be described, and their applicability for drilling fluids will also be discussed.

2.5.1.1 Eulerian-Eulerian Approach, Applicability, Advantage and Disadvantages

The fluid and the solid phases are treated by two-phase models (hydrodynamic models) as two continuous interpenetrating phases. For granular flow, the solid form is modelled by using the analogies from kinetic theory; Particle-Particle interactions are reported based on the Kinetic Theory of Granular Flow [66]. This model is applicable from dilute to dense particulate flows (Fig. 2.4). Particle size distribution can also be accounted for by assigning a separate secondary phase for each particle diameter. The Eulerian is the most complicated model of the multiphase patterns in **FLUENT**. It solves a set of equations (continuity, momentum and energy) for each phase [67].

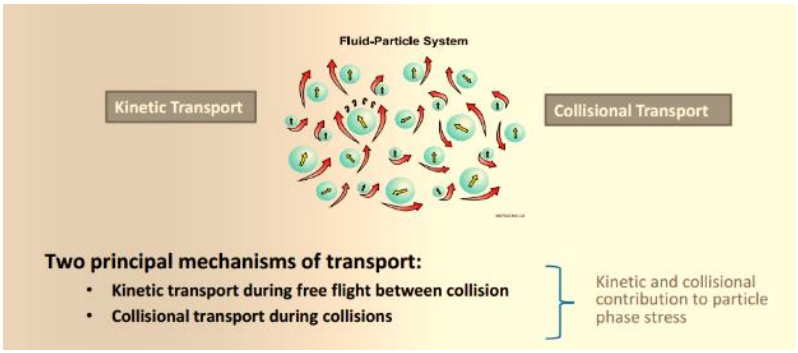

Figure 2-4 Schematic diagram of Kinetic Theory of Granular Flow [66].

The applicability of models depends on flow regime, particle loading (volume fraction) and phase coupling. According to the table (2-1), the best multiphase model applicable is Eulerian and Dense Discrete phase model. There are a number of publications that deal with Eulerian-Eulerian simulations for the drilling fluid process [68, 69]. However, there is no paper that describes a full

model. These publications indicate that the Eulerian-granular approach is valid for cuttings-drilling fluid simulation.

Table 2-1 Applicability of Multiphase models [67].

	Eulerian Model	DPM	Mixture Model	VOF Model	DDPM model
Flow Regime	Bubbly flow, droplet flow, slurry flow, fluidized beds, particle-laden flow	Bubbly flow, droplet flow, particle-laden flow	Bubbly, droplet, and slurry flows	Slug flow, stratified/free-surface flow	Fluidized beds
Particle Loading	Dilute to dense	Dilute (VF<12%)	Dilute to moderately dense	Dilute to dense	Dense
Phase Coupling	Weak to strong Coupling between phases	Weak to strong coupling between phases	Weak coupling between phases	Weak to moderate coupling between phases	Moderate to strong coupling
Stokes Number	All ranges	All ranges of Stokes number	St <<1	All ranges	All ranges

The advantages of the two-fluid models (Eulerian – Eulerian Approach) can be summarized as follows:

- Lower computational cost when compared to the DEM method.
- Including chemical reactions is easy.
- The existence of many commercial solvers such as Fluent and MFIX.

On the other hand, the disadvantages can be summarized as follows:

- It is very complicated.
- Only one size can be used for the solid phase as well as one shape (sphere) while the drilled cuttings have different sizes and shapes.
- Dependency on constitutive relationships required to model additional terms of the solid phase.

- The discrete property of the solid particles is absent in the Eulerian-Eulerian approach due to the continuum modelling of the dispersed phase [70].
- The 3-D model is not reported for use for many applications.

2.5.1.2 Euler – Lagrange Approach, Applicability, Advantage and Disadvantages

The calculation of dispersed flow is frequently established on a coupled hybrid approach: CFD (fluid flow) and DEM (particle phase). The main advantages of this coupling are particle size distribution and detailed modelling [71]. However, The Lagrangian discrete phase model in FLUENT acts as the Euler-Lagrange approach. The liquid state is handled as a continuum by solving the time-averaged Navier-Stokes equations, while the dispersed phase is solved via tracking a high number of particles into the measured flow domain. In the regular formulation of the Discrete Lagrangian model (DPM), the theory is that the volume fraction of the discrete phase is adequately low, so it is not taken into account when constructing the equations of the continuous phase. The volume fraction of the particulate phase is accounted for in the dense discrete phase model (DDPM) to surmount this lack of the Discrete Lagrangian model [67].

In this approach, Newton's law of motion is applied to simulate each particle separately [72]. The forces summation depends on certain factors, such as gravity, lift, drag, contact, friction, buoyancy and so on. Certain forces can be assumed to be included, depending on the system type that will be modelled [73].

This approach consists of F forces calculations and the ordinary differential equations solution. The properties of the particle can be included in the ordinary differential equations and calculated for a specific position, time, temperature, velocity, diameter, mass, or concentration of the particle. This can be done by adding another equations such as material and energy balance [72].

The Euler-Lagrange approach is an effective tool to model particle deposition inside the fractured permeable formation. A coupling between computational fluid dynamics (CFD) and discrete element method (DEM) is enabled to utilize both concurrently. The CFD is employed to solve the continuous phase (fluid) by Navier–Stokes equations and DEM is used to interpret the movement of the particles-phase (dispersed), which applies Newton's laws of motion for each particle [71]. A coupling takes charge of the exchange of information between the phases.

The advantages of the two-fluid model (Euler – Lagrange Approach) can be summarized as follows [73]:

- Drilled cuttings of various sizes and shapes can be injected into the drilling fluid flow.
- Easy to understand and simple terms of modelling.
- Comparatively easy to perform and various commercial sources already exist such as MIFX, Star CCM+, LIGGGHTS/LAMMPS and OpenFOAM.

The disadvantages can be summarized as follows:

- Very expensive regarding computational cost.
- Some empirical alterations are needed.

2.5.1.3 Summary

There are several techniques that can be used for- modelling multi-phase flow systems. Choosing a suitable model is a real serious concern. Multiphase flow modelling is a difficult responsibility, but it is a useful tool that can be used to infer more about these flows.

As discussed earlier, the Eulerian-Eulerian strategy usually requires much less computational resources when compared to the Eulerian-Lagrangian schemes. Thus, it can be employed to model pilot scale [74, 75]. However, the discrete nature of the solid phase is missed in the Eulerian-Eulerian strategy due to the continuous representation of the dispersed phase. This weakness can be surmounted with the discrete element method [76, 77]. In

this approach, the solid particles are tracked separately based on Newton's laws of motion, aside from particle–particle and particle-wall collisions.

It is not only the Eulerian approach that faces limitations, the Lagrangian approach also suffers from several limitations. One of the main shortcomings of the DEM technique is the cost computational demands that reduce its application to the small-scale [78]. The dense discrete phase model (DDPM) has been established to avert this limitation, in which the details of particle-particle and particle-wall collisions are not overtly tracked; as an alternative, a force is employed to represent these collisions [79]. Moreover, the hypothesis of the parcel is utilized to lessen the number of particles included in the computations, resulting in an important acceleration of the speed of simulations. Therefore, the DDPM looks promising, especially considering the advantages of Lagrangian methods, and this applies to large scales.

The DDPM model is suggested in this work to overcome the main shortcomings of the Eulerian–Eulerian and CFD-DEM approaches. DDPM has the powers of easy implementation of realistic particle size distribution and tracking of the discrete character of particles. It also has less computational cost than the Eulerian-Eulerian approach [80], because the coarse grid can be employed to perform grid-size-independent simulations and the application of the idea of the parcel.

2.5.2 Previous Approaches

During the past decade, the commercial computational fluid dynamic CFD codes, such as FLUENT, have been employed to simulate mudflow behaviour through the drill pipe and the wellbore under various conditions. Overall, not one of these studies tackled the effects of nanoparticles on the performance of a drilling mud. Pereira et al. [81] investigated the profiles of velocity and pressure of a non-Newtonian drilling fluid in laminar flow using the computational fluid dynamics (CFD) technique. The effects of viscosity, flow, eccentricity, and shaft rotational motion, on the radial and axial velocity, have been investigated. Good agreement was obtained between the study results and the results reported in the literature. Also, it appears that the pressure drops in the annular increases with the shift rotational motion.

Mme and Skalle [65] utilized CFD computations to determine the effects of the rotational motion of the drill pipe, annular flow behavior, and the cuttings physical properties on the cuttings transport. The discrete phase model is used in the simulation, which is two-way coupling between the cutting and fluid. As a result of using DPM, the volume fraction of the discrete phase should not be in excess of 10%, otherwise, weak accurate predictions will be obtained. In terms of studying the shear thinning behavior of the mud based on the drill pipe rotation, they mentioned that the molecular viscosity of mud decreases reasonably near the rotational drill pipe due shear rate. Furthermore, the cutting size inversely effects the carrying capacity and cleaning performance of the mud. Fluid inlet velocity improves the transport of cuttings, which have a particular shape and size.

The cuttings particles transport process has been investigated based on particle shape influence [82]. Three different particle shapes, namely round-shaped, cubic-shaped, and disc-shaped, beside the spherical particle, have been used. The effects of these samples on the hole cleaning process have been examined using a coupled CFD–DEM approach. Fluid-particle interaction has been taken into account by a two-way coupling scheme, while particle-particle and particle-wall interactions have been considered via the Hertz–Mindlin model. The shape of the cutting particle plays a major role in the hole cleaning process. The results show that particles with higher sphericity are easier to clean and transport at low fluid flow velocities and at higher inclination angles. On the other hand, the concentration of the disc-shaped particles is lower than that of the ideal spherical particles, along with the particle motion and deposit in a horizontal wellbore for the three different. In summary, this work has been carried out using a model that is a combination of CFD and Discrete Element Method (DEM).

The cuttings transport was also investigated by Bilgesu, Ali [83], by utilizing CFD software to study the effects of cuttings and mud properties on the cuttings motion and distribution. According to this study, the mud velocity in the annular plays a vital role in the cuttings removal process. The smaller cutting particle size transports easier through the flow domain, while the larger cutting particle size needs a higher circulation rate than that of smaller cuttings

to achieve similar transport efficiency. Overall, close agreement was obtained between the simulation results and the lab results.

The cuttings transport efficiency in deviated wellbores has been numerically predicted, but this time using a foam-based drilling fluid. Foam drilling fluid is a non-Newtonian pseudo plastic fluid, which is suitable to be used in drilling and stimulation operations. Rooki, Ardejani [84] predicted the effects of foam quality, drilling pipe rotational velocity, fluid velocity, and well inclination on the cutting transport process through both concentric and eccentric annuli. Their results show that foam quality enhances fluid carrying capacity with increasing fluid inlet velocity. For consistent foam quality, pipe rotation enhances the amount of transported cuttings. In contrast with the pipe rotation, deviation angle reduces cuttings transport ratio for a particular rotational speed. This implies that the cuttings transport efficiency in vertical wells is higher than in horizontal wells.

2.6 State-of-The-Art Summary

It's clear from the literature review that the studies of functional drilling fluids are insufficient, and the applications of nanoparticles is still in its infancy, with many inconsistent results. There are a range of limitations for existing drilling fluids studies, which can be summarized as,

- Little attention has been given to the complex interaction between drilling fluid properties and functions, as well as between drilling fluid properties itself.
- Little attention has been given to the unstable nature of drilling fluid movement, and it is essential to design a single recipe of drilling fluid that display appropriate capabilities both at static and in dynamic conditions.
- There is a lack of detailed study on the viscoelastic properties and structural recovery (thixotropy) of drilling fluids.

Employing nanoparticles to improve the function of drilling fluids is a recent development, and a range of experiment have been performed by using nanoparticles to control mud filtrate volume [33, 85, 86], minimize differential

pipe sticking [42], improve drilling and production at high pressure and high temperature (HPHT) conditions [11, 28, 87], enhance shale stability [88-90] and improve rheological properties [58, 91, 92]. Some of the results are very promising, however there are a number of limitations, as commented in this area,

- The understanding of the properties of nanoparticle-based drilling fluids is insufficient. Most of the studies have been focused on one single property, such as rheological property or filtration property [47, 93, 94]. As a drilling fluid provides multi-functions during the drilling operation, such as cooling, lubrication and cutting transport, the addition of nanoparticles would clearly affect these functions. It is essential to understand the variations of related properties in order to have a complete assessment of the nanoparticle effects.
- There are limited nanoparticles used, and in most of the applications, only one type of nanoparticle is used. The addition of one nanoparticle may improve one property, but not on the others [95]. There is strong need to consider hybrid nanoparticles, with different nanoparticles used to address different functions, in order to achieve an overall improvement of drilling fluids.
- It is unclear about the influences of nanoparticles on erosion-corrosion and cutting transport during a practical drilling operation.

Addressing these limitations, this work aims to conduct a systematic study on the influence of nanoparticles, especially hybrid nanoparticles, on the performance of water-based drilling fluids. Two drilling fluids will be studied, with biopolymer and without biopolymer. New nanoparticle based functional drilling fluids will be developed and characterized, and the influence of nanoparticles on the rheology, filtration and fluids loss, corrosion and erosion rate will be assessed, supported by numerical simulation of the cutting transportation process.

3 Research Methodology

This chapter is divided into three main parts: in the first part, the preparation of nano-based drilling fluids and the experimental study will be demonstrated, and the second section deals with corrosion and the erosion-corrosion of drill pipes that caused by drilling fluids, while in the third section numerical method will be discussed.

3.1 Experimental Methodology

This chapter describes the experimental procedures, the methods and instruments used to characterise the nanoparticles, and the performance of the product fluid. The nanoparticles and nanofluids were characterised using TEM, SEM, XRD, TGA and DLS. The drilling fluid, on the other hand, was characterized using a Fann viscometer for viscosity and the gel strength measurements and Anton Paar Rheometer for viscoelasticity and thixotropy, respectively. The NPs-based drilling fluid lubricity and filtration properties were measured by a differential sticking tester. Finally, the swelling of prepared drilling fluids was measured using swelling tester. Each experiment was repeated two times in order to verify the validity of all the tests.

3.1.1 Materials

Sodium bentonite was purchased from the Mistral Industrial Chemicals Company. The physical and chemical characteristics of sodium bentonite are shown in Table 1. Alumina and graphite nanoparticles are provided from NanoTek® and Nanoshel respectively.

Table 3-1 physical and chemical characteristics of sodium bentonite

Typical Chemical Analysis		Typical Mineralogy		Other Typical Properties	
SiO_2	57.1%	Montmorillonite	92%	Bulk Density	800 – 900 Kg/m3
Na_2O_3	3.27%	Calcite	4%	Swelling Volume	29 ml/2g
Al_2O_3	17.79%	Feldspars	2%	Moisture	Maximum 14%
K_2O	0.9%	Quartz	1%	Cation Exchange Capacity	78 meq / 100g
Fe_2O_3	4.64%	Dolomite	1%	Sieve Analysis	Maximum 5% retained on a 150µm sieve
TiO_2	0.77%				
CaO	3.98%				
Mn_2O_3	0.06%				
MgO	3.68%				
LoI	7.85%				

Silica NPs was supplied from US Research Nanomaterials Inc with a uniform particle size distribution (99+%, 20-30 nm, amorphous). Carbon nanotubes and carbon black nanoparticles are supplied from Sigma-Aldrich and Alfa Aesar respectively.

3.1.2 Characterization

The morphology of nanoparticles and nanofluids was identified via a transmission electron microscopy (Hitachi SU8230: high-performance cold field emission (CFE) SEM) and a transmission Electron microscope (The FEI Tecnai TF20 is a 200kV FEG high resolution Transmission Electron Microscope (TEM). The hydrodynamic nanoparticles size distribution in distilled water was checked by using a Malvern Nanosizer based on the dynamic light scatting (DLS) method (DLS, Mavern Zetasizer, Marvern, UK). X-ray diffraction (XRD), generated using a Bruker D8 producing x-rays of 1.5406 Å wavelength from a generator working at 40 keV and 40 mA and Fourier transform infrared (FTIR), along with spectra obtained using a Nicolet iS10 FT-IR Spectrometer within the range of 500-4000 cm^{-1}, were used to check mineralogical compositions and to analyse potential bonding formed between the nanoparticles and xanthan gum respectively. The thermal stabilities of the xanthan gum, NPs/XG were investigated using a thermogravimetric analysis (TGA) with a Netzsch-STA 449 Jupiter (Germany).

3.1.2.1 Morphology Analysis

A) SEM Analysis

By using a focused electronic beam to scan the surface of specimens, and by collecting emitted secondary electrons from the sample, which are excited by primary focused electrons, the scanning electron microscopes (SEM) allows imaging surfaces of the samples, thus investigating the roughness, quality and the “visual” appearance of the samples. Conventionally, SEM relies on electron interactions at the surface, therefore in order to avoid an accumulation of electrostatic charges on the sample surfaces, the specimens

should be conductive. Nonconductive specimens can be coated with an ultrathin gold or carbon layer (nanometres thick), either by low-vacuum sputter coating or by high-vacuum evaporation. In this thesis, the morphologies of all nanoparticles, nanofluids samples and corrosion coupons were observed by SEM (FEI Quanta 650 FEG-ESEM). Drops of liquid samples were applied onto the aluminium stubs and they were vacuum dried overnight at 40 ^{o}C. The samples were then carbon coated prior to SEM analysis.

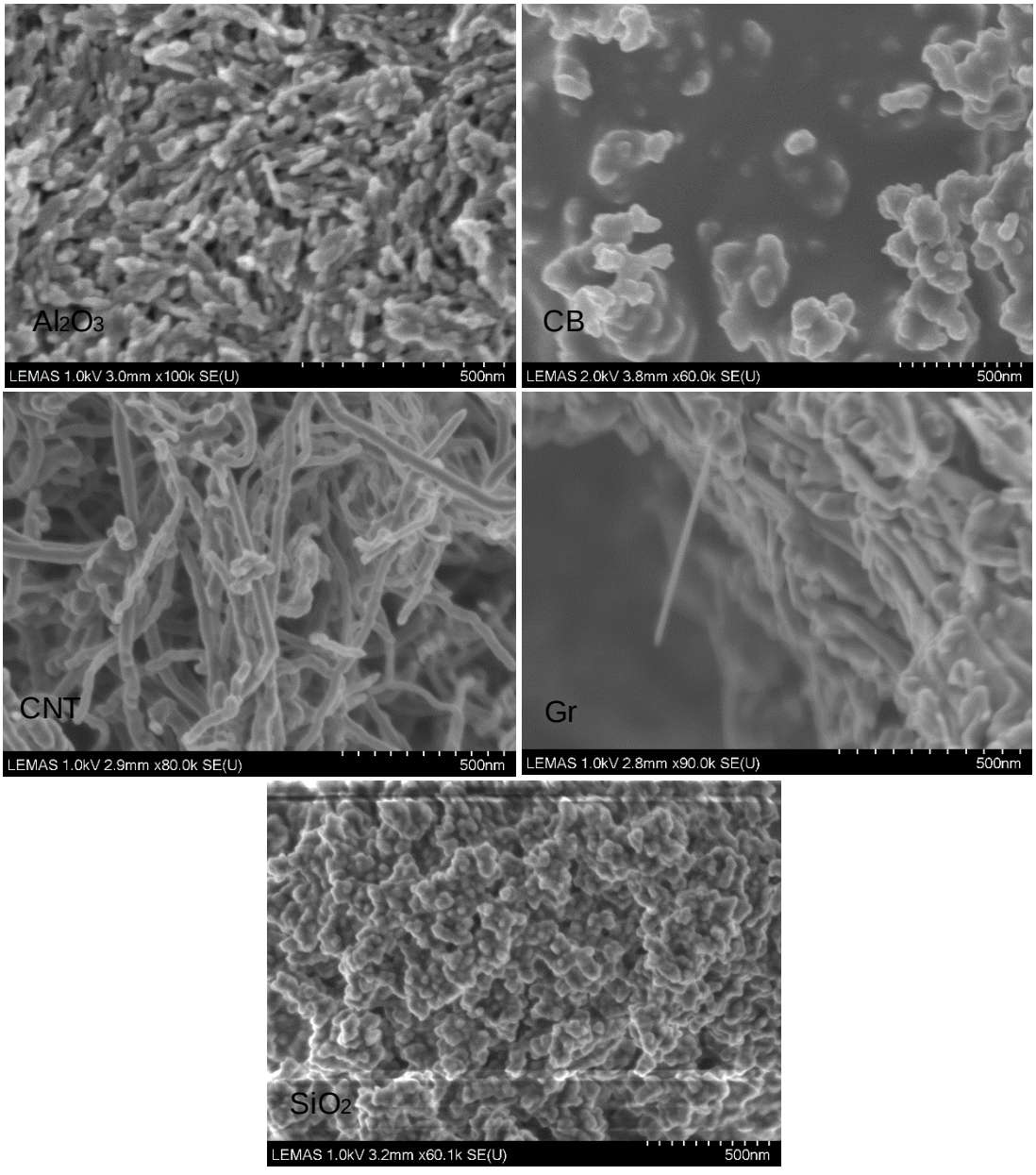

Figure 3-1 SEM images of Al_2O_3, CB, CNT, Gr and SiO_2 nanoparticles

Figures 3-1 shows field emission scanning electron microscope images of the typical morphological features of Al_2O_3, CB, CNT, Gr and SiO_2 nanoparticles.

These images show that the nanoparticles exhibit an aggregate phenomenon. The SEM of Al_2O_3 nanoparticles demonstrates the rod-like morphology. The SEM analysis of graphite and silica nanoparticles exhibits layered sheets and a needle structure morphology for graphite and nearly spherical particles for silica.The SEM analysis reveals tubular nanotubes for CNT and non-uniform size spherical particles for carbon black.

The optimal dispersion and distribution of nanoparticles in the polymer matrix is key to obtaining new materials that have synergy with the constituent compounds' properties. This synergy depends on the degree and nature of the intermolecular interactions between the polymer matrix and the nanoparticles. The morphology of the prepared nanofluid and xanthan gum were studied using ultra high resolution with nanoscale resolution to examine the filler dispersion and the compatibility between polymer and nanoparticles. The SEM morpphoogy analysis of nanoparticles in the polymer matrix is presented in Chapter 5.

B) TEM Analysis

The morphology of the nanoparticles was also characterized by a transmission Electron microscope (TEM) as shown in Figure 3-2. This technology uses an accelerated beam of electrons, which passes through a very thin specimen to enable the observation of features such as structure and morphology. The TEM shows the same particle morphology that is indicated by using SEM. The sample preparation protocol started by dispersion of the nanoparticles in distilled water then the dispersion was ultrasonicated to separate the particles. Drops of the dispersion were taken on the TEM grid and were dried in a vacuum oven overnight at 40 ^oC. Finally, the grid was inserted in the TEM machine. It is obvious, from the images that all the nanotubes are hollow and tubular in shape and graphite exhibits a layered sheets structure morphology. For Al_2O_3 and SiO_2 nanoparticles, it is clear that nanoparticles are aggregated together and exhibit same shape as indicated previously in the SEM analysis.

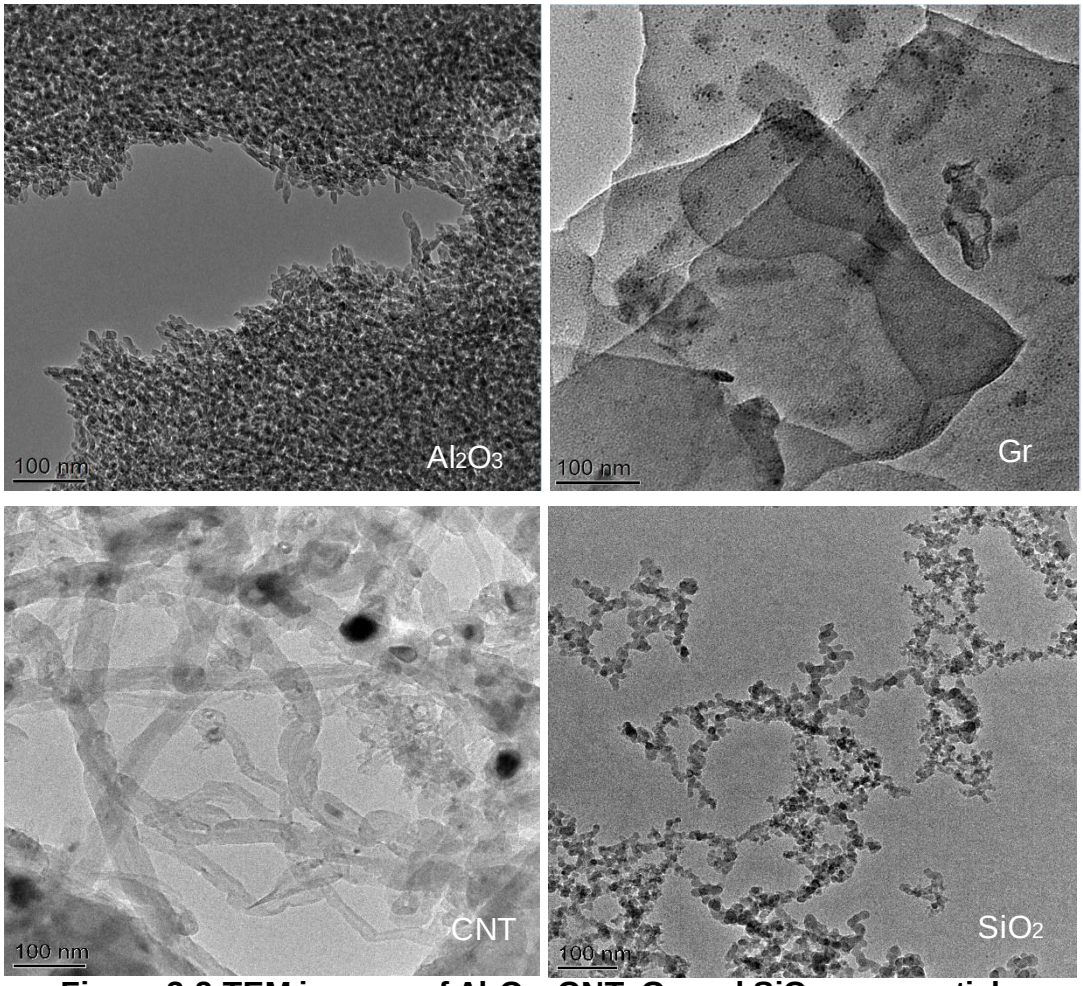

Figure 3-2 TEM images of Al_2O_3, CNT, Gr and SiO_2 nanoparticles

3.1.2.2 Particle Size Distribution

The particle size distribution of Al_2O_3, CB, Gr, CNT, SiO_2 nanoparticles was examined via the dynamic light scattering (DLS) method. Zetasizer nano zs manufactured by Malvern (UK), was used for this purpose. The principle of dynamic light scattering is that fine particles and molecules that are in constant random thermal motion (known as Brownian motion) diffuse at a speed related to their size, where smaller particles diffuse faster than larger particles. To measure the diffusion speed, the speckle pattern produced by illuminating the particles with a laser is observed [96]. The scattering intensity at a specific angle will fluctuate over time, which is detected using a sensitive avalanche photodiode detector (APD). The intensity changes are analysed with a digital auto correlator which generates a correlation function [97]. This curve can be

analysed to determine the size and the size distribution as shown in Figure 3-3.

Figure 3-3 Schematic of light scattering (DLS) method [98]

Figure 3-4 shows the particle size distribution by number for Al_2O_3, CB, Gr, CNT and SiO_2 nanoparticles. The contributions in terms of Number% are shown as a function of particle diameter. For the Al_2O_3 nanofluid, the peak is located at 78.82 nm, at 22.4%. On the other hand, the peak is located at 68.07nm with 17% for the CB nanofluid. The particle size distribution of CNT shows a single peak at 50.75nm (27.8%). Finally, the SiO_2 nanofluid shows two peaks at 50.75nm (37%), 164nm (1%). It is therefore clear that is hydrodynamic particles size disruption of all employed nanoparticles in nano size. However, the DLS results show a larger size of nanofluid, in comparison with manufacturing size, due to agglomeration and clustering, as there is no surfactant used to stabilize the nanoparticles.

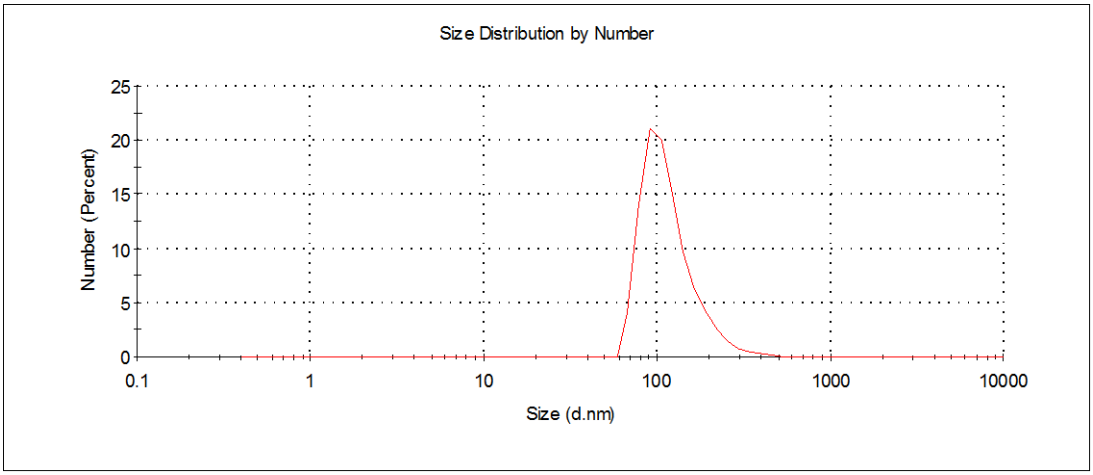

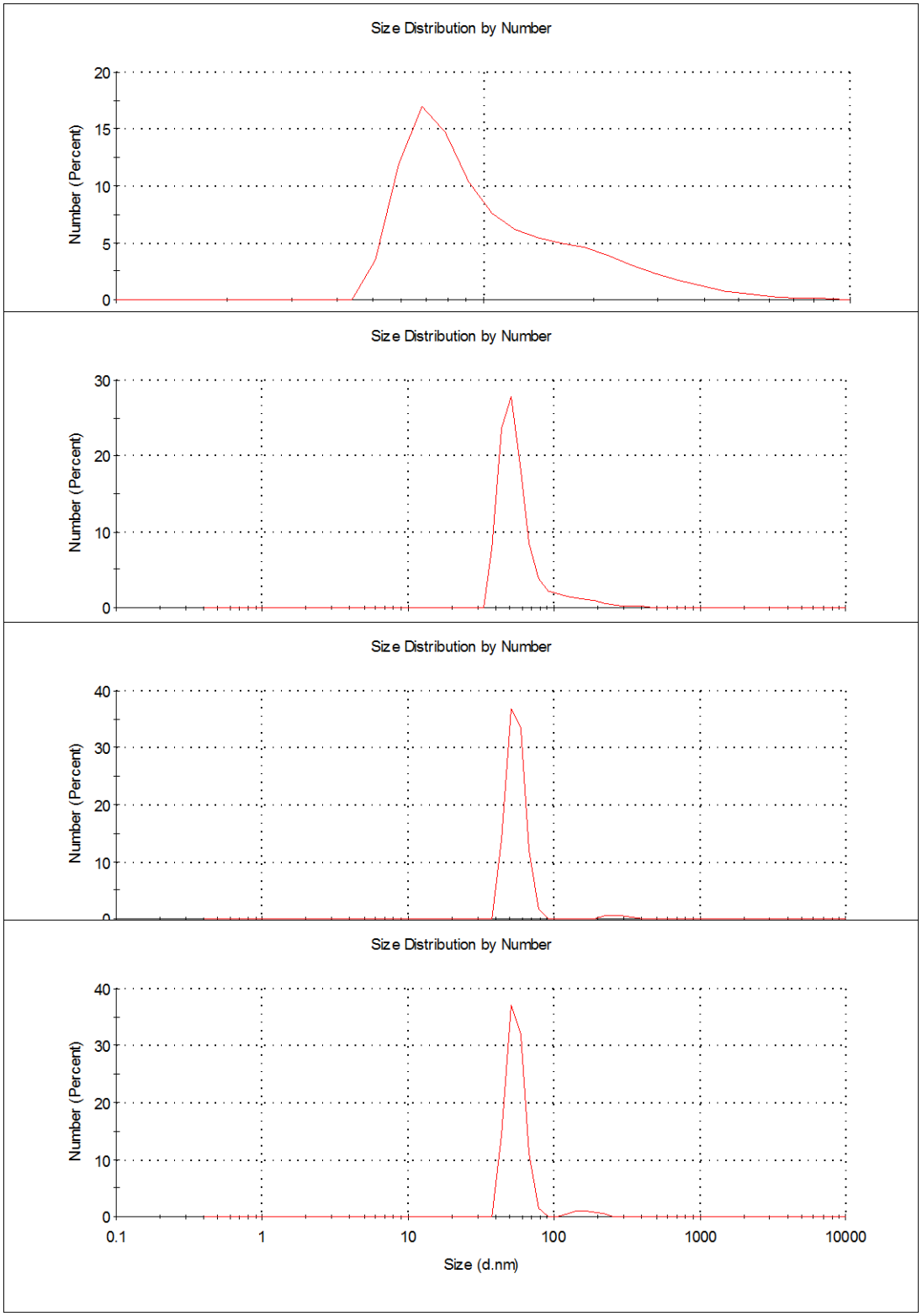

Figure 3-4 Particle size distribution of Al_2O_3, CB, CNT, Gr and SiO_2 nanoparticles.

3.1.2.3 X-Ray Diffraction Analysis

The mineralogical compositions of xanthan gum, NPs, and NPs-Xanthan mixtures were investigated by X-ray diffraction (XRD), generated using a Bruker D8 producing x-rays of 1.5406 Å wavelength from a generator working at 40 keV and 40mA. The xanthan gum, NPs, and NPs-Xanthan were dried in dried in a vacuum oven overnight at 40 ^{o}C, and then applied to the silicon holder, making sure that the surface is smooth and flat. Each sample was analysed for 15 minutes, with the reflection peaks range (2θ) between 10° and 70°C. The data obtained was analysed using high score plus software.

3.1.2.4 FTIR Analysis

In order to identify the underlying factors regarding why adding nanoparticles could increase the fluid performance, FTIR spectroscopy was used to analyse potential bonding formed between different types of nanoparticles and xanthan gum. The structure analysis of xanthan gum, NPs, and NPs -xanthan were investigated using Fourier transform infrared (FTIR), with the spectra obtained using a Nicolet iS10 FT-IR Spectrometer, within the range of 500-4000 cm^{-1}. The background was collected every 7 minutes and the dry powder samples were used making sure they applied uniformly to obtain the better resolution peaks. The equipment was cleaned in between samples in order to avoid the chance of contamination.

3.1.2.5 Thermogravimetric Analysis

The thermal stabilities of the xanthan gum, NPs, and NPs-Xanthan based drilling fluids were investigated using thermogravimetric analysis (TGA) using a Netzsch-STA 449 Jupiter (Germany). A 15mg sample sealed in aluminium pans was scanned from 30°C to 500°C, at a rate of 10°C/min under a nitrogen gas environment.

3.1.3 Methods

3.1.3.1 Preparation of Nano and Hybrid Nano based Drilling Fluids

The drilling fluids were prepared in the laboratory according to a general mud composition. A typical formulation includes 335ml of water and 20g of sodium bentonite particles. They were mixed using an overhead high shear speed

mixer for 20 minutes until there was complete hydration of the bentonite. During the first stage, single types of nanoparticles (Al_2O_3, CB, Gr, CNT, and SiO_2) at different concentrations (0.0, 0.2, 0.4, 0.6, and 0.8 wt %) were dispersed, mixed using a Hamilton beach mixer for 20 minutes into the formed mud. The next step was to test this fluid system in the presence of hybrid nanoparticles. Three hybrid nanoparticles recipes were added to the base drilling fluids, as shown in the experimental flow chart (Figure 3-6). In all cases, the hybrid NPs-based fluids were compared with NPs-based fluids and based drilling fluids samples.

3.1.3.2 Preparation of Nano/Xanthan based Drilling Fluids

The polymer nanofluid was prepared using direct mixing (solution method), which is suitable for a water-based mud (WBM). In this way, the specified amount of xanthan polymer was added to a pre-prepared aqueous nanofluid and mixed for 1 hour by using an overhead high shear speed mixer at 11000 rpm. 17g of sodium bentonite was added to 350 ml of prepared XG/SiO_2 solution while being stirred at 11000 rpm by a commercial Hamilton Beach stirrer for 20min, in order to prepare a stable mud, as evidenced in Figure 3-5. The experimental flow protocol is shown in Figure 3-7.

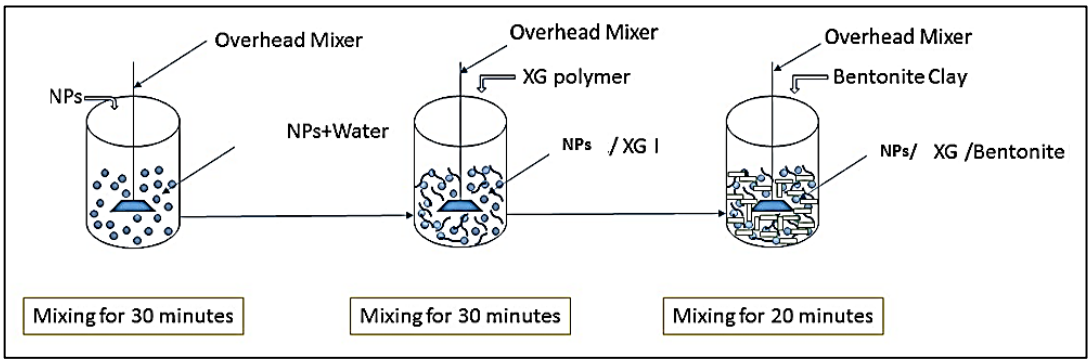

Figure 3-5 Schematic diagram for the preparation process

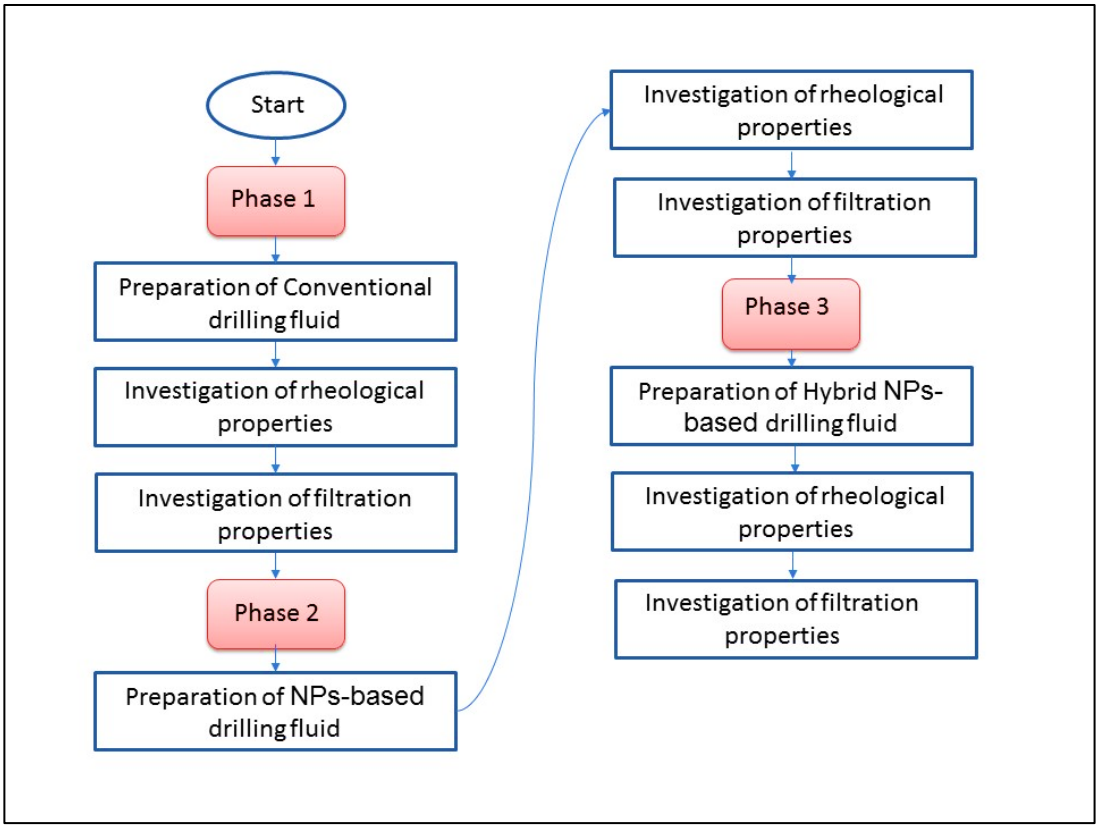

Figure 3-6 Experimental procedure flowchart of Hybrid NPs-based drilling fluid

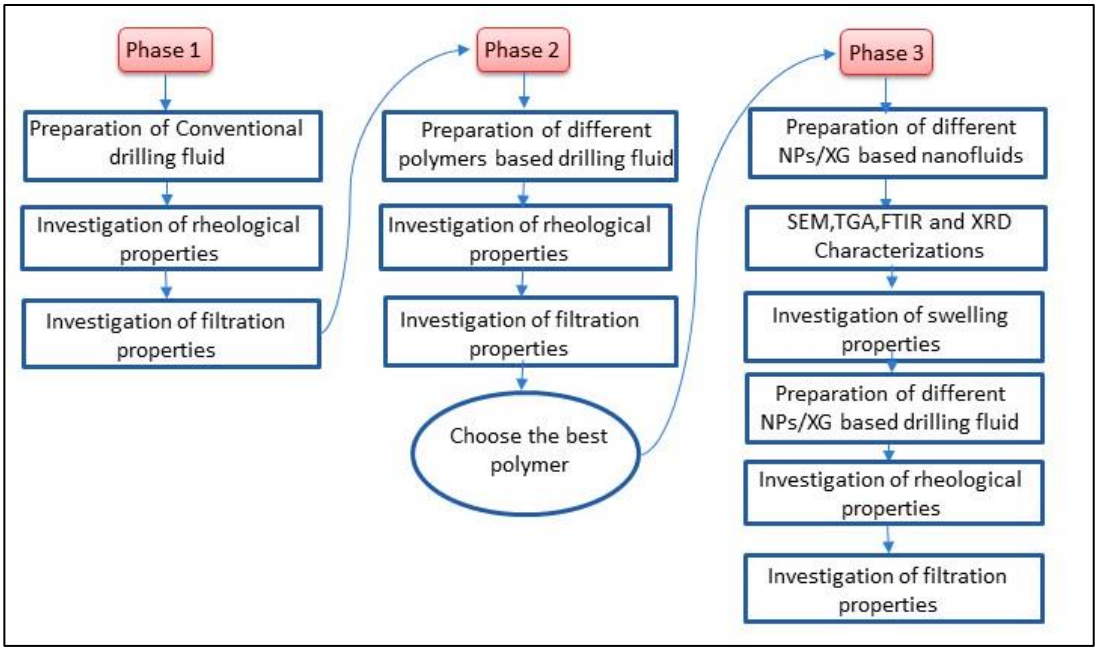

Figure 3-7 Experimental procedure flowchart of NPs/XG-based drilling fluid

3.1.4 Experimental Setup and Procedures

3.1.4.1 Anton Paar MCR301 Rheometer

In general, the Fann 35 Viscometer is used to measure the rheology of the drilling fluid in most oil fields across the world. However, in this research, viscosity measurements are done by the Anton Paar MCR301 Rheometer and the Fann 35 Viscometer. This Rheometer is more precise and more advanced: it can measure viscosity and related attributes. The MCR301 was used to conduct further analysis of fluids, while the Fann 35 failed [31, 99, 100]. The rheological properties were assessed by the Anton Paar MCR301 according to the API standard [101].

a) Flow Test

The viscosity is tested as a function of the shear rate in a rotational rheometer system in order to define the general flow behavior of the drilling fluid. The data displayed either the viscosity or the shear stress, which is plotted against the shear rate as in Figure (3-8). The obtained diagram is called flow curve. In many situations, the flow curve is the first and usually also the most important rheological measurement. It exhibits the flow behavior at low shear rates as well as high shear rates [102].

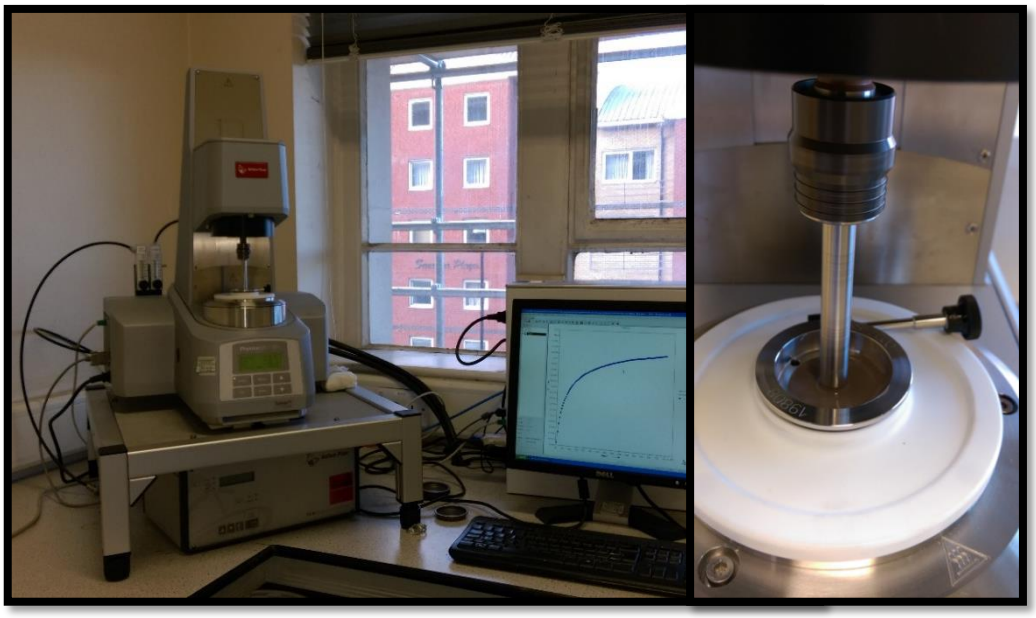

Figure 3-8 Anton Paar MCR301 Rheometer with the viscometer measuring cell (Bob and cylindrical cup).

The measuring system consists of a rotating cylinder called a bob and cylindrical cup, where the fluid rests (Fig. 3.9). In a working situation, the cylindrical bob rotates inside the cylindrical cup which is filled with fluid. This situation can be considered analogous to the rotation of a drill string inside a vertical wellbore filled with fluid.

Figure 3-9 Viscosity measuring cell; Bob and cylindrical cup [103].

When the bob starts to rotate inside the cylindrical cup, which is filled with fluid, shear stress and shear rate curve is plotted automatically by the Rheoplus software (Fig. 3.1). The rotation speed can be adjusted depending on the type of experiment. The shear stress at the bob surface can be calculated from the calculated torque and the geometry (eq.3.1), whereas the shear rate is measured from the angular velocity and the geometry of the system (eq. 3.2).

$$\boldsymbol{\tau} = \frac{\boldsymbol{M}}{\boldsymbol{2\pi {R_b}^2 L}} \qquad 3\text{-}1$$

$$\boldsymbol{\gamma} = \frac{\boldsymbol{2\ \omega\ {R_C}^2}}{\boldsymbol{{R_C}^2 - {R_b}^2}} \qquad 3\text{-}2$$

Where:

Rc = radius of the cylinder cup, Rc = radius of the cylinder bob, L = Length of the bob

ω = angular velocity, M = measured torque, τ = shear stress [104].

All input parameters should be set before running the test. The temperature and the rotation speed ramp of 3, 6, 100, 200, 300 and 600rpm are set to the Rheoplus software. After the test is finished, the graphs and data from their windows can be observed (Figure 3-8), then the equipment is cleaned and the MCR and the temperature circulation system is switched off.

b) ***Viscoelastic Test***

Oscillatory tests are used to determine viscoelastic properties of materials. The basic principle is that the fluid is exposed to periodic oscillations (Fig. 3-10). The bob and cylindrical cup kit can be utilized to illustrate the test. The sample is set between a stationary cylindrical cup and an oscillating bob. The oscillating bob dynamically moves back and forth, causing shares of the sample [105].

The oscillation amplitude sweep test is applied in order to find the linear portion of the viscoelasticity and to observe the structural characteristics of the fluids. This was done with an angular frequency of 1 1/s, with the strain changing from 0.01 % to 1000 %.

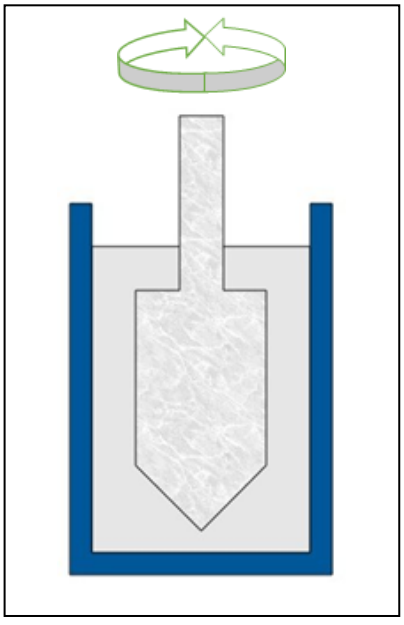

Figure 3-10 Schematic diagram of oscillation test

The sample is evaluated at a constant frequency (usually ω = 1 1/s) with increasing strain or stress from 0.01 to 1000. The temperature is held at a

constant (20°C). The observing values are storage modulus (G'), loss modulus (G'') and phase shift (tan delta). These data yield information about the viscoelastic properties, e.g., whether a material is mainly elastic or mainly viscous and its structural durability. Further, the strain range for the linear viscoelastic range (LVE) can be determined. In this range, the textile properties are independent of the applied strain which means that the sample structure is not tempted by the measurement. Thus, information about the sample structure can be obtained by measurements in this scope. All test types that are practiced gathering information about the construction of a material at rest should be transported out this strain range.

c) Thixotropy Test

The thixotropy of the drilling fluid is related to the important task of holding cuttings and weighting particles suspended in the drilling fluid. A gel-like structure forms when the shear stress is removed from the drilling fluid. This gel structure suspends heavy particles and prevents the cuttings from precipitating and settling in the wellbore wall. The gel structure is created by the rebuilding the structure, because viscoelastic fluids have the ability to store energy as in Figure 3-11. The time it needs for the drilling fluid to establish a gel structure is one of the most significant ways to classify the drilling fluid.

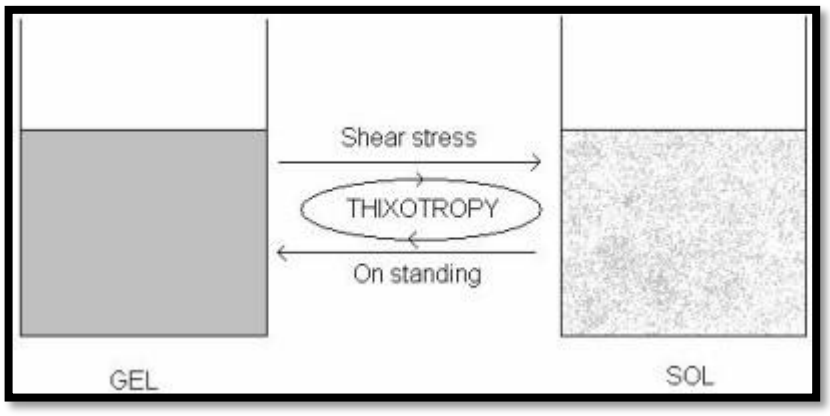

Figure 3-11 Schematic diagram of Thixotropy

The thixotropy (3ITT) test consists of three intervals:

- 1st interval: low shear rate or strain inside LVE at a constant frequency

- 2nd interval: high shear rate

- 3rd interval: as in first interval

The first interval is used as a reference because here the material is measured at rest. In the second interval the structure of the material is destroyed. In the third interval the material is evaluated at rest again and the degree and speed of the structural recovery can be assessed [106]. The combination of oscillation-rotation-oscillation should be utilized because the available information on the measurement data allows for a more precise explanation of phenomena observed in the application (Figure 3-12). For a drilling fluid application, the material is mainly viscous, it can flow, during and directly after the shearing. At rest, the properties need to change from mainly viscous to mainly elastic after a certain time. This time, as well as the degree of recovery can be determined using this type of test.

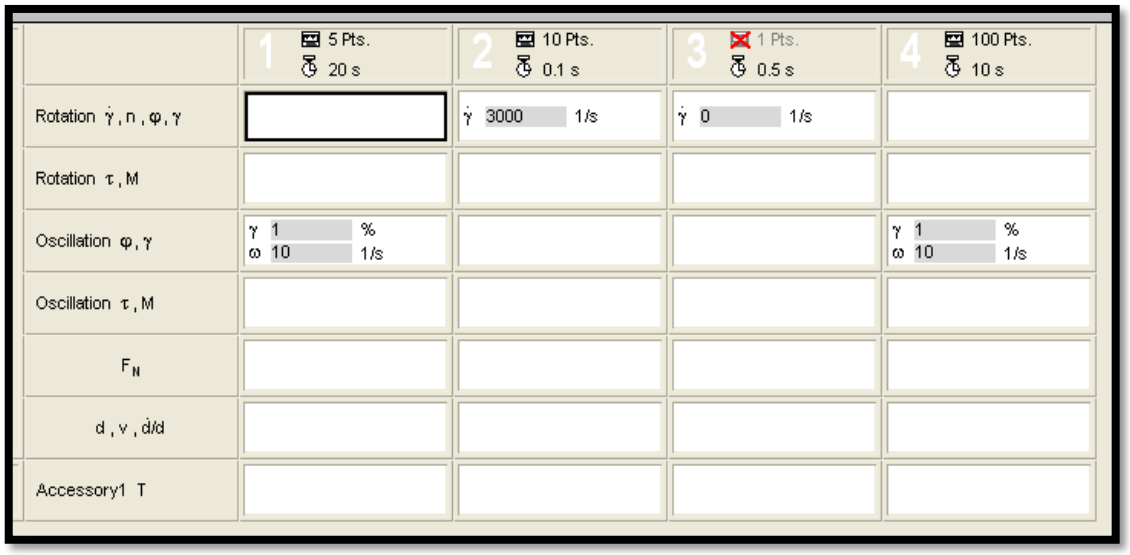

Figure 3-12 Setting of Thixotropy test parameters into Rheoplus software

3.1.4.2 Fann 35 Viscometer

The rheology of the formulated drilling fluids were measured using a Fann Model 35 Viscometer and an Anton Paar rheometer. Rheological properties such as apparent viscosity (AV), plastic viscosity (PV), yield point (YP), 10-s and 10- min gel strengths (GS), were all determined at room temperature. Either the Fann cup, or the Anton Paar cell, was filled with the prepared drilling fluid. The rotor was immersed precisely to the scribe line. Shear stresses and

viscosities were measured at 600, 300, 200, 100, 6 and 3 rotations per minute (RPM). Each RPM was recorded when the viscometer dial reached a steady reading. Flow properties were determined with the help of equations:

$$\boldsymbol{AV = \theta 600/2} \qquad 3\text{-}3$$

$$\boldsymbol{PV = \theta 600 - \emptyset 300} \qquad 3\text{-}4$$

$$\boldsymbol{YP = 0.511(\theta 300 - PV)} \qquad 3\text{-}5$$

10 sec GS was determined after the drilling fluid was stirred for 10 sec and undisturbed for 10 sec. Then, the dial reading was turned to 3rpm; the initial dial reading is the required 10 sec GS. A similar procedure was carried out for the determination of 10 min GS. However, the stirred time was 10 sec and undisturbed for 10 min.

3.1.4.3 Shale Swelling Tester

It is necessary to take a proper drilling fluid to obtain maximum inhibition and wellbore stability regarding the swelling characteristics of shale formations. During drilling a well, a clay mineral rich formation will potentially start to rapidly swell if the drilling fluid is not sufficiently well-suited to the formation. Many challenges can result from clay swelling, such as bit balling, pipe drag, hole sloughing, or other related problems. Accordingly, choosing the appropriate drilling fluid before (or during the drilling wellbore), can be very helpful in attaining a stable wellbore. A ZNP-01 expansion quantity meter was used to examine the communication between water-based fluids and sodium bentonite clay, with a view to determine shale hydration or dehydration by gauging the increase or decrease in length over time of intact shale core on normal temperature and pressure, and further to assess the ability of NPs/XG fluid to inhibition to shale. Shale swelling was recorded in millimeters and the percentage of expansion was based on the original length. The working principle of the apparatus is that pressed shale powder in the fluid cup expands and pushes against the piston. The expansion value is displayed by the percentage gauge.

3.1.4.4 Differential Sticking Tester

In this part of the research, the differential sticking tester will be used to check the improvement of the lubrication behavior of drilling fluids by adding nanoparticles into the water-based mud. The main motivation of this test is to investigate lubrication properties of water-based mud with and without nanoparticles. This kind of test is important when monitoring the friction coefficient between the drilling string and the filter cake, in order to handle the drilling fluids and improve lubricity character in time, which can effectively prevent the accident of differential sticking occurring and provide accurate reliable data for ensuring fast and safe well drilling.

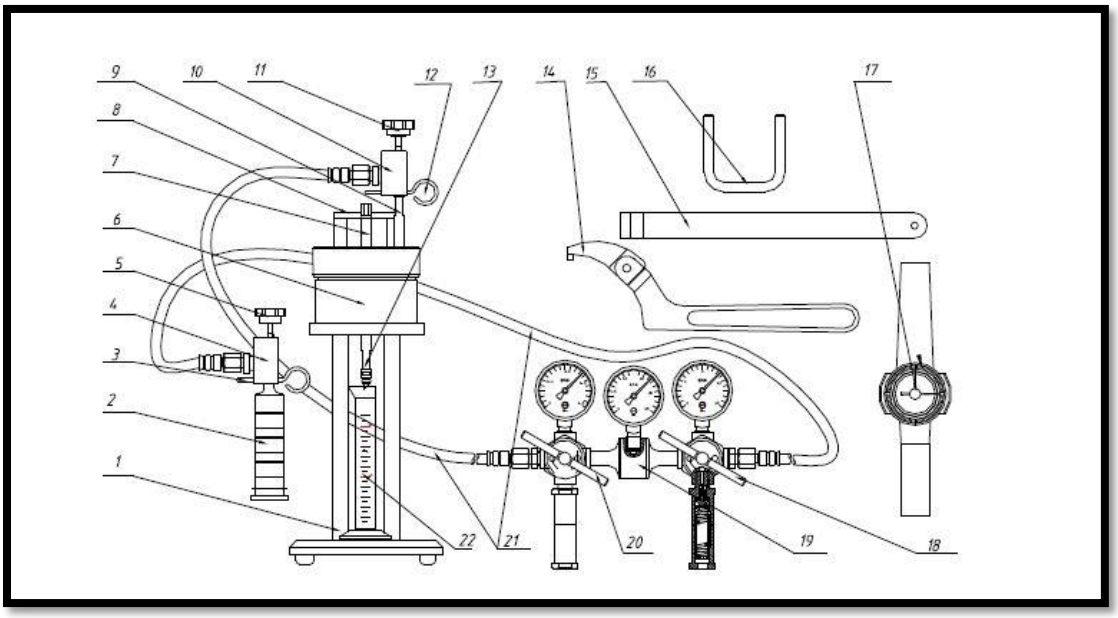

Figure 3-13 Structure Diagram of Differential Sticking Tester

A) Expermental Up

The Differential Sticking Tester is used to measure the Tendency Coefficient of a drilling fluid and investigate how useful treatments might be with any given drilling fluid. This test considers both the stickiness of the filter cake, as well as the quantity of cake building that must occur in order to stick the pipe in the hole. The Tendency or Adhesion coefficient is determined by running a Timed Pressurized Filtration then measuring the adhesion coefficient at a normal

temperature with the torque tester after pressing the adhesion plate to adhere strongly to the filter cake. The experiment setup is shown in Figure 3-13.

B) ***Prodedure***

- **Checking**

Before running the test, the air supply, manifold, hoses and pressure gage should be safe and reliable. In addition, the status of the unit should be clean and dry.

- **Preparation of the cell**

Firstly, the filter paper, rubber ring and nylon ring were placed in order onto the screen on the inner cap. Then the screen and clamping ring were pressed tightly on the nylon ring using a U-wrench as in Figure (3-14A)

Secondly, the cell should stand on the holder. The four holes in the base aim at the four pins of the holder then the drilling fluid sample was poured into the cup to the scale mark as in Figure (3-14B). Also, the adhesive disk should be installed on the drilling fluid cup cover.

Thirdly, the connectivity valve stem should be installed on the drilling fluid cup cover, then the air supply hose and tee components connect to the upper valve stem.

- **Filtration Step**

Firstly, the inlet pressure must be 3.5Mpa (the output pressure of the regulator handle (20) of Figure 3-13 should be 3.5Mpa). Secondly, the upper valve stems should be open (9) and turned counterclockwise 1/4 round to ensure the pressure of the drilling fluid cup is 3.5Mpa, then a 25ml graduate was placed on the lower part of the lower valve stem (13). We then begin to time when the counterclockwise opening lower valve stem is 1/4 round.

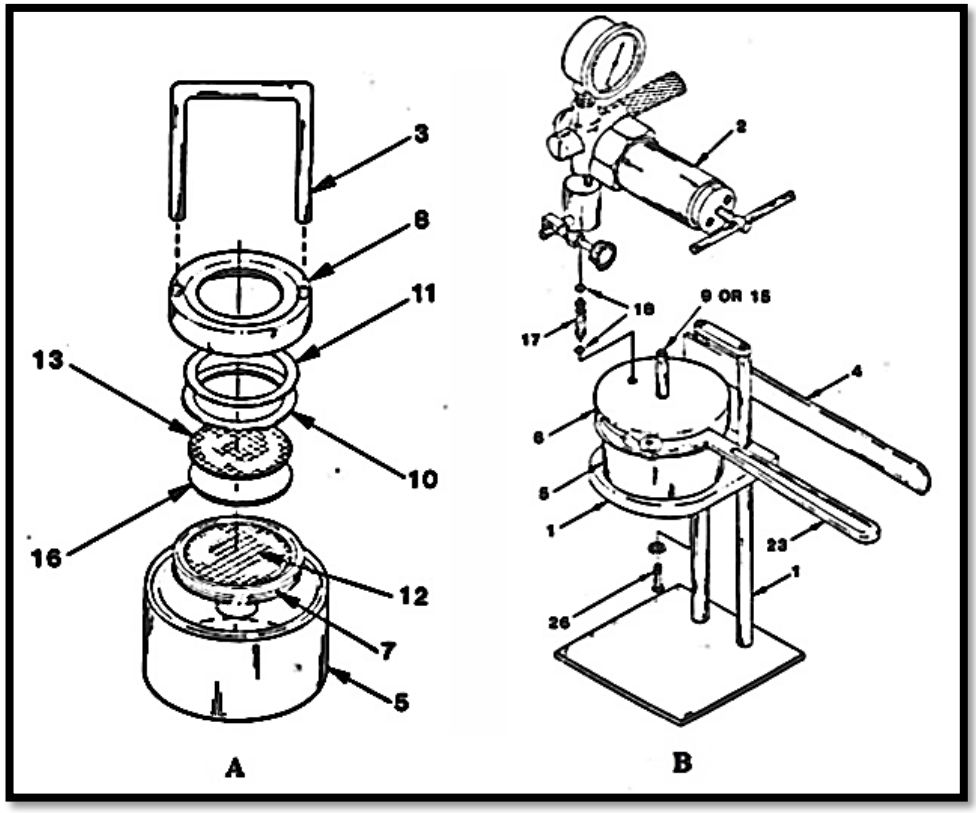

Figure 3-14 A- preparation of the cell B- cell standing situation [107].

- **Adhesion Step**

After filtration, the adhesive disk should firmly stick to the filter cake by pressing the support beam to the pressure rod as in Figure (3-15) then, the air supply should be closed.

The adhesive plate should be stick to filter cake for 5 minutes or more than the torque meter, which should be held on top of the adhesive disk. The torque meter should be slowly forced, with a view to measure the maximum torque value caused when the adhesive disk and filter cake begin to slide. In general, the torque measurements should be repeated 3 to 6 times every 5 minutes until the torque value is up to a maximum. The value should be reported, and the test is thus complete.

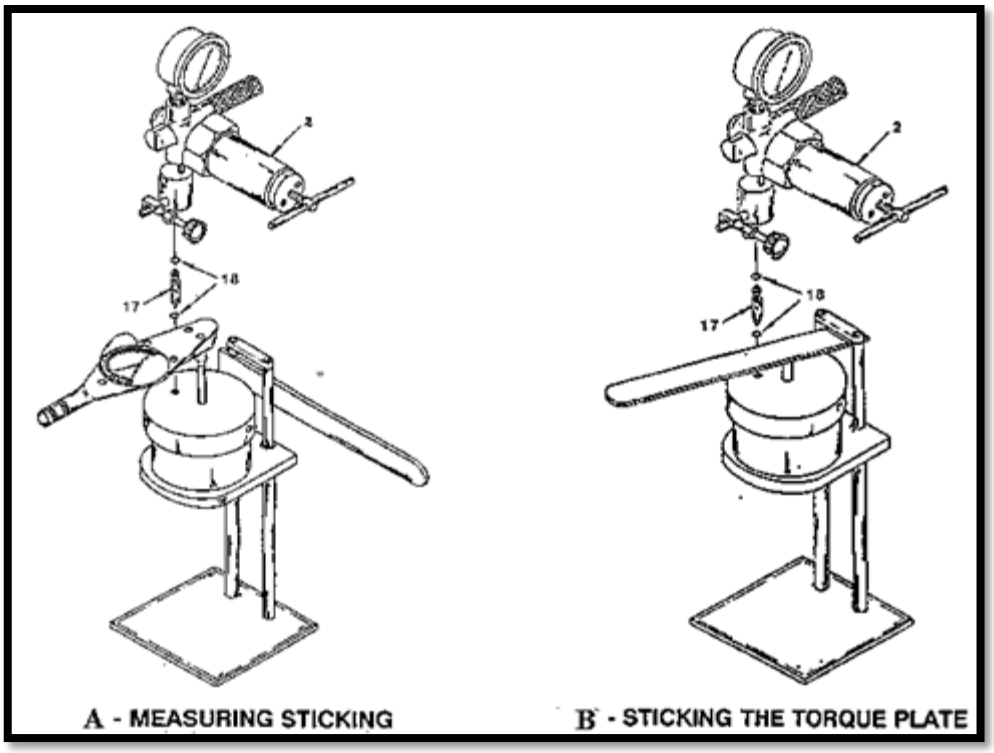

Figure 3-15 A-Adhesion measurement B-Sticking the Torque plate [107].

- **Calculation of Adhesion Coefficient**

The working principle of the instrument is based on Newton's friction law. The smallest slide will be produced when the diameter of the adhesion plate is equal to 50. mm and the pressure differential are equal to 3.5 MPa.

The adhesion coefficient (f) is determined based on the value of torque measured with the torque tester.

$$f = M \times 0.845 \times 10^{-2} \qquad 3\text{-}6$$

Where

f = adhesion coefficient

M = Adhesion value

3.2 Corrosion and Erosion Corrosion

3.2.1 Preparation of Drill Pipe Corrosion Coupons

A cylindrical coupon was used in the present study. AutoCAD software was employed to design the corrosion coupon and insulator. The dimensions of the drill pipe specimen are shown in Figure 3-16. The internal and external diameters of the coupon were 4.8mm and 10 mm, respectively. The height of the coupon and its total surface area exposed to the corrosive environment was 5 mm and 1.5708 cm^2, respectively. Furthermore, the coupon was made of API drill pipe grade X-95 and the coupon holder was made of PTFE to prevent the galvanic corrosion and to fit it on an autoclave rotating shaft. The specimen was polished with 400- and 600-grit silicon carbide papers using water and cleaned with acetone in an ultrasonic bath. Then, the sample was weighted using OHAUS Discovery semi-micro and analytical balance (model: DV114C), which has an accuracy of 0.0001 g, which was used to determine the mass of the coupon before immersion.

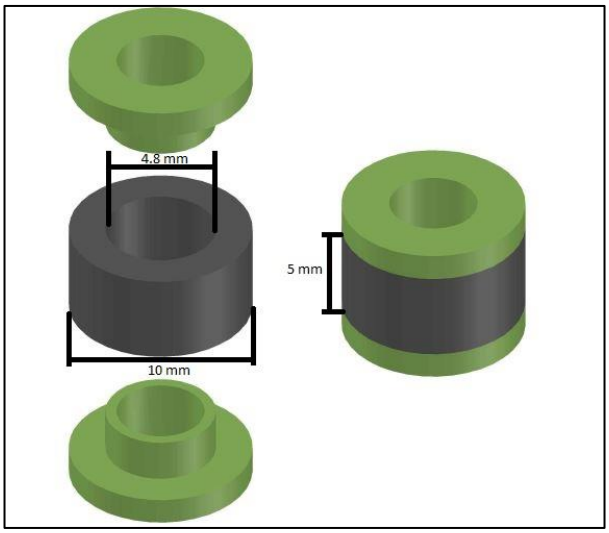

Figure 3-16 Corrosion coupon and PTFE insulator Design

3.2.2 Corrosion and Erosion-corrosion Tests

Our experimental setup bears are practically the same as the one proposed by our previous research [57]. We chose the stirred autoclave apparatus to simulate the drilling process. A 100-ml stirred autoclave was used for erosion-

corrosion tests. The drill-pipe coupon was suspended by rotating the shaft, which was immersed in the base drilling fluids/drill cuttings mixture at room temperature and 300rpm speed for at least 40hr inside the stirred autoclave. Before and after each test, the coupon was cleaned with distilled water, then acetone was applied, and it was dried with hot air, after which it was weighted. The weight loss within the immersion period was determined as the difference between the initial and final weights. Each experiment was at least repeated twice to obtain reproducible data. The surface characteristics were analysed using SEM imaging. Then, the corrosion rate (mm/year) was calculated using the following formula [13]:

$$Erosion\text{-}corrosion\ Rate\ (\boldsymbol{mm/year}) = \frac{\boldsymbol{87.60 \times weight\ loss\ (mg)}}{\boldsymbol{density\ \left(\frac{mg}{cm^3}\right) \times area\ (cm^2) \times time\ (hours)}} \quad 3\text{-}7$$

Figure 3-17 Erosion-corrosion experiment set up

3.2.3 Morphology Observation

The surface morphologies of the drill-pipe coupons were inspected via SEM (Hitachi TM3030 Benchtop SEM). This observation is essential to study the surface roughness of the coupons and to conclude the influence of drill cuttings at different sizes and concentrations as well as the drilling base fluid on the surface damage, such as cracks or wears, to the drill-pipe coupon. In addition, Hitachi SU8230 SEM was used to investigate the morphological studies of the nanofluid.

3.3 Computational Simulation Methodology

Fundamentally, drilling fluid is injected at a certain pressure and flow rate, as shown in Figure 3-18, from the inlet of a drill-pipe. Subsequently, the fluid leaves the drilling pipe at the bottom of the wellbore and then flows to the surface in the inverse direction, due to high pressure at the bottom. The flow in the drilling pipe is fully developed with uniform velocity under a static drilling pipe and a radial velocity near the inner the pipe wall during the rotation. The flow in annular experiences different phenomena due to high pressure and wall shear stress. Large eddies are formed at the bottom of the borehole and negative velocity can be obtained. Before starting with the simulation procedure, some assumptions have been made, which are as follows:

1. The wellbore wall is non-porous (low porosity media is considered).
2. There are no nozzles at the end of the drill-pipe.

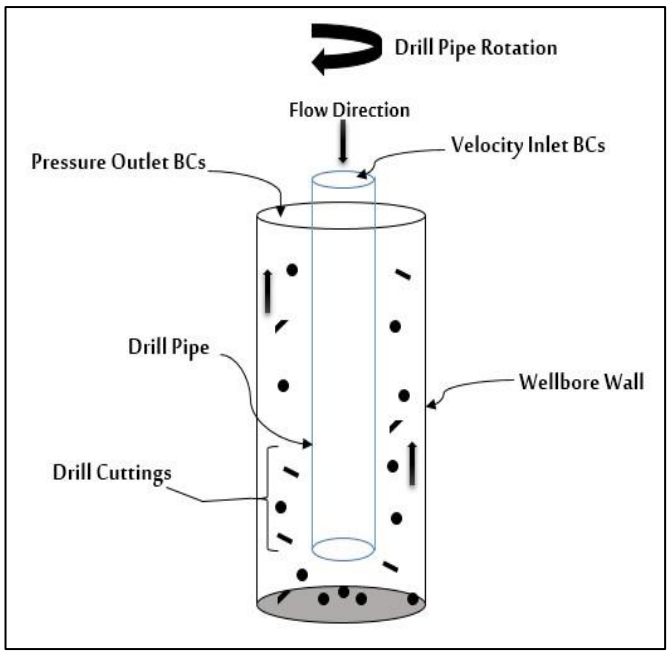

Figure 3-18 Drilling fluid flow through the drilling system

3.3.1 Base-case Flow Geometry with Dimensions

The 3D geometry consists of two overlapping cylinders: an internal cylinder (drilling pipe), and an external cylinder (wellbore), as illustrated in Figure 3-19. The geometry has been created using Design Modeler/ANSYS pre-processor, and the dimensions are in Table 3.2.

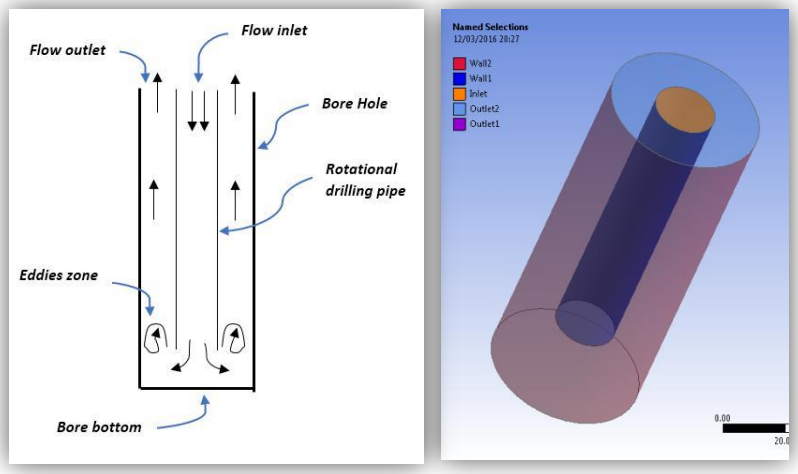

Figure 3-19 Schematic drawing the flow path, B. Base-case flow geometry from the DM

Table 3-2 Geometry dimensions

Drilling pipe	**Diameter, cm**	**20**
	Length, cm	100
Well-bore	Diameter, cm	50
	Length, cm	120

3.3.2 Mesh Size and Characteristics

The grids of the base case flow geometry have been generated using ICEM CFD v.15 pre-processor. Three different sizes of mesh have been used to eliminate dependency on the mesh size (see Table 3-3). Figure 3-20 demonstrates a good agreement between the grids in terms of velocity magnitude, turbulent kinetic energy (*k*), wall shear stress, and turbulence intensity. The refined medium grid has been selected for further simulation to

create a balance between the computational time and the predictions accuracy. The 3-mesh size and characteristics are presented in Table 3-3.

Table 3-3 Meshes size and characteristics

Mesh	Cells	Faces	Nodes	Cell zone	Face zones	Max Aspect Ratio	Min. Orthogonal Quality
Coarse	77520	237460	82477	1	7	34.8	0.7
Medium	127182	388003	133712	1	7	23	0.715
Fine	172250	525239	180820	1	7	20.8	0.716

The final mesh is an unstructured mesh of hexahedral cells and quadrilateral faces, as illustrated in the Figure 3-21. Versteeg and Malalasekera [108] reported that the optimal mesh should be non-uniform and fine in zones of high flow variation, and coarse in zones with low flow change. A hexahedral mesh offers an excellent accuracy for RANS calculations at high Reynolds number and high viscous flow regions [109]. Good agreement between the grid results can be noticed from the Figure 3-20. This indicates that mesh size has no significant impact on flow predictions.

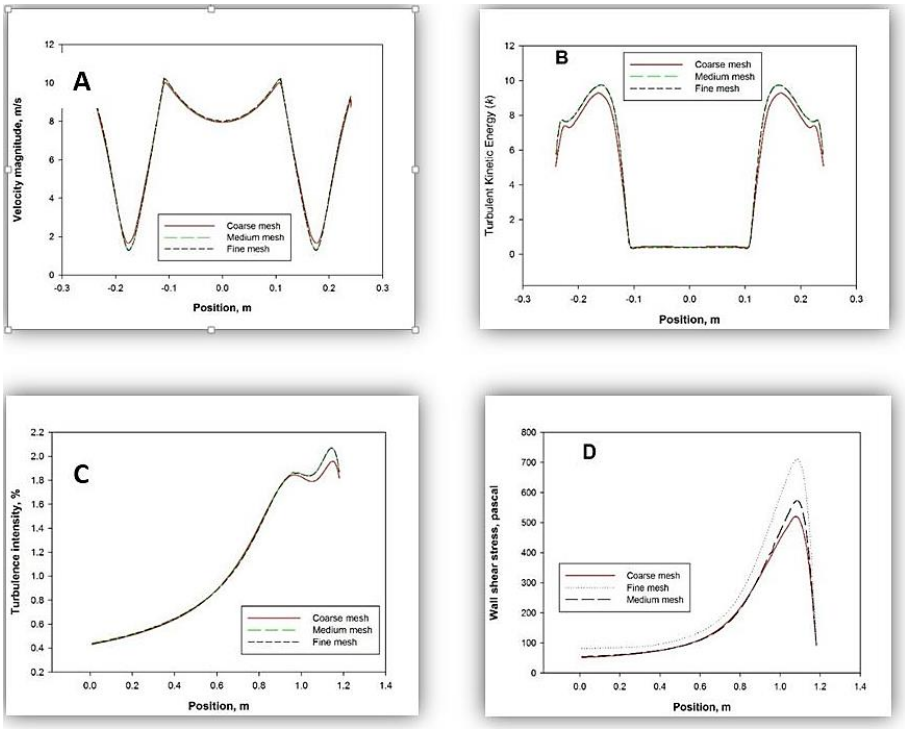

Figure 3-20 Velocity magnitude (m/s), B. Turbulent kinetic energy (k), C. Turbulent dissipation rate (Epsilon), and D. Wall shear stress.

3.3.3 Governing Equations Solved

3.3.3.1 Multiphase Flow Model: Eulerian-Lagrangian Approach

The Eulerian multiphase flow model is linked to a dense discrete phase model (Lagrangian Frame) with a view to simulate cuttings and nanoparticles transport with a drilling fluid as the continuous phase. The volume fraction equation and conservation of momentum, mass, and energy equations included in the Eulerian-Lagrangian model are described in further detail in the forthcoming sections.

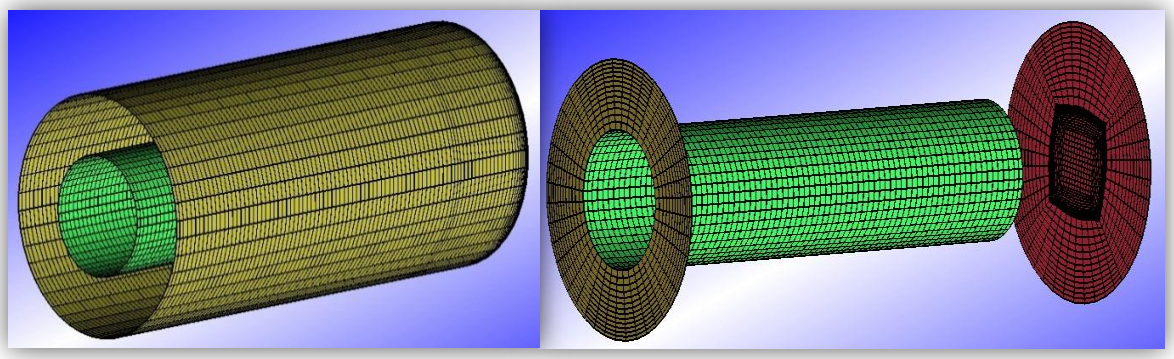

Figure 3-21 the computational grid of the model.

3.3.3.2 Volume fraction equation

The equations of volume fraction for each phase are individually solved using implicit time discretization.

$$V_q = \int_V \alpha_q \, dV \qquad 3\text{-}8$$

Where,

$$\sum_{q=1}^{n} \alpha_q = 1 \qquad 3\text{-}9$$

3.3.3.3 Mass Conservation Equation

The general form of mass conservation (continuity equation) for multiphase incompressible flows can be written as follows:

$$\frac{\partial}{\partial t}(\alpha_q \rho_q) + \nabla.(\alpha_q \rho_q \overrightarrow{v_q}) = \sum_{p=1}^{n}(\dot{m_{pq}} - \dot{m_{qp}}) + S_q \qquad 3\text{-}10$$

3.3.3.4 Momentum Conservation Equation

The equation of momentum conservation (Newton's Second Law) can be written as follows:

$$\frac{\partial}{\partial t}\left(\alpha_q \rho_q \vec{v}_q\right) + \nabla.\left(\alpha_q \rho_q \vec{v}_q \vec{v}_q\right) = -\alpha_q \nabla p + \nabla.\overline{\overline{\tau_q}} + \alpha_q \rho \vec{g} \qquad 3\text{-}11$$

$$+ \sum_{p=1}^{n} (\overrightarrow{R_{pq}} + \overrightarrow{v_{qp}}\dot{m}_{pq} - \overrightarrow{v_{qp}}\dot{m}_{qp})$$

$$+ \left(\overrightarrow{F_q} + \overrightarrow{F_{lift,q}} + \overrightarrow{F_{wl,q}} + \overrightarrow{F_{vm,q}} + \overrightarrow{F_{td,q}}\right)$$

3.3.3.5 Energy Conservation Equation

To describe energy conservation in Eulerian multiphase flow model, the independent steady state enthalpy can be written for each phase *q&p.*

$$\frac{\partial}{\partial t}\left(\alpha_q \rho_q h_q\right) + \nabla.\left(\alpha_q \rho_q \overrightarrow{u_q} h_q\right) = \alpha_q \frac{\partial p_q}{\partial t} + \overline{\overline{\tau_q}}:\nabla\overrightarrow{u_q} - \overrightarrow{q_q} \qquad 3\text{-}12$$

$$+S_q + \sum_{p=1}^{n}\left(Q_{pq} + m_{pq}h_{pq} - m_{qp}h_{qp}\right)$$

3.3.3.6 Turbulence Model: Standard *k-ε* Model

A standard k-ε turbulence model has been employed as a viscous model in this simulation study. This model is robust, well-established, and generates reasonable predictions for a board range of turbulent flows [110]. A standard k-ε model is an example of two transport equations, which involve calculating the turbulent kinetic energy (*k*) and turbulent dissipation rate (*ε*), as described below:

$$\frac{\partial}{\partial_t}(\rho k) + \frac{\partial}{\partial_{xi}}(\rho k v_i) = \frac{\partial}{\partial x_j}\left[\left(\mu + \frac{\mu_t}{\sigma_k}\right)\frac{\partial k}{\partial xj}\right] + G_k + G_b - \rho\varepsilon - Y_M + S_k \qquad 3\text{-}13$$

$$\frac{\partial}{\partial t}(\rho\varepsilon) + \frac{\partial}{\partial x_i}(\rho\varepsilon v_i) = \frac{\partial}{\partial x_j}\left[\left(\mu + \frac{\mu_t}{\sigma_\varepsilon}\right)\frac{\partial \varepsilon}{\partial x_j}\right] + C_{1\varepsilon}\frac{\varepsilon}{k}(G_k + C_{3\varepsilon}G_b) - C_{2\varepsilon}\rho\frac{\varepsilon^2}{k} + S_\varepsilon$$

3-14

$$\boldsymbol{\sigma_\varepsilon = 1.30, \sigma_k = 1.00, C1 = 1.44, C2 = 1.92, C\mu = 0.09}$$

3.3.3.7 Equation of Motion for Particles

In the Lagrangian approach, FLUENT predicts the trajectory of particles by integrating the force balance on the particles. The force balance equates the particle inertia with forces that apply to particles such as drag force, gravity force, etc. [110]. Particle force balance can be written as follows:

$$\frac{d\vec{u}_p}{dt} = \boldsymbol{F_D}\left(\vec{u} - \overrightarrow{u_p}\right) + \frac{(\rho_p - \rho)\vec{g}}{\rho_p} + \vec{F} \qquad 3\text{-}15$$

Where, $\vec{F}$ refers to forces term that may include different possible forces such as gravity force, Saffman's lift force, pressure gradient force, etc., depending on the configurations. The drag force per unit particle mass F_D is described as

$$\boldsymbol{F_D = \frac{18\mu}{\rho_P d_P^2} \frac{C_D Re}{24}} \qquad 3\text{-}16$$

The pressure gradient in the fluid:

$$\boldsymbol{\vec{F} = \frac{\rho}{\rho_P} u_P \nabla u} \qquad 3\text{-}17$$

And particle lift due to shear which is also knowing as Saffman's lift force [111]:

$$\boldsymbol{\vec{F} = \frac{2Kv^{\frac{1}{2}}\rho d_{ij}}{\rho_p d_p (d_{kl} d_{lk})} (\overline{u} - \overline{u_p})} \qquad 3\text{-}18$$

3.3.4 Numerical Methods Used

Three-dimensional, transient numerical simulations of non-Newtonian, turbulent flow of drilling fluid through a rotational, concentric annulus drilling pipe, have been carried out using an ANSYS-FLUENT 15.0 CFD commercial code. The flow is turbulent, and a standard *k-ε* turbulence model has been used for turbulence modelling. The Eulerian-Lagrangian approach has been employed for the multiphase modelling of drilling mud and suspended solids. For all simulation cases, a *double-precision* solver has been employed in order to cope with geometry complexity and produce more accurate results. The time step size for continuous phase solver to provide satisfactory convergence is selected at 0.001 sec. The time required for the solution to converge, varies from simulation to simulation, ranging from 15 to 37 hours. The vast majority of simulations have been run on High-Performance Computing (HPC)/ARC2 at the University of Leeds.

The SIMPLE algorithm has been employed for Pressure-Velocity coupling in an unsteady flow of drilling fluid. The convection terms of the Reynolds-averaged Naiver-Stokes (RANS) equations are discretized using the *second order upwind discretization scheme*. In all simulation cases, *gravity force* has been applied to the positive X-direction where the bottom of the wellbore.

3.3.5 Coupling Regime between Discrete and Continuous Phases

The cutting particles and nanoparticles motion and distribution have been modelled using the Eulerian-Lagrangian Approach. The momentum equation of the Eulerian model predicts the flow characteristics of the continuous phase, and the Lagrangian model calculates the cell volume fraction of the discrete phase. The Eulerian multiphase parameter that was used to simulate the particles flow is the Dense Discrete Phase Model (DDPM). DDPM was upgraded from the Discrete Phase Model (DPM), with a view to overcome the volume fraction drawback in the DPM [110]. The fluid-particle interaction can be expressed through the coupling scheme under consideration. In the current study, two regimes of coupling will be employed, which are detailed below.

3.3.5.1 Two-Way Coupling Scheme

The effects of the continuous phase on the particles motion (and vice-versa) have been considered for the first part of the particles flow simulation. In DDPM, moving particles can be mimicked as moving mass points; the abstractions are utilised for the shape and volume. The information about flow characteristics around the particles (such as vortex shedding and flow separation) are ignored. In this approach, the continuum phase field is solved to satisfy convergence; the discrete phase is then processed, and the particles trajectories and other properties are computed. Thus, the solution of continuous phase equations will not be affected by the particle addition.

According to the particle force balance equation (3.8), two force terms are commonly used. First, there is drag force per unit particle mass, and then there is additional forces term. The additional forces term can incorporate different forces, which could be important under specific conditions. Under our study's circumstances, two particular additional forces, besides the force of gravity, can be influential, namely Two-Way Turbulence Coupling and Saffman's lift force. The Two-Way Turbulence Coupling model enables the effects of variation in turbulent quantities due to flow vortexes and particles damping. Saffman's Lift Force represents the lift due to a shear. The trajectory of a particle is predicted using unsteady particle tracking. Stochastic tracking has been used to compute the trajectories of particles utilising the mean continuous phase velocity [110].

3.3.5.2 Four-Way Coupling Scheme

The term of “four-way”, refers to four different interactions, which include the fluid-particle, particle-fluid, particle-particle, and solid surface-particle interactions. This implies that the particle flow behaviour manipulates the motion of adjacent particles, as well as the overall particles’ motion, which can be affected by contact dynamics with solid surfaces. Fluid-particle interaction (and vice-versa) is considered via a DDPM calculation frame, while the interactions of particle-particle, particle-well wall, and the particle-drilling pipe are considered via a Discrete Element Method (DEM) model. In FLUENT, the DEM option is a part of DDPM’s capability, as with the other additional forces. Cundall and Strack [112] reported that the DEM application takes into consideration the forces that are produced from the collision of particles. These forces are called the *soft sphere* approach and are included in the particle motion equation through an additional forces term.

The laws that manage the particle-particle and particle-solid surface collision, include spring, spring-dashpot, and friction [110]. In summary, particle position, velocity, and mass can all change after a collision due to particles overlapping. The trajectory of a particle is predicted using unsteady particle tracking with a time step size of 0.001, using stochastic tracking for turbulent particle dispersion. Predictions regarding cutting particles’ motion after a collision offers more a realistic overview of the cuttings transport process. Once the physical collision takes place, particle-particle and particle-wall momentum and heat exchange occur. In this work, a four-way coupling regime has been employed for mimicking the cuttings transport process. Constants for contact force laws are provided to control the particles motion after the collision, as listed in Table 3.4.

Table 3-4 Constants of Contact Force Laws

Collision Pairs	Contact Force Laws Constants	Value
Basalt rock - Cutting particle	Spring-dashpot: k	1000
	Spring-dashpot: eta	0.9
	Friction-dshf: μ_{stick}	0.5
	Friction-dshf: μ_{glide}	0.2
	Friction-dshf: μ_{limit}	0.1
Carbon Steel - Cutting Particle	Spring-dashpot: k	1000
	Spring-dashpot: eta	0.9
	Friction-dshf: μ_{stick}	0.5
	Friction-dshf: μ_{glide}	0.2
	Friction-dshf: μ_{limit}	0.1
Particle-Particle	Spring-dashpot: k	900
	Spring-dashpot: eta	0.7
	Friction-dshf: μ_{stick}	0.5
	Friction-dshf: μ_{glide}	0.2
	Friction-dshf: μ_{limit}	0.1

3.3.6 General Configurations for Drilling Fluid Flow Simulation

The base mud physical properties and the boundary conditions are listed in tables 3-5 and 3-7, respectively. The fluid flow is non-Newtonian, the viscosity changes according to shear rate and the dependent temperature method of the non-Newtonian power law model. The constants for the PL model and Herschel-Bulkley models, as well as the fluid physical properties, have been determined by the experimental investigations, as shown in Table 3-5. Thermal conductivity and specific heat for water were considered for drilling fluid. The absolute criteria of convergence for equations residuals were 10^{-4} for the continuity equation, 10^{-6} for the energy equation, and 10^{-5} for the rest of the equations. The under-relaxation factor of the momentum equation was 0.4 and the other equations were FLUENT defaults.

Table 3-5 Base mud physical properties

Properties	Values
Density, kg/m^3	1055
Activation energy/R, K	1374.1
Thermal conductivity, W/m.K	0.6
Cp (specific heat), J/kg.K	4128
Yield Stress Threshold, pascal	5.75
Critical shear rate, 1/s	3.87

3.3.7 Configurations of Cuttings Transport through a Wellbore

The effects of fluid flow, drilling stem rotational speed, and the cuttings characteristics on the cuttings transport and distribution in a wellbore have been investigated. The cuttings particulates have been injected from the bottom of the wellbore with a size distribution, using the ROSIN-RAMMLER method. The simulations involve two schemes of coupling of continuous-dispersed phases: two-way coupling, and four-way coupling. The parameters for particles (cuttings) modelling and size distribution that were used in the simulation have been listed in Table 3.7. The cuttings material has been assumed to be Sandstone rock. The tangent and normal coefficients of restitution, in table 3.7, have been adopted from [113].

Table 3-6 Boundary conditions

Zone	Parameters	Value
Inlet	Type	Velocity inlet
	Velocity magnitude, m/s	10
	Hydraulic diameter, m	0.25
	Temperature, K	298
	Turbulent intensity, %	5
	DPM	Escape
Outlet	Type	Pressure Outlet
	Outlet backflow turbulent intensity, %	5
	Backflow hydraulic diameter	0.25
	DPM	Escape
Wellbore Wall	Type	Wall
	Wall motion	Stationary
	Wall roughness constant	0.5
	Roughness height, m	0.0003
	Material of construction	Basalt Rock
	Thermal condition	UDF
	Thickness of wall, m	0.05
	DPM	Reflect
Wellbore Bottom	Type	Wall
	Wall motion	Stationary
	Wall roughness constant	0.5
	Roughness height, m	0.0003
	Material of construction	Basalt Rock
	Temperature, K	370
	Thickness of wall, m	0.05
	DPM	Reflect
Drilling Pipe	Type	Wall
	Wall motion	Rotational motion
	Wall roughness constant	0.5
	Roughness height, m	0
	Material of construction	Carbon steel
	Thermal condition	Coupled
	Thickness of wall, m	0.01

These coefficients were used for the polynomial profile, as a function of an impingement angle, for discrete phase reflection on the aluminium wall.

However, an experimental test for determining the native coefficients of the wall material used in this simulation (Basalt rock), is not an easy task to achieve, as discussed in the study of van Buijtenen et al. [114].

Table 3-7 Particle (cutting) parameters

Parameter		Values
Max. diameter, *m*		0.001
Min. diameter, *m*		10^{-6}
Mean diameter, *m*		0.0004
Spread parameter		3
Particle density, *kg/m³*		2300
Mass flow rate, *kg/s*		0.4
Particle volume, *m³*		5.24×e-10 – 5.23e-19
Particle weight, *gm*		1.95 – 0.0019
Temperature, *K*		300
X-velocity, *m/s*		0
Y-velocity, *m/s*		0.008
Normal restitution coefficients	C_1	0.993
	C_2	-0.0307
	C_3	4.75e-04
	C_4	-2.61e-06
Tangent restitution coefficients	C_1	0.998
	C_2	-0.029
	C_3	6.43e-04
	C_4	-3.56e-06

4 Performance Evaluation of Hybrid Nanoparticles Drilling Fluids

The outline of this Chapter is as follow. Firstly, an experimental analysis was performed on the base drilling fluid (which mostly contained water and sodium bentonite), to examine the shortcomings of the base drilling fluid's properties. The next step was to test this fluid system in the presence of nanoparticles and hybrid nanoparticles. The hybrid NPs-based fluids were compared with NPs-based fluids and based fluid samples. The characteristics of the prepared fluids were evaluated by measuring viscosity, gel strength, viscoelasticity, thixotropy, filtrate loss and lubricity as described in Chapter 3. The results of the particular performance of CB-SiO_2, Al_2O_3-CNT, and SiO_2-Al_2O_3 based drilling fluids are also presented in this chapter.

4.1 Rheological and Filtration properties of Single Type Nanoparticles based Drilling Fluids

Figure 4-1 shows the influence of NPs on the apparent viscosity (AV), plastic viscosity (PV), yield point (YP), and gel strength (10 sec and 10 min) compared to the regular water-based drilling fluid. Based on this, it can be demonstrated that both apparent viscosity and yield point increased with 1g of SiO_2, CB and Al_2O_3 nanoparticles additions. The drilling fluids apparent viscosity increased by ~13.5%, when only 1 g of CB NPs was added to 350mL of the base drilling fluid.

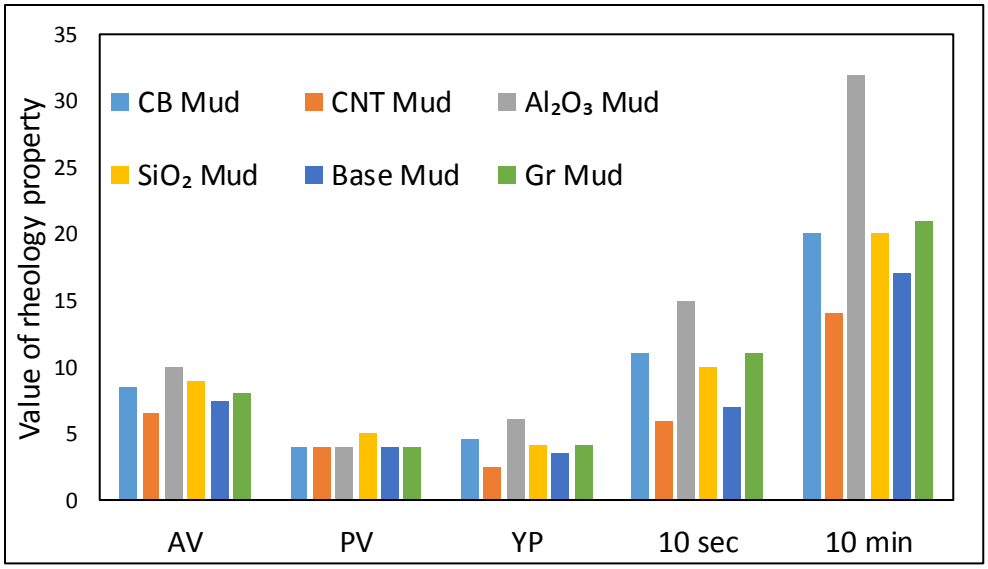

Figure 4-1 Rheological properties of single type nanoparticles (CB, CNT, Al_2O_3, SiO_2 and Gr) based drilling fluids.

In addition, an approximate 20% increase in the viscosity was obseved with the SiO_2 addition, and 6.6% with the addition of 1 g of graphite nanoparticles. Furthermore, around 36% viscosity enhancement was noted when Al_2O_3 was added, as shown in Figure 4-1, while apparent viscosity and yield point decreased with the addition of CNT nanoparticles. Generally, a drilling fluid with lower plastic viscosity and higher yield point is recommended as the lower plastic viscosity provides turbulence at the drill bit, which enables better hole cleaning and a higher yield point ensures enhanced carrying capacity and strong shear thinning behaviour. The plastic viscosity of the drilling fluid remains at the same value with the addition of nanoparticles. The silica nanoparticles increase the plastic viscosity from 4 to 5 pa. The drilling fluids' yield point increased by ~28.5% when only 1 g of CB NPs is added to 350mL of the base drilling fluid. Furthermore a yield point approaching a 14.3% increment was measured with the addition of SiO_2 and Gr in the same conditions. Moreover, a 71.4% yield point enhancement was noted when Al_2O_3 was added.

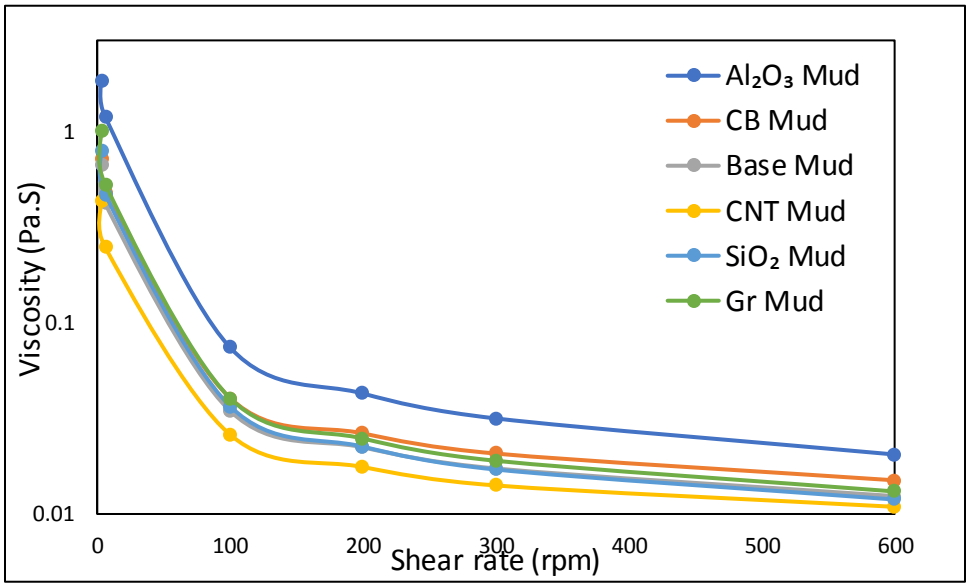

Figure 4-2 the viscosity of the prepared drilling fluids as a function of shear rate.

The gel strength is likewise a significant property, given that it quantifies the ability of the drilling fluid and keeps the drill cuttings in suspension. Experimentally, it was observed that the SiO_2, CB, Gr, and Al_2O_3 based fluids also demonstrated appropriate gel strengths at 10 secs and 10 minutes, as shown in the Figure 4-1. The 10 sec gel strengths for the water-based drilling fluid was 7pa, which increased with 1g of SiO_2 nanoparticles to 10pa and 11pa for Gr, CB. Furthermore, 15pa was found with the introduction of 1g of Al_2O_3.

One reason behind this enhancement could be that the nanoparticles work as chain joiner points between the bentonite molecules, which support the gelation behaviour of the drilling fluid [23]. In the same way, the 10 minute gel strength of the water-based drilling fluid was 17pa, and 20pa for both SiO_2 and CB. Furthermore, 32pa was found with the addition of 1g of Al_2O_3 and 21 pa with Gr. It is evident from the results that NPs-based drilling fluids have a relatively higher effect on the rheological parameters of the developed drilling fluids. Different enhancement trends can be observed based on the addition of nanoparticles associated with different parameters, such as the zeta potentials of the nanoparticles, dispersion ability, the size, and the shape of nanoparticles. In addition to the aforementioned effect of different nanoparticles on the rheology properties of the suspension, drastic increases in viscosity, yield stress and gel strength observed with Al_2O_3 could be justified by the reflection of synergy of homo-coagulation of between the aluminium oxide particle and hetero-coagulation of aluminium oxide, with the bentonite particle in the suspension. In order to btter explain the particles' interactions and to verify the validity of the rheological results that were investigated through the viscometer, we carried out a more advanced rheological measurement using both rotational and oscillation systems, via the Anton Paar rheometer. The viscosity of the drilling fluid decreases with increasing shear rate. This flow behaviour is called shear-thinning, as in Figure 4-2. Therefore, it is insufficient to only indicate the viscosity. It is interesting to note that the viscosity of the drilling fluid increased with addition of nanoparticle. The drilling fluids viscosity increased by 1.38 times when only 1 g of SiO_2 is added to 350 ml of the base drilling fluid. In addition, about 1.5 times viscosity increment was measured when 1 of Gr was added in the same conditions. Also, about two times viscosity increment was measured when the 1 g of CB nanoparticles were added in the same conditions. Furthermore, around 3 times viscosity enhancement was noted when 1 g of Al_2O_3 was added.

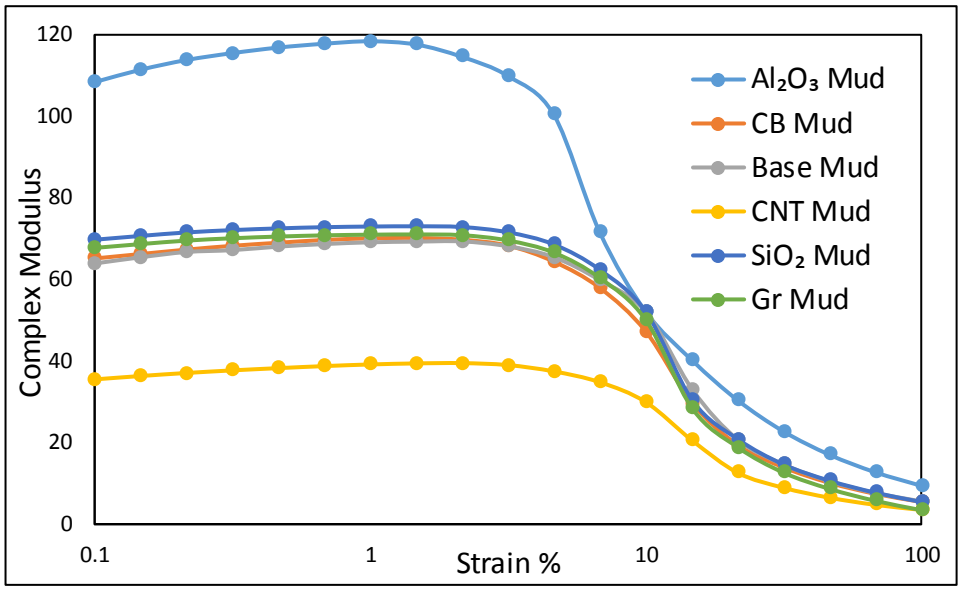

Figure 4-3 Complex modulus of the prepared drilling fluids as a function of deformation percentage

Characteristics such as loss and storage modulus, complex modulus, dynamic yield point, structural stability, and phase angle, all help describe the viscoelastic behavior of drilling fluids. The inter-particle interaction plus the particle networks in the drilling fluids can be measured by noting its passage from a solid-like condition to a liquid-like condition. The presentation of variation complex modulus (overall resistance to deformation) as a function of the strain is obtained through an oscillatory amplitude test, which is used as a suitable tool for the investigation of the strength of the particle connection in the fluid (the stiffness of material; the higher the modulus, the more stringent the material) [115, 116]. As can be seen imoren Figure 4-3, the complex modulus increases with the addition of nanoparticles. This means that nanoparticles offer more elastic properties (better suspension capability of the cuttings) to the fluid before the flow point. This is relevant, given that this state helps retain cuttings and weighting materials suspended in the drilling fluid, instead of allowing for them to settle into the wellbore. The results also indicate that nanoparticles can develop the structure of the drilling fluid. Moreover, even nanoparticles give better suspension capability of the cuttings to the drilling fluid; the flow point is still the same. This means that nano drilling fluids demonstrate appropriate abilities both at rest and in movement, since they have better gel structure, which is easily broken when drilling fluid pumps are shut off or are running at very low speed, the drilling fluid will take on a gel-like state. This state helps retain cuttings and weighting materials suspended in the drilling fluid instead of allowing them to settle into the wellbore.

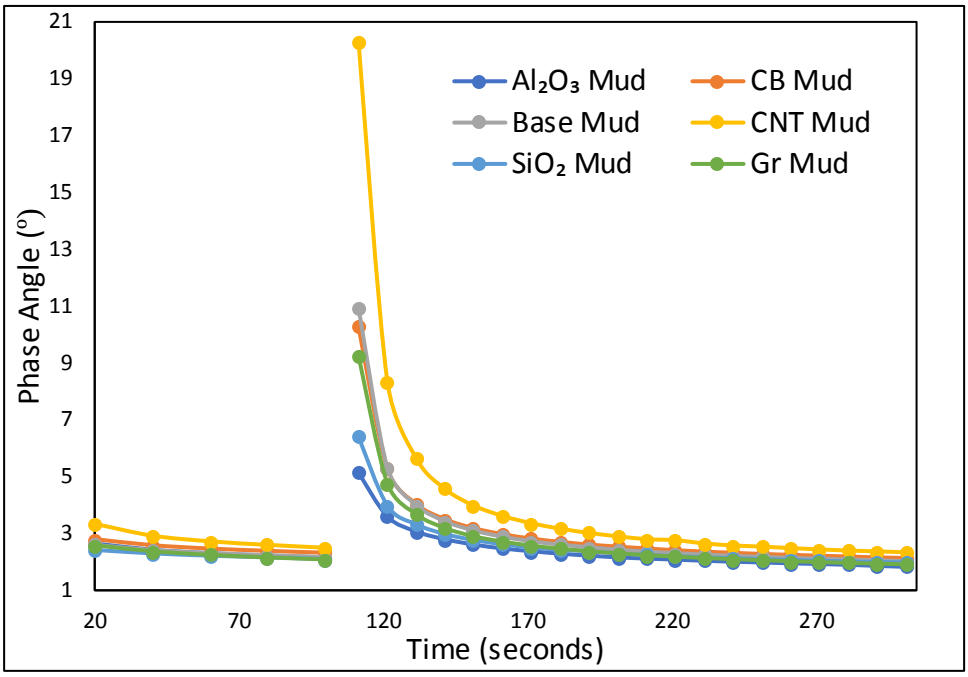

Figure 4-4 Thixotropy (structural recovery) of nano-prepared drilling fluids (Al_2O_3, CB, CNT, SiO_2 and Gr) as a function of time.

It is appropriate that the drilling fluid quickly develops high gel strength in order to resist the settling of massive particles out of suspension. These results agree with [117, 118] and also confirms our previous findings [95]. The laboratory results also prove that the addition of nanoparticles could develop the thixotropic properties of drilling fluids. Apparent tendency in Figure 4-4 (in accordance with aforementioned results in Figure 4-3 conforms that the addition of different nanoparticles ensures more elastic behaviour of the drilling fluid and increases the degree and the speed of the structural recovery, through reducing the time required for rebuilding. It is preferable to minimise the reconstruction time to prevent the sedimentation of the weighting materials and drilled cuttings. Our findings appear to be consistent with previous results [43, 119]. Figure 4-5 outlines the effect of Al_2O_3, CB, SiO_2, Gr and CNT nanoparticles on the filtrate volume, compared with the conventional water-based drilling fluid. It is obseved that not only Gr and SiO_2 decrease the filtrate volume, the addition of CB nanoparticles also decrease the filtrate volume, although this is a lower percentage when compare to the addition of SiO_2. The theory behind the idea that adding NPs could decrease the filtrate volume of drilling fluid is that the applied pressure force the NPs to plug the small pores in the filter cake, which will in turn reduce its permeability. Therefore, the filtrate volume will be lower. The filtrate volume of the traditional drilling fluid was 6.8ml for 10 minutes, and this volume decreased to 6.4ml with the addition of 1g of CB NPs. The results also show that that the addition of 1g of

silica and graphite NPs reduce the filtrate volume to 5.8ml, which is a reduction of around 14.7% in the filtrate volume.

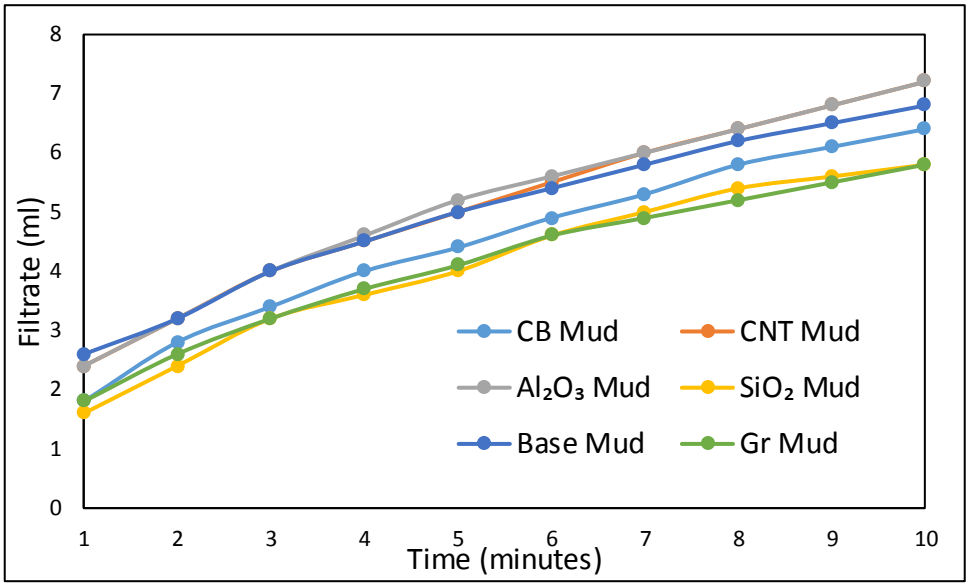

Figure 4-5 The effect of Al_2O_3, CB, SiO_2, Gr and CNT NPs on the filtrate volume, compared with the conventional water-based drilling fluid.

While notably increasing with the addition of CNT and Al_2O_3, the results indicate that such plugging does not occur. This is possibly due to the size and morphology of these particles. Figure 4-6 shows the dispersion of SiO_2, Al_2O_3 and Gr on bentonite fluid and clearly shows the effect of nanoparticles on the morphology of NPs-Bentonite. Al_2O_3 nanoparticles embedded in the randomly formed pore structure on the surface of the clay particle might increase the filtrate loss. On the other hand, SiO_2 was also embedded randomly on the surface of the clay particle, which implies a link between bentonite particles, which in turn might decrease the filtrate loss, while the graphite sheets increase the strength of bentonite against filtration.

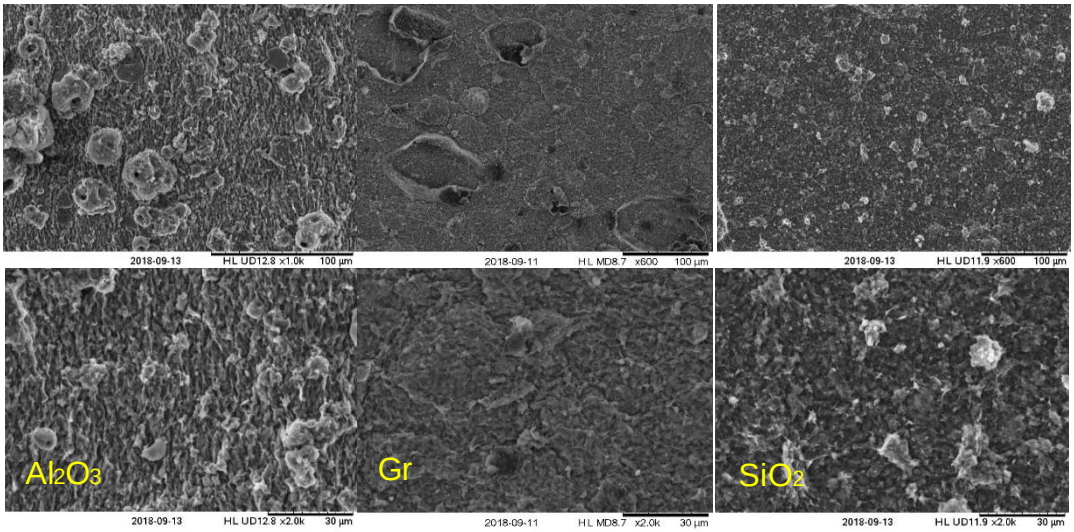

Figure 4-6 the SEM images of Al_2O_3, Gr and SiO_2 drilling fluids

4.2 Effect of Nanoparticles Concentration

In addition to the aforementioned effect of different nanoparticles on drilling fluid viscosity, apparent viscosity (AV), yield point (YP), gel strength (10 sec and 10 min), viscoelasticity and thixotropy compared to the regular water-based drilling fluid, there has been an increase in rheology properties with observed rising nanoparticles concentration. Figures 4-7, 4-8, 4-9 show that the increase in concentration of adding nanoparticles (SiO_2, Gr, and Al_2O_3) into bentonite drilling fluid results in increased viscosity. The drilling fluid viscosity increases 1.5 times when only 1g of SiO_2 is added to 350mL of the original drilling fluid. Besides, an almost double times viscosity increment was measured when 3g of SiO_2 were added in the same conditions, as revealed in Figure 4-7. On the other hand, the drilling fluid viscosity increases by 1.38 times when only 1g of Gr is added to 350mL of the original drilling fluid. Additionally, an approximate 1.62 times viscosity increment was measured when the 3g of Gr was added in the same conditions, as presented in Figure 4-8. In addition to the above effect of the concentration increase of SiO_2 and Gr on the viscosity of the suspension, a drastic increase in viscosity was observed when increasing the Al_2O_3 nanoparticles concentration. Figure 4-9 shows that the viscosity increases in concentration when adding Al_2O_3 nanoparticles into the bentonite drilling fluid. The addition of just 0.5 Al_2O_3 increases the viscosity of drilling fluids by 2 times, and 3.5 times viscosity increment was measured when the 3g of Al_2O_3 was added in the same conditions.

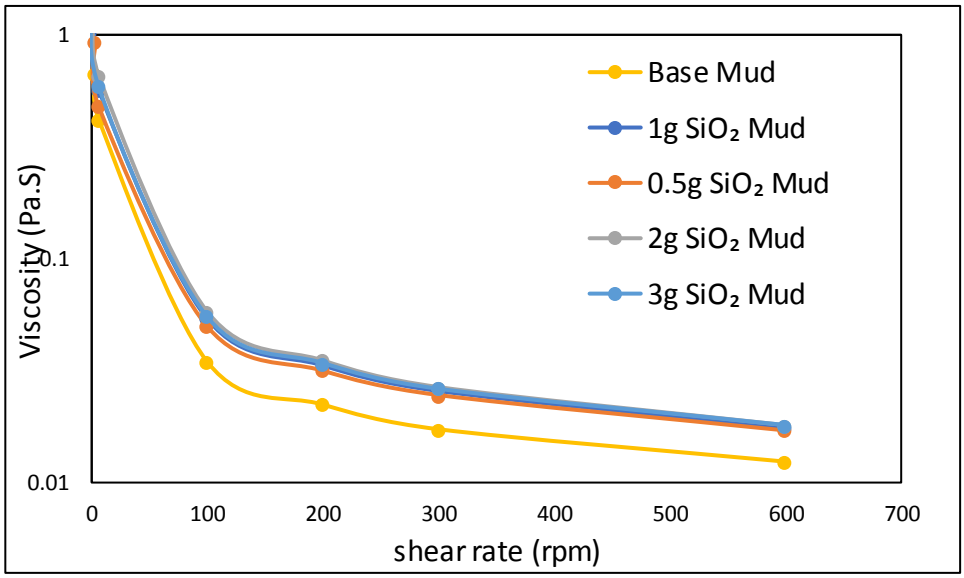

Figure 4-7 Effect of increasing SiO_2 concentration on the viscosity of the prepared drilling fluids

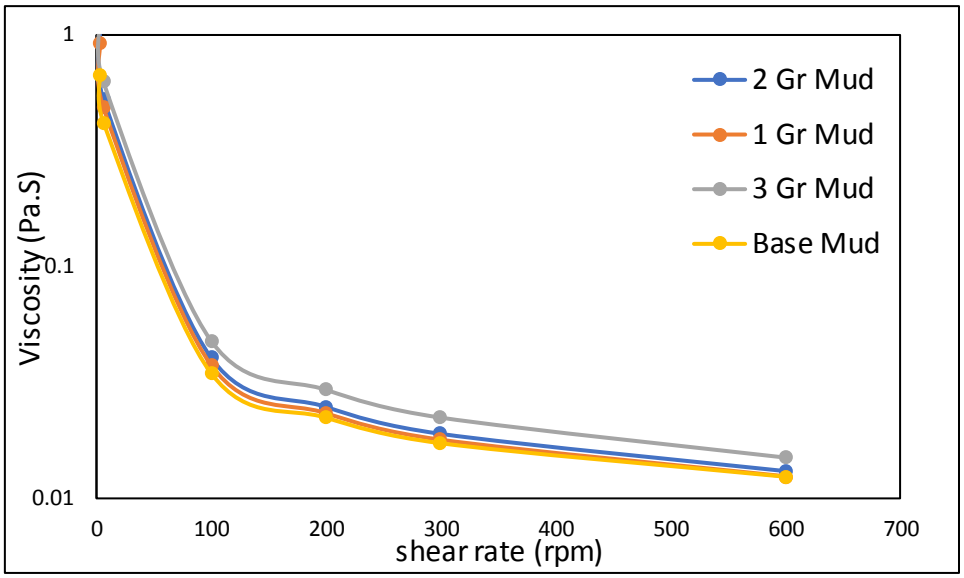

Figure 4-8 Effect of increasing Gr concentration on the viscosity of the prepared drilling fluids

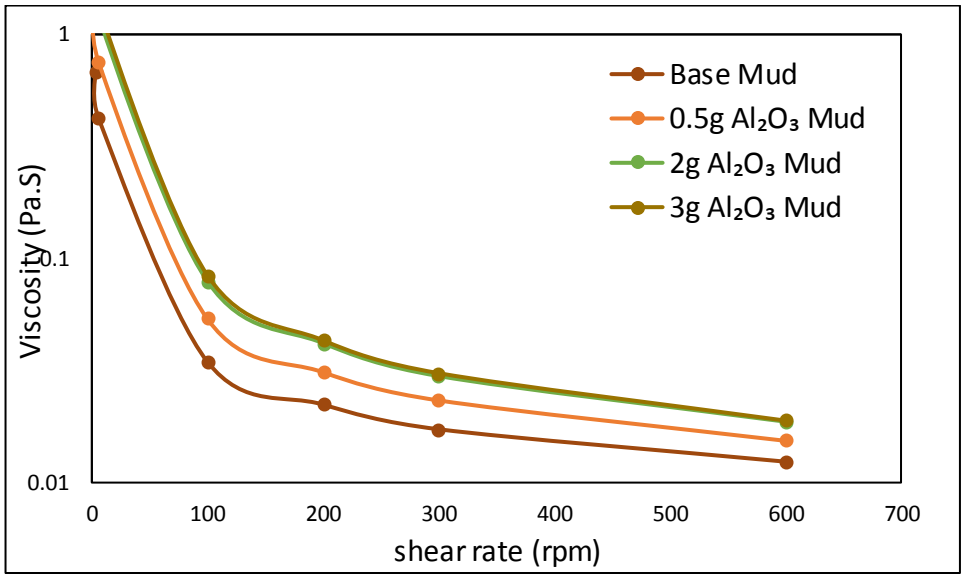

Figure 4-9 Effect of increasing Al_2O_3 concentration on the viscosity of the prepared drilling fluids

The following assessment to analyse the effect of increasing nanoparticles concentration on the strength of inter-particle interaction via examination of viscoelastic performance in prepared fluid samples oscillatory tests was carried out and is demonstrated in Figures 4-10,11,12.

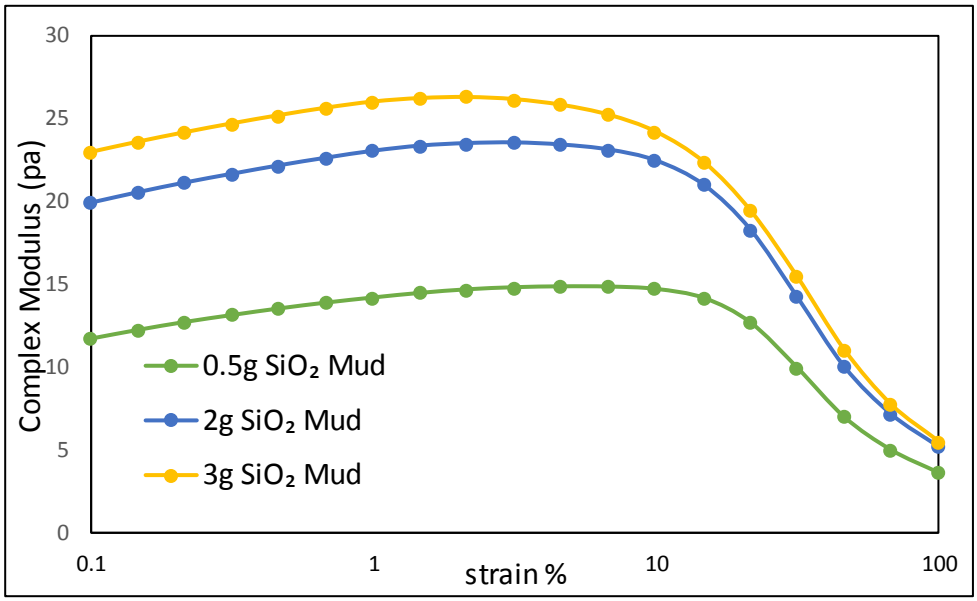

Figure 4-10 Effect of SiO_2 NPs concentration on the strength of inter-particle interaction (Complex Modulus) of drilling fluids.

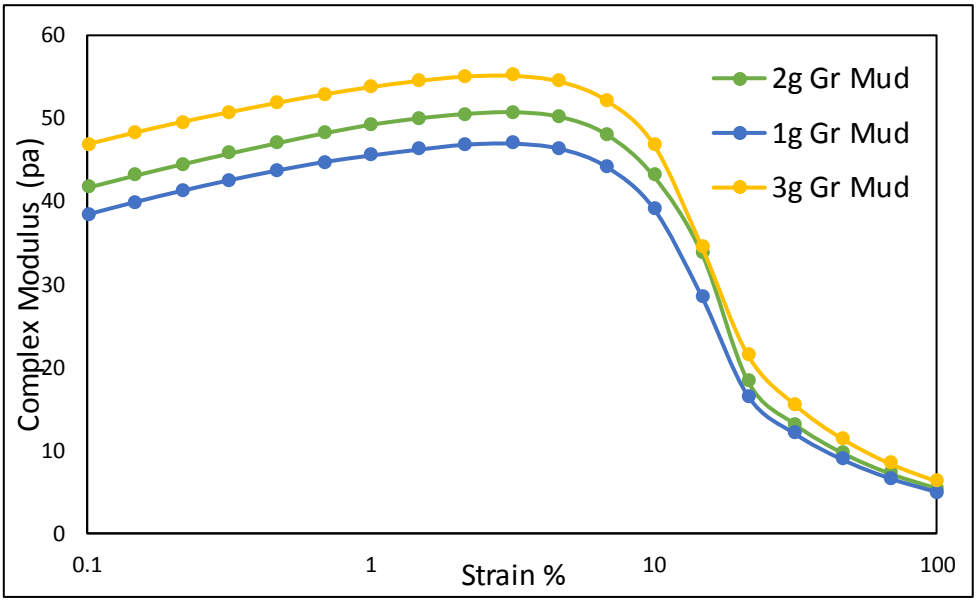

Figure 4-11 Effect of Gr NPs concentration on the strength of inter-particle interaction (Complex Modulus) of drilling fluids.

As can be seen in Figure 4-10, the complex modulus rises with increased SiO_2 nanoparticle concentrations. Similar behaviour is observed when increasing graphite and alumina concentrations, but with different levels. More significant increases were experienced by increasing Al_2O_3 NPs concentration, followed by Gr NPs and lastly with SiO_2 NPs. This strength in the fluid structure would be attributed to increase in interaction strength related to the synergy effect

between both homo-coagulation and hetero-coagulation between the particles in the suspension.

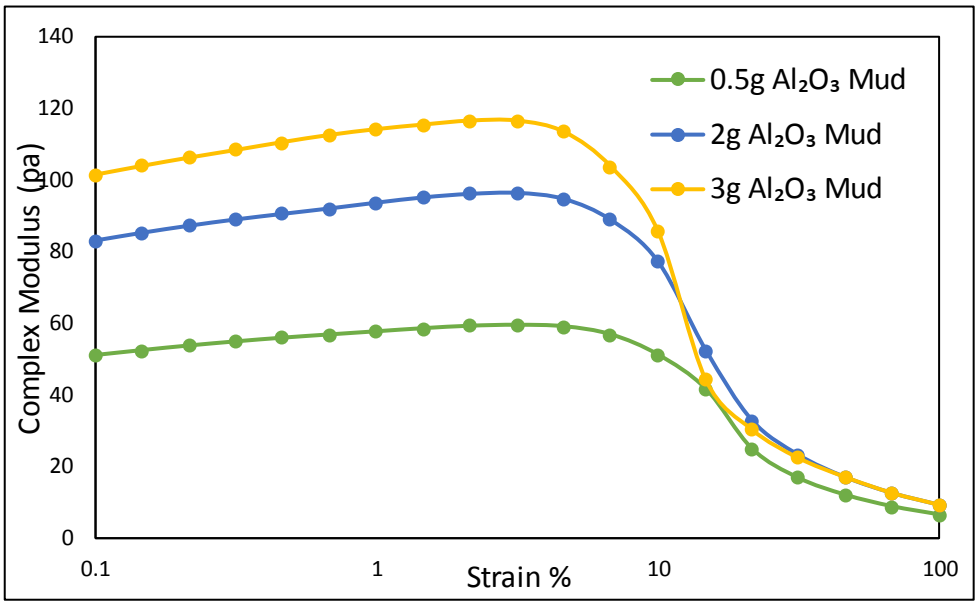

Figure 4-12 Effect of Al_2O_3 NPs concentration on the strength of inter-particle interaction (Complex Modulus) of drilling fluids.

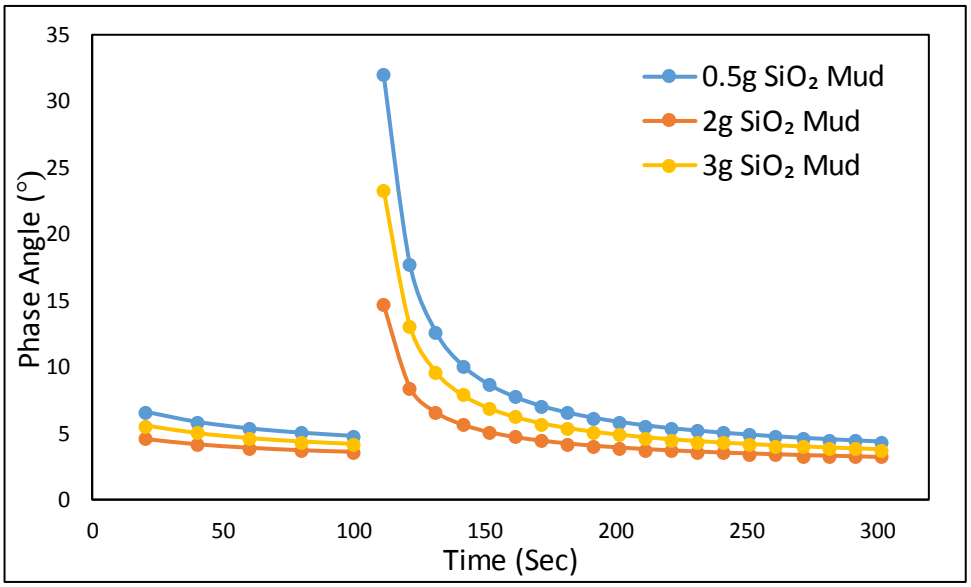

Figure 4-13 Effect of increasing SiO_2 concentration on the thixotropy of the prepared drilling fluids

The laboratory results also ascertained that increasing the nanoparticles concentration develops the thixotropic properties of the drilling fluids. Apparent tendency in Figure 4-13 (in accordance with the aforementioned results in Figure 4-10) confirms that the increase in SiO_2 nanoparticles

concentration ensures more elastic behaviour of the drilling fluid and increase the degree and the speed of the structural recovery through reducing the time required for rebuilding. As can be seen in Figure 4-13, the phase angle decreases from 32° to 23.3° then to 14.67° when the concentration increases from 0.5g to 3g, passing through to 2g. Likewise, a clear reduction in rebuilding time has been observed. The rebuilding required time for 3g SiO_2 is 60 sec and 130 secs for 2g SiO_2, whereas it is 300 secs for 0.5g SiO_2.

A similar trend was exhibited by increasing graphite and alumina concentrations, but with different levels. Higher reduction in phase angle was seen when increasing Al_2O_3 NPs concentration, followed by Gr NPs, and lastly SiO_2 NPs. This strength in fluid structure can be attributed to increases in the interaction strength related to the synergy effect of both homo-coagulation and hetero-coagulation between the particles in the suspension.

The phase angle decreases from 10.7° to 9.25°, then to 7.9° when the concentration of graphite NPs increases from 1g to 3g passing through 2g, as shown in Figure 4-14. Also, a clear reduction in the rebuilding time has been observed. The rebuilding required time for 3g Gr is 90 secs and 110 secs for 2 g Gr, while it is130 secs for 0.5g Gr.

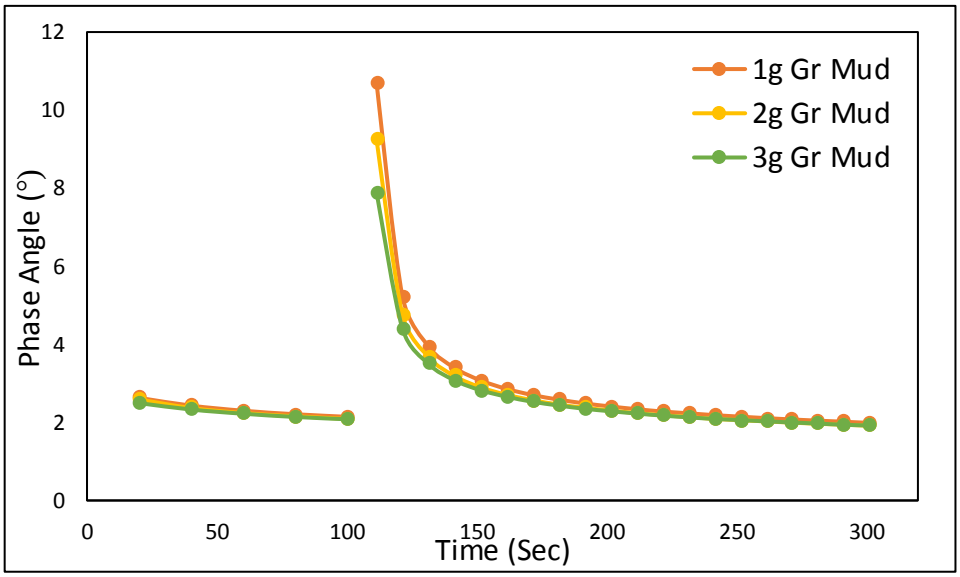

Figure 4-14 Effect of increasing Gr concentration on the thixotropy of the prepared drilling fluids

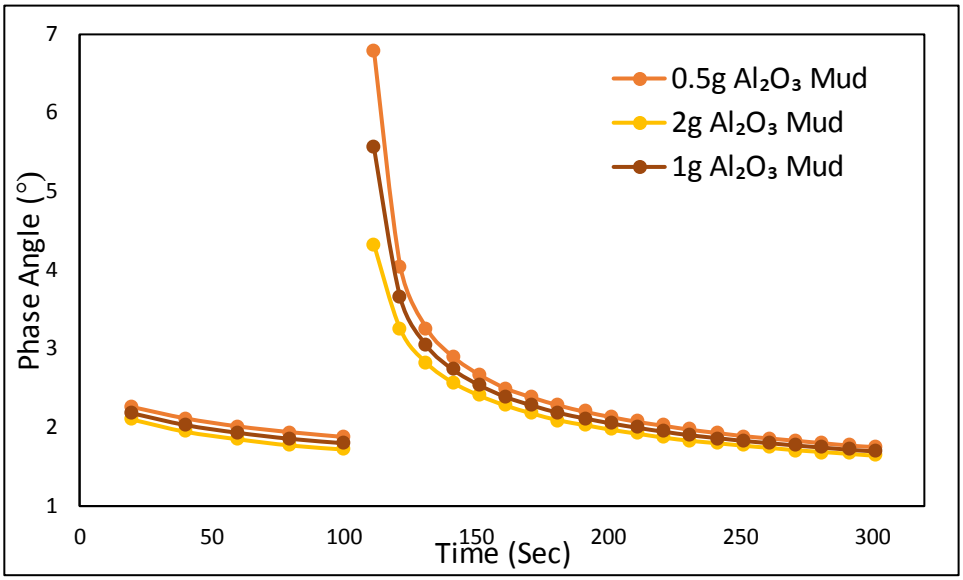

Figure 4-15 Effect of increasing Al_2O_3 concentration on the thixotropy of the prepared drilling fluids

Similarly, with Al_2O_3, the phase angle decreases from 6.8° to 5.5º, then to 4.3º, when the concentration of Al_2O_3 NPs increases from 1g to 3g passing through to 2g, as shown in Figure 4-15. Also, a clear reduction in rebuilding time has been observed. The rebuilding required time for 3 g Al_2O_3 is 130 Sec and 110 Sec for 2g Al_2O_3, while it is 160 Sec for 0.5g Al_2O_3.

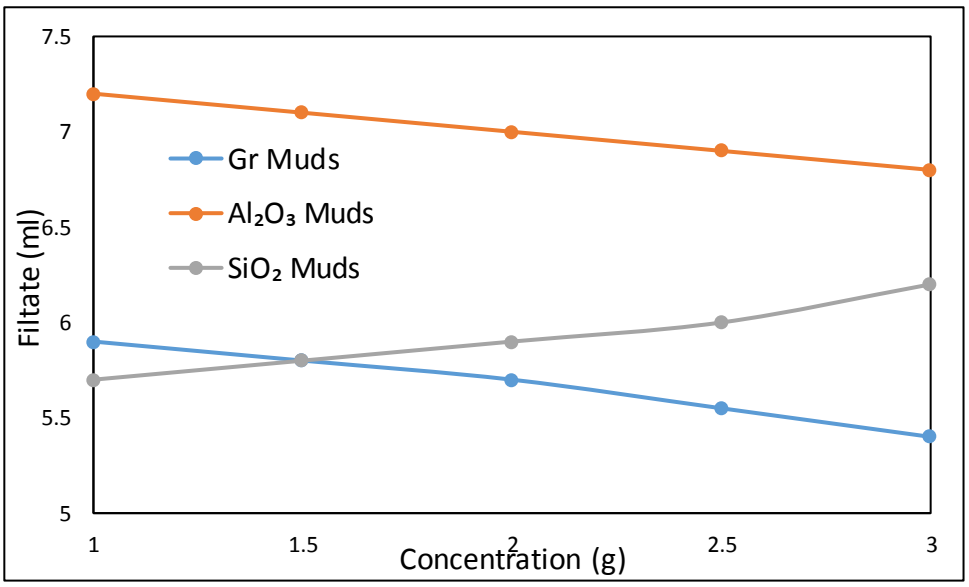

Figure 4-16 The effect of Al_2O_3, SiO_2, and Gr on the filtrate volume of prepared drilling fluids

Figure 4-16 illustrates the effect of increasing the concentration of adding nanoparticles (SiO_2, Gr, and Al_2O_3) into the bentonite drilling fluid on the filtrate

loss. It is clear that increasing the concentration of Al_2O_3 nanoparticles slightly reduces the filtrate loss of the drilling fluid. This reduction could be explained by the presence of micro particles, which result from exceeding Al_2O_3 as shown in the SEM analysis, in Figure 4-17. Also, the increased concentration of Gr nanoparticles reduces the filtrate loss of the drilling fluid.

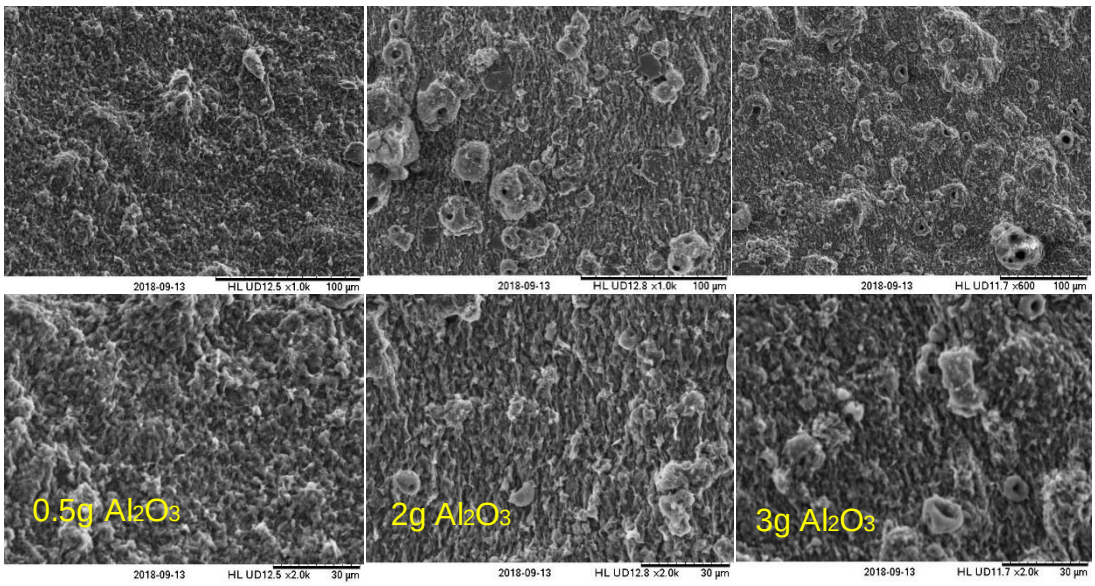

Figure 4-17 SEM analysis at different Al_2O_3 concentrations

The filtrate loss decreases from 5.9 ml to 5.4 ml when the concentration of Gr increases from 1g to 3g. This reduction could be linked to the morphology of Gr nanoparticles. The presence of 1g of Gr sheets reduces the filtrate loss from 6.8 ml to 5.9 ml, since the graphite sheets confer better structure to the drilling fluid, which aid them in resisting the filtration process. Moreover, increasing the concentration leads to the accumulation and overlapping of graphite sheets, which confers a strong composition to resist filtration as shown in Figure 4-18. The SEM analysis shows that the increase of SiO_2 nanoparticles in the bentonite drilling fluid results in a rough surface, as can be observed in Figure 4-19. This indicates that the nano silica may have undergone a chemical reaction with the surface charge of bentonite.

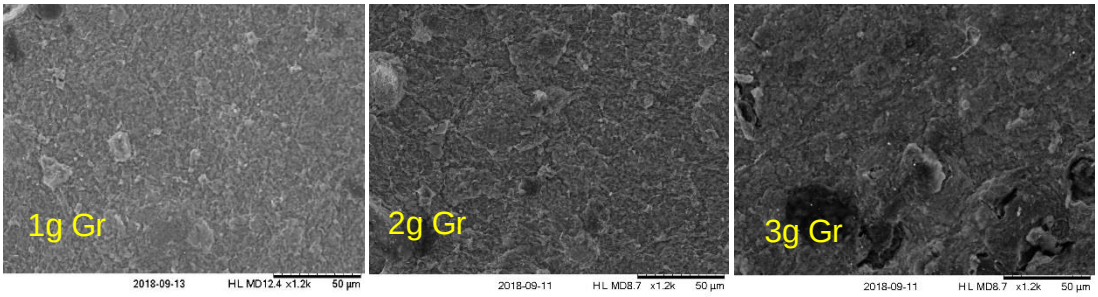

Figure 4-18 SEM analysis at different Gr concentrations

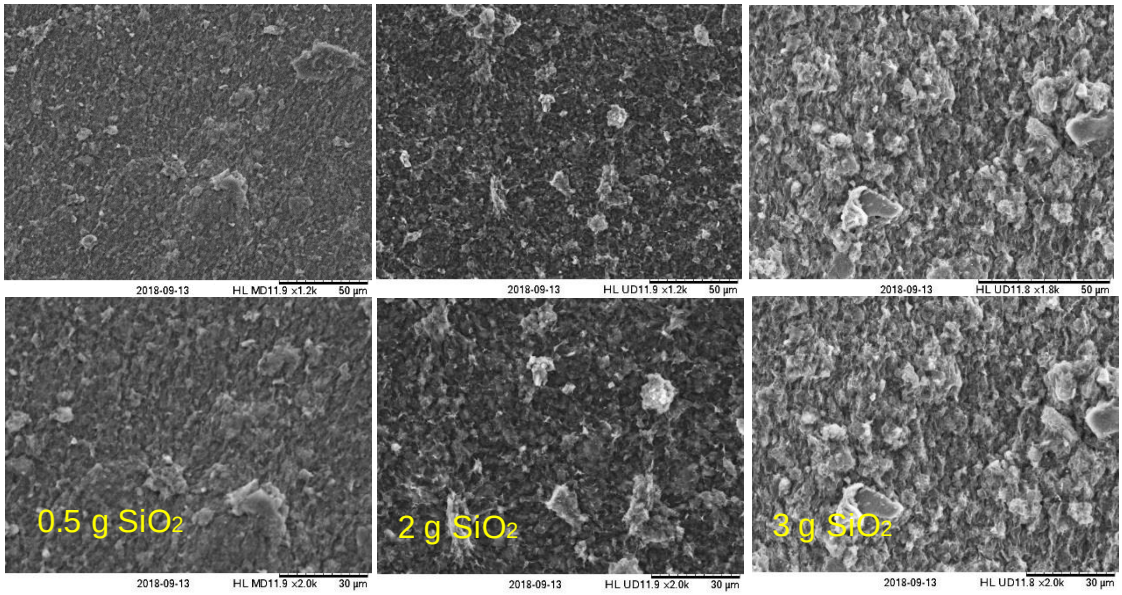

Figure 4-19 SEM analysis at different SiO_2 concentrations

Based on these results we build the hypothesis that the impact of nanoparticles is multi-faceted, and their influence on different properties varies. The addition of one nanoparticle may improve one property, but may in turn retract from another. It is unlikely that the addition of one type of particle could improve all related features. With a view to address these limitations, we develop novel hybrid nanoparticle systems, which will be discussed in detail in the following section.

4.3 Rheological and Filtration properties of Hybrid Nanoparticles based Drilling Fluids

Three hybrid nanoparticle recipes were chosen depending on the results of the single type nanoparticles, along with the chemical and physical features of these nanoparticles, with a view to enhance the drilling fluid's performance. The rheology and filtration properties were investigated for CB-SiO_2, CNT-Al_2O_3, SiO_2-Al_2O_3 nanoparticles-based fluids. The first hybrid nanoparticles recipe contains CB and SiO_2 nanoparticles. There are two main reasons behind choosing both SiO_2 and CB nanoparticles. Firstly, carbon black nanoparticles are used to improve rheological and thermal properties. Secondly, nano silica is used to reduce the fluid loss. Figure 4-20 presents the influence of CB-SiO_2 hybrid NPs-based fluids on the apparent viscosity (AV), plastic viscosity (PV), yield point (YP), and gel strength (10 sec and 10 min), compared to SiO_2 and CB NPs based fluids and conventional water-based drilling fluid. It can be seen that the 10 sec and 10 minutes gel strength from the addition 1g of 1:1 CB-SiO_2 hybrid nanoparticles are higher than the values at the same concentration of 1g SiO_2, 1g CB nanoparticles. This could be linked with the dispersion of SiO_2 and CB nanoparticles on the surface of bentonite particles and suggests links between bentonite particles, which might promote the gelation of the bentonite.

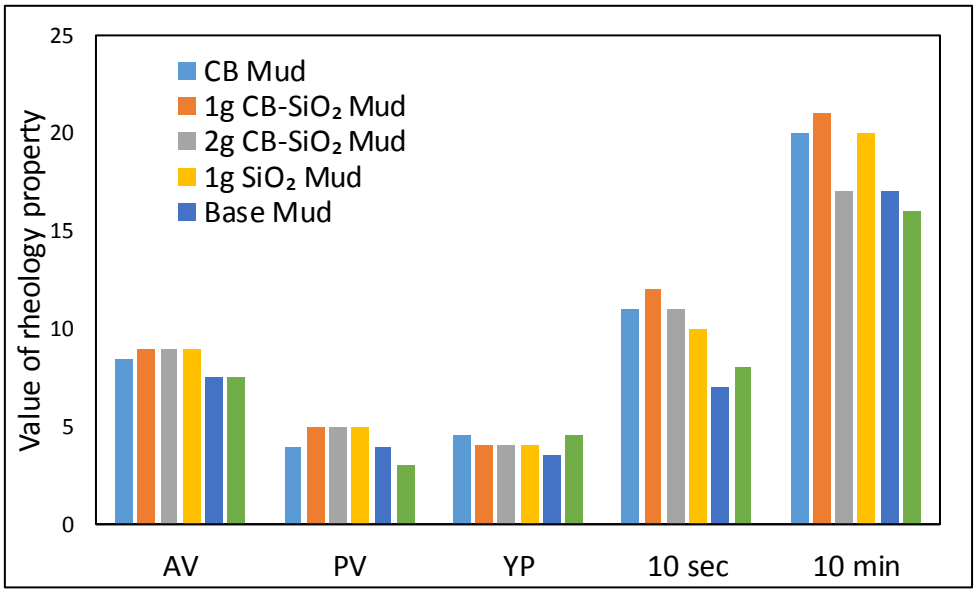

Figure 4-20 Rheological properties (AV, PV, YP, 10 sec and 10 minutes gel strength) ofCB-SiO_2 Nanoparticles based Drilling Fluids

Figure 4-21 presents the influence of CB-SiO_2 hybrid NPs-based fluids on the viscosity, compared to SiO_2 and CB NPs based fluids and conventional water-based drilling fluid. It can be seen that viscosities of the drilling fluids with 1g

and 2g of 1:1 CB-SiO_2 are higher than with SiO_2 alone at the same concentrations. This could be linked with the dispersion of CB-SiO_2 nanoparticles on the surface of bentonite particles and suggests links between bentonite particles, which might promote the gelation of the bentonite.

The viscosities of the drilling fluids with 1g and 2g of 1:1 CB-SiO_2 are higher than with SiO_2 alone at the same concentrations, as shown in Figure 4-21.

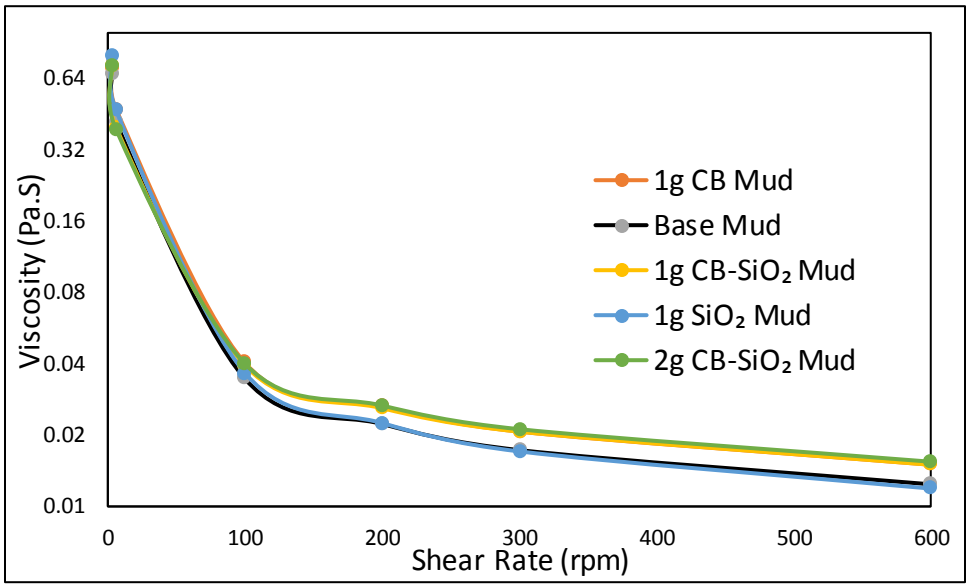

Figure 4-21 Effect of SiO_2 and CB combination on drilling fluid viscosity

Figure 4-22 shows a filtrate loss of CB, SiO_2, CB-SiO_2 and base mud. It is clear that 1g of CB-SiO_2 nanoparticles reduces the filtrate loss of the drilling fluid better than CB nanoparticles alone and the same is true for SiO_2. The laboratory results also ascertained that increasing the concentration of CB, SiO_2 and CB-SiO_2 nanoparticles increases the filtrate loss of the drilling fluid. The trends apparent in Figure 4-23 (in accordance with the aforementioned results in Figure 4-22). It is evident that the combination of CB and SiO_2 nanoparticles reduces the filtrate loss better than the CB NPs alone. Also, the increase concentration of CB-SiO_2 nanoparticles increase the filtrate loss of the drilling fluid. It's clear from the results that the hybrid CB-SiO_2 NP recipe works better than either the CB NP or SiO_2 NP alone.

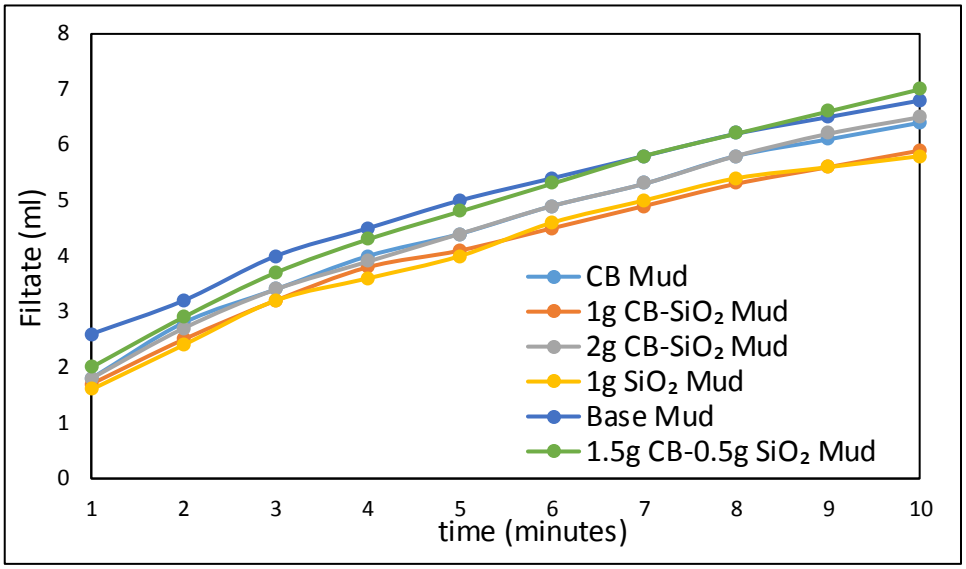

Figure 4-22 Effect of SiO_2 and CB combination on filtrate loss

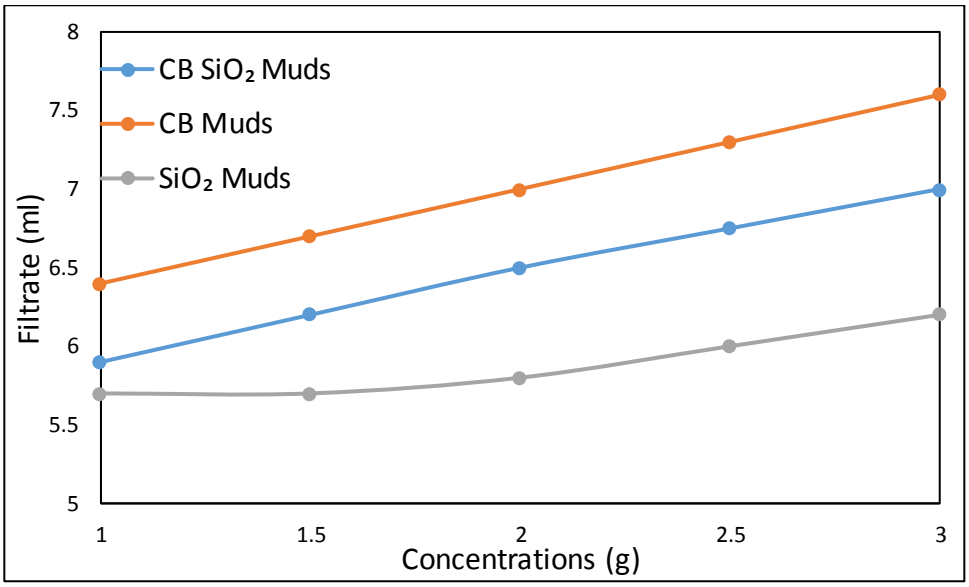

Figure 4-23 Effect of SiO_2, CB and CB-SiO_2 Concentration on filtrate loss

The second hybrid nanoparticles recipe is CNT-Al_2O_3. Figure 4-24 shows the influence of 1g of CNT-Al_2O_3 on the apparent viscosity (AV), plastic viscosity (PV), yield point (YP), and gel strength (10 sec and 10 min) compared to CNT and Al_2O_3 NPs alone. It can be seen that the combination of CNT and Al_2O_3 NPs exhibits better rheological properties than CNT NPs. This enhancement is attributed to the presence of Al_2O_3 nanoparticles. The drilling fluids apparent viscosity increased by ~38.5% when only 1g of CNT-Al_2O_3 NPs was added, instead of 1g of CNT only. The drilling fluids' yield point doubles (approximately), and it is also noted that the combination of CNT and Al_2O_3 NPs exhibited better 10 sec and 10 minute gel strength than CNT NPs.

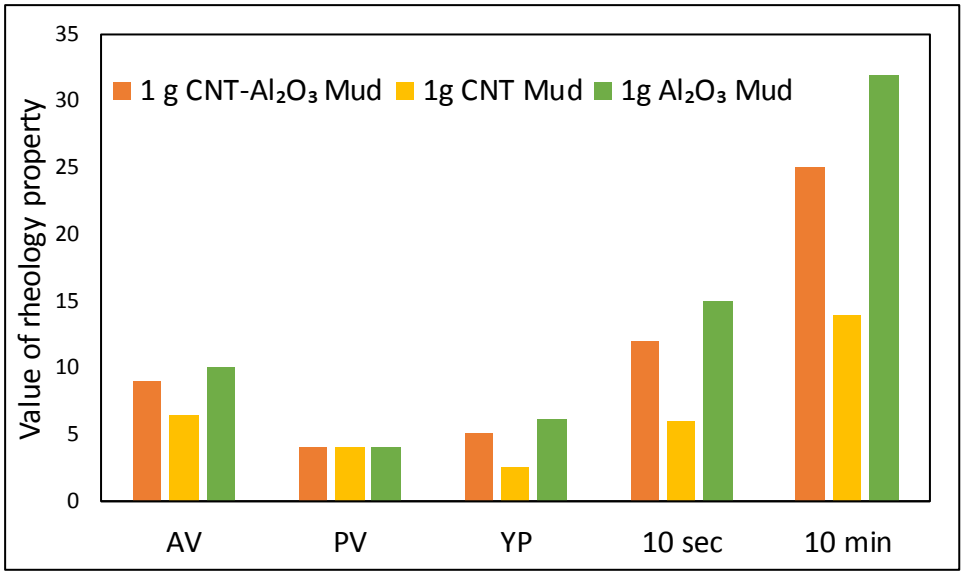

Figure 4-24 Rheological properties of CNT-Al_2O_3 Nanoparticles based Drilling Fluids

Experimentally, it was observed that the 10 sec gel strength doubled, and was enhanced by 78.6 % for 10 min gel strength.

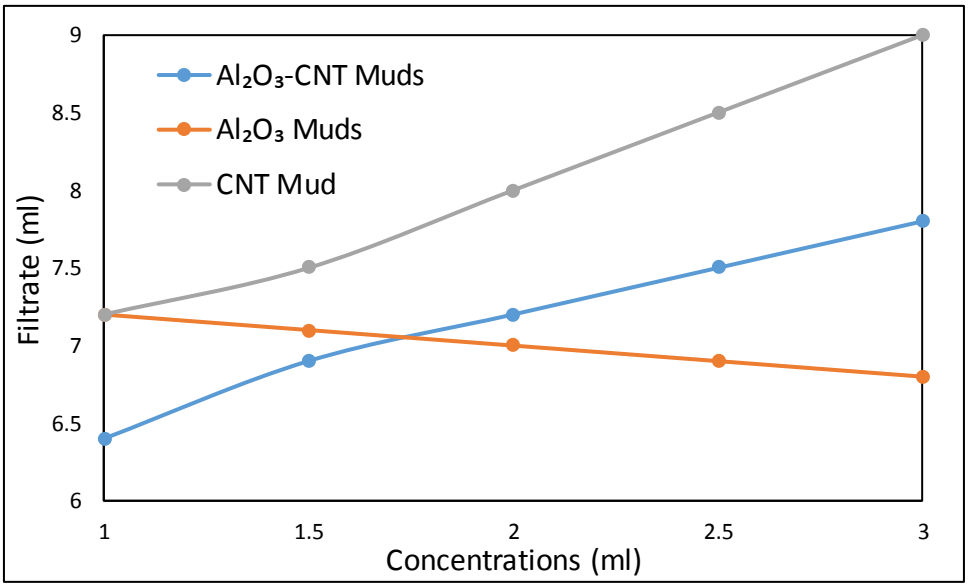

Figure 4-25 Effect of CNT, Al_2O_3 and CNT-Al_2O_3 Concentration on filtrate loss

Figure 4-25 shows the filtrate loss of the CNT, Al_2O_3, CNT-Al_2O_3 and base muds. It is evident that the combination of CNT and Al_2O_3 NPs exhibit better filtration properties than CNT NPs. The filtrate loss of CNT-Al_2O_3 was 6.4 ml while it was 7.2 ml for CNT. It can also be observed that an increase in nanoparticles concentration increases the filtrate loss of the drilling fluids. We carried out a more advanced rheological measurement using an Anton Paar

rheometer. The viscosity of drilling fluids decreases with an increasing shear rate. This flow behaviour is known as shear-thinning. Figure 4-26 shows that the combination of CNT and Al_2O_3 NPs exhibit more viscous fluid than CNT NPs and base mud. Figure 4-27 shows that the complex modulus increases with a combination of CNT and Al_2O_3 NPs. This means that nanoparticles offer more elastic properties to the fluid before the flow point and this what we require given that this state helps retain cuttings and weighting materials suspended in the drilling fluid instead of allowing them to settle into the wellbore. The results also indicate that the combination of CNT and Al_2O_3 NPs developed the structure of the drilling fluid through quickly develops high gel strength that can resist the settling of massive particles out of suspension, as shown in Figure 4-28. When the drilling fluid pumps are shut off (or running at very low speed), the drilling fluid will take on a gel-like state. This state helps retain cuttings and weighting materials suspended in the drilling fluid, instead of allowing them to settle into the wellbore.

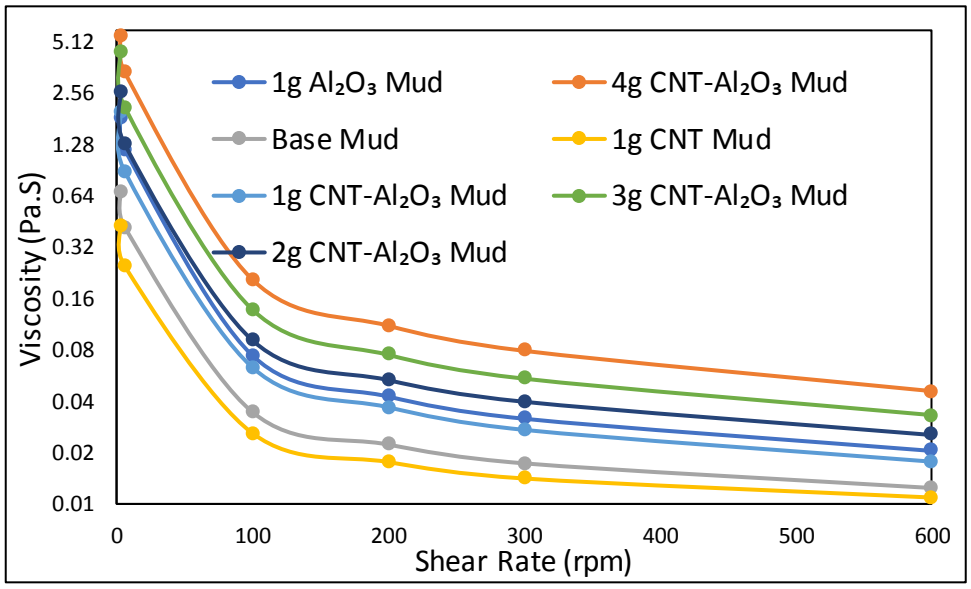

Figure 4-26 Effect of CNT and Al_2O_3 combination on drilling fluid viscosity

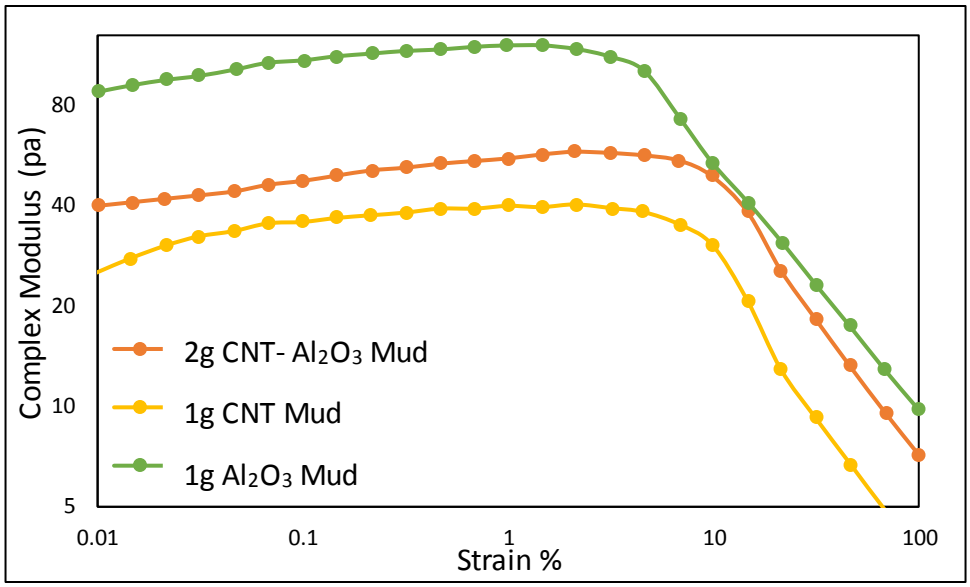

Figure 4-27 Effect of CNT and Al_2O_3 combination on the strength of inter-particle interaction (complex modulus) of the prepared drilling fluids as a function of deformation percentage.

The final hybrid NPs recipe was Al_2O_3-SiO_2. This recipe was chosen according to the results of the addition of each alumina and silica to the drilling fluids. The alumina NPs, as previously shown, can enhance the rheological properties of drilling fluids, while silica NPs can eliminate the filtrate loss that is caused by alumina.

Figure 4-29 shows the influence of Al_2O_3-SiO_2 NPs on the apparent viscosity (AV), plastic viscosity (PV), yield point (YP), and gel strength (10 sec and 10 min) compared to Al_2O_3, SiO_2 and the regular water-based drilling fluid. It can be observed that Al_2O_3-SiO_2 enhances the rheological properties of base mud better than SiO_2 alone. The drilling fluids apparent viscosity increased by ~26.7% when only 1g of Al_2O_3-SiO_2 NPs was added to 350mL of the base drilling fluid and increased by around 20.5% with SiO_2 alone. The laboratory results also ascertained that the Al_2O_3-SiO_2 NPs develop the yield point of the drilling fluids. The addition of 1g and 2g of SiO_2 NPs improves the yield point by 14.3% and 28.6 compared to Al_2O_3-SiO_2 NPs by around 28.6 and 114.4% at the same concentration. Furthermore, it has been observed that the addition of Al_2O_3-SiO_2 also exposed appropriate gel strengths at 10 sec and 10 min better than SiO_2 NPs alone.

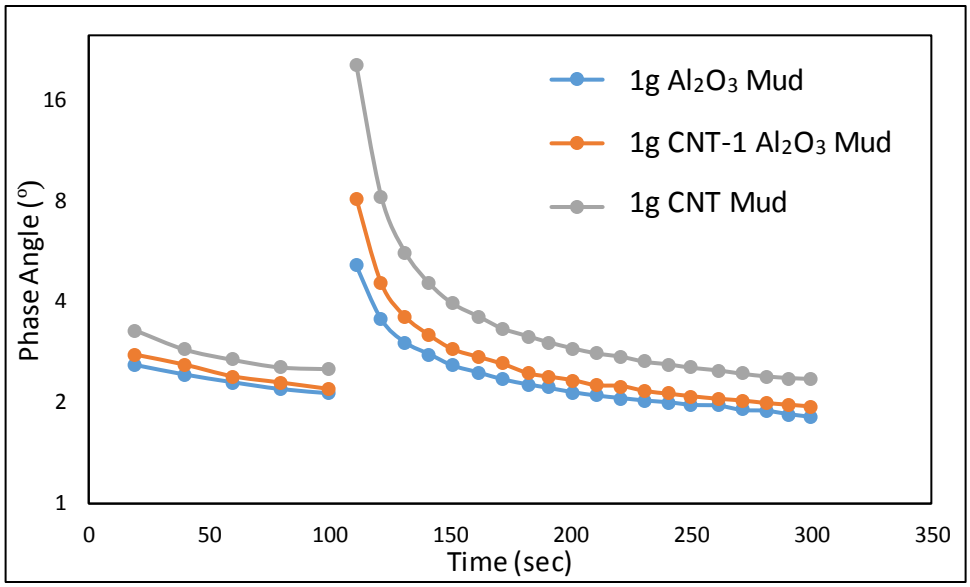

Figure 4-28 Effect of CNT and Al_2O_3 combination on the thixotropy (structural recovery) of the prepared drilling fluids as a function of shear rate and time.

The 10 sec gel strength for water-based drilling fluid was seven pa, which increased with 1g of SiO_2 nanoparticles to 10pa and 12pa for Al_2O_3-SiO_2. Likewise, the gel strength remained at 10pa with the addition of 2g of SiO_2, while it increased to 20pa when 2g of Al_2O_3-SiO_2 was added. In the same way, the 10 min gel strength of the water-based drilling fluid was 17pa, which increased to 20pa with 1g SiO_2 and 23pa for Al_2O_3-SiO_2. Furthermore, it was found to decrease to 17pa with the addition of 2g of SiO_2 and it increased to 33pa with Al_2O_3-SiO_2. It is quite apparent from the results that Al_2O_3-SiO_2 NPs-based drilling fluids have a relatively higher effect on the rheological parameters of the developed drilling fluids than SiO_2 alone. This enhancement is associated with the presence of Al_2O_3 in a hybrid recipe. Viscosity, viscoelasticity and thixotropy measurements were carried out using rotational, oscillation and oscillation-rotational-oscillation systems to observe the potential effect of Al_2O_3-SiO_2 on inter-particle interaction, along with the particle networks in the drilling fluids' suspension.

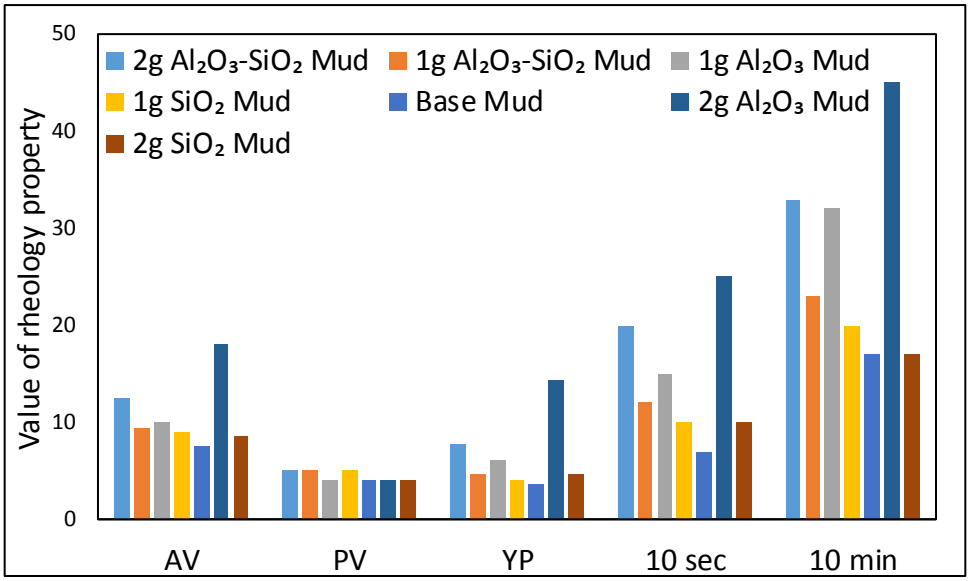

Figure 4-29 Rheological properties of Al_2O_3-SiO_2 Nanoparticles based Drilling Fluids

Figure 4-30 shows that the viscosity increases in concentration when adding Al_2O_3-SiO_2 nanoparticles into the bentonite drilling fluid. it is evident that the increase in concentration of Al_2O_3-SiO_2 increases the viscosity of the drilling fluids. The drilling fluid viscosity increased 1.5 times when only 1g of Al_2O_3-SiO_2 was added to 350mL of the original drilling fluid. An increase of 2.25 times viscosity was measured when the 2g of Al_2O_3-SiO_2 was added in the same conditions. On the other hand, the drilling fluid viscosity increased by 5.5 times when the concentration increased to 3g of Al_2O_3-SiO_2.

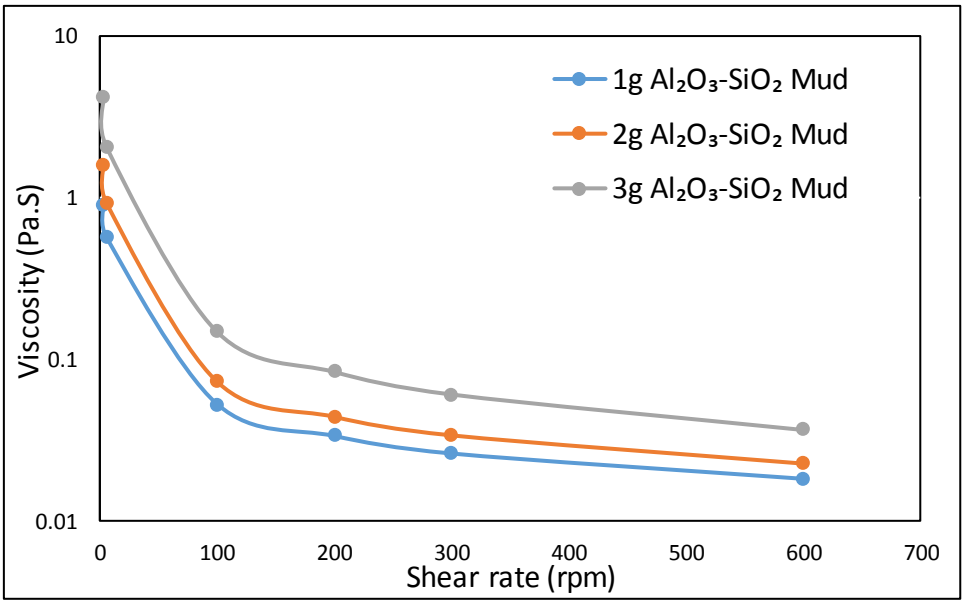

Figure 4-30 Effect of SiO_2-Al_2O_3 Concentration on drilling fluid viscosity as a function of shear rate.

Oscillatory tests were then carried out (detailed in Figure 4-31) to evaluate the effect of increasing the concentration of Al_2O_3-SiO_2 nanoparticles on the strength of inter-particle interaction via an examination of the viscoelastic performance in prepared fluid samples. As can be seen in Figure 4-31, the complex modulus rises with corresponding increases SiO_2, Al_2O_3 and Al_2O_3-SiO_2 nanoparticle concentrations. Similar behaviour was displayed, but at different levels. More significant increases were experienced by increasing Al_2O_3 NPs concentration, then increasing Al_2O_3-SiO_2 NPs and lastly by increasing SiO_2 NPs. This strength in the fluid structure can be attributed to increases in the interaction strength related to the synergy effect of both SiO_2 and Al_2O_3 NPs.

Thixotropy tests were carried out and are illustrated in Figure 4-32 to evaluate the impact of increasing Al_2O_3-SiO_2 nanoparticles concentration on the rebuilding time. It is evident that the rebuilding time was reduced with the increase in SiO_2, Al_2O_3 and Al_2O_3-SiO_2 nanoparticle concentrations. As can be observed rom Figure 4-32, the phase angle decreases from 32° to 23.3º then to 14.67º when the concentration increases from 1g to 3g, passing through to 2g. In addition, a clear reduction in rebuilding time was also noticed. The rebuilding required time for 3g of SiO_2 is 130 seconds and 150 seconds for 2 g SiO_2, while it was 300 seconds for 1g SiO_2. The same was true for Al_2O_3, where the phase angle decreases from 6.8° to 5.5º then to 4.3º when the concentration of Al_2O_3 NPs increases from 1g to 3g passing through to 2g. Also, a clear reduction in the rebuilding time was also observed. The rebuilding required time for 3g of Al_2O_3 is 110 seconds and 120 seconds for 2g Al_2O_3, while 160 seconds for 1g Al_2O_3. Likewise, for Al_2O_3-SiO_2, the phase angle decreases from 12.26 to 6.55 then to 4.87 when the concentration increases from 1 g to 3 g passing through 2 g. Also, a clear reduction in rebuilding time was noticed. The rebuilding required time for 3 g Al_2O_3-SiO_2 is 100 seconds, whereas 110 seconds and 130 seconds to 2g and 1g, respectively. Figures 4-33 and 4-34 show the influence of increasing SiO_2, Al_2O_3 and Al_2O_3-SiO_2 concentration on the filtrate loss volume. It is clear that increasing the concentration of Al_2O_3 nanoparticles slightly reduces the filtrate loss of the drilling fluid. This reduction could be explained by the presence of microparticular aggregates, which results from excess Al_2O_3. The combination of Al_2O_3 and SiO_2 reduce the filtrate loss better than Al_2O_3 NPs alone. Also, the increase concentration of Al_2O_3, SiO_2 and Al_2O_3-SiO_2 nanoparticles increased the filtrate loss of the drilling fluid as presented in Figure 4-23. It is also evident that the Al_2O_3-SiO_2 recipe works better than Al_2O_3 and SiO_2 alone.

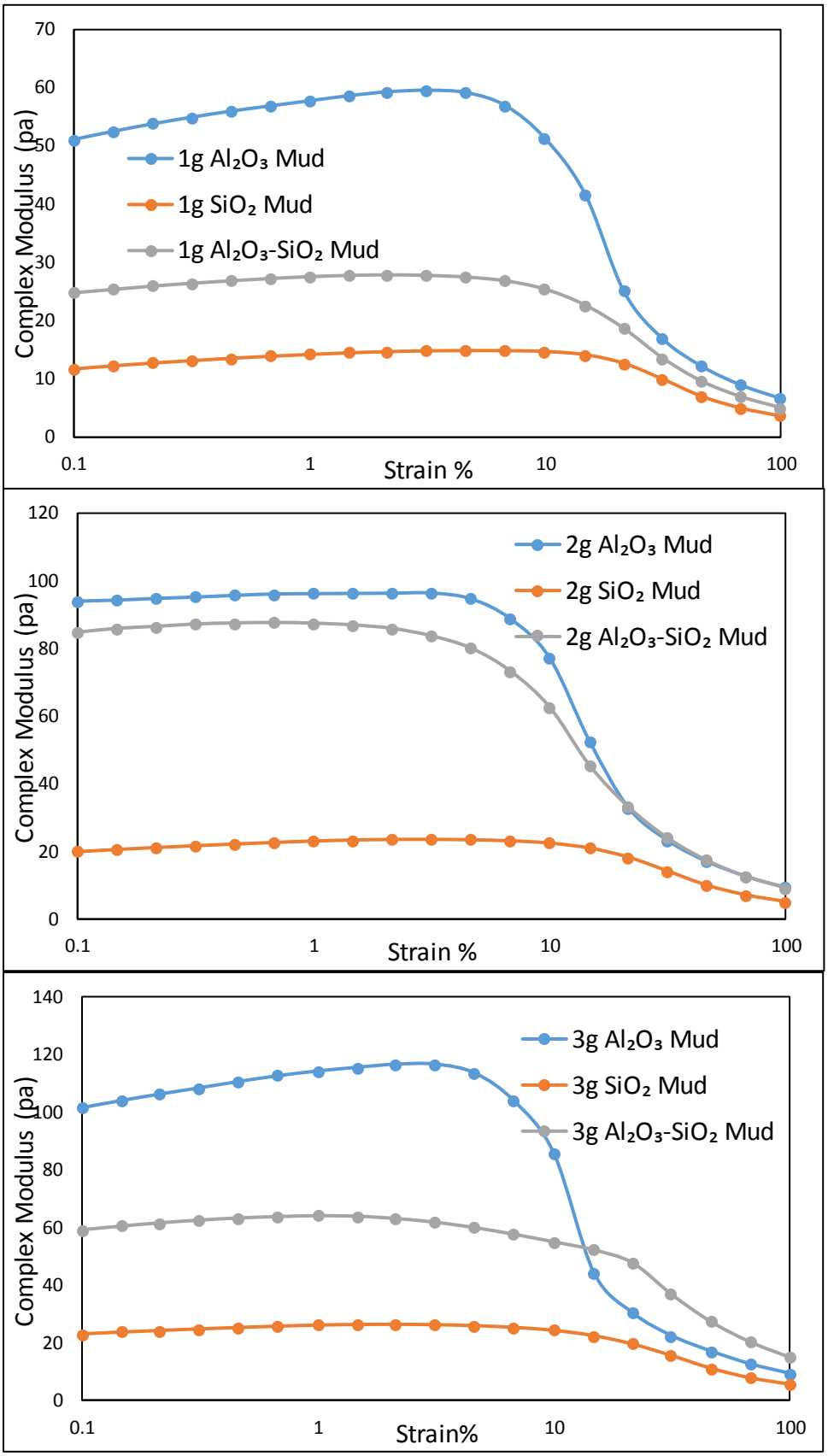

Figure 4-31 Effect of SiO_2, Al_2O_3 and SiO_2-Al_2O_3 concentration the strength of inter-particle interaction (complex modulus) of the prepared drilling fluids as a function of deformation percentage.

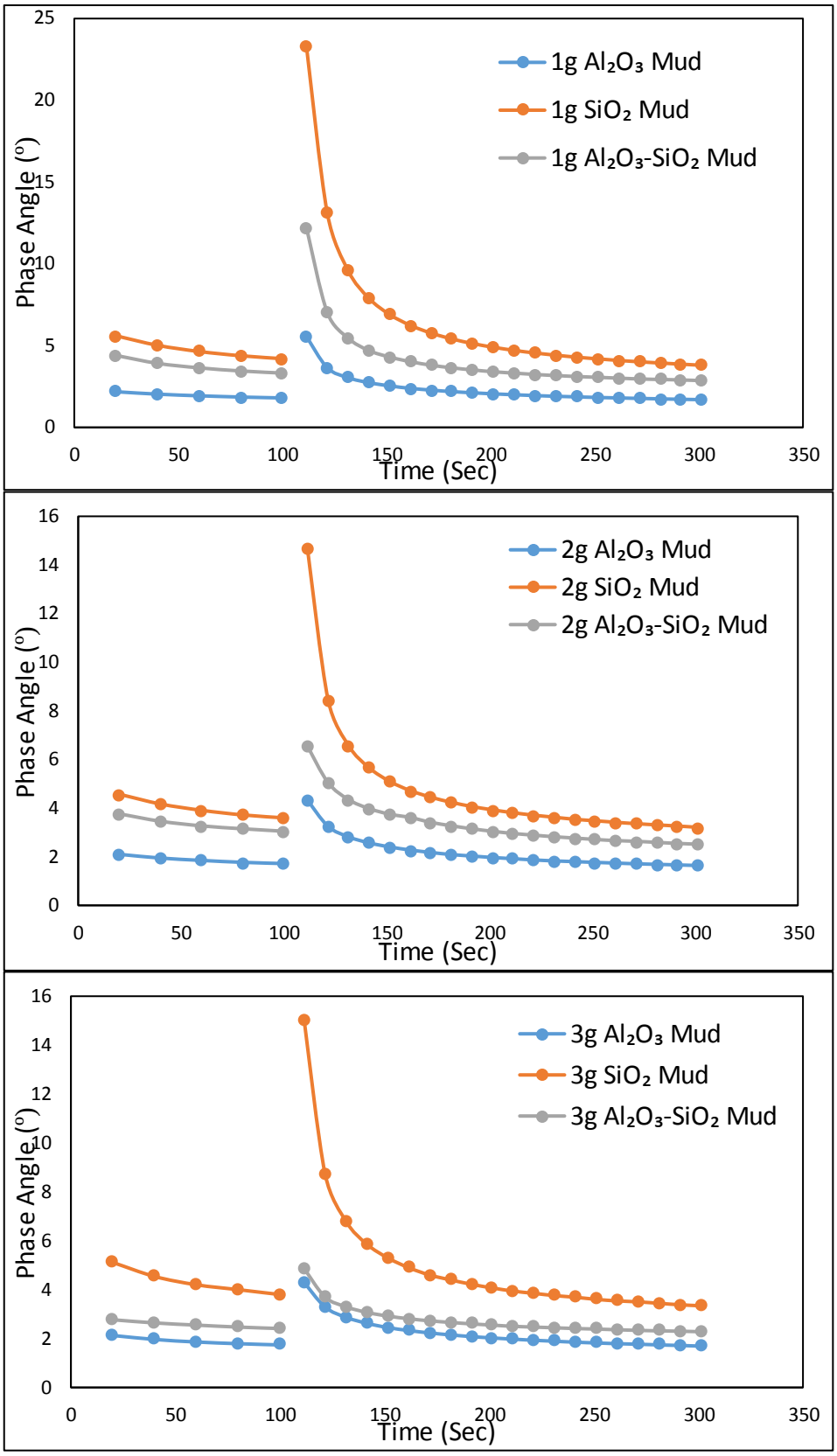

Figure 4-32 Effect of SiO_2, Al_2O_3 and SiO_2-Al_2O_3 concentration on the thixtropy (structural recovery) of the prepared drilling fluids as a function of shear rate and time.

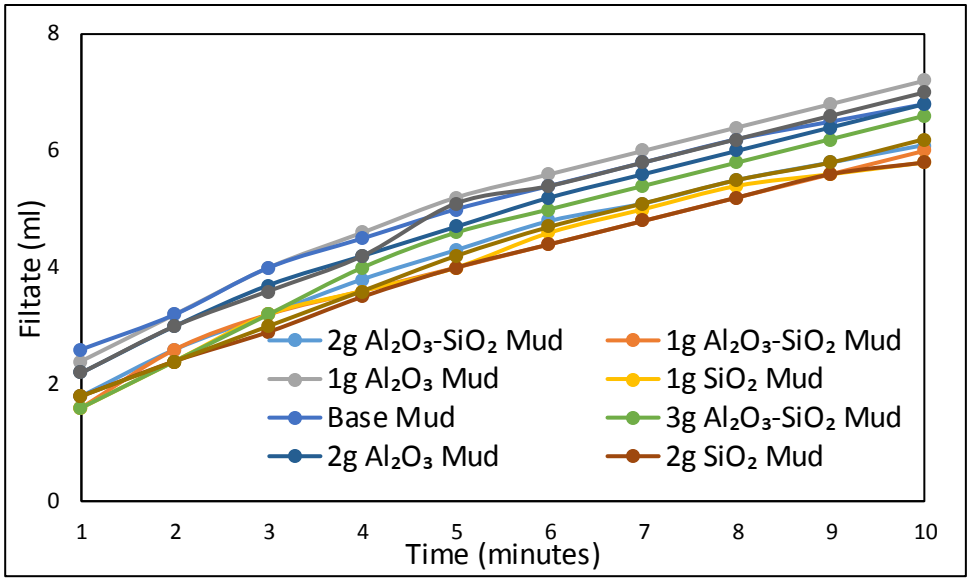

Figure 4-33 Effect of SiO_2 and Al_2O_3 combination on the thixotropy (structural recovery) of the prepared drilling fluids as a function of shear rate and time.

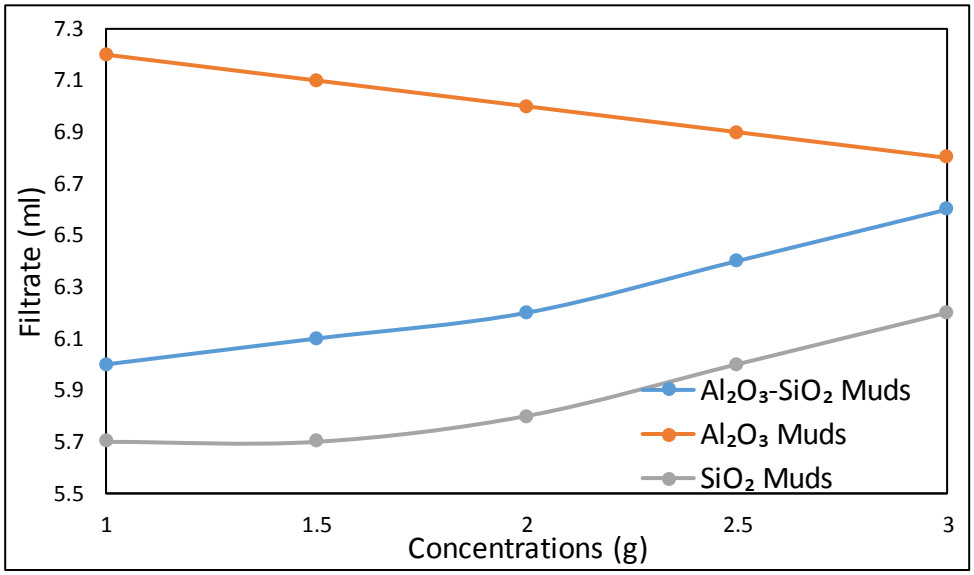

Figure 4-34 Effect of SiO_2, Al_2O_3 and SiO_2-Al_2O_3 Concentration on filtrate loss

4.4 Summary

To summarise, the aims of this chapter were to discover role of the addition of nanoparticles and to evaluate the impact of hybrid nanoparticles on the water-based drilling fluids. The Chapter has shown that the addition of single nanoparticles can improve the effectiveness of water-based mud (WBM), both

in static and dynamic situations, due to the establishment of an appropriate gel structure that can be easily broken under low shear stress. Furthermore, these nanoparticles improve the degree and the speed of the structural recovery by reducing the relaxation time, which is necessary in order to avoid the sedimentation of weighting materials and drilled cuttings. Besides, it is also observed that the nanoparticles could penetrate the porous wall of the wellbore and clog the pores, forming a thin and impermeable cake that reduces drilling fluid loss. The hybrid NPs-based fluids are compared with single NPs-based fluids and based fluid samples. The main conclusions drawn from the experimental investigations are summarised below:

- The inter-particle interaction of the nanoparticles within the bentonite platelets is the key drilling fluid property enhancement in this study.
- An important observation shown in Figures 4-1, 4-2, 4-3 and 4-4 is that the addition of Al_2O_3 NPs have greater rheological properties when compared to the CB, CNT, SiO_2 and Gr NPs.
- The addition of Al_2O_3 NPs into water-based drilling fluid promotes the attraction of positive charges on the surface of NPs, with negative charges on the face of bentonite. This attraction modifies the connection modes between the bentonite platelets (inter-particle interaction to face-to-face (F-F) and face-to-edge (F-E)). This intercalation of Al_2O_3 NPs into the interlayer space of bentonite clay endow new functional properties to the clay. This rigid clay platelet network increases the viscosity, viscoelasticity and thixotropy of the water-based drilling fluids.
- It is noted that the addition of Al_2O_3 nanoparticles increases the fluid loss quantity. The fluid loss, which increases with Al_2O_3 nanoparticles, is attributed to the increase in permeability of the filter cake due to the hero-coagulated structure. This hetro-coagulated structure forms a strong clay platelet network, which did not experience compaction during filtration testing, thus resulting in high a permeability filter cake.
- Gr, CB and SiO_2 nanoparticles reduce the filtrate loss and could not enhance the rheological properties in the same way as Al_2O_3.
- The addition of CB, SiO_2 and Gr NPs into water-based drilling fluid promotes repulsive forces between the negative charges on the

surface of NPs with negative charges on the face of bentonite. This repulsion force weakens the connection modes between bentonite platelets (inter-particle interaction to face-to-face (F-F) and face-to-edge (F-E)). This rigid clay platelet network does not increase the viscosity, viscoelasticity and thixotropy of water-based drilling fluids. This strong electrostatic repulsion prevents coagulation and the subsequent formation of a strong clay platelet network.

- The repulsion forces between the negative charges of SiO_2 and Gr NPs with negative charges on the face of bentonite ensured the drilling fluid was well dispersed (non-coagulated), thus reducing the permeability of the filter cake due to the subsequent compaction of well-dispersed drilling fluid.
- It was noted that there is an increase in rheology properties that corresponds with rising nanoparticles concentration, especially for Al_2O_3 dispersions
- The increase in nanoparticles concentration increases the carrying capacity of the drilling fluid (increase suspension capability of the cuttings) and increase the degree and the speed of the structural recovery through reducing the time required for it to be rebuilt.
- It is o observed from Figure 4-16 that; the increase in concentration of Gr nanoparticles reduces the filtrate loss of the drilling fluid and the increase in concentration of Al_2O_3 nanoparticles slightly reduces the filtrate loss of the drilling fluid.
- It is unlikely that the addition of one type of particle could improve all related features. Aiming to address these limitations, we suggest adding hybrid system of SiO_2-Al_2O_3 nanoparticles.
- The rheology and filtration properties were investigated for CB-SiO_2, CNT-Al_2O_3, SiO_2-Al_2O_3 nanoparticles-based fluids.
- The results show that the combination of two different nanoparticles type-based drilling fluids can address the limitations of using one NPs type.

5 Improving Drilling Fluid Properties using Nanoparticles and Water-Soluble Biopolymers

In this Chapter, employing nanoparticles and biopolymer as a solution to enhance the performance of water-based-drilling fluids is studied. Silica nanoparticles with different biopolymers (croscarmellose sodium, Arabic gum, Carboxymethyl Cellulose Sodium and xanthan gum) were carried out and the results of the detailed enhancement in viscosity, filtration and lubrication properties are presented. Then, different types of nanoparticles (SiO_2, CNT, CB, Gr and Al_2O_3) with xanthan gum are conducted and the outcomes regarding the performance of Al_2O_3-XG, SiO_2-XG, CB-XG, Gr-XG and CNT-XG based drilling fluids are presented.

5.1 Effect of Biopolymer Type

The rheology and filtration properties of different drilling fluids based Crscarmellose sodium (CS), Arabic gum (Ag), Carboxymethyl Cellulose Sodium (CMC) and xanthan gum (XG) and base muds were investigated with a view to choose the best biopolymer for drilling fluid application. Figure 5-1 shows the rheological properties (AV, PV, YP, 10 sec gel strength and 10 min gel strength Croscarmellose sodium, Arabic gum, Carboxymethyl Cellulose Sodium and xanthan gum and base muds). The finding highlights that xanthan possesses higher rheological properties when compared to other biopolymers and base drilling fluids.

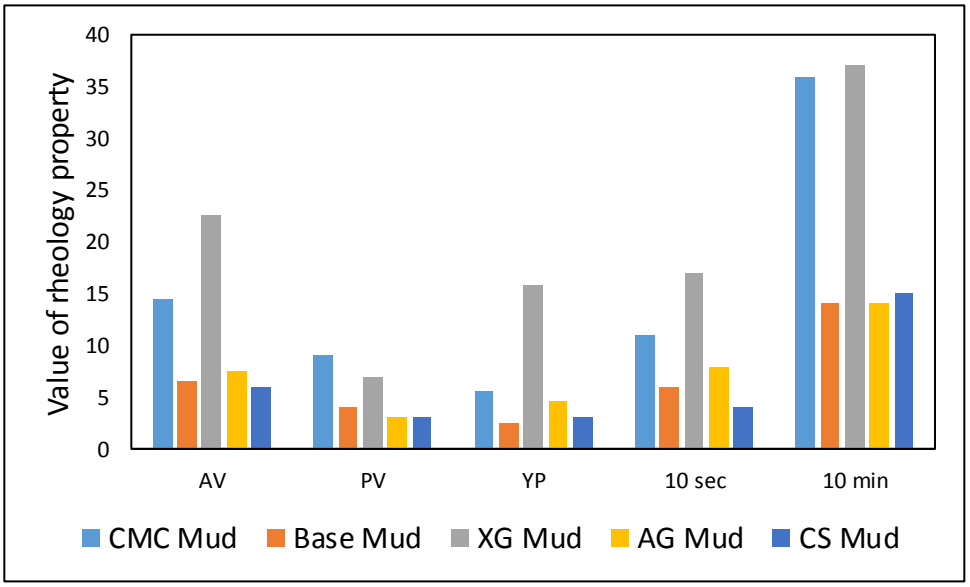

Figure 5-1 Rheological properties of biopolymers and base muds

The filtrate loss results provide additional evidence that xanthan is better than other polymers for application of drilling fluids. As presented in Figure 5-2, the filtrate loss of xanthan mud is 5.8ml while in a base mud of 9.4ml, 8.2 for CS mud and 6.8 for Ag mud.

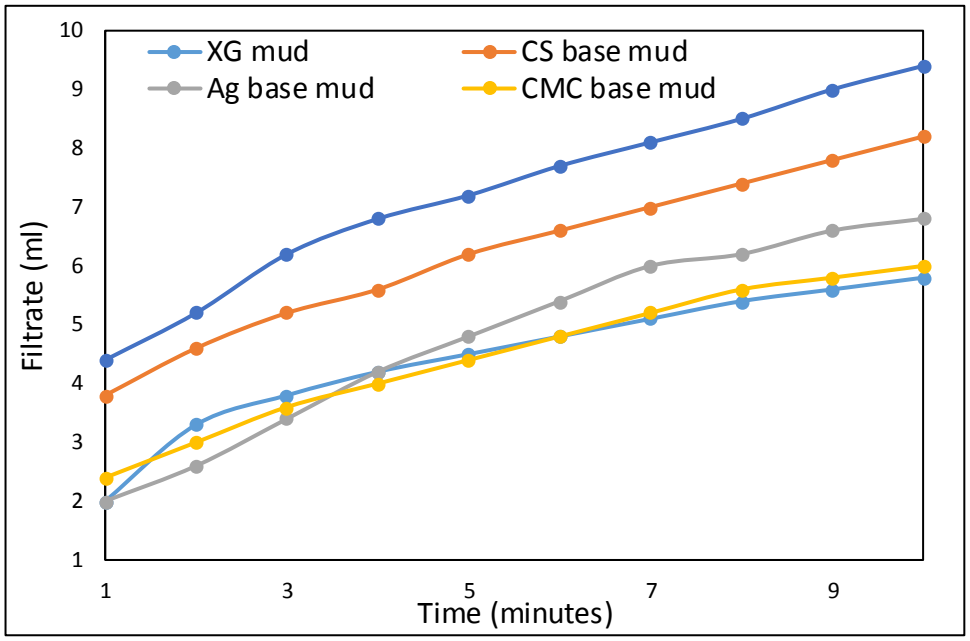

Figure 5-2 Filtration properties of biopolymers and base muds

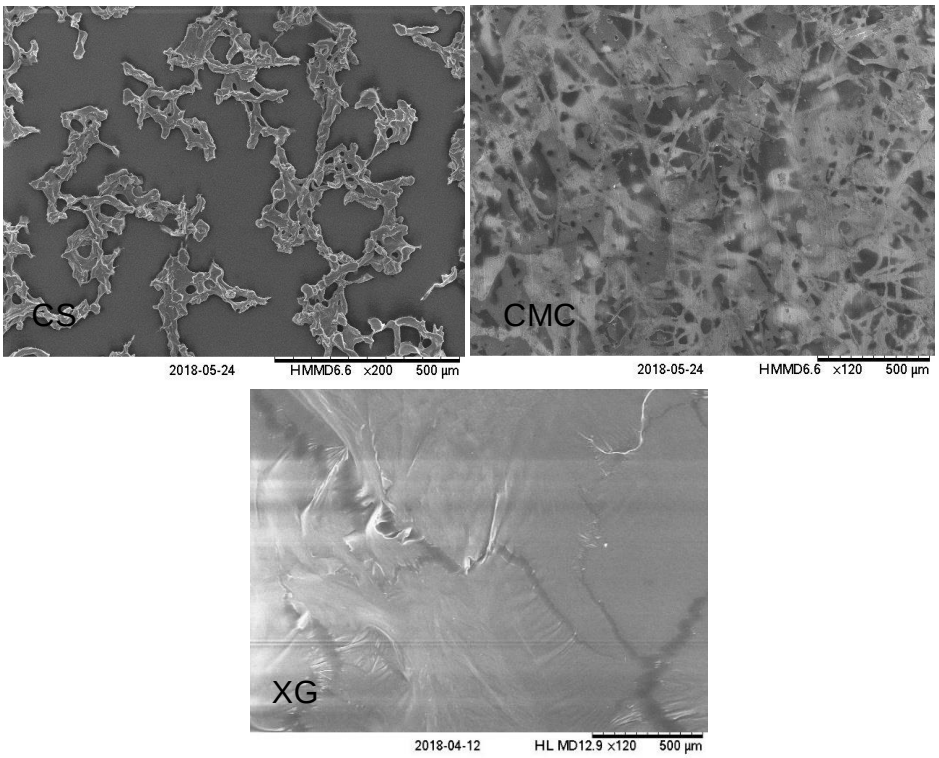

Figure 5-3 SEM Images of CS, CMC, and XG Biopolymers

The morphological structure of these polymers was investigated to find how each polymer matrix connected. It is evident from Figure 5-3 that the XG

polymer matrix has a fibrous nature, a slightly better structure than CMC and a much better structure than CS. This explains the rheology and filtration results that have been obtained. The filtration properties enhancement through adding 1g of silica nanoparticles to these polymers drilling was also investigated. The results of this are shown in Figure 5.4. It's clear that the addition of silica nanoparticles reduces the filtrate loss for all polymers as well as for the base drilling fluid. Nevertheless, xanthan gum offered superior enhancement. Hence, different types of nanoparticles, along with xanthan gum, will be considered as recipes to improve drilling fluid performance.

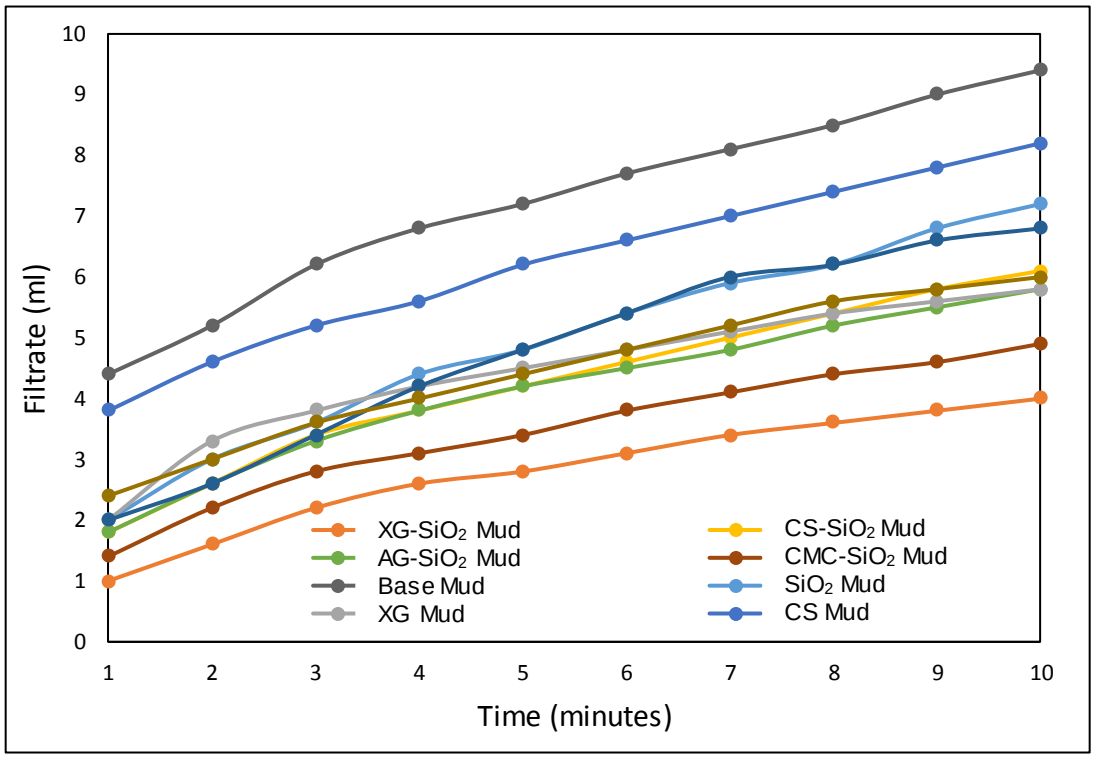

Figure 5-4 Effect of SiO_2 nanoparticles addition on filtrate loss

5.2 Micro and Chemical Structure of prepared Nanofluids

The SEM images of the SiO_2 XG, CB XG, CNT XG, Al_2O_3 XG and GR XG nanofluids and XG polymer are shown in Figure 5-5. The SEM images show the fibrous polymer matrix of the xanthan gum, and bridges between the polymer structures. The SEM analysis of the dried SiO_2-xanthan fluid allows us to distinguish between the xanthan polymer and the SiO_2 nanoparticles. The distribution of the nanoparticles and their orientation, as well as the aggregation of nanoparticles, can clearly be observed in the SEM of the SiO_2-

xanthan. The morphology of CNT, CB and Gr nanoparticles with xanthan has been altered from their morphology alone due to the interaction between polymer and graphitic material [120]. The X-ray and FTIR were used to indicate the interaction between the xanthan gum and the nanoparticles.

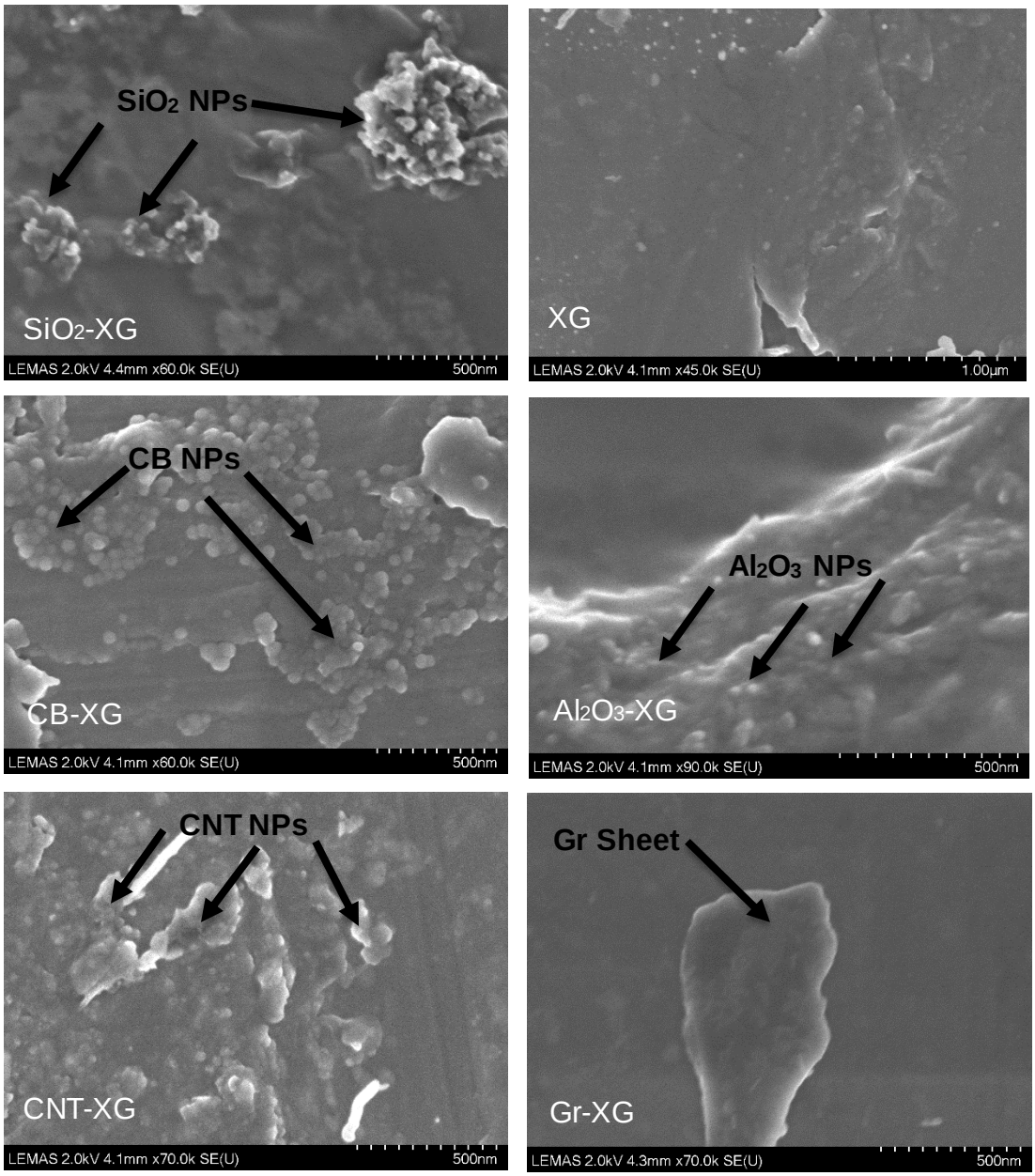

Figure 5-5 Scanning electron micrographs of (a) the SiO_2-XG, XG, CB-XG, Al_2O_3-XG, CNT-XG and Gr-XG

The crystal structure of 11 samples of nanofluids (XG, SiO_2, SiO_2 XG, CNT, CNT XG, Al_2O_3, Al_2O_3 XG, CB, CB XG, Gr and Gr XG) are shown in Figure 5-6 to Figure 5-11. Based on the SiO_2 XRD pattern, the characteristic diffraction broad peak centred on 22° (2θ) and its amorphous nature was confirmed

[121]. The Xanthan XRD pattern shows two peaks focused on 20 and 37° (2θ). The presence of the peaks centred at 22° (2θ) and 37° (2θ) in the SiO_2-Xanthan XRD pattern confirmed the mineralogical compositions of the prepared nanofluid.

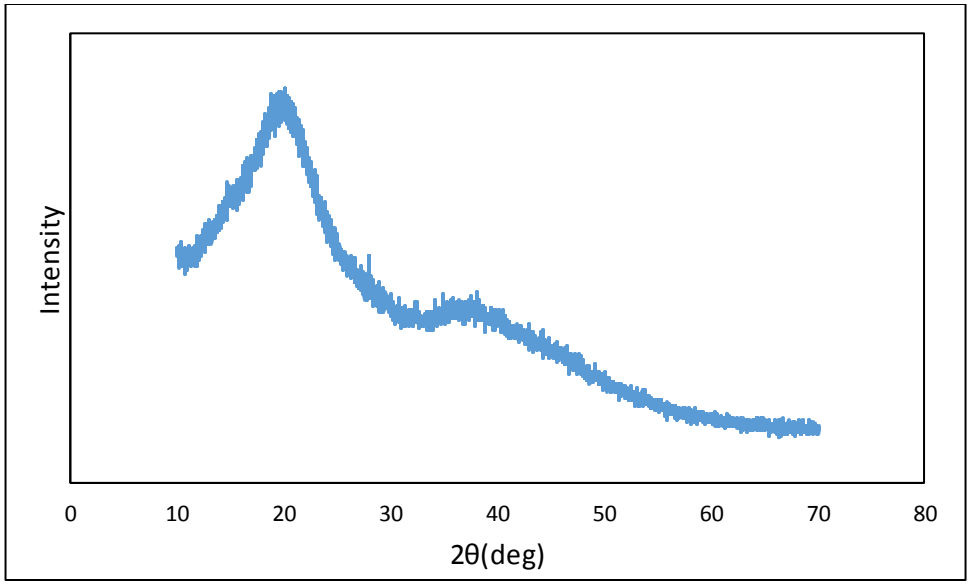

Figure 5-6 XRD Pattern for xanthan gum

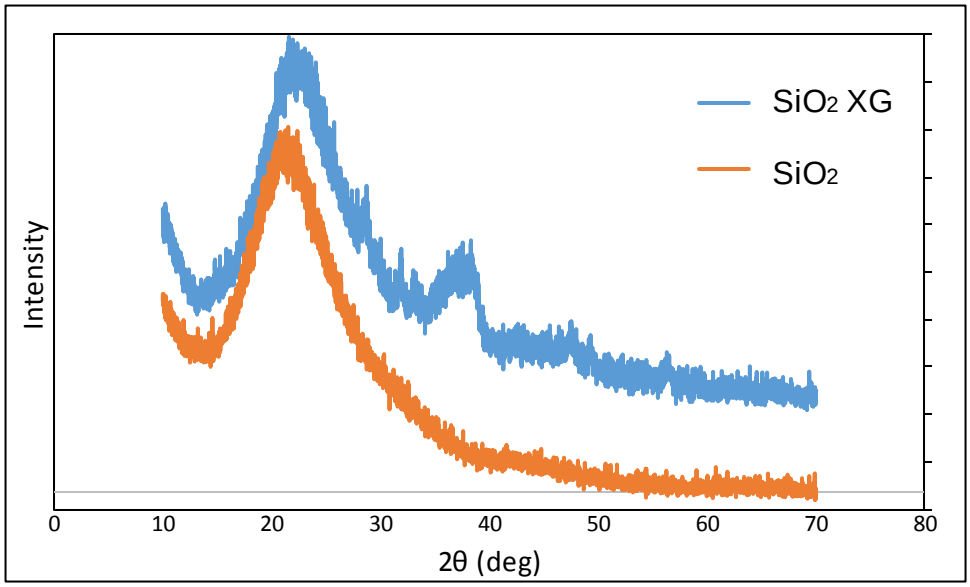

Figure 5-7 XRD Patterns for SiO_2 and SiO_2 XG

The XRD patterns of CNT, CNT XG nanofluid are presented in Figure 5-8. The sample CNT displays a well resolved and sharp peak at 2 θ = 25.3°, which could be indexed as (002) plane of the hexagonal graphite structure. The other characteristics diffraction peaks of MWCNT at 2 θ = 43.5° and 53°

are associated with (100) and (004) planes of graphitic structure in MWCNT, respectively [122-126]. The broad diffraction band between 13° to 29° in Figure 5-8 can be assigned to the amorphous nature of XG. However, the diffractogram obtained for CNT XG presents a broad diffraction band, adjacent to (002) plane of the hexagonal graphite structure, which is associated with the amorphous nature of XG. The incorporation of CNT could be observed with reduced intensity, indicating an interaction between the XG polymer matrix and CNT NPs.

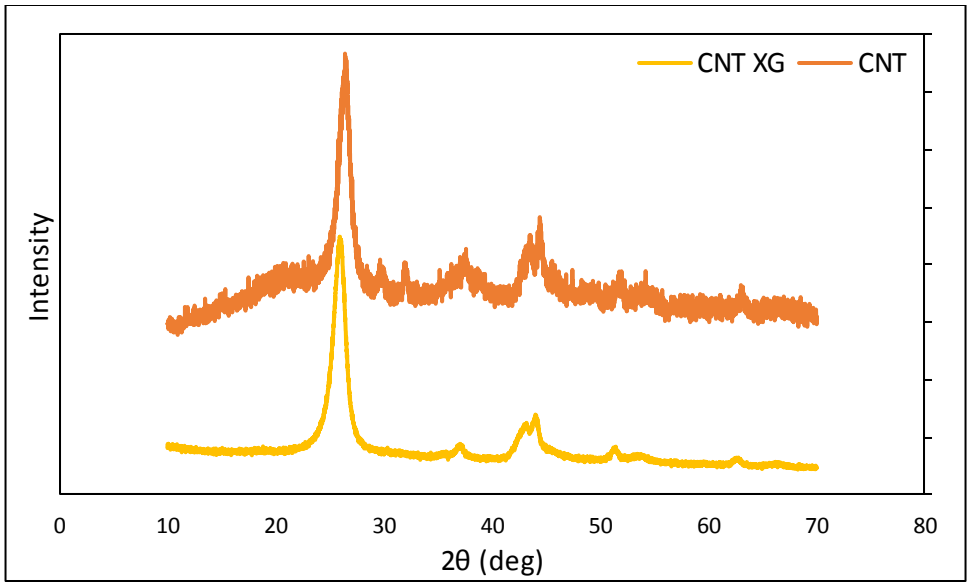

Figure 5-8 XRD Patterns for CNT and CNT XG

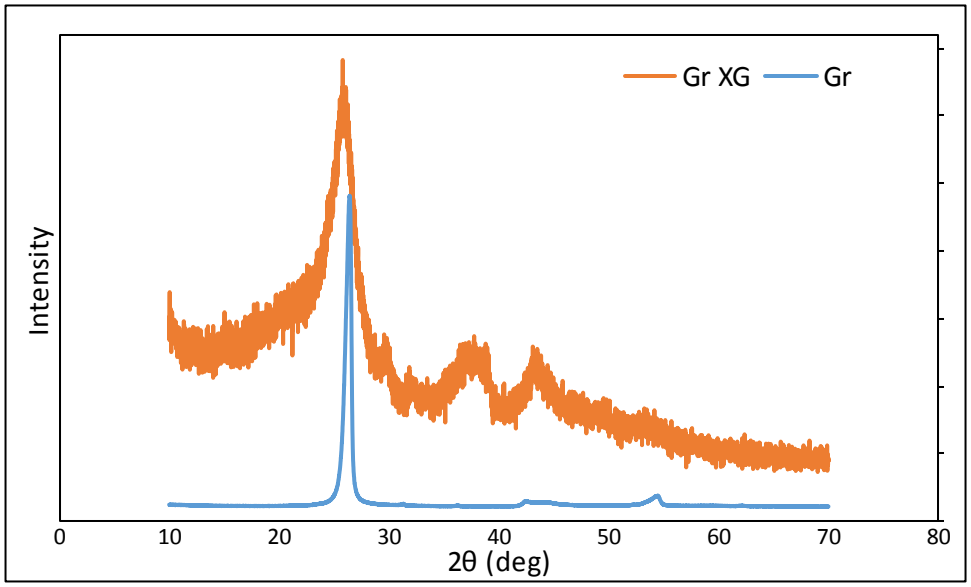

Figure 5-9 XRD Patterns for Gr and Gr XG

The X-ray diffraction patterns of Gr and Gr XG are presented in Figure 5-9. The XRD pattern of graphite shows a characteristic peak at 2θ= 26.5° corresponding to the plane of the hexagonal graphite structure. Also, the graphite XRD pattern exhibit another peak at 2θ= 54.7°, which represents the (004) planes of the graphitic structure. The broad diffraction band between 10° to 25° in Figure 5-9 can be allocated to the amorphous nature of XG. However, the diffractogram obtained for Gr XG presents a broad diffraction band, adjacent to (002) plane of the hexagonal graphite structure, which is associated with the amorphous nature of XG.

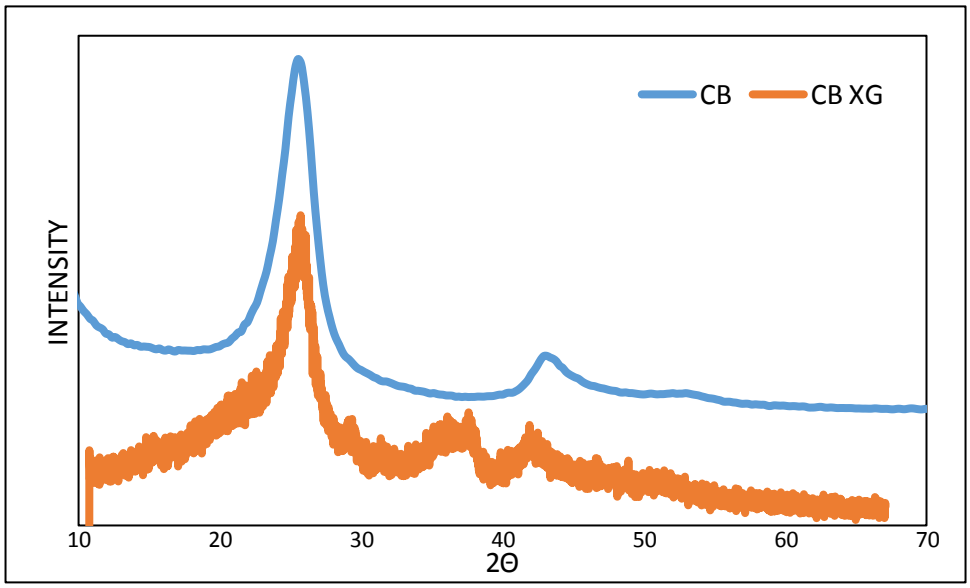

Figure 5-10 XRD Patterns for CB and CB XG

The XRD patterns for the carbon black nanoparticles and carbon black/xanthan are exhibited in Figure 5-10. The XRD pattern of carbon black shows two peaks at 2θ= 25.7° and 2θ= 43.4°, which are attributed to (002) and (100) planes [127]. The interaction of the XG polymer matrix with carbon black was the same as CNT XG and Gr-XG through the association of (002) plane with the amorphous nature of XG.

Figure 5-11 shows the crystalline phase of the Al_2O_3 nanoparticle and Al_2O_3 XG nanofluid. It shows the existence of the gamma (γ) and delta (δ) phases. The recorded diffraction pattern matches with the combined JCPDS patterns of γ -Al_2O_3 (JCPDS 10-0425) and δ-Al2O3 (JCPDS 00-016-0394). The crystal characteristics are: γ -Al2O3: cubic and δ-Al2O3: tetragonal. The XRD pattern of Al_2O_3 exhibited peaks at 2θ at 20, 22, 32, 33, 35, 37, 39, 40, 46, 62, and 67, which were respectively assignable to the diffraction of the (111), (220), (311),

(222), (400), (511) and (440) planes of Al_2O_3 nanoparticles. The XRD pattern of Al_2O_3 XG shows the associated between the amorphous XG and γ -Al_2O_3.

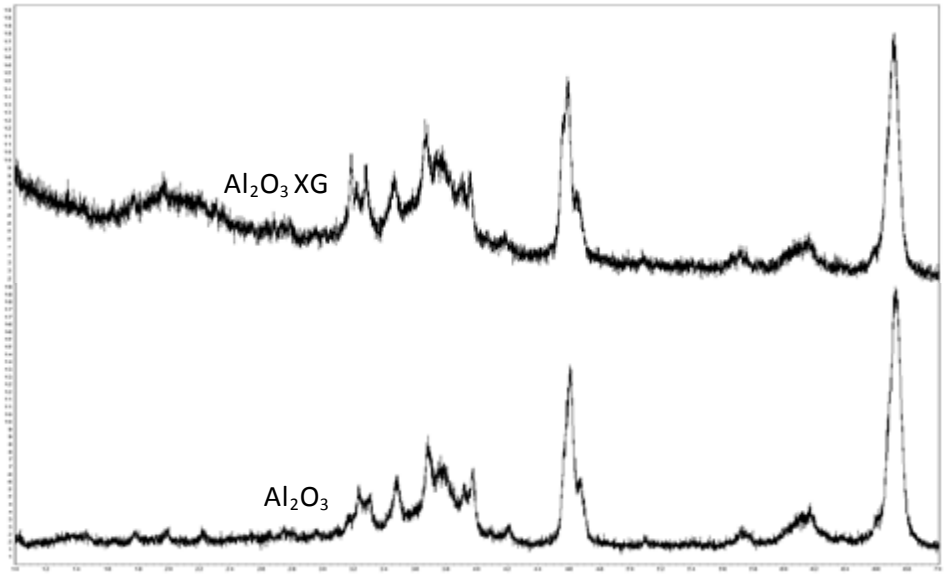

Figure 5-11 XRD Patterns for Al_2O_3 and Al_2O_3 XG

The presence of nanoparticles in the polymer matrix was investigated via the FTIR spectra. The FTIR spectrum of Xanthan, SiO_2, and SiO_2-Xanthan nanofluid are shown in Figure 5-12. In the spectrum of xanthan, the peaks from 2500 to 3300 and 3423 cm^{-1} are attributed to stretching vibrations O−H [128]. The peaks at 1423 to 1622 cm^{-1} are assigned to stretching vibrations of the COO− group [129, 130]. The presence of a peak at 1047 cm^{-1} corresponds with the acetyl group and the peak at 1724 cm^{-1} is due to the C−O axial deformation [131].

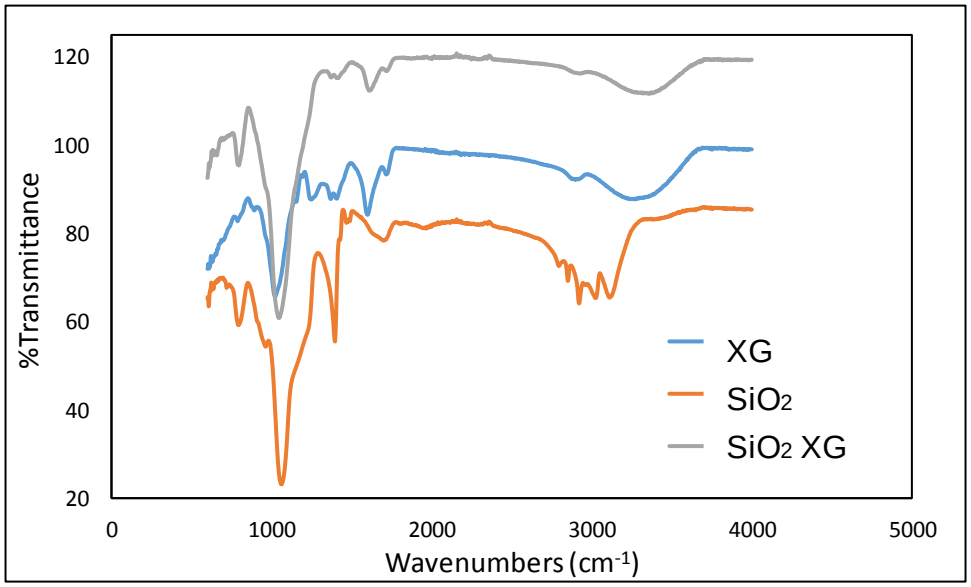

Figure 5-12 FTIR Spectra of XG, SiO_2 and SiO_2 XG

For SiO_2 nanoparticles, the peak of 1047 cm^{-1} is attributed to the Si-O-Si stretching. The peaks of 1375, 1415 and 3355 cm^{-1} correspond to hydrogen boned- O-H groups. Si-OH-Si bending vibration is observed at 796cm^{-1} . The presence of the peaks of 1048 and 790 cm^{-1} in the SiO_2-xanthan spectrum indicate the formation of SiO_2-Xanthan nanofluid. Also, the disappearance of some xanthan peaks with SiO_2-xanthan indicate the participation of xanthan in the formation of the silica nanoparticles.

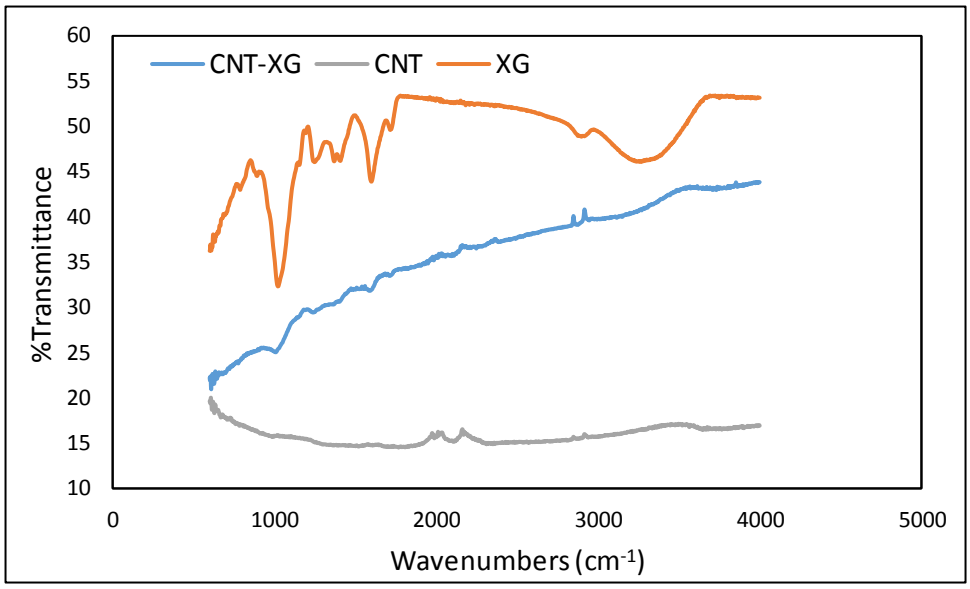

Figure 5-13 FTIR Spectra of XG, CNT and CNT XG

The FTIR spectrum of Xanthan, CNT, and CNT-Xanthan nanofluid are shown in Figure 5-13. For CNT nanoparticles, the presence of hydroxyl groups and carbonyl groups corresponds to the appearance of broad peaks at 3443 cm^{-1} and 1602 cm^{-1}, respectively [132]. The peaks of 2851 and 2960 represent symmetric and asymmetric C-H stretching of methyl and methylene groups. The spectral peaks at 2200 and 2075 are attributed to C=C stretching bond of the alkynes molecule. The presence of peaks 3443, 2960, 2851, 2200, 2075, 1622, 1423 cm^{-1} in the CNT-xanthan spectrum indicate the formation of a CNT-Xanthan nanofluid. Also, the disappearance of some xanthan peaks with CNT-xanthan indicate the participation of xanthan in the formation of the CNT.

The FTIR spectrum of Xanthan, Gr, and Gr-Xanthan nanofluid are shown in Figure 5-14. Many functional groups can be introduced in graphite nanoparticles, which have a peak of around 3413 cm^{-1} arising from the O-H stretching vibrations and a peak of nearly 1807 cm^{-1} of carboxyl C=O, approximately 1629 cm^{-1} of C-C groups. In addition, there is a peak of nearly 1407 cm^{-1} of C-H, and 1110 cm^{-1} of C-O. The peak at 2960 cm^{-1} indicates that the asymmetric C-H is stretching the methylene groups and the peak at 1614

cm^{-1} arises from C=C stretching symmetric. Meanwhile, in the spectrum of Gr-XG, most of the characteristic peaks of XG and Gr appeared with slightly less intensity than the peaks of pure Gr and XG.

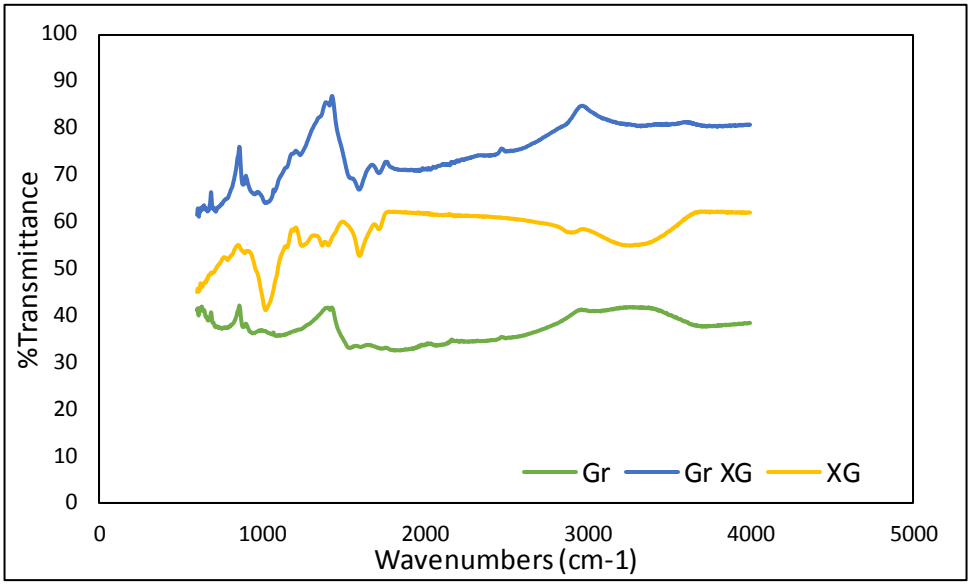

Figure 5-14 FTIR Spectra of XG, Gr and Gr XG

Figure 5-15 shows the FTIR spectra of XG, CB and CB XG. In all spectra, a peak of 2946 cm^{-1} is seen, which is attributed to the asymmetric C-H stretching of the methylene groups. For CB, the peak of 1785 cm^{-1} is assigned to the C=O stretching of the COOH group and 1437 cm^{-1} is assigned to C-O stretching [133]. The peak of 1550 cm^{-1} is attributed to the hydroxyl groups or the carbonyl groups [134] and the peak of 1670 cm^{-1} is ascribed to the C=C stretching vibration [135]. The peak of 1087 cm^{-1} is attributed to C−O stretching. Meanwhile, in the spectrum of CB-XG, most of the characteristics peaks of XG and CB appeared with slightly less intensity than the peaks of pure material, which indicates an interaction between carbon black nanoparticles and xanthan gum. Also, the disappearance of some xanthan peaks with CB-xanthan indicate the participation of xanthan in the formation of the CB.

The FTIR spectrum of Xanthan, Al_2O_3, and Al_2O_3-Xanthan nanofluid are shown in Figure 5-16. For Al_2O_3 nanoparticles, the *γ-Al_2O_3* structure was considered a hydrogen spinel between 3110 and 3310 cm^{-1} and the complex Al-O infrared absorption band between 1100 and 350 cm^{-1} as shown in Figure 5-16. The presence of Al_2O_3 nanoparticles in the polymer matrix was observed at a peak in wave number of 752 cm^{-1}, which is Al-O functional groups of the alumina particles.

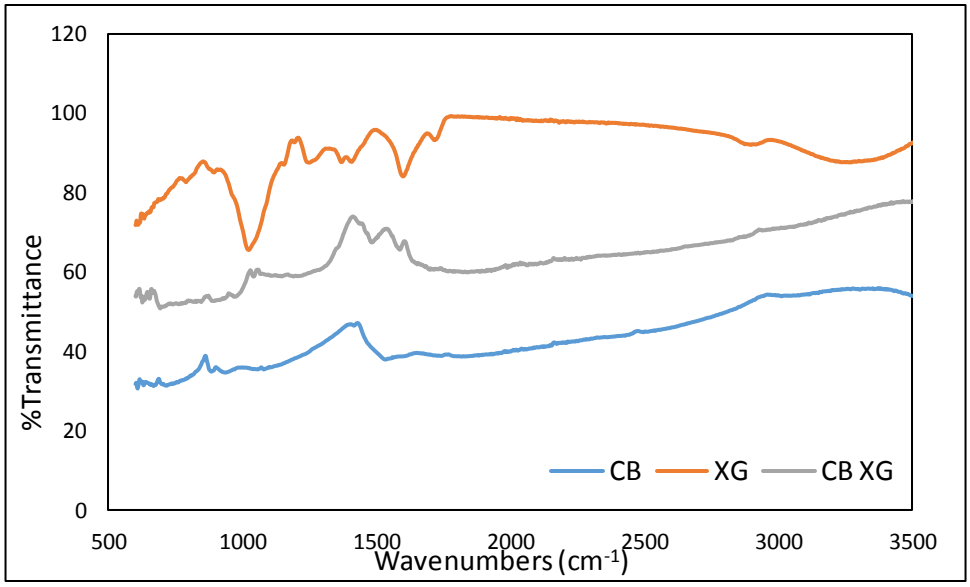

Figure 5-15 FTIR Spectrum for XG, CB and CB-Xanthan.

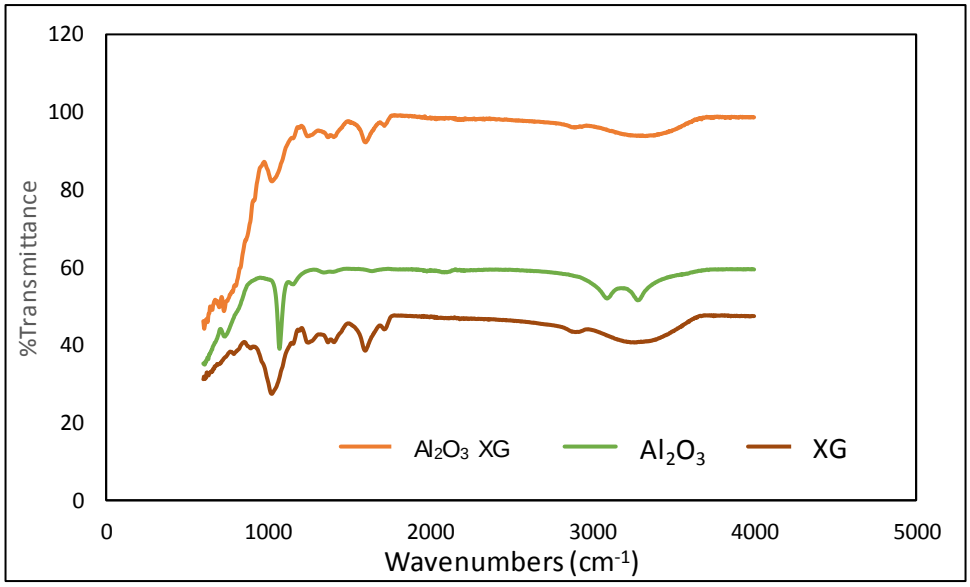

Figure 5-16 FTIR Spectrum for XG, Al_2O_3 and Al_2O_3-XG.

The TGA curves of the XG gum, SiO_2 XG, Al_2O_3 XG, CNT XG, Gr XG and CB XG fluids are presented in Figure 5-17. Three temperature stages were chosen to simulate the downhole temperature environments, such as the elevated temperature (ET) range (0 °F to 300°F), high temperature (HT) range (300 °F to 400 °F), and ultra HT range(400 °F to 500 °F) in the wells [136]. It is clear from the TGA results that the weight loss percentage of all nanofluids with a temperature increase is lower than the xanthan gum. This means that the addition of these nanoparticles to the xanthan polymer enhanced the

thermal stability of the nanofluid. This could be due to the incorporation of the nanoscale dispersement of the nanoparticles and the xanthan polymer matrix. The TGA curve of xanthan gum shows three stages of decomposition. The first decomposition of about 11% weight loss occurred under 130°C, which was due to the desorption of water. The second degradation of xanthan gum occurred at about 283°C. The rate of weight loss increased when the temperature increased. Nearly 65% of weight loss occurred at this stage, then, the rate of weight loss reduced to around 69% at 400°C.

The CNT-Xanthan exhibit similar behaviour to CB XG and Gr XG. Approximately 4% weight loss occurred under 130°C, which was due to desorption of water. Nearly 27% weight loss occurred at 330°C; then, the rate of weight loss reduced. The total weight loss of the xanthan gum in the range of 30°C to 500°C was 87%, while the total weight loss for CNT XG nanofluid was around 32%. The TGA curve of Al_2O_3 XG nanofluid has shown a high resistance to temperature. It can be observed that the total weight loss percentage of Al_2O_3 XG nanofluid is 14%. The behaviour of SiO_2 XG is the same as Al_2O_3 XG, but with a higher loss. The total weight loss of SiO_2 XG is around 48%. These results show that the nanofluid has a worthy characteristics of temperature resistance. If we exclude the first degradation of all samples due to the presence of moisture in the samples, the CNT XG, CB-XG, Gr-XG, SiO_2 XG and Al_2O_3 XG nanofluids show one stage of decomposition, while the XG fluid shows two stages. These results agree with previous studies regarding thermal stability enhancement caused by nanofluids [60, 91, 137].

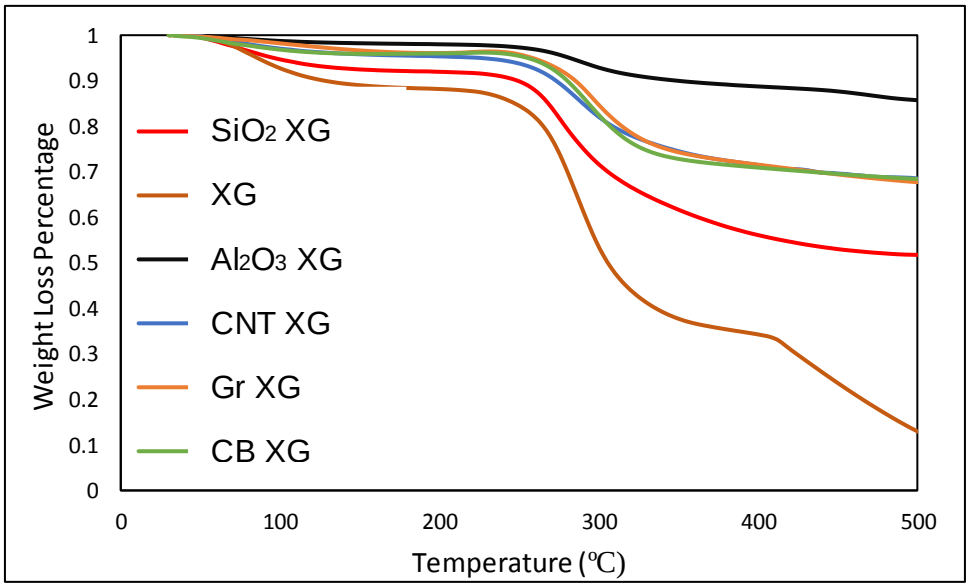

Figure 5-17 TGA Curves for Xanthan, SiO_2-XG, Al_2O_3-XG, CNT-XG

5.3 The Effect of Nanofluids on Drilling Fluid Rheology Properties

Drilling fluid rheology is a crucial property that impacts different significant elements of the drilling operation. The most significant rheological properties are apparent viscosity, plastic viscosity, yield point and the gelling properties of the fluid. These rheological parameters are notably present in nanofluid based drilling fluids. The effect of nanofluid on the rheological parameters, namely plastic viscosity, apparent viscosity, yield point and gelling properties of the developed drilling fluid formulations is shown in Figure 5-18.

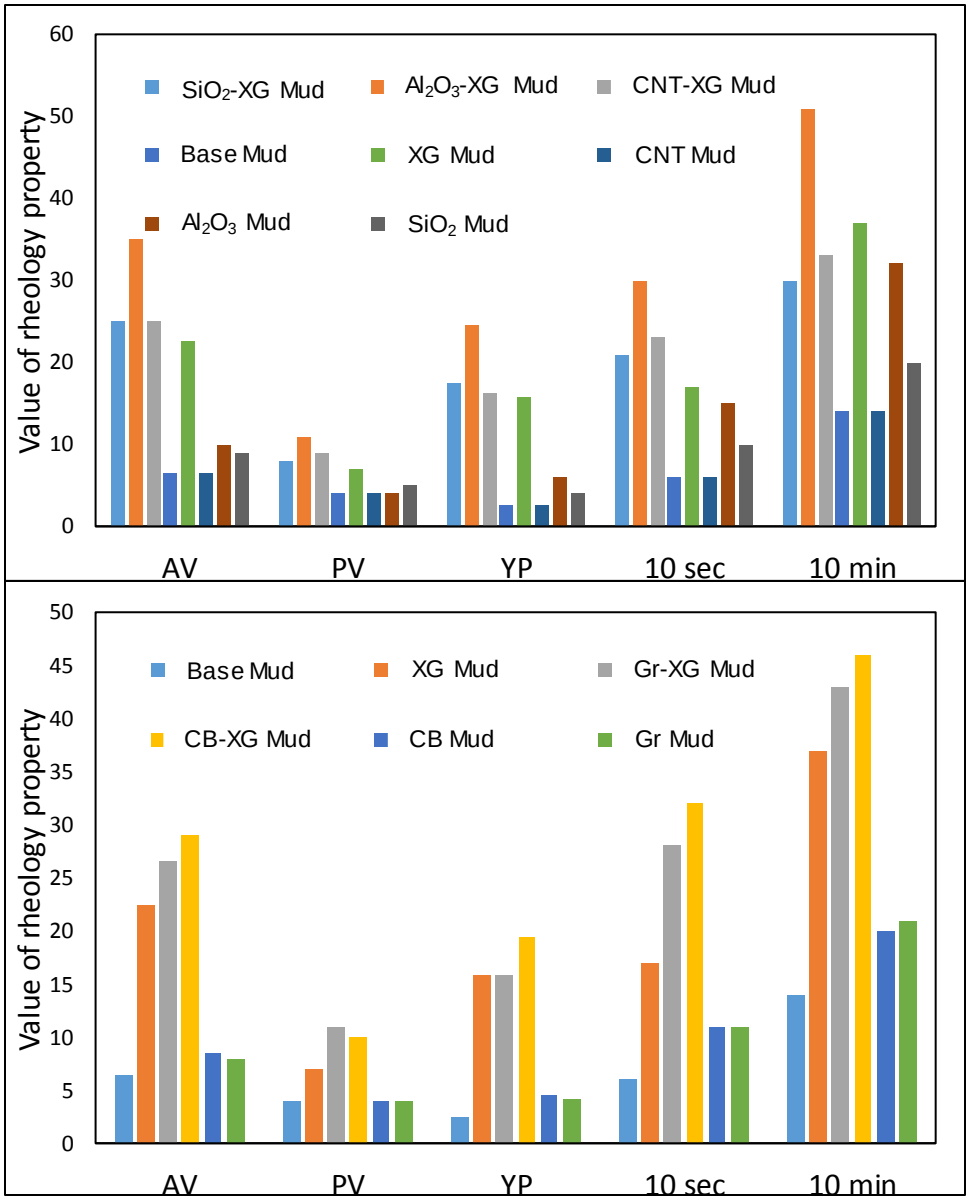

Figure 5-18 Rheological properties of prepered drilling fluids

Figure 5-18 shows the influence of SiO_2, CNT, Al_2O_3, Gr and CB nanoparticles, along with SiO_2-XG, CNT-XG, Al_2O_3-XG, Gr-XG and CB-XG on apparent viscosity, plastic viscosity, yield point and the gelling properties of the fluid compared to the regular water-based drilling fluid. It is observed that both plastic and yield point increases with the addition of polymers and nanofluid. This is due to the presence of nanofiller chain joiner points that post viscosity increasing and flexible segments of the biopolymer in the polymer matrix. The drilling fluids apparent viscosity has increased with the addition of Al_2O_3, SiO_2, CB and Gr NPs to around 10, 9, 8.5 and 8 sequentially (as explained in the previous chapter). On the other hand, the apparent viscosity remains at the same value with the addition of CNT NPs. Therefore, it's obvious that addition of alumina NPs has the highest apparent viscosity, followed by silica then Carbon black and graphite. However, the addition of NPs-XG does not provide the same role as NPs addition. The addition of Al_2O_3-XG, CB-XG, Gr-XG, CNT-XG and SiO_2-XG increase the apparent viscosity to 35, 29, 26.5, 25 and 25 (respectively), while it increase by 22 with XG alone. It is clear that the combination of NPs-XG exhibits better apparent viscosity than NPs and XG alone. Also, carbon NPs-XG (CB-XG, Gr-XG and CNT-XG) show superior apparent viscosity than SiO_2-XG, while the addition of SiO_2 NPs demonstrated better apparent viscosity than CB, Gr and CNT NPs. This attributed to good carbon NPs-XG interaction as shown previously in the FTIR and XRD analysis.

In addition, the yield point has increased with the addition of Al_2O_3, SiO_2, CB and Gr NPs to around 6.132, 4.088, 4.599 and 4.088 respectively, however it does not change with the introduction of CNT NPs. The addition of Al_2O_3-XG, CB-XG, Gr-XG, CNT-XG and SiO_2-XG increase the yield point to 24.5, 19.4, 15.8, 16.35, 17.37 and 15.8 for XG alone. It is obvious that the combination of NPs-XG display a better yield point than NPs and XG alone.

Gel strength is also a significant property, since it measures the ability of the drilling fluid to hold the drill cuttings in suspension. Experimentally, it was observed that the NPs-XG WBM also exposed appropriate gel strength both at 10 sec and 10 min. The 10 sec gel strength of water-based drilling fluid was 6 pa, which increased to 10 pa with the addition of 1g of SiO_2 nanoparticles. Furthermore, 21pa was achieved with the addition of SiO_2-XG. Likewise, the addition of 1 g of Gr, CB, CNT and Al_2O_3 increase the gel strength to 11,11,6, 15 respectively, whereas the addition of Gr-XG, CB –XG, CNT-XG and Al_2O_3-XG increase the gel strength to 28, 32, 23 and 30 respectively. The reason behind this enhancement could be that the nanoparticles work as chain joiner

points between the polymer matrixes, which support the gelation behaviour of nanofluid drilling fluid [23]. In the same way, the 10 min gel strength of water-based drilling fluid was 19pa, which increased with 1 g of SiO_2 nanoparticles to 20pa. Furthermore, 35pa was achieved with the addition of nanofluid. It is therefore evident from the results that synthesised nanofluid has a relatively higher effect on the rheological parameters of the developed drilling fluid system than the xanthan polymer and the nanoparticles.

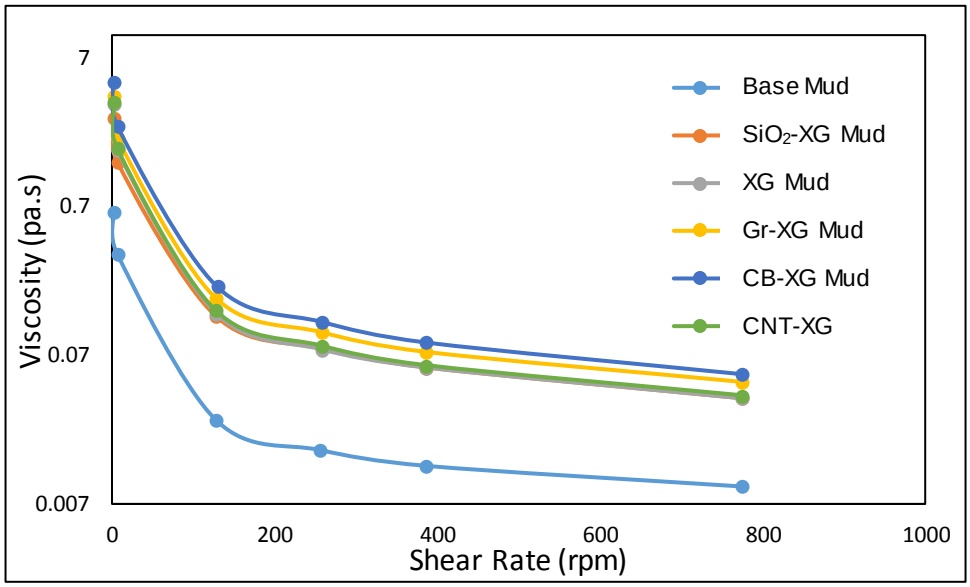

Figure 5-19 Viscosities of the prepared NPs-XG drilling fluids samples

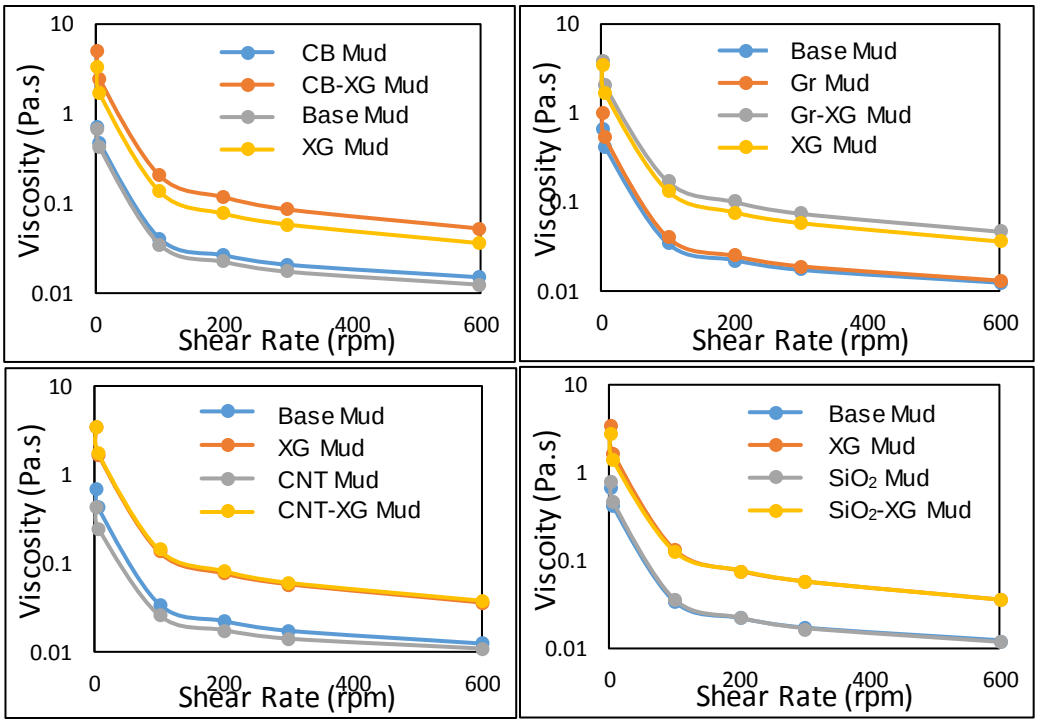

Figure 5-20 Viscosities of the prepared drilling fluids samples

Viscosity affects the efficiency of hole cleaning. Thus, it is evident from Figure 5-19 and Figure 5-20 that the rheological properties of water-based drilling fluids slightly increases with 1g addition of each SiO_2, CNT, Al_2O_3, Gr and CB nanoparticles and sharply increases with the addition of 1g of xanthan polymer. As a result, the rheological properties dramatically increase with the introduction of nanofluid. The viscosity increasing behaviour of xanthan polymer is normal because its works as a Viscosifier, while with different nanofluids, the nanoparticles work as chain joiner points that support the increase in viscosity. In order to support this hypothesis, FTIR spectroscopy was used to check whether there were some potential bonding effects formed between nanoparticles and xanthan. Also, scanning electron microscopy (SEM) was employed to examine the intermolecular interaction between the polymer matrix and the nanoparticles. Both the FTIR and SEM results support the hypothesis in terms of why rheological properties increase with the addition of nanoparticles.

Viscoelasticity tests were carried out to investigate the impact of NPs-XG on the strength of drilling fluid suspension. Figure 5-21 shows that CB-XG, Al_2O_3-XG and Gr-XG have a better structure than xanthan. This strength in fluid structure can be attributed to increase in interaction strength related to the synergy effect between both NPs and xanthan polymer. The laboratory results also discovered that the addition CB-XG, Al_2O_3-XG and Gr-XG develop the thixotropic properties of drilling fluids more significantly when compared to the addition of XG.

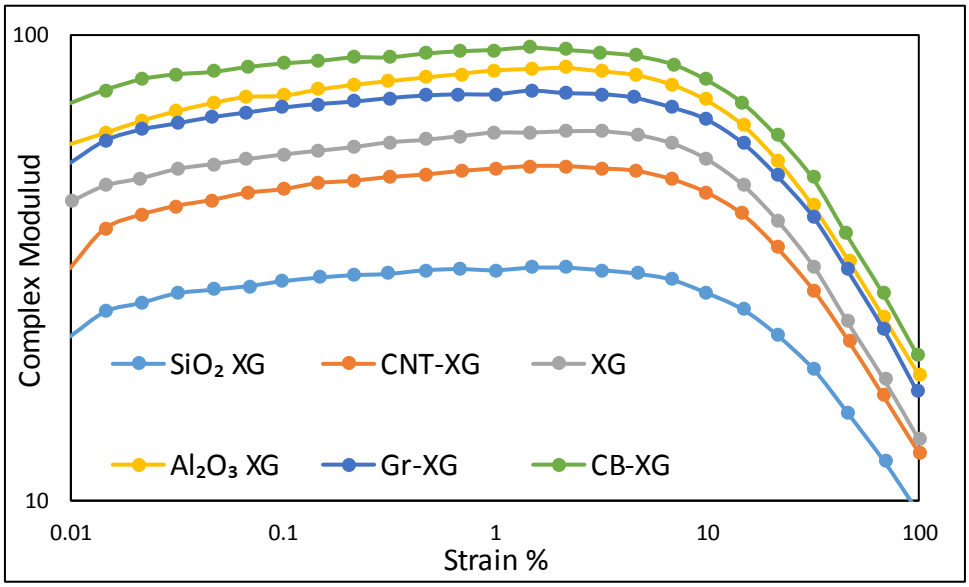

Figure 5-21. Yield points of the prepared drilling fluids samples

Apparent tendency in Figure 5-22 in accordance with the aforementioned results in Figure 5-21, confirms that CB-XG, Al_2O_3-XG and Gr-XG provides more elastic behaviour to the drilling fluid and increases the degree and the speed of the structural recovery by reducing the time required for rebuilding. As can be observed from Figure 5-21, the phase angle decreases from 11.7° for XG to 10.6º for Gr-XG then to 9.67º for CB-XG. In addition, there is a clear reduction in rebuilding time. The required rebuilding time for CB-XG is 50 secs and 90 secs for Gr-XG, while it is 110 secs for Al_2O_3-XG and 150 secs for xanthan.

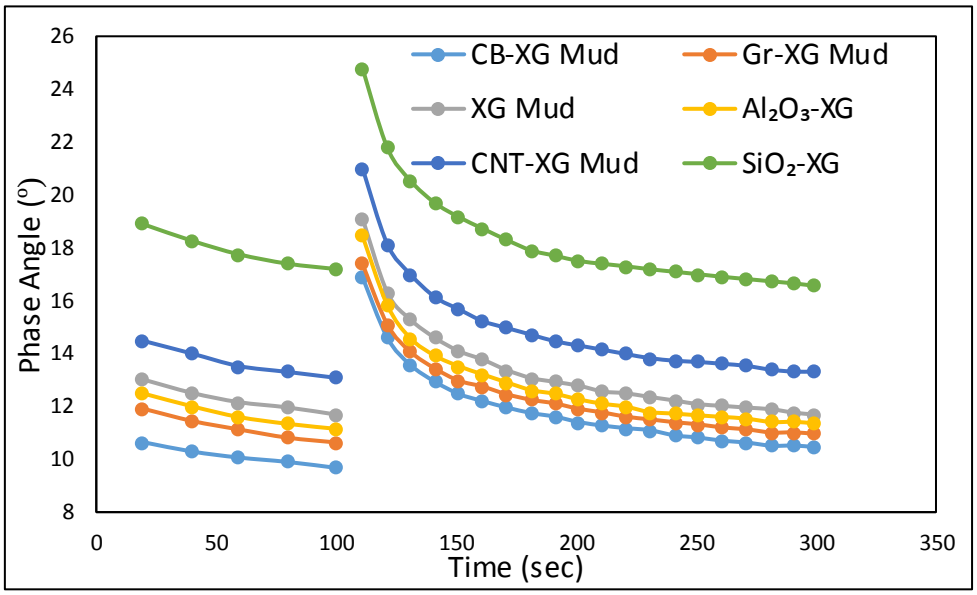

Figure 5-22 Effect of NPs-XG on the thixotropy of drilling fluids

5.4 The Effect of NPs-XG Nanofluids on Fluid Filtration Properties

Figure 5-23 shows the influence of SiO_2, CNT, Al_2O_3, Gr and CB nanoparticles and SiO_2-XG, CNT-XG, Al_2O_3-XG, Gr-XG and CB-XG on the filtrate volume compared to the conventional water-based drilling fluid. It can be obseved that the addition of different nanoparticles with xanthan gum decreases the filtrate volume. The results show that the combination of different NPs and Xanthan polymer exhibits better reduction in filtrate loss volume than the addition of NPs and Xanthan polymer alone. Even CNT XG demonstrated a better reduction than CNT and XG alone. As it is obvious from the below Figure that the addition of CNT alone increases the filtrate loss, whereas the addition of CNT XG decreases the filtrate loss due to the presence of dispersed CNT; it acts as a plaster between the polymer particles and seals the permeable mud

cake, which reduces the filtrate loss [138]. Micro-Nano particles in NPs-xanthan nanofluid drilling fluid could bridge together under the polymer matrix molecular chain, which in turn could block the matched micro-pore. Thus, it improves rheological and filtration properties. The above results indicate that NPs-xanthan nanofluid was an efficient filtrate loss reducer. The filtration properties also depend on NPs size and shape, which explains the difference between the NPs-XG nanofluids' filtrate loss results.

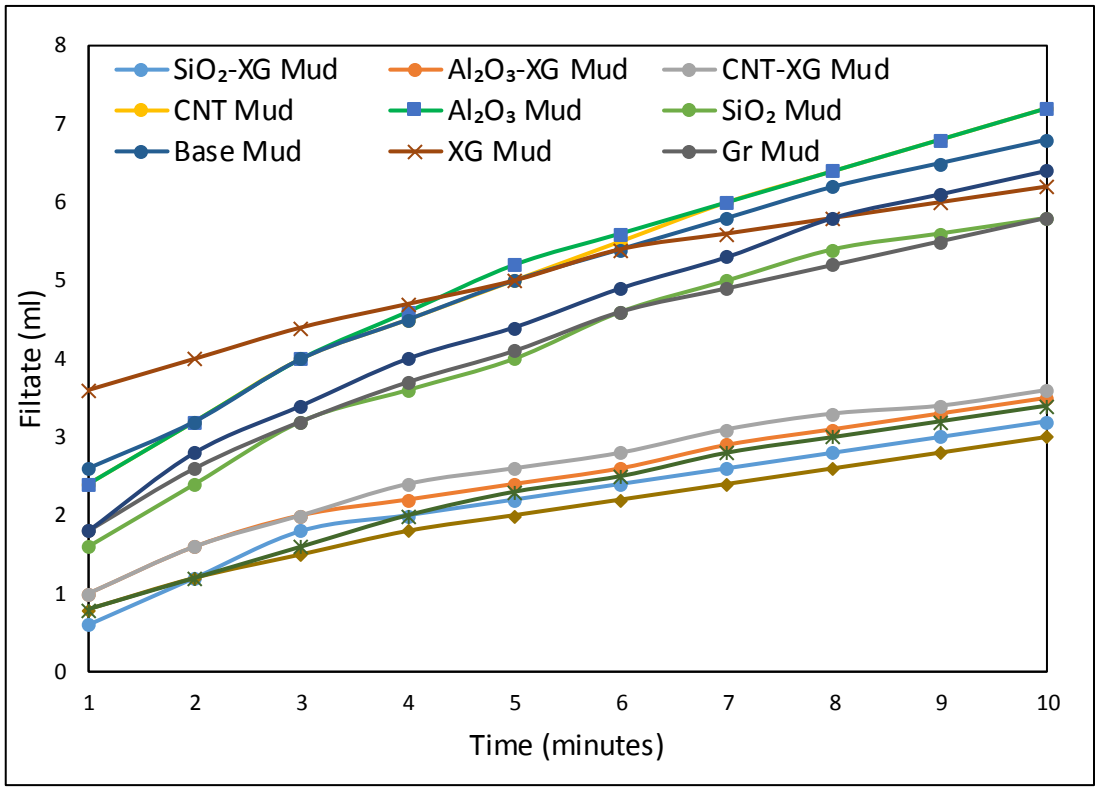

Figure 5-23. Filtrates of the prepared drilling fluids samples

5.5 The Effect of NPs-XG Nanofluids on Fluid Swelling Behaviour

Figure 5-24 displays the expansion quantity meter results reported for the sodium bentonite shale when exposed to four different drilling fluids: fresh water, XG, SiO_2-XG, CNT-XG, Al_2O_3-XG, Gr-XG and CB-XG nanofluid. After 16hr exposure to these systems, the SiO_2-XG nanofluid shows less than 4% expansion and 2.8% expansion for Gr-XG occurred to the bentonite. Nevertheless, about 13% expansion occurred to the bentonite with fresh water in 16 hours. The experimental outcomes confirm that the shale swelling of the water-based drilling fluid is brought down to less than 2.8% in the presence of the Gr-XG nanofluid. The enhancement in the shale inhibition is to be

observed from about 13 to 10 with xanthan, due to the polymer matrix plugging the void space and repelling water molecules in order to absorb into the bentonite [139]. On the other hand, the addition of different nanoparticles reduce the swelling percentage, which is because of nanoparticles' potential to plug the Nano pores of clay, which in turn prevents shale swelling [140]. It's appears that the bentonite absorbed less amount of water in the nanofluid system to achieve the expansion, because of the synergetic properties of nanoparticles and the polymer, and this behaviour weakens the clay swelling and enhances the shale strength.

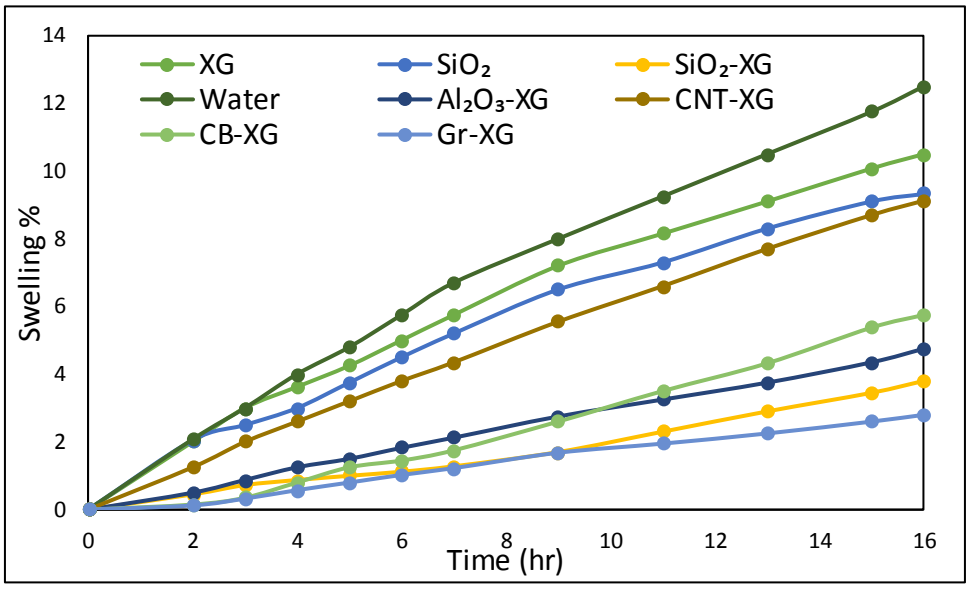

Figure 5-24. Swelling Percentage of Sodium Bentonite Exposed to Fresh Water and prepared drilling fluids

5.6 Summary

Employing nanoparticles and biopolymers as a solution to enhance the performance of water-based-drilling fluids was investigated in this Chapter. The rheology and filtration properties of different drilling fluids based on Croscarmellose sodium (CS), Arabic gum (Ag), Carboxymethyl Cellulose Sodium (CMC) and xanthan gum (XG) and base muds were investigated to choose the best biopolymer for drilling fluid application. It shows that Xanthan has higher rheological properties compared to other biopolymers and base drilling fluids. The filtrate loss results provide additional evidence that xanthan is better than other biopolymers for the application of drilling fluids. As shown

in Figure 5-2, the filtrate loss of xanthan mud is 5.8 ml, while for base mud 9.4ml, 8.2ml for CS mud and 6.8ml for Ag mud. The results show that the combination of different NPs and Xanthan polymer exhibited better reduction in filtrate loss volume than the addition of NPs and Xanthan polymer alone. The main conclusions drawn vie the experimental investigations are summarised below:

- The rheological and filtration properties depend on NPs-Polymer interaction, which explains the difference between NPs-XG nanofluids filtrate loss results.
- SiO_2-XG WBM exposes appropriate gel strength both at 10 sec and 10 min. The 10 sec gel strengths for water-based drilling fluid was 7pa, which increases with 1g of SiO_2 nanoparticles to 10pa. Furthermore, 23pa was achieved with the addition of nanofluid. The reason behind this enhancement could be that the nanoparticles work as chain joiner points between the polymer matrixes, which support the gelation behaviour of nanofluid drilling fluid. Likewise, the same is true for other NPs-XG recipes.
- Even CNT XG showed better reduction than CNT and XG alone. As it is obvious from the Figure 4-5 that the addition of CNT alone increases the filtrate loss, whereas the addition of CNT-XG decreases the filtrate loss due to the presence of dispersed CNT, which acts as a plaster between the polymer particles and seals the permeable mud cake to reduce the filtrate loss.
- The bentonite absorbs less water in the nanofluid system in order to achieve expansion, because of the synergetic properties of nanoparticles and polymer; this behaviour weakens the clay swelling and enhanced the shale strength.

6 Corrosion and Erosion-Corrosion Control of Drill Pipe by using Nanoparticles and biopolymer

This chapter presents the experimental results of the measurement of the corrosion and erosion-corrosion rate of carbon steel API X-95 drill pipe specimens in drill cuttings/a water-based-drilling fluid system. The corrosion rate in a reservoir-like environment under both static and dynamic conditions is investigated, along with and the influence of wellbore conditions, including temperature, pressure, and the salinity of water-based drilling fluids. Then, the erosion-corrosion rate in cuttings/water systems at different sizes (0.841,1.7, 3.3) and different concentrations (5%, 10%, 15%) actual drill cuttings are presented. Finally, The erosion-corrosion rate at SiO_2-XG nanofluid (NPs with xanthan) is discussed with a view to support the applicability of nanofluids in control erosion-corrosion in solid-fluid systems.

6.1 Effect of Temperature and Pressure on Corrosion Rate

Experiments were performed to investigate the effects of temperature and pressure on the corrosion rate values of carbon steel. For temperature tests, experiments were performed at 50 bar pressure and 100 rpm. Four temperature values (20 °C, 45 °C, 70 °C and 95 °C) were studied to ascertain the consequences of temperature on corrosion rates. The data from Figure 6-2 show that temperature has a significant impact on corrosion rates. The corrosion rate increased by nearly four times when the temperature increased from 20 °C to 95 °C. An increase in the temperature evidntly accelerates all reactions, thereby accelerating the diffusion rate of the O_2 species. Therefore, corrosion rate values increased because more O_2 species transport from the bulk and react at the surface [141-144].

In contrast, for the pressure test, experiments were performed at a constant temperature of 25 °C and a rotation speed of 100 rpm. Figure 6-1 shows the effect of pressure on the corrosion rate. An increase in pressure has a negligible impact on the corrosion rate values when compared with temperature. It is believed that an increase in pressure affects corrosion by increasing the solubility of O_2. In addition, an increase in pressure indicates

an increase in the O_2 concentration. Thus, more species react at the surface [145].

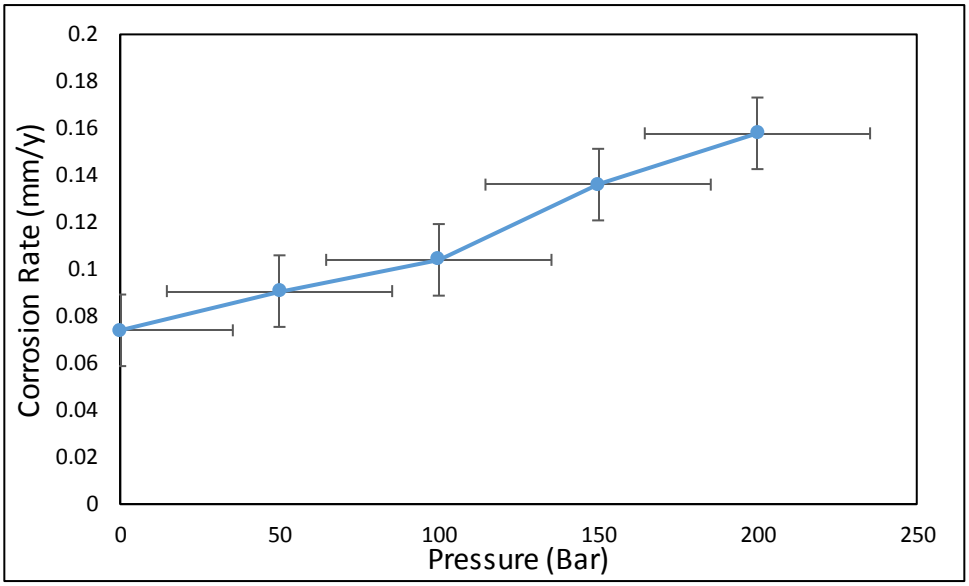

Figure 6-1 Effect of pressure on corrosion rate (50 bar and 100 rpm)

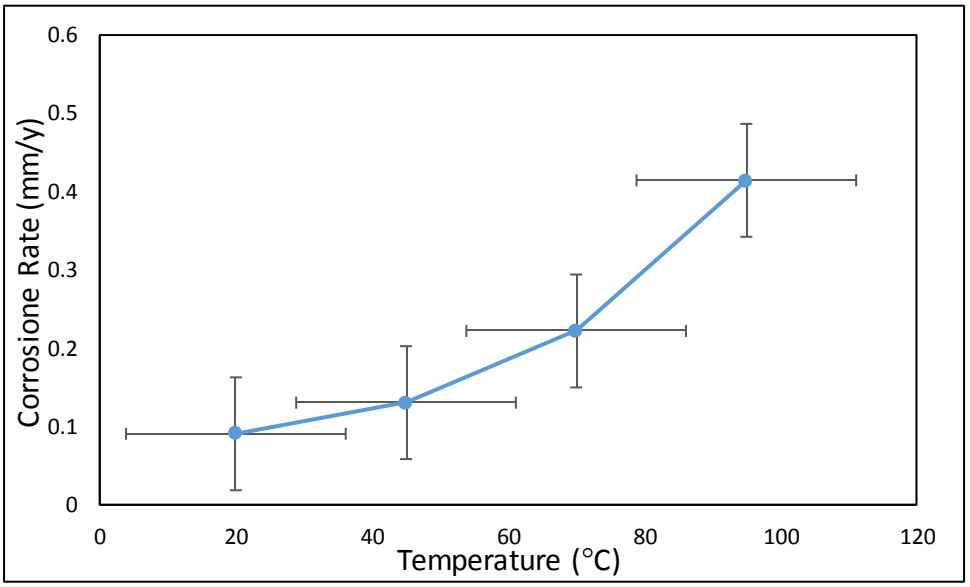

Figure 6-2 Effect of temperature on corrosion rate

6.2 Effect of Rotation Speed on Corrosion Rate

Figure 6-3 shows variations in the corrosion rates with the drill-string rotation speed at both ambient temperature and pressure. The corrosion rate gradually increases with an increase in rotation speed, which promotes high turbulence and causes effective mixing, leading to an increased O_2 transport rate and corrosion rate. In contrast, an increase in rotation speed can reduce the thickness of the water boundary layer next to the metal surface. This thin boundary layer allows dissolved O_2 to corrode the steel surface [146]. Thus, the experimental results show that the corrosion rate is increased fourfold (approximately) when the rotation speed increased to 600 rpm.

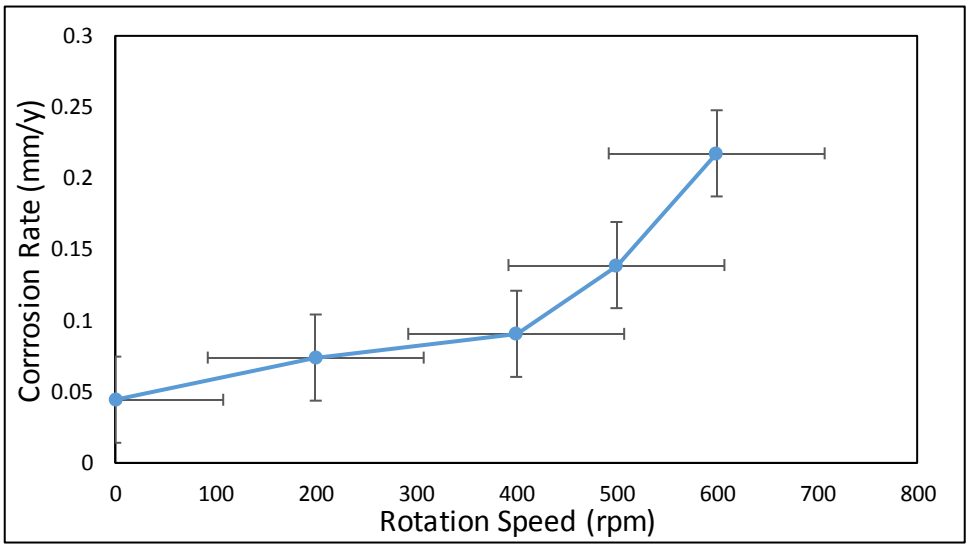

Figure 6-3 Effect of rotation speed (in rpm) on corrosion rate

At a high speed of 600 rpm, to distinguish between the mass transfer and erosion effects using the chemical composition of the particles, a deaerated erosion test was performed to determine the amount of metal loss by the drilling fluid at both ambient temperature and pressure. It is believed that a high particle velocity increases the erosion rate [147-149]. However, the weight loss measurement shows that the corrosion rate from erosion is considerably small, i.e. up to 0.004633 mm/year. These results confirm that the main source of corrosion is the dissolved species rather than the erosion caused by the drilling fluid chemicals. Figure 6-4 shows the SEM images before and after the erosion test (600 rpm; 1 bar; 20 °C). The SEM images in Figure 6-4 show that there is no change in the surface texture after the pure erosion test. In addition, it is evident that there is no apparent wear or cracks

on the metal surface, indicating that the erosion caused by the drilling fluid is negligible.

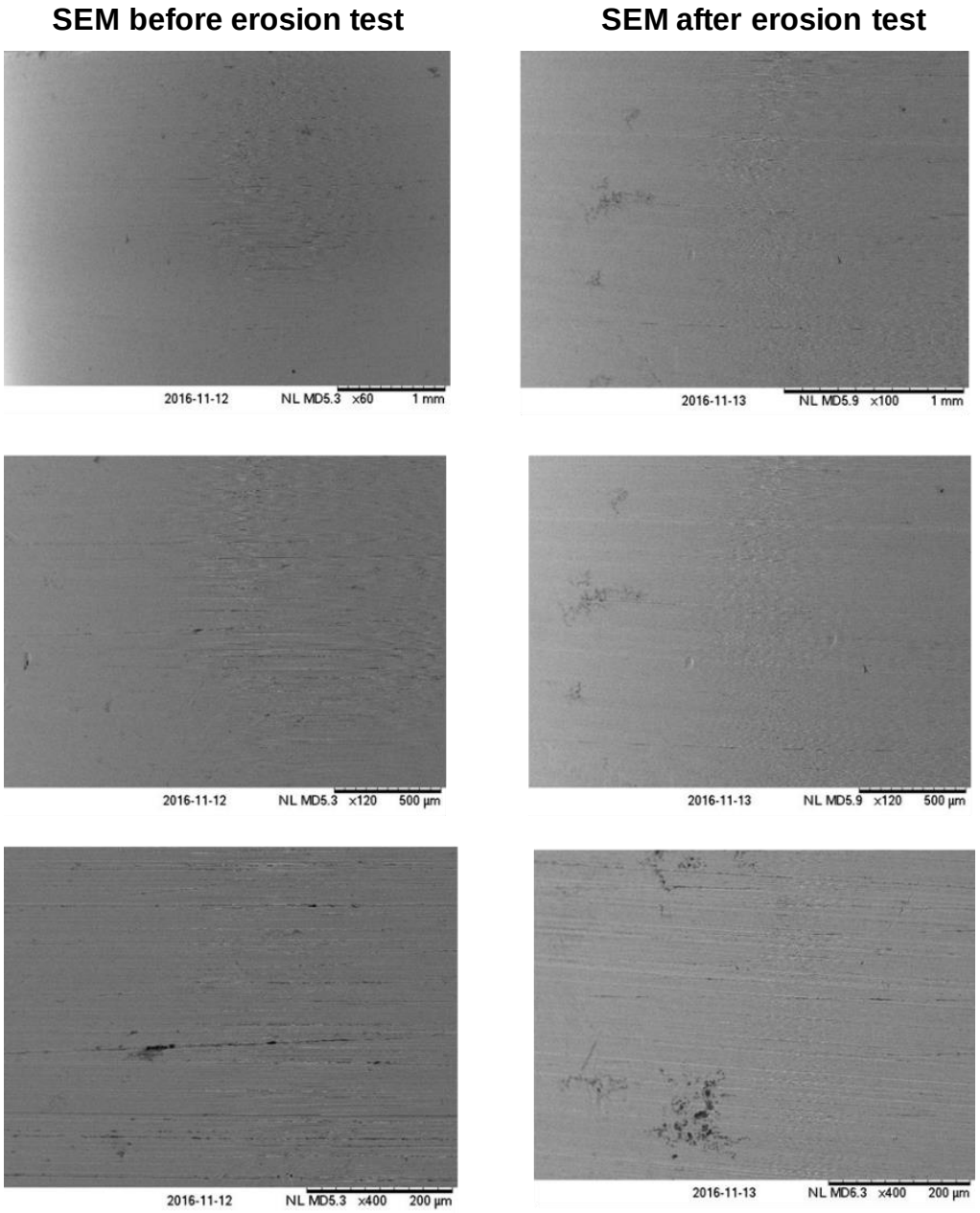

Figure 6-4 Scanning electron microscopy (SEM) images before and after the pure erosion test to indicate if there any wear or cracks on the metal surface caused by drilling fluid.

6.3 The Effect of Salinity Concentration on Corrosion Rate

The variations in the corrosion rates with the drilling fluid salinity at ambient temperature and pressure, at a constant rotation speed of 400 rpm, are shown

in Figure 6-5. It is evident from Figure 6-5 that the corrosion rate decreases with an increase in the salinity concentration. This occurs because a higher concentration of NaCl causes an increase in the fluid's density and viscosity. In addition, a high NaCl concentration increases the ionic strength, which decreases the amount of dissolved O_2 present in the system [52, 150].

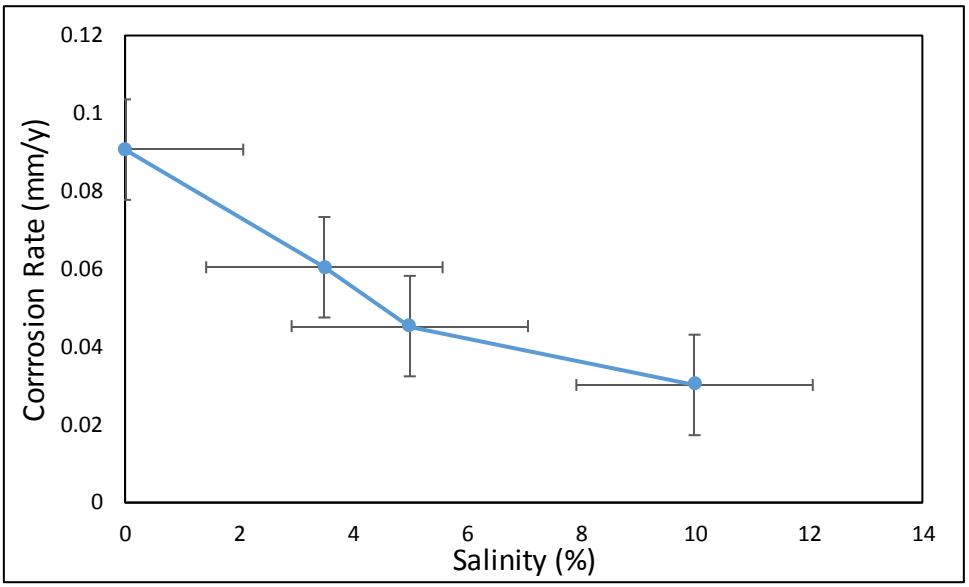

Figure 6-5 Effect of salinity concentration on corrosion rate

These results show that this simple method can be used to simulate the corrosion behaviour of drilling fluids under reservoir-like conditions, which enables us to investigate the effect of various influencing parameters. The corrosion data that was difficult to obtain under flow and high temperature and high-pressure conditions can be easily achieved by this new method, which can also be extended to simulate other complicated conditions.

6.4 The Effect of Drill Cuttings Size on Erosion-corrosion Rate

Three different sizes of actual limestone drilled cuttings are used to investigate the impact of drill cuttings size on drill pipe corrosion/ erosion. Figure 6-6 shows the drill pipe erosion-corrosion rates at 300rpm and 5% cuttings concentration (weight) with increased drilling cuttings size from 0.841 to 3.3 mm. The results demonstrate higher erosion-corrosion at bigger drill cuttings size due to erosion, as indicated in Figures 6-6 and 6-7. The large size drill cuttings have considerable kinetic energies when compared with small size

cuttings. Therefore, these bigger drill cuttings transfer more kinetic energy to the pipe wall and thus accelerate wear.

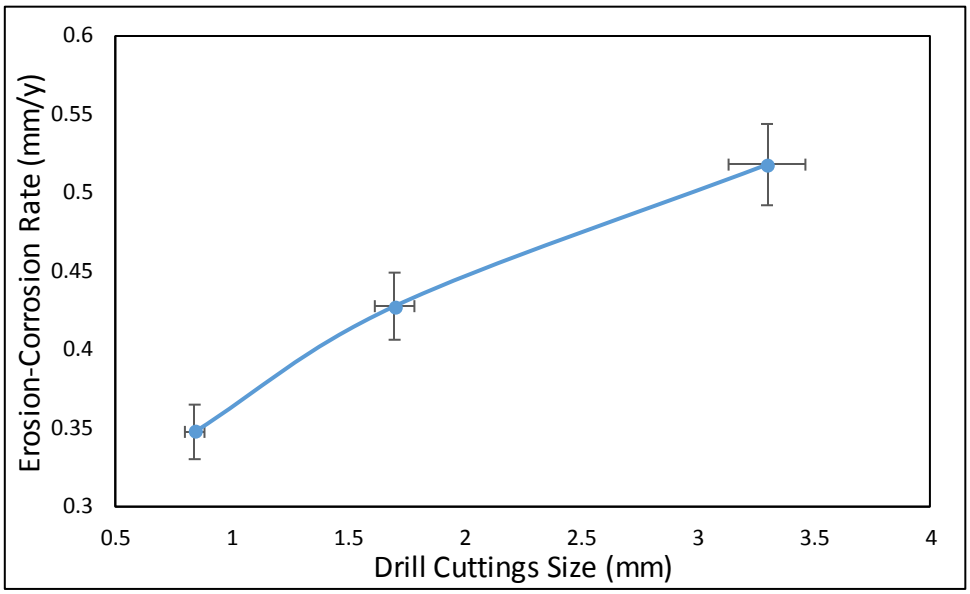

Figure 6-6 Erosion-corrosion rates at different drill cuttings size

The SEM results from the erosion-corrosion tests for 0.841 and 3.3 mm drill cuttings sizes are shown in Figure6-8. The SEM images prove that the collision efficiency of drilling cuttings concerning the specimen surface increases with an increase in drill cuttings particle size, as shown in Figure6-8 C&D. The SEM results also show that the size of the crater formed upon impact with the target material is directly proportional to the size of the particle, as displayed in Figure 6.8 (A&B). Therefore, increasing the particle size will result in a more significant erosion factor. These outcomes are consistent with previous results [151-156].

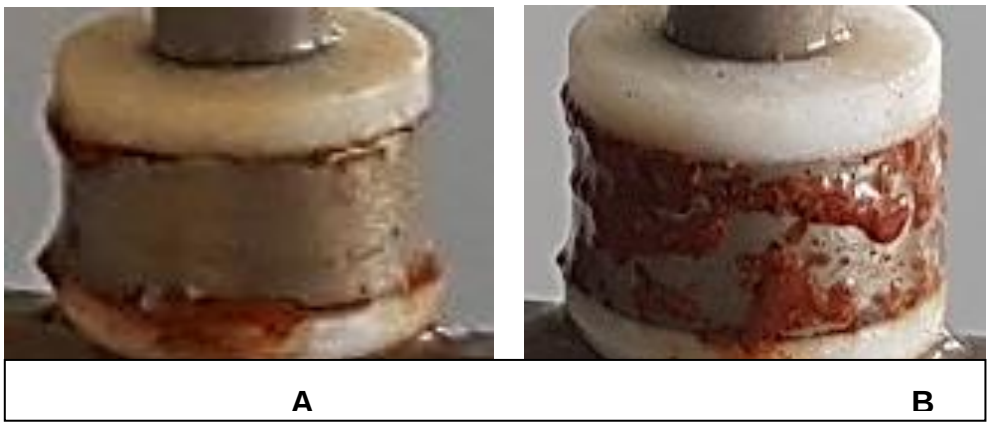

Figure 6-7 Drill pipe coupons after erosion-corrosion for a) 5% of 0.841mm cuttings, b) 5% of 3.3mm cuttings

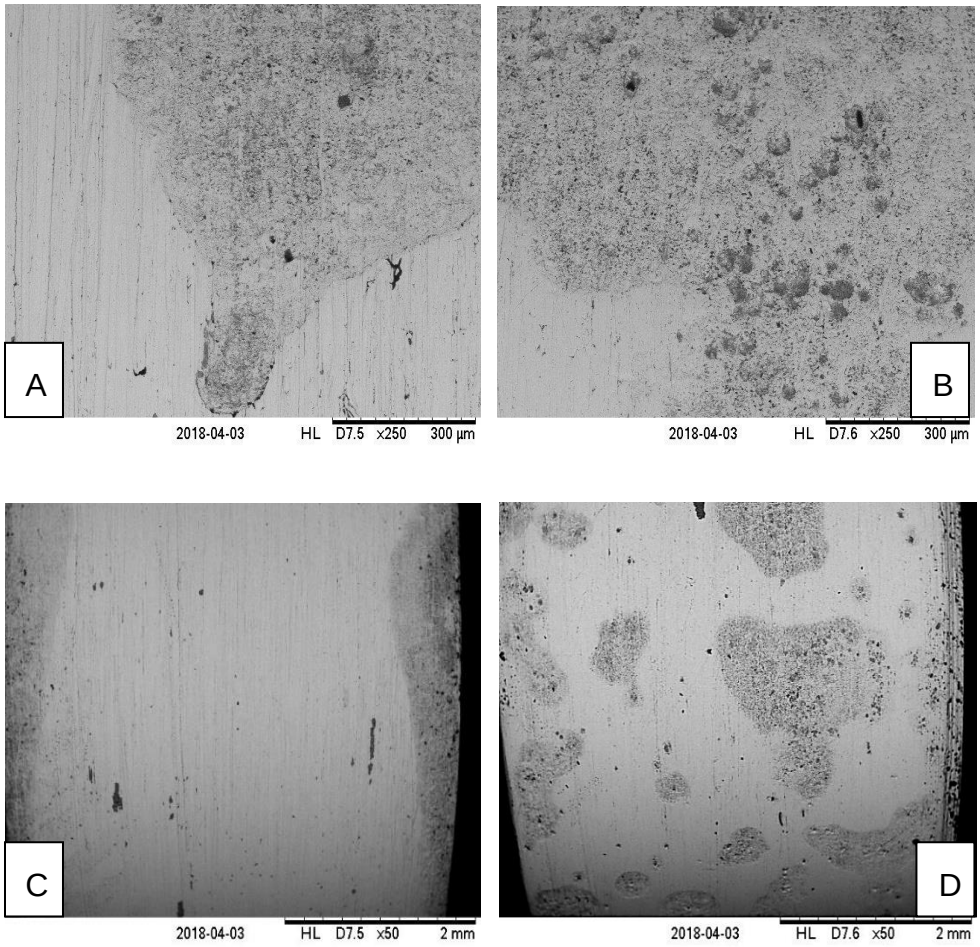

Figure 6-8 SEM after corrosion erosion with (a&c) 5% of 0.841mm cuttings, (b&d) 5% of 3.3mm cuttings

6.5 The Effect of Drill Cuttings Concentration on Drill pipe Erosion-corrosion Rate

The drill pipe erosion-corrosion rates of 300rpm and 0.841 mm with increased drill cuttings concentration (where the cuttings concentration varies from 5, 10, and 15% (wt/volume)) are graphically presented in Figure 6-9.

The results show a decrease in the drill pipe erosion-corrosion, since the cuttings concentration increased from 5% to 15%. This is expected, since an increase in the number of drill cuttings impacts the drill pipe material, which will result in a layer of particles building up on the surface, preventing direct impact, but causing material removal by abrasion as the layer is dragged across the target surface [157, 158]. The particles approaching the wall surface collide with other particles near the wall and lose a certain amount of

kinetic energy. This is known as the “shielding effect”, which is provided by the particles near the target wall. Thus, particles strike the surface with less kinetic energy, or they may even rebind away from the target wall. Hence, it has been determined that the number of particles striking the wall does not increase at the same rate as the concentration of the particle in the slurry increases [155]. The SEM images after the erosion-corrosion tests for 5% and 15% drill cuttings sizes, as shown in Figure 6-10 allow us to visualise the impact drill cuttings concentration on the drill pipe material. The outcomes agree with previous findings [159].

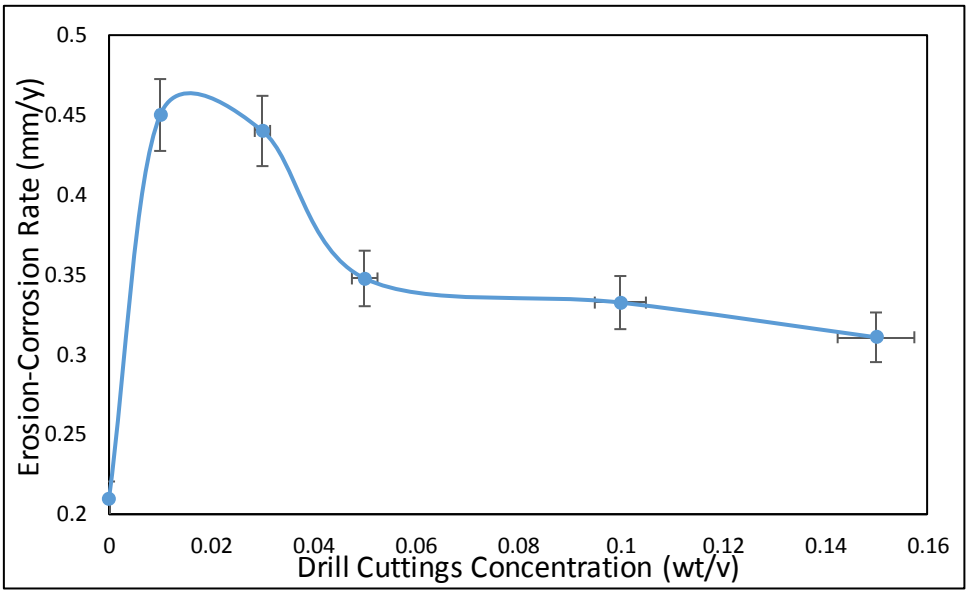

Figure 6-9 Erosion-corrosion rate at different drill cuttings concentration

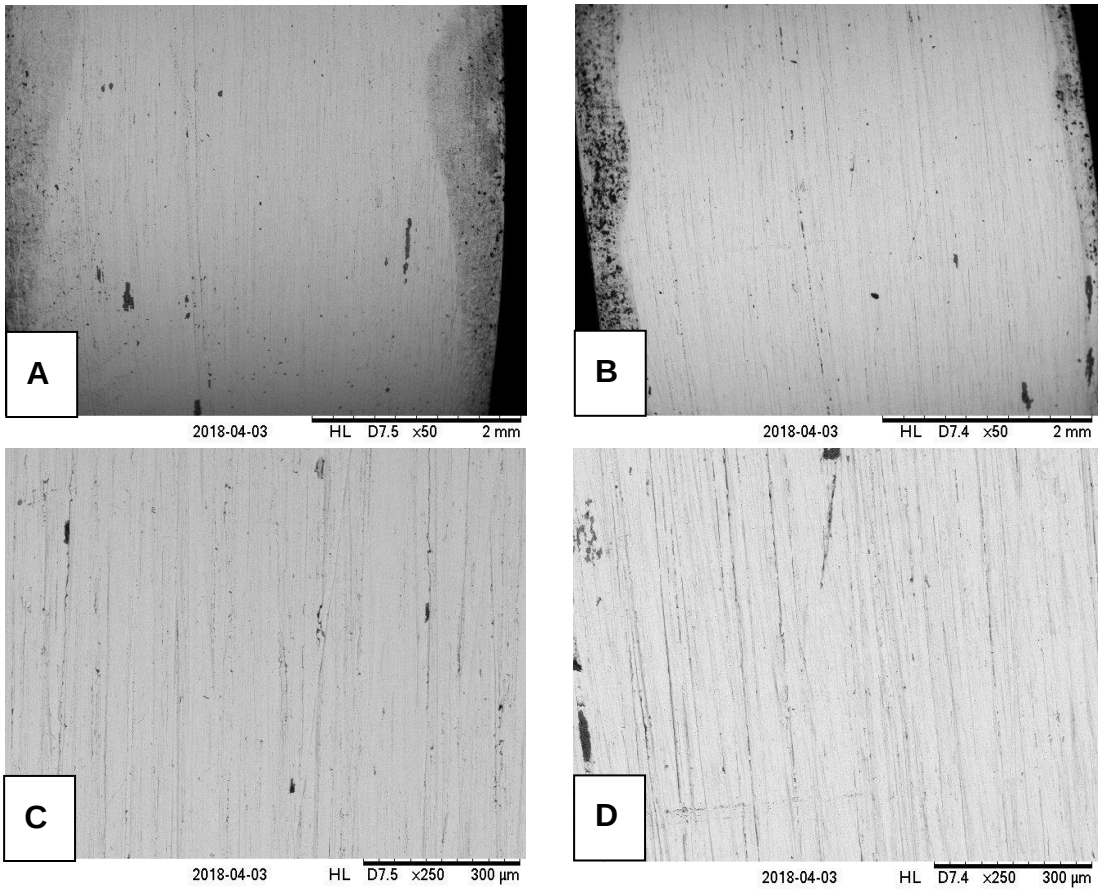

Figure 6-10 SEM after corrosion erosion with (a&c) 5% of 0.841mm cuttings, (b&d) 15% of 0.841mm cuttings

6.6 The Effect of Base Fluids on Drill pipe Erosion-corrosion rate

Three different base drilling fluids are employed to examine the influence of base drilling fluid type on erosion-corrosion. These investigations highlighted the impact of water, Xanthan polymer and SiO_2-Xanthan nanofluid on drill pipe erosion-corrosion behaviour. Figure 6-11 shows the drill pipe erosion-corrosion rates at 300rpm and 5% drill cuttings for water, Xanthan polymer and SiO_2/ Xanthan nanofluid. The results show that water as a base fluid has experience corrosion than the others. The most remarkable achievement to emerge from the data is that the erosion-corrosion rates of the drill pipe using the SiO_2/Xanthan nanofluid is the lowest when compared to the corrosion

rates using water and xanthan polymer. We believe that nanofluids show lower and more stable friction coefficients and they also have self-healing lubricating effects [160, 161]. This could be the main reason for the low corrosion rates of metals in the nanofluid. Another reason for the low corrosion rates of the nanofluid is the presence of polymer in the solution [162]. Since these SiO_2-nanofluids use xanthan polymer as their dispersant, the inhibitory characteristics of the nanofluid are indirectly enhanced. As a result, a lower corrosion rate of erosion-corrosion is recorded in the experiment using the SiO_2- nanofluid.

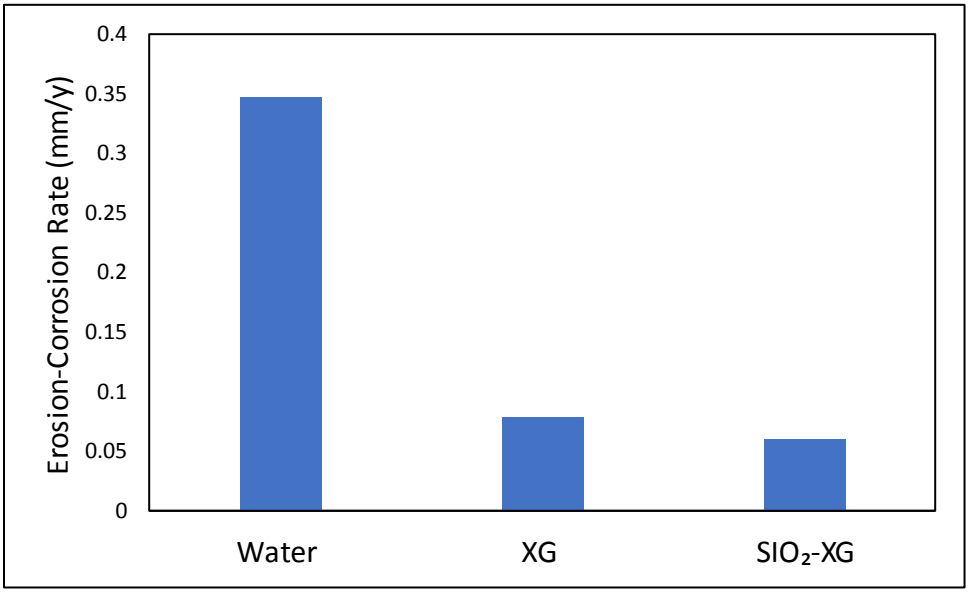

Figure 6-11 Erosion-corrosion rates at different base fluids

The erosion rate should also be expected to decrease, since increasing fluid viscosity serves to increase the drag force on a particle. As the viscosity of the carrier liquid increases, for given flow conditions and sizes of particles and target, the collision efficiency should likewise decrease, as should the particle impact velocity at the stagnation point. The viscosities of fluids have been investigated experimentally, as in Figure 6-12. The results show that the viscosity of the xanthan polymer is a little higher than the viscosity of SiO_2-nanofluid. Nevertheless, a higher erosion-corrosion reduction was obtained with SiO_2- nanofluid, as shown in Figure 6-11. The reason for this erosion-corrosion reduction is that the nanofluid has the potential to form a protective lubricating film in the wall pipe interface [163].

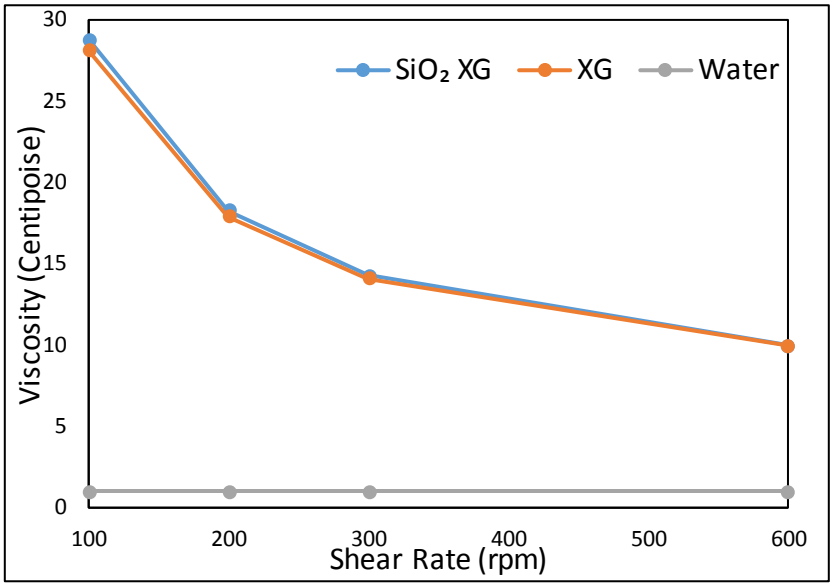

Figure 6-12 Viscosities of different base fluids

6.7 Summary

A novel simple method to examine pipe corrosion in a reservoir-like environment was proposed in this research, and a parametric study investigating the factors influencing the corrosion rate was conducted. Based on the research that has been undertaken, it can be summarized:

- The parametric study results demonstrate that the corrosion rate increases with an increase in temperature, pressure and rotational speed. However, it decreases with an increase in the salinity concentration.
- The erosion rate of the drilling fluid shows a negligible effect compared to those observed in the corrosion experiments under the same conditions, which confirms the dominant effect of corrosion.
- The erosion-corrosion of the drill pipe increases with an increase of drill cuttings sizes.
- The erosion-corrosion rate of the drill pipe decreases with the increase of cuttings concentration, and drilling fluids viscosity

- The SEM results clearly show that the collision of drilled cuttings concerning the specimen surface increases with an increase in drill cuttings particle size. The size of the crater formed upon impact with the target material is directly proportional to the size of the particle.
- The erosion-corrosion rates of the drill pipe using the SiO_2-Xanthan nanofluid is the lowest when compared to the corrosion rates using water and xanthan polymer.

7 Computational Fluid Dynamics Study of Drilled Cuttings Transport through Vertical Well

7.1 Power-Law Index (n), Consistency Index (k) Yield Stress Estimation:

A flow test for the non-Newtonian fluids can be conducted by estimating the viscosity as a function of deformation rate (shear rate). This test may be regarded as a fundamental test of the drilling muds in order to evaluate a viscosity profile under a deformation rate. Various deformation rates are produced from a drilling pipe to drill different layers, which are mostly equivalent to 3, 6, 100, 200, 300, and 600 rpm. The mud has been tested to determine the Power Law Index (n) and Consistency Index (K), as shown in Figure 7-1. These constants have been calculated by approximating the viscosity curve to Herschel Bulkley model equations using the curve fitting method.

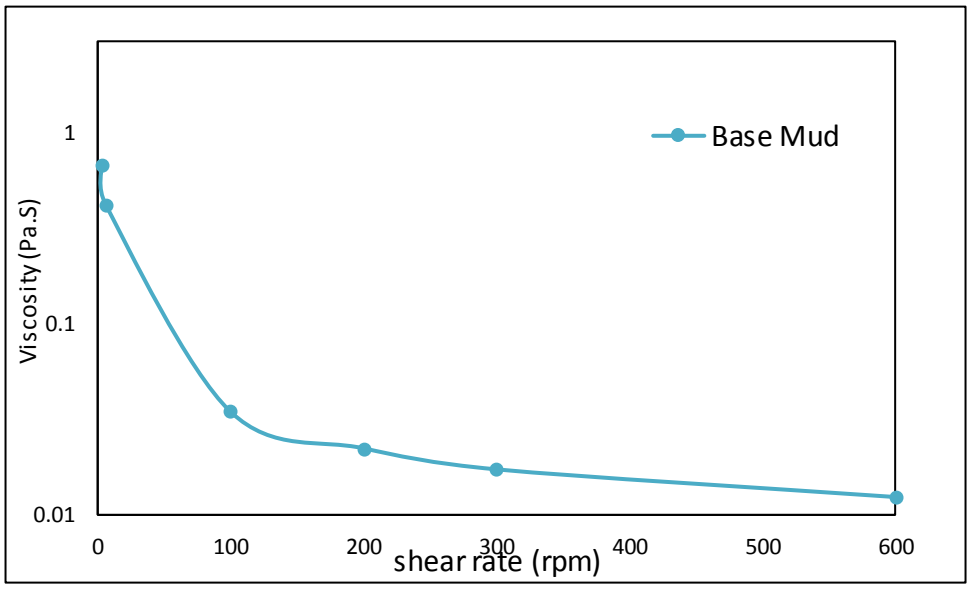

Figure 7-1 Flow curve for the base mud.

The drilling fluid shows both viscous and elastic behaviour depending on the deformation. The viscoelasticity property of a drilling fluid can be tested with an oscillatory amplitude test, which includes calculating the storage modulus (G') and loss modulus (G") as a function of the shear strain. As previously discussed, G' and G" curves contain several parameters related to the fluid

viscoelasticity, such as yield stress point. Figure 7-2 illustrates the storage modulus (G') and loss modulus (G") profiles for the mud, and the red circle refers to the yield point, which is 5.75 pa.

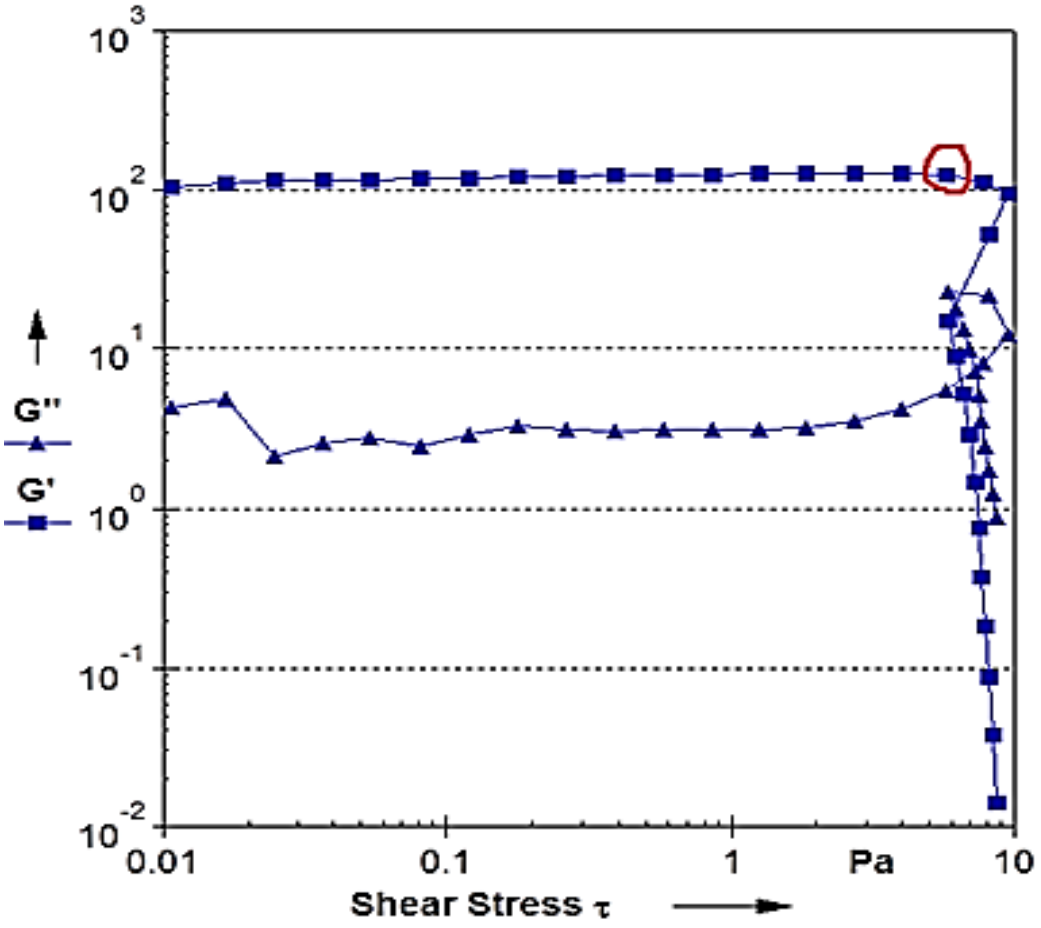

Figure 7-2 Viscoelasticity curve for base mud.

7.2 Model Validation

The CFD model developed in this study is validated by the experimental findings of Samsuri et al. [46], who studied the effect of a Multiwall Carbon Nanotubes (MWNTs) additive on the carrying capacity of the drilling mud in a vertical well model. MWNTs were added at different concentrations for various flow rates, with a view to investigate mud lifting performance. To validate the model's results, 0 and 0.01 wt % of nanoparticles are simulated at flow velocity ranges from 0.05 to 0.15 m/s. Two cases, one for the base drilling fluid and the other for the nano drilling fluid, which contains 0.01wt% CNT nanoparticles, were performed in conjunction with

experiments. The orthorhombic cutting particles were injected from the bottom of a well, with a fixed size of 4.8 mm. As presented in Figure 7-3, solid agreement was obtained between the simulation results and those results obtained by Samsuri and Hamzah [46]. Thus, the closest cuttings recovery percentage is achieved at a higher mud flow rate.

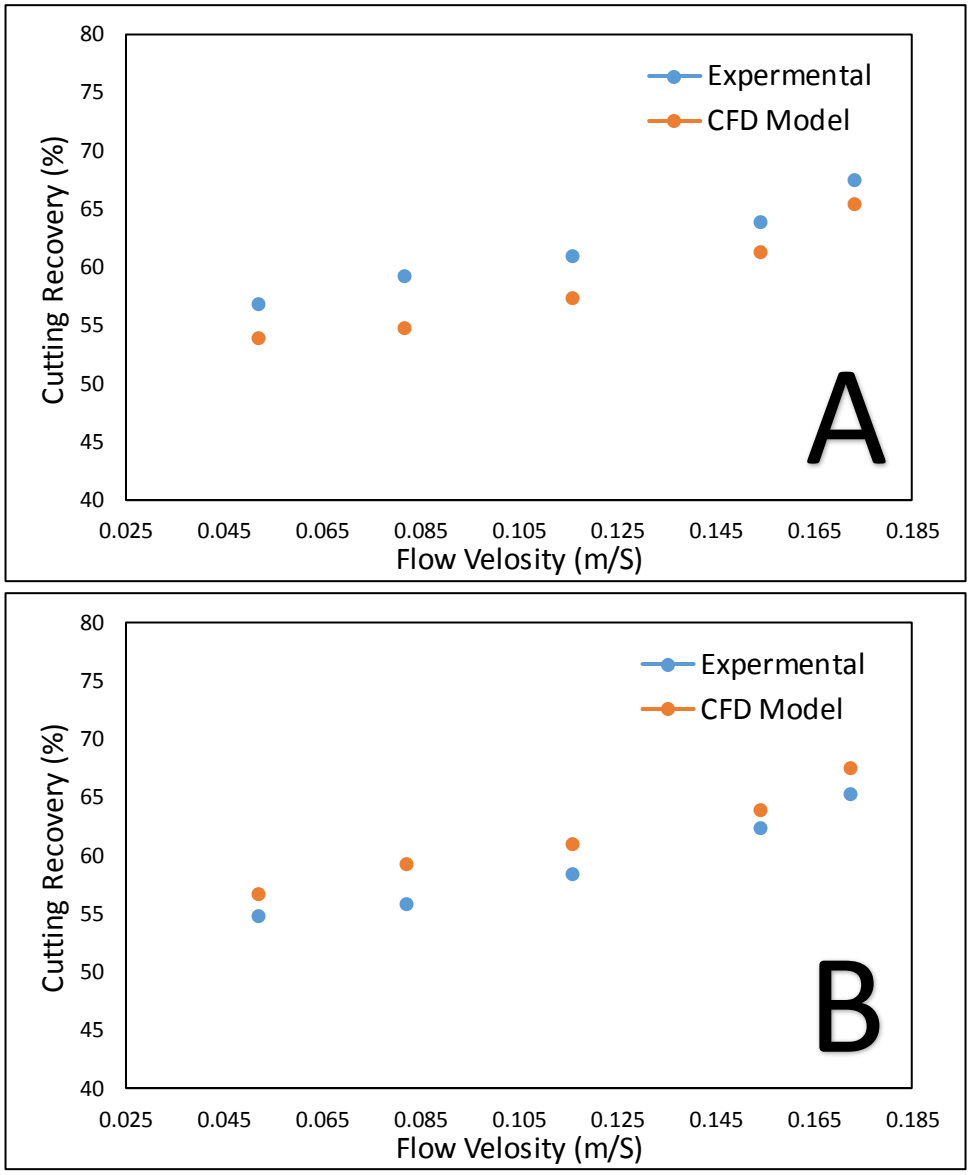

Figure 7-3 The experimental validation for the numerical findings; A) cuttings particle size 4.8 mm and CNT NPs content of 0.01 wt. %. B) Without NPs

7.3 Fluid Flow

The flow pattern of a water-based drilling fluid through a rotating drill pipe and a wellbore has been investigated. Figure 7-4 reveals the streamlines and flow direction in the flow domain. Recirculation zones are formed near the corners of the wellbore bottom due to the great Reynolds number and sudden expansion in the flow area. The turbulent eddies in these zones could results in a loss of fluid, loss of heat and a drop in pressure [164]. The contour of the fluid's velocity shows a variation in the velocity components, as shown in Figure 7-4. The effects of drill pipe rotation onfluid viscosity have been analysed. Dynamic viscosity decreases when the rotational speed increases as shown in Figure 7-5.

The fluid viscosity contributes to the overall performance of the drilling fluid in the hole cleaning process. The dynamic viscosity of a non-Newtonian fluid has been studied with variation of the shear rate and the addition of nanoparticles. The most critical parameter that affects the fluid's viscosity is the drill pipe rotation speed (i.e. shear rate). Figure 7-5 presents the effects of rotational speed and nanoparticles on the fluid's viscosity. Adding nanomaterials in two concentrations promotes the fluid's viscosity under different shear rates. The NPs concentration of 0.9 wt. % shows a significant improvement in the fluid's viscosity, thus, it has been considered for the cuttings transport investigations. The effective dispersion ability of nanoparticles within the fluid structure could be the responsible for viscosity improvement. Figure 7-6 depicts fluid viscosity distribution in the model through a cross-sectional view of the viscosity contour. Figure 7-5 shows that the flow behaviour of nanoparticle seeded drilling fluid is similar to the base fluid (drilling fluid without nanoparticles). Both drilling fluids with and without nanoparticles followed the shear thinning behaviour. The difference between them is that the addition of nanoparticles renders higher viscosity, which could be linked with the effective dispersion ability of the nanoparticles on the surface of the bentonite.

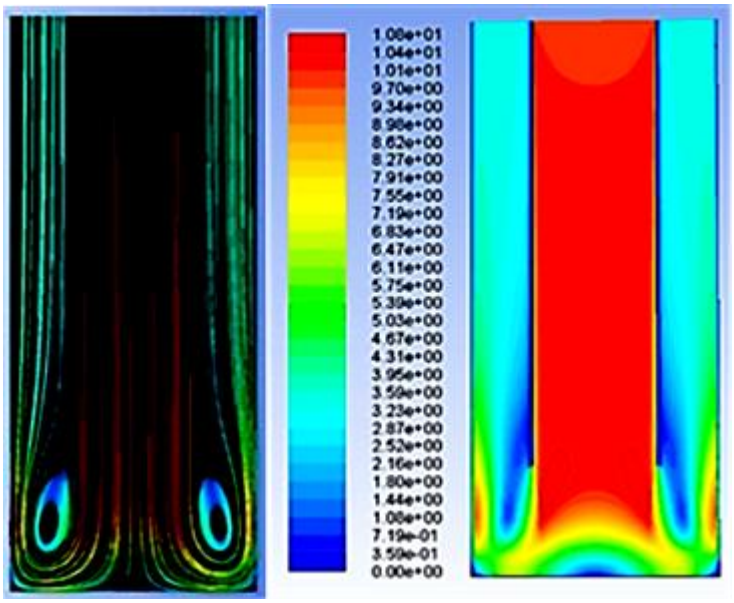

Figure 7-4 (Left) the streamlines and flow direction in the flow domain in 2D view (Right) velocity magnitude contours.

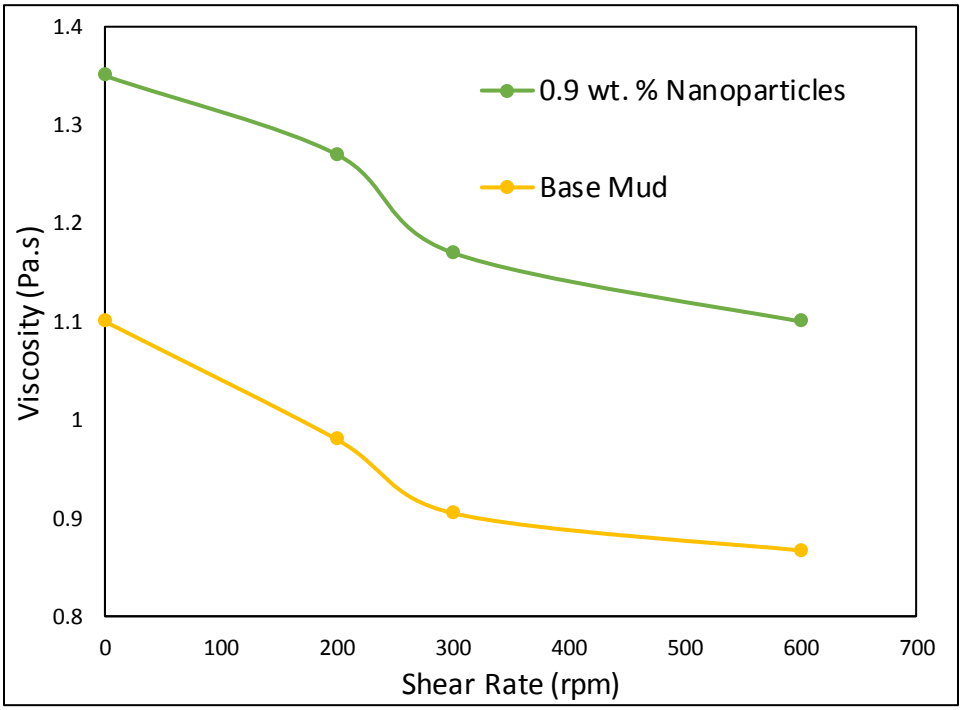

Figure 7-5 Effects of nanoparticles addition on the fluid viscosity

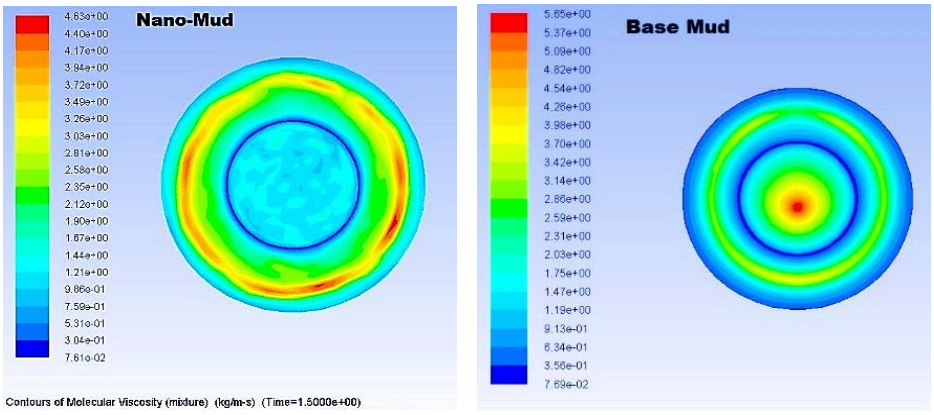

Figure 7-6 Cross-sectional contour of the fluid viscosity for base mud and nano-based mud (100 rpm)

7.4 Carrying Capacity Enhancement

The efficiency of nanofluid in the hole cleaning process was examined for different fluid flow rates and drilling cutting characteristics. In the present model, the cutting transport process was studied based on the cuttings volume faction in the effluent fluid. As described in the previous section, the selection of NPs concentration (0.9 wt. %) was made to satisfy both cleaning efficiency and economic considerations. In this study, the fluid inlet velocity is varied at both base and 0.9 wt. % nano drilling fluids. The addition of nanoparticles and fluid inlet velocity both improve the fluid carrying capacity for drilling cuttings. Figure 7-8 present the impact of fluid velocity on the carrying capacity of the nanoparticle-based mud and base mud. An increase in cutting recovery is observed when the inlet velocity increases for both fluids. Nevertheless, this increase is more with 0.9 wt. % of the nano drilling fluid. During drilling, when a mud engineer noticed that the hole is not being cleaned of cuttings at a satisfactory rate, the engineer would increase the circulation rate and thicken the drilling fluid, and thus justify why there is more cuttings recovery with nanofluid. This can be explained mathematically by using equations 7.1 and 7.2, as well as schematic Figure 7-7.

$$V_{particle} = V_{fluid} - V_{slip} \qquad 7\text{-}1$$

$$V_{slip} = \frac{\mathbf{138}\,(\rho_s - \rho_f)\,d_s^{\,2}}{\mu} \qquad 7\text{-}2$$

Therefore, there is increased cuttings recovery when the fluid velocity and viscosity are increased. On the other hand, the increment of the annular fluid velocity results in open hole erosion and uncontrolled losses after fracturing, and furthermore, the viscosity increment can cause differential sticking problems. All these aforementioned parameters should be carefully controlled. An important observation from Figure 7-8 is that the cutting recovery of the nano drilling fluid at a low inlet velocity is more than the base drilling fluid (51% at 0.5ms^{-1} for the nano fluid and 48% for the base fluid). This behaviour can help reduce the cuttings' deposition when the circulation velocity insufficient to overcome the gravitational force.

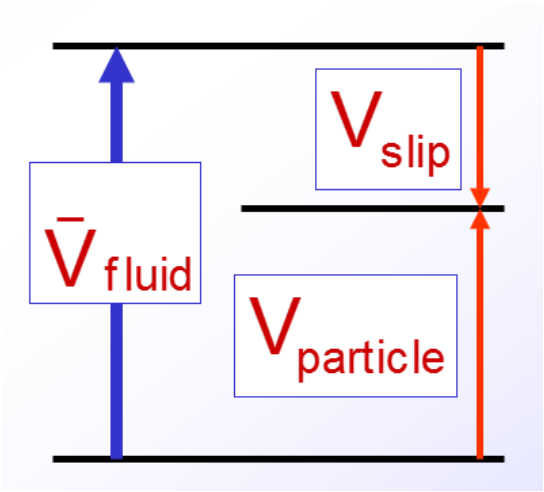

Figure 7-7 Schematic diagram of velocities balance during drilling

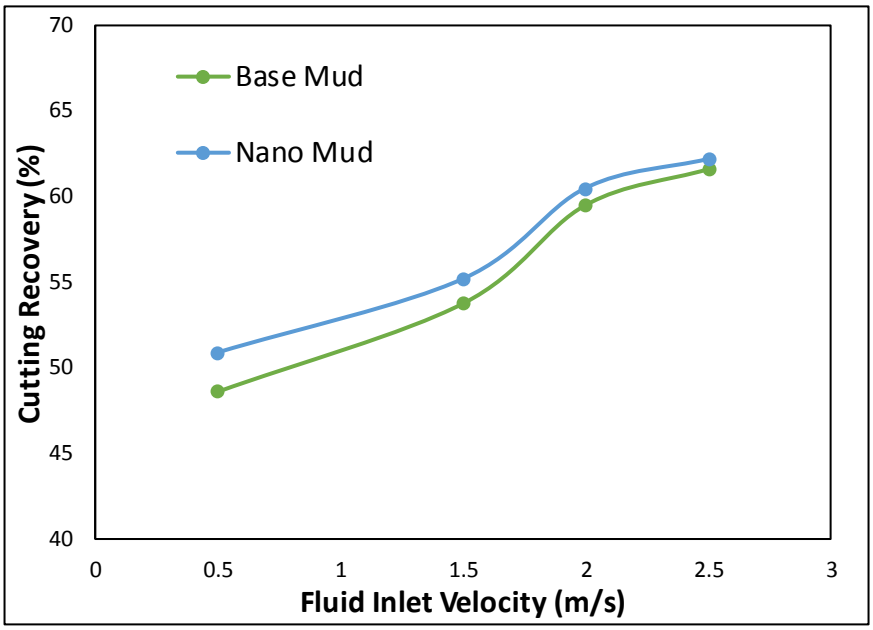

Figure 7-8 Cuttings recovery vs fluid inlet velocity for drill pipe rotation speed of 100 rpm.

A drill cutting in suspension is acted upon by different forces. The diagram below (Figure 7-9) illustrates this by showing the acting forces on drilling cuttings. The major forces acting on cuttings transport include drag, buoyancy and gravity forces. The cutting characteristics and the fluid properties are very important in determining which force is most active and dominates the system. These forces can be grouped into static and hydrodynamic forces. Gravity and buoyancy forces are static forces due to the properties of the particles and its surrounding fluid. Drag is the hydrodynamic force incurred from the fluid flow. Particles start accumulating when the fluid drag is unable to enable further motion of the particles. In vertical wells, the drag force should surpass the gravitational force which is almost moving in the opposite direction of the drag force. Otherwise, the upwards particle motion will terminate and particle settling will occur. Figure 7-10 (A) demonstrates that the higher in-situ concentration of drilling cuttings, the higher the cuttings' transport rate. As the height of the cutting bed becomes more prominent, the fluid can hold more cuttings and attain the critical carrying capacity. The increasing flow turbulence results in uniform drug distribution that lifts the cuttings to the surface. These results agree with Hussaini and Azar [165] findings; they

suggested that mud annular velocity decreases in-situ cuttings concentration. However, the mud flow rate needs to be systematically restricted for controlling the pressure drop, pumping cost and wellbore stability.

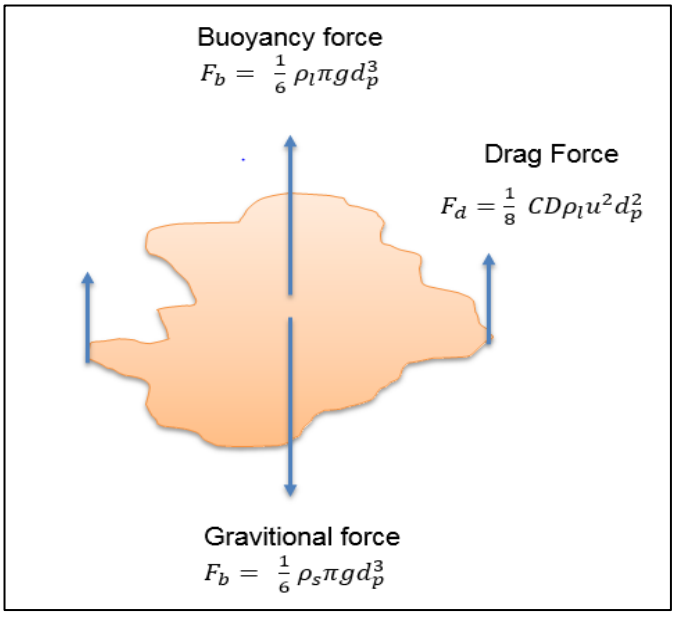

Figure 7-9 Forces acting on a drilled cutting

The shape of the cutting particle could affect the hole cleaning process. Beside the spherical particles, the transport of the particles with a shape factor of 0.9 and 0.8 was tested at fixed in-situ concentration of 40 wt. %. Figure 7-10 (B) indicates that the particles with higher sphericity are carried more easily; the spherical particles easily transport from the bottom of a wellbore due to its good sliding capability. This is also theoretically confirmed by Haider and Levenspiel [166] approach for non-spherical particles drag. They state that the shape factor lowers the drag coefficient, hence the resistance to particles' transport is more likely to be lower.

The last parameter that has been investigated is cuttings' density. The particles with low relative density are more efficient at cleaning. The heavier cuttings tend to settle to the wellbore bottom, as illustrated in Figure 7-10C. The results obtained by the present study are confirmed by Li and Wilde's (2005) study, who pointed out that a particle with a higher density is harder to transport through a wellbore. The reason behind this is that the gravitational force increases when the density of the cutting particles increases (Figure 7-

9 and equation 7.2). Increases in cutting density tend to increase slip velocity, which adversely affects hole cleaning as result of more cuttings settling. Whereas, the opposite occurs when the density of the drilling fluid is increased. The increased fluid density causes the buoyancy force to increase, which in turn increases cutting recovery. An important observation from in Figure 7-8 and Figure 7-10 is that the cutting recovery of drilling fluids can increase with the addition of nanoparticles. The addition of nanoparticles to water-based mud improves the viscosity, viscoelasticity and thixotropy properties of water-based mud, as well as the ratio of yield point to plastic viscosity. Generally, a drilling fluid with a lower plastic viscosity and higher yield point is recommended, given that the lower plastic viscosity provides turbulence at the drill bit, which in turn provides better hole cleaning, and a higher yield point ensures enhanced carrying capacity and strong shear thinning behaviour.

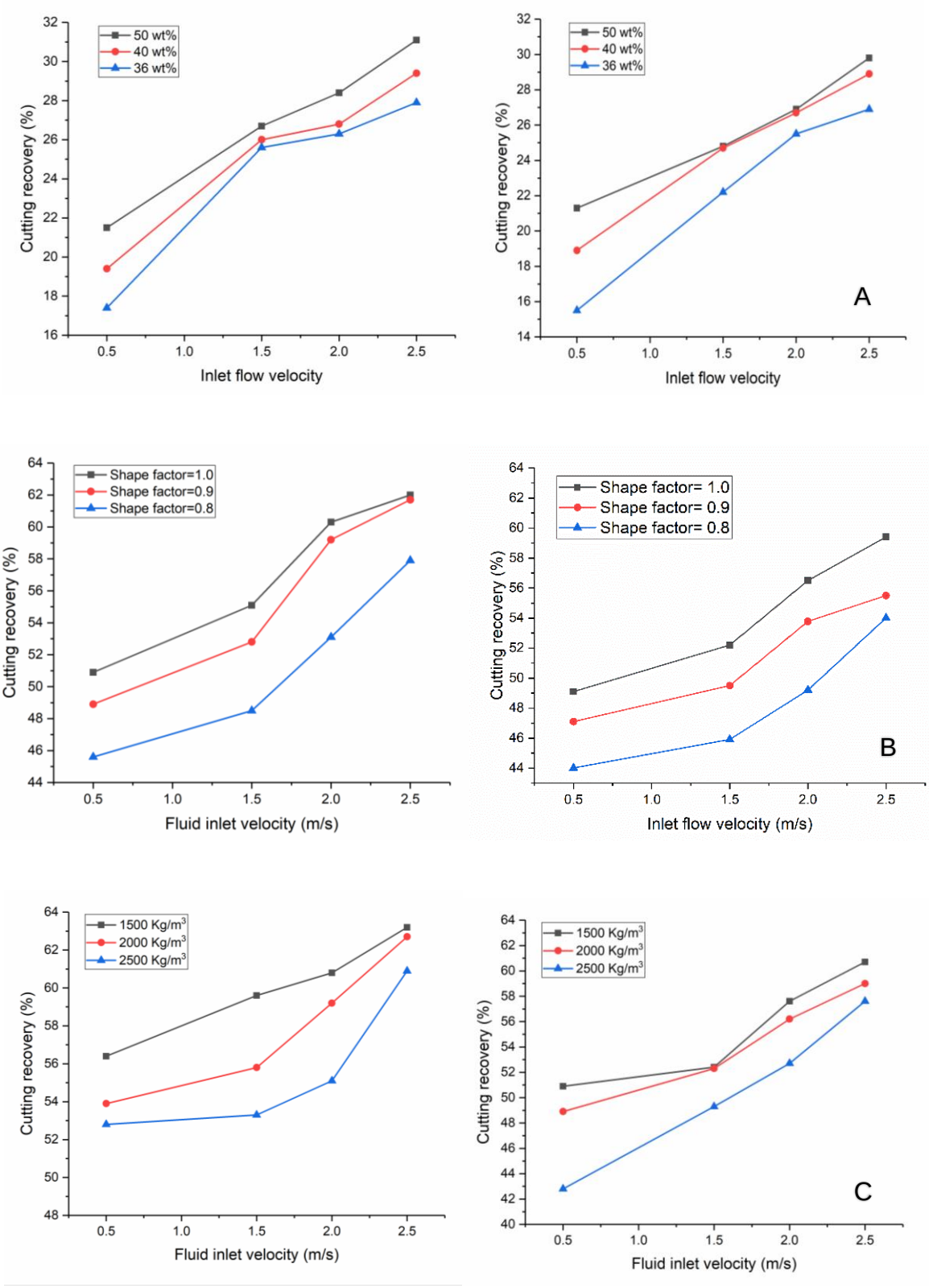

Figure 7-10 Effect of cuttings *in-situ* concentration, shape and density, on the cuttings transport process for 0.9 wt. % CuO-Al_2O_3 nanoparticle mud and base mud, at 100 rpm

7.5 Comparison between Two-Way (DDPM) and Four-Way Coupling

Figure 7-11 compares two-way (DDPM) and four-way coupling (DDPM+DEM) regimes, which define the relationship between the continuous phase and the discrete phase. Employing a four-way coupling regime fulfils a realistic and robust interaction between the two phases. On the other hand, particle movement will be restricted due to collisions with adjacent particles or solid surface. This collision can lead to a loss of particle kinetic energy, and thus reduce cuttings transport.

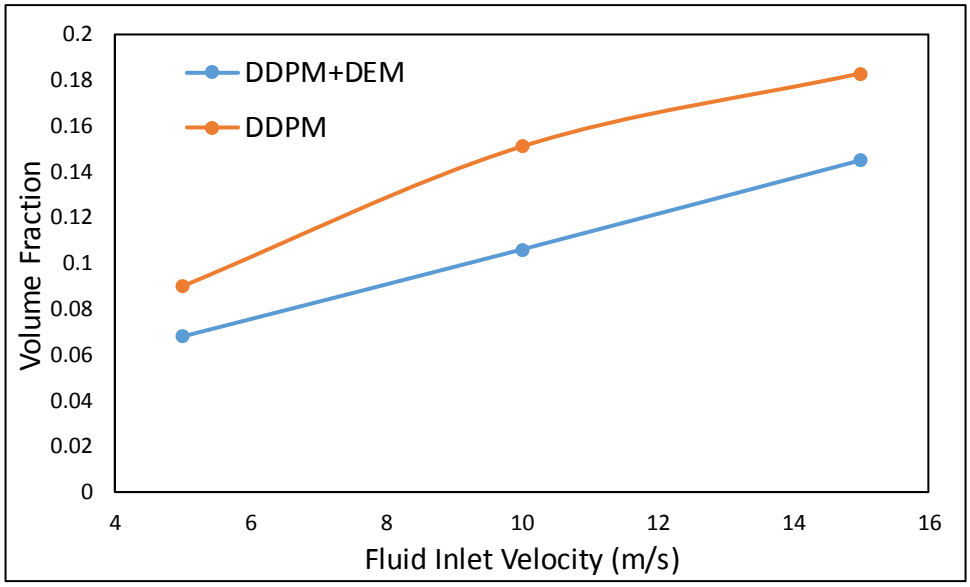

Figure 7-11 Comparison of Two-Way and Four-Way coupling regimes

Figure 7-11 supports this argument, where there is pronounced variation between volume fraction between two-way and four-way coupling methods. As the cutting particle in two-way coupling (DDPM) does not affect contact dynamics, the accessible particle transports to a surface. Therefore, the quantity of drilling cuttings leaving the wellbore in the case of DDPM is higher than that in of the DDPM+DEM case. The longitudinal sectional contours of cuttings volume fraction depict a frivolous difference in the cuttings distribution between the DDPM and DDPM+DEM cases, as shown in Figure 7-12.

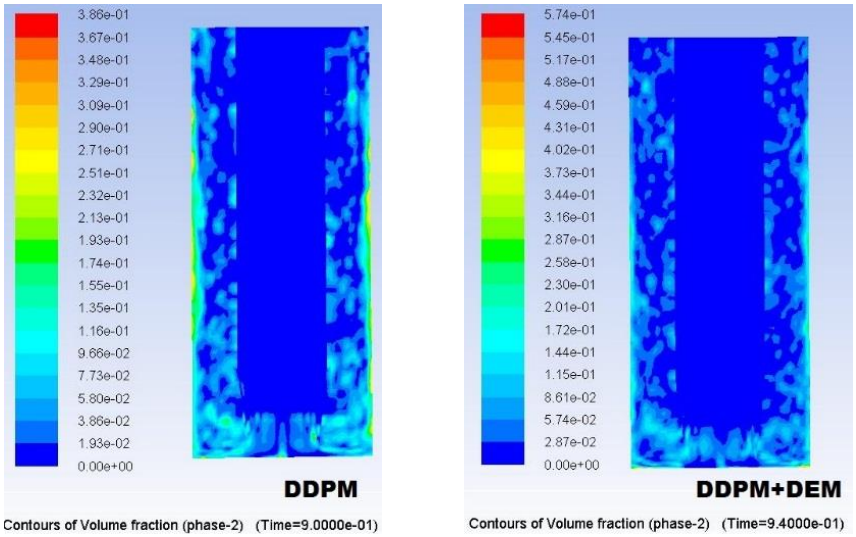

Figure 7-12 Contours of cuttings volume fraction using Two-Way and Four-Way coupling regimes.

7.6 Summary

The Chapter investigate numerically the influence of nanoparticles and the effects of various parameters such as drilling fluid rheology, flow rate, pipe rotation, cuttings density, shape, concentration and drilling fluid- cuttings particle coupling regimes on the cuttings transport in a vertical wellbore. A CFD simulation was carried out by using the transient solver of ANSYS-FLUENT commercial code. The dense discrete phase model (DDPM) is used to overcome the main shortcomings of previous Eulerian based approaches. In addition, agreement has been achieved between the simulation results and the published experimental study. The simulation show that the cuttings transport process and fluid viscosity can be significantly enhanced by adding nanomaterials to the fluid, and further, it has shown that the process is highly influenced by cutting characteristics, such as in-situ concentration, shape, and density, which can be summarised as follows:

- The flow pattern is turbulent, complex and disordered in the bottom of a wellbore.
- Adding nanoparticles with adequate concentration significantly boosts fluid viscosity and carrying capacity.

- Nanoparticles show the proper attitude towards enhancing carrying capacity of the drilling fluid, particularly at the lower and moderate flow rates.
- Increasing fluid inlet velocity enhances the cleaning performance.
- Cuttings with higher sphericity have better transport efficiency
- Density has an inverse influence on cutting transport.
- The CFD coupling regime of continuous and discrete phases significantly affects the cuttings transport process. The outlet volume fraction of cuttings using a two-way coupling regime is greater than that of a four-way coupling regime. Four-way coupling is much closer to reality, when taking the contact dynamics into account.

8 Conclusion and Recommendations for future work

8.1 Conclusions

In addressing the difficulties that face traditional drilling fluids, with wellbore instability, lost circulation, pipe sticking, toxic gasses and high torque, the present thesis has performed a systematic experimental study to assess the influence of various nanoparticles on the performance of two water-based muds. The changes in property depend on nanoparticle concentration, charge and shape.

The study has demonstrated that the addition of nanoparticles can modify various properties of a drilling fluid, depending on particle morphology, surface characteristics and concentrations. In general NPs can be employed to assist the traditional WBM via several ways:

1. NPs can be used as additives to improve drilling fluid properties. The results suggest that the impact of nanoparticles is multi-faceted, and the influences of nanoparticles on different properties are different. It is unlikely that the addition of one type of particle could improve all related features, since one nanoparticle may improve one property but may not improve anther.
2. Hybrid nanoparticle systems can be used to address the limitations of using a single type of NPs. With complementary properties, the hybrid nanoparticle-based drilling fluids can be used to overcome the problems associated with single type nanoparticles, and can improve the chemical and physical features of these nanoparticles with enhanced drilling fluid performance.
3. For WBM with biopolymer, NPs can be used as a cross linker to reinforce physio-chemical, mechanical and thermal properties of the drilling fluids, leading to improved performance.
4. NPs can also be used to reduce-wear and friction by forming a thin film covering the drill pipe, and improving carrying capacity, thus reducing the cutting collision with the drill pipe.

More specifically, the following conclusions can be reached based on experimental and numerical studies:

Rheological properties

- The addition of nanoparticles to water-based mud, developed the drilling fluid structure. The expected enhancements depend on the selected nanoparticles types, morphology and the nanoparticles concentration.
- For single NPs addition, the positive surface charge NPs showed better enhancement in rheological properties then the negative surface charge.
- The addition of Al_2O_3 CB, Gr and SiO_2 nanoparticles helps the drilling fluid to rapidly develop high gel strength to resist the settling of heavy particles out of suspension.
- An increase in nanoparticles concentration increases the elastic behaviour of the drilling fluid and increase the degree and the speed of the structural recovery through reducing the time required for it to be rebuilt.
- The combination of negative charge NPs and positive charge NPs exhibited better rheological properties than negative charge NPs. This enhancement can be attributed to the presence of positive charge NPs.
- Based on the rheological investigations, the addition of nanoparticles has the power to form a drilling fluid that demonstrates appropriate abilities both at rest and in movement.

Fluid loss and swelling

- Nanoparticles can decrease the filtration and fluids loss. For example, while the filtrate volume of traditional drilling fluid was 6.8ml after 10 minutes, this volume decreased to 6.4ml with the addition of 1g of CB NPs. Similarly, the addition of 1g of silica and graphite NPs reduces the

filtrate volume to 5.8ml and around 14.7% reduction percentage in filtrate volume, respectively.

- Using hybrid nanoparticles could further improve the filtration and loss behaviour.
- The combination of negative charge NPs and positive charge NPs also exhibited better filtration properties than positive charge NPs, as clearly shown in Al_2O_3-SiO_2 NPs. The filtrate loss enhancement is attributed to the presence of negative charge NPs.
- The rheology and filtration properties of different drilling fluids based on Croscarmellose sodium (CS), Arabic gum (Ag), Carboxymethyl Cellulose Sodium (CMC) and xanthan gum (XG) and base muds were investigated to choose the best biopolymer for drilling fluid application. The finding highlights that xanthan has higher rheological and filtration properties when compared to other biopolymers and base drilling fluids
- The results showed that the addition of different NPs into Xanthan based drilling fluids exhibited better rheological, filtration, and swelling than the addition of NPs and xanthan polymer alone.
- Even CNT XG showed a better reduction than CNT and XG alone. As can be seen from Figure 5-23 the addition of CNT alone increases the filtrate loss, whereas the addition of CNT XG decreases the filtrate loss due to the presence of dispersed CNT; it acted as a plaster between the polymer particles and seals the permeable mud cake to reduce the filtrate loss
- The rheological, filtration and swelling properties depend on NPs-Polymer interaction which explains the difference between the NPs-XG nanofluids filtrate loss results.

Corrosion and erosion-corrosion

- A novel design of coupon rotating inside an autoclave was developed to appropriately simulate the drilling pipe corrosion behaviour in the

wellbore, which is more beneficial than using an HPHT flow loop, which is generally large and expensive.

- The corrosion rate in wellbore conditions increases with an increase in the temperature, pressure and rotational speed, but decreases with an increase in salinity concentration
- The erosion rate of the drilling fluid showed a negligible effect when compared to those observed in the corrosion experiments under the same conditions, which confirm the dominant effect of corrosion.
- The SEM results showed that the collision of drilling cuttings concerning the specimen surface rise with an increase in drill cuttings particle size, and further, the size of the crater formed upon impact with the target material is directly proportional to the size of the particle.
- The rate of erosion-corrosion decreases with the increase of drill cuttings concentration. Also, a high erosion-corrosion rate is observed in the case of large drill cuttings particles. A new approach to control drill pipe erosion-corrosion rate is proposed by using SiO_2-nanofluid, which resulted in the lowest corrosion rate when compared to those of water and xanthan polymer.

Lifting capacity

- A CFD analysis of the nanoparticles influence on fluid viscosity shows an agreement with the experimental outcomes. Two types of nanomaterials with a total concentration of 0.9 wt. % and sizes like those in the experimental work have been simulated.
- Nanoparticles show a positive impact on enhancing the carrying capacity of the drilling fluid, particularly at lower and moderate flow rates. The effective viscosity increases with an increase in nanoparticle concentration.
- Cuttings with higher sphericity have better transport efficiency and the density has an inverse influence on cutting transport.

- The CFD coupling regime of continuous and discrete phases significantly affects the cuttings transport process. The outlet volume fraction of cuttings using a two-way coupling regime is greater than that of a four-way coupling regime. Four-way coupling is much closer to reality when taking the contact dynamics into account.

8.2 Recommendations for future work

The drilling fluids research area still needs further effort and novel developments to overcome different drilling challenges. CFD investigations alongside lab experiments are required to discover the proper solutions for various problems. There is great potential to extend the current research and build upon the knowledge within this field. Such points to be considered are outlined below:

1. Much of the ambiguity and contradiction surrounds using one NPs type to develop drilling fluids. Most researcher's present nanomaterials as the best solution in their results. Hence, further studies should be carried to discover the role of each type of NPs on a specific property.
2. So far, researchers have mainly focused on drilling fluids containing only one nanoparticle type. Hence, further studies should focus on the use of different nanoparticles in combination, with a view to address the limitations of using one NPs type.
3. Further research could utilise a dynamic filtration system, which could generate high pressure and high temperature.
4. Further research could also encapsulate the NPs/polymer in nano-capsule and emulsion controlled release when being delivered to the interested area.
5. In-situ synthesis of nano-drilling condition under wellbore conditions should be considered.
6. Different nanoparticle hybrids with different polymer should be tested.
7. It would also important to produce nanoparticle/polymer hybrids in one step and check their influence on drilling fluid properties.

8. Future studies could perform the simulations presented in this work using fractured and porous media. The necessary data for setting up porous zones in a geometry such as porosity and viscous and inertial resistances need to be evaluated experimentally.
9. Further research could Design and attach the entire geometry of a dynamic drill bit with nozzles to the drill pipe. This could vastly affect the flow pattern and pressure drop in a flow domain.
10. Research could employ an erosion model for examining the potential erosion in the wellbore wall caused by cuttings particles, nanoparticles, and the mud itself.
11. Studies could investigate the contribution of nanoparticles building a high-quality filter cake along a wellbore wall.
12. Studies could also offer a CFD analysis to study the effects of different factors on differential pipe sticking.
13. The CFD study of nanoparticles effects can be expanded to include nanoparticles characteristics such as density, size, shape, and structure.

9 List of References

1. Van Dyke, K. (1998). *Drilling fluids, mud pumps, and conditioning equipment*. University of Texas at Austin Petroleum.
2. Nasser, J., Jesil, A., Mohiuddin, T., Al Ruqeshi, M., Devi, G., & Mohataram, S. (2013). Experimental investigation of drilling fluid performance as nanoparticles. *World Journal of Nano Science and Engineering*, *3*(03), 57..
3. Shah, S. N., Shanker, N. H., & Ogugbue, C. C. (2010, April). Future challenges of drilling fluids and their rheological measurements. In *AADE fluids conference and exhibition, Houston, Texas*. sn.
4. Awele, N. (2014). Investigation of Additives on Drilling Mud Performance With 'TØNDER GEOTHERMAL DRILLING'As A Case Study. *Master. Aalborg University Esbjerg*.
5. Mellot, J. (2008, February). Technical Improvements in Wells Drilled with a Pneumatic Fluid. In *SPE paper 99162, presented at the SPE/IDAC drilling Conference, Miami, Florida, USA, February* (pp. 21-23).
6. Oakley, D. J., James, S. G., & Cliffe, S. (1991, January). The Influence of Oil-Based Drilling Fluid Chemistry and Physical Properties on Oil Retained on Cuttings. In *Offshore Europe*. Society of Petroleum Engineers.
7. Apaleke, A. S., Al-Majed, A. A., & Hossain, M. E. (2012, January). Drilling fluid: state of the art and future trend. In *North Africa Technical Conference and Exhibition*. Society of Petroleum Engineers..
8. Oakley, D. J., Morton, K., Eunson, A., Gilmour, A., Pritchard, D., & Valentine, A. (2000, January). Innovative drilling fluid design and rigorous pre-well planning enable success in an extreme HTHP well. In *IADC/SPE Asia Pacific Drilling Technology*. Society of Petroleum Engineers.
9. McLean, M. R., & Addis, M. A. (1990, January). Wellbore stability analysis: a review of current methods of analysis and their field application. In *SPE/IADC Drilling Conference*. Society of Petroleum Engineers.
10. Nabhani, N., & Emami, M. (2012). The potential impact of nanomaterials in oil drilling industry. *Nano con*, *201*, 23-25.
11. Singh, S. K., Ahmed, R. M., & Growcock, F. (2010, January). Vital role of nanopolymers in drilling and stimulations fluid applications. In *SPE Annual Technical Conference and Exhibition*. Society of Petroleum Engineers.
12. Roy, R. S., & Sharma, M. M. (2001, January). The Relative Importance of Solids and Filtrate Invasion on the Flow Initiation Pressure. In *SPE European Formation Damage Conference*. Society of Petroleum Engineers.
13. Abdo, J., & Haneef, M. D. (2012). Nano-enhanced drilling fluids: pioneering approach to overcome uncompromising drilling problems. *Journal of Energy Resources Technology*, *134*(1), 014501.
14. Mostafavi, V., Ferdous, M. Z., Hareland, G., & Husein, M. (2011, June). Design and application of novel nano drilling fluids to mitigate

circulation loss problems during oil well drilling operations. In *Nanotech Conference and Expo* (Vol. 13, pp. 13-16).

15. Bicerano, J. (2009). *U.S. Patent Application No. 12/178,785*.
16. Skalle, P. (2011). *Drilling fluid engineering*. Bookboon.
17. Paiaman, A. M., & Al-Anazi, B. D. (2008). Using nanoparticles to decrease differential pipe sticking and its feasibility in Iranian Oil fields. *Сетевое издание «Нефтегазовое дело»*, (2).
18. Jahanbakhshi, R., & Keshavarzi, R. (2016). Intelligent Classifier Approach for Prediction and Sensitivity Analysis of Differential Pipe Sticking: A Comparative Study. *Journal of Energy Resources Technology*, *138*(5), 052904.
19. Bowes, C., & Procter, R. (1997). Drillers Stuck Pipe Handbook. *Ballater, Scotland: Procter & Collins Ltd*.
20. Amanullah, M., & Al-Tahini, A. M. (2009, January). Nano-technology-its significance in smart fluid development for oil and gas field application. In *SPE Saudi Arabia Section Technical Symposium*. Society of Petroleum Engineers.
21. Paiaman, A. M., & Al-Anazi, B. D. (2008). Using nanoparticles to decrease differential pipe sticking and its feasibility in Iranian Oil fields. *Сетевое издание «Нефтегазовое дело»*, (2).
22. Amanullah, M., AlArfaj, M. K., & Al-abdullatif, Z. A. (2011, January). Preliminary test results of nano-based drilling fluids for oil and gas field application. In *SPE/IADC Drilling Conference and Exhibition*. Society of Petroleum Engineers.
23. Jung, Y., Barry, M., Lee, J. K., Tran, P., Soong, Y., Martello, D., & Chyu, M. (2011, April). Effect of nanoparticle-additives on the rheological properties of clay-based fluids at high temperature and high pressure. In *AADE National Technical Conference and Exhibition* (pp. 12-14). Houston, TX: American Association of Drilling Engineers.
24. Abdo, J., & Haneef, M. D. (2010, August). Nanoparticles: Promising solution to overcome stern drilling problems. In *Nanotech Conference and Exhibition, Anaheim, California* (pp. 6-8).
25. Abdo, J., & Haneef, M. D. (2013). Clay nanoparticles modified drilling fluids for drilling of deep hydrocarbon wells. *Applied Clay Science*, *86*, 76-82.
26. Riveland, F. A. (2013). *Investigation of nanoparticles for enhanced filtration properties of drilling fluid* (Master's thesis, Institutt for petroleumsteknologi og anvendt geofysikk).
27. Ragab, A. M., & Noah, A. (2014). Reduction of formation damage and fluid loss using nano-sized silica drilling fluids. *Petroleum Technology Development Journal*, *2*, 75-88.
28. William, J. K. M., Ponmani, S., Samuel, R., Nagarajan, R., & Sangwai, J. S. (2014). Effect of CuO and ZnO nanofluids in xanthan gum on thermal, electrical and high pressure rheology of water-based drilling fluids. *Journal of Petroleum Science and Engineering*, *117*, 15-27.
29. Jabrayilov, E. (2014). *Friction reduction by using nanoparticles in oil-based mud* (Master's thesis, Institutt for petroleumsteknologi og anvendt geofysikk).
30. Jahns, C. (2014). *Friction Reduction by using Nano-Fluids in Drilling* (Master's thesis, Institutt for petroleumsteknologi og anvendt geofysikk).

31. Jabrayilov, E. (2014). *Friction reduction by using nanoparticles in oil-based mud* (Master's thesis, Institutt for petroleumsteknologi og anvendt geofysikk).
32. Jung, Y., Son, Y. H., Lee, J. K., Phuoc, T. X., Soong, Y., & Chyu, M. K. (2011). Rheological behavior of clay–nanoparticle hybrid-added bentonite suspensions: specific role of hybrid additives on the gelation of clay-based fluids. *ACS applied materials & interfaces*, *3*(9), 3515-3522.
33. Contreras, O., Hareland, G., Husein, M., Nygaard, R., & Al-Saba, M. (2014, February). Application of in-house prepared nanoparticles as filtration control additive to reduce formation damage. In *SPE International Symposium and Exhibition on Formation Damage Control*. Society of Petroleum Engineers.
34. Vryzas, Z., Zaspalis, V., Nalbantian, L., Mahmoud, O., Nasr-El-Din, H. A., & Kelessidis, V. C. (2016, November). A comprehensive approach for the development of new magnetite nanoparticles giving smart drilling fluids with superior properties for HP/HT applications. In *International Petroleum Technology Conference*. International Petroleum Technology Conference.
35. Ponmani, S., Nagarajan, R., & Sangwai, J. S. (2016). Effect of nanofluids of CuO and ZnO in polyethylene glycol and polyvinylpyrrolidone on the thermal, electrical, and filtration-loss properties of water-based drilling fluids. *SPE Journal*, *21*(02), 405-415.
36. Halali, M. A., Ghotbi, C., Tahmasbi, K., & Ghazanfari, M. H. (2016). The role of carbon nanotubes in improving thermal stability of polymeric fluids: Experimental and modeling. *Industrial & Engineering Chemistry Research*, *55*(27), 7514-7534.
37. Salih, A. H., Elshehabi, T. A., & Bilgesu, H. I. (2016, September). Impact of nanomaterials on the rheological and filtration properties of water-based drilling fluids. In *SPE Eastern Regional Meeting*. Society of Petroleum Engineers.
38. Ismail, A. R., Aftab, A., Ibupoto, Z. H., & Zolkifile, N. (2016). The novel approach for the enhancement of rheological properties of water-based drilling fluids by using multi-walled carbon nanotube, nanosilica and glass beads. *Journal of Petroleum Science and Engineering*, *139*, 264-275.
39. Li, M. C., Wu, Q., Song, K., Qing, Y., & Wu, Y. (2015). Cellulose nanoparticles as modifiers for rheology and fluid loss in bentonite water-based fluids. *ACS applied materials & interfaces*, *7*(8), 5006-5016.
40. Li, M. C., Wu, Q., Song, K., De Hoop, C. F., Lee, S., Qing, Y., & Wu, Y. (2015). Cellulose nanocrystals and polyanionic cellulose as additives in bentonite water-based drilling fluids: Rheological modeling and filtration mechanisms. *Industrial & Engineering Chemistry Research*, *55*(1), 133-143.
41. Amarfio, E. M., & Abdulkadir, M. (2016). Effect of Al2O3 nanoparticles on the rheological properties of water based mud. *Int. J. Sci. Eng. Appl*, *5*, 7-11.
42. Javeri, S. M., Haindade, Z. M. W., & Jere, C. B. (2011, January). Mitigating loss circulation and differential sticking problems using

silicon nanoparticles. In *SPE/IADC Middle East Drilling Technology Conference and Exhibition*. Society of Petroleum Engineers.

43. Parizad, A., & Shahbazi, K. (2016). Experimental investigation of the effects of SnO2 nanoparticles and KCl salt on a water base drilling fluid properties. *The Canadian Journal of Chemical Engineering*, *94*(10), 1924-1938.
44. Saboori, R., Sabbaghi, S., Mowla, D., & Soltani, A. (2012). Decreasing of water loss and mud cake thickness by CMC nanoparticles in mud drilling. *International Journal of Nano Dimension*, *3*(2), 101-104.
45. Fereydouni, M., Sabbaghi, S., Saboori, R., & Zeinali, S. (2012). Effect of polyanionic cellulose polymer nanoparticles on rheological properties of drilling mud. *International Journal of Nanoscience and Nanotechnology*, *8*(3), 171-174.
46. Samsuri, A., & Hamzah, A. (2011). Water based mud lifting capacity improvement by multiwall carbon nanotubes additive. *Journal of Petroleum and Gas Engineering*, *5*(2), 99-107.
47. Taha, N. M., & Lee, S. (2015, December). Nano graphene application improving drilling fluids performance. In *International petroleum technology conference*. International Petroleum Technology Conference.
48. Borisov, A. S., Husein, M., & Hareland, G. (2015). A field application of nanoparticle-based invert emulsion drilling fluids. *Journal of Nanoparticle Research*, *17*(8), 340.
49. Wang, Z., Yin, D., Luo, Y., Liang, H., Yang, L., & Lu, H. (2013). Corrosion and Its Inhibition in Water-Based Drilling Fluid Used in Onshore Oilfied. *Natural Resources*, *4*(07), 456.
50. Wei, B. M. (1984). Metal corrosion theory and application.
51. Dhiman, A. S. (2012). Rheological properties & corrosion characteristics of drilling mud additives. *Halifax: Dalhousie University*.
52. Kadhim, F. S. (2011). Investigation of carbon steel corrosion in water base drilling mud. *Modern Applied Science*, *5*(1), 224.
53. Adeboye, Y. B., & Oyekunle, L. O. (2016). Experimental study of hole cleaning performance of underbalanced drilling at downhole conditions. *Nigerian Journal of Technology*, *35*(2), 375-380.
54. Farquhar, G. B., Kane, R. D., Abayarathna, D., & Sanders, D. H. (1997, January). Prediction of corrosion inhibitor performance using simulated CO2/H2S environmental autoclave and flowloop tests. In *Corrosion97*. NACE International.
55. Nesic, S., Bienkowski, J., Bremhorst, K., & Yang, K. S. (2000). Testing for erosion-corrosion under disturbed flow conditions using a rotating cylinder with a stepped surface. *Corrosion*, *56*(10), 1005-1014.
56. Haaland, E., Pettersen, G., & Tuntland, O. B. (1976). Testing of iron oxides as weight materials for drilling muds.
57. Al-Yasiri, M., Al-Khateeb, M., & Wen, D. (2018). Examination of drill pipe corrosion in water-based drilling fluids under wellbore conditions. *Corrosion Engineering, Science and Technology*, *53*(3), 183-187.
58. Jain, R., Mahto, V., & Sharma, V. P. (2015). Evaluation of polyacrylamide-grafted-polyethylene glycol/silica nanocomposite as potential additive in water based drilling mud for reactive shale

formation. *Journal of Natural Gas Science and Engineering*, *26*, 526-537.

59. Jain, R., & Mahto, V. (2015). Evaluation of polyacrylamide/clay composite as a potential drilling fluid additive in inhibitive water based drilling fluid system. *Journal of Petroleum Science and Engineering*, *133*, 612-621.
60. Jain, R., Mahto, T. K., & Mahto, V. (2016). Rheological investigations of water based drilling fluid system developed using synthesized nanocomposite. *Korea-Australia Rheology Journal*, *28*(1), 55-65.
61. Alizadeh, S., Sabbaghi, S. A. M. A. D., & Soleymani, M. (2015). Synthesis of Alumina/Polyacrylamide nanocomposite and its influence on viscosity of drilling fluid. *International Journal of Nano Dimension*, *6*(3), 271-276.
62. Sadeghalvaad, M., & Sabbaghi, S. (2015). The effect of the TiO2/polyacrylamide nanocomposite on water-based drilling fluid properties. *Powder Technology*, *272*, 113-119.
63. Aftab, A., Ismail, A. R., Khokhar, S., & Ibupoto, Z. H. (2016). Novel zinc oxide nanoparticles deposited acrylamide composite used for enhancing the performance of water-based drilling fluids at elevated temperature conditions. *Journal of Petroleum Science and Engineering*, *146*, 1142-1157.
64. Huang, X., Sun, J., Lv, K., Liu, J., Shen, H., & Zhang, F. (2018). Application of core-shell structural acrylic resin/nano-SiO2 composite in water based drilling fluid to plug shale pores. *Journal of Natural Gas Science and Engineering*, *55*, 418-425.
65. Mme, U., & Skalle, P. A. (2012). CFD calculations of cuttings transport through drilling annuli at various angles. *International Journal of Petroleum Science and Technology*, *6*(2), 129-141.
66. Ding, J., & Gidaspow, D. (1990). A bubbling fluidization model using kinetic theory of granular flow. *AIChE journal*, *36*(4), 523-538.
67. Fluent, I. N. C. (2006). FLUENT 6.3 user's guide. *Fluent documentation*.
68. Kabir, M. A., & Gamwo, I. K. (2011). Filter cake formation on the vertical well at high temperature and high pressure: Computational fluid dynamics modeling and simulations. *Journal of Petroleum and Gas Engineering*, *7*(2), 146-164.
69. Won, S., Bilgesu, H. I., & Ameri, S. (2008, January). Investigation of mud-filtrate invasion using computational fluid dynamics. In *SPE Eastern Regional/AAPG Eastern Section Joint Meeting*. Society of Petroleum Engineers.
70. Chen, X., & Wang, J. (2014). A comparison of two-fluid model, dense discrete particle model and CFD-DEM method for modeling impinging gas–solid flows. *Powder technology*, *254*, 94-102.
71. Oliveira Jr, J. A. A., Zago, J., Fontes, C., Waldmann, A. T. A., & Martins, A. L. (2012, January). Modeling Drilling Fluid Losses in Fractured Reservoirs. In *SPE Latin America and Caribbean Petroleum Engineering Conference*. Society of Petroleum Engineers.
72. Radjaï, F., & Dubois, F. (2011). *Discrete-element modeling of granular materials* (pp. 425-p). Wiley-Iste..
73. Valle, M. R. (2012). Numerical modeling of granular flows in rotary kilns. *SURVEY, L. Delft: Delft University of Technology*.

74. Chen, X. Z., Shi, D. P., Gao, X., & Luo, Z. H. (2011). A fundamental CFD study of the gas–solid flow field in fluidized bed polymerization reactors. *Powder Technology*, *205*(1-3), 276-288.
75. Zhang, N., Lu, B., Wang, W., & Li, J. (2010). 3D CFD simulation of hydrodynamics of a 150 MWe circulating fluidized bed boiler. *Chemical Engineering Journal*, *162*(2), 821-828.
76. Tsuji, Y., Kawaguchi, T., & Tanaka, T. (1993). Discrete particle simulation of two-dimensional fluidized bed. *Powder technology*, *77*(1), 79-87.
77. Xu, B. H., & Yu, A. B. (1997). Numerical simulation of the gas-solid flow in a fluidized bed by combining discrete particle method with computational fluid dynamics. *Chemical Engineering Science*, *52*(16), 2785-2809.
78. Xu, M., Chen, F., Liu, X., Ge, W., & Li, J. (2012). Discrete particle simulation of gas–solid two-phase flows with multi-scale CPU–GPU hybrid computation. *Chemical engineering journal*, *207*, 746-757.
79. Popoff, B. and M. Braun.(2007). *A Lagrangian approach to dense particulate flows*. in *International Conference on Multiphase Flow, Leipzig, Germany*.
80. Cloete, S., Johansen, S., Braun, M., Popoff, B., & Amini, S. (2010, May). Evaluation of a Lagrangian discrete phase modeling approach for resolving cluster formation in CFB risers. In *International Conference on Multiphase Flow, Leipzig, Germany, May*.
81. Pereira, F., M. Barrozo, and C. Ataíde. (2007) *CFD predictions of drilling fluid velocity and pressure profiles in laminar helical flow.* Brazilian Journal of Chemical Engineering. **24**(4): p. 587-595.
82. Akhshik, S., M. Behzad, and M. Rajabi (2007), *CFD–DEM model for simulation of non-spherical particles in hole cleaning process.* Particulate Science and Technology. **33**(5): p. 472-481.
83. Bilgesu, H. I., Ali, M. W., Aminian, K., & Ameri, S. (2002, January). Computational Fluid Dynamics (CFD) as a tool to study cutting transport in wellbores. In *SPE Eastern Regional Meeting*. Society of Petroleum Engineers.
84. Rooki, R., Ardejani, F. D., Moradzadeh, A., & Norouzi, M. (2014). Simulation of cuttings transport with foam in deviated wellbores using computational fluid dynamics. *Journal of Petroleum Exploration and Production Technology*, *4*(3), 263-273.
85. Srivatsa, J. T., & Ziaja, M. B. (2011, January). An experimental investigation on use of nanoparticles as fluid loss additives in a surfactant-polymer based drilling fluids. In *International Petroleum Technology Conference*. International Petroleum Technology Conference.
86. Barry, M. M., Jung, Y., Lee, J. K., Phuoc, T. X., & Chyu, M. K. (2015). Fluid filtration and rheological properties of nanoparticle additive and intercalated clay hybrid bentonite drilling fluids. *Journal of Petroleum Science and Engineering*, *127*, 338-346.
87. Nguyen, P. T., Do, B. P. H., Pham, D. K., Nguyen, Q. T., Dao, D. Q. P., & Nguyen, H. A. (2012, January). Evaluation on the EOR potential capacity of the synthesized composite silica-core/polymer-shell nanoparticles blended with surfactant systems for the HPHT offshore

reservoir conditions. In *SPE International Oilfield Nanotechnology Conference and Exhibition*. Society of Petroleum Engineers.

88. Friedheim, J. E., Young, S., De Stefano, G., Lee, J., & Guo, Q. (2012, January). Nanotechnology for oilfield applications-hype or reality?. In *SPE international oilfield nanotechnology conference and exhibition*. Society of Petroleum Engineers.
89. Li, G., Zhang, J., & Hou, Y. (2012, January). Nanotechnology to improve sealing ability of drilling fluids for shale with micro-cracks during drilling. In *SPE international oilfield nanotechnology conference and exhibition*. Society of Petroleum Engineers.
90. Riley, M., Young, S., Stamatakis, E., Guo, Q., Ji, L., De Stefano, G., ... & Friedheim, J. (2012, January). Wellbore stability in unconventional shales-the design of a nano-particle fluid. In *SPE oil and gas India conference and exhibition*. Society of Petroleum Engineers.
91. Mao, H., Qiu, Z., Shen, Z., & Huang, W. (2015). Hydrophobic associated polymer based silica nanoparticles composite with core–shell structure as a filtrate reducer for drilling fluid at utra-high temperature. *Journal of Petroleum Science and Engineering*, *129*, 1-14.
92. Sadeghalvaad, M., & Sabbaghi, S. (2015). The effect of the TiO2/polyacrylamide nanocomposite on water-based drilling fluid properties. *Powder Technology*, *272*, 113-119.
93. Vryzas, Z., & Kelessidis, V. C. (2017). Nano-based drilling fluids: A review. *Energies*, *10*(4), 540.
94. Muhsan, A. S., Mohamed, N. M., Siddiqui, U., & Shahid, M. U. (2017). Nano Additives in Water Based Drilling Fluid for Enhanced-Performance Fluid-Loss-Control. In *ICIPEG 2016* (pp. 669-675). Springer, Singapore.
95. Alyasiri, M., Antony, J., & Wen, D. Enhancement of Drilling Fluid Rheology by Nanoparticles.
96. Hiemenz, P. C., & Rajagopalan, R. (1997). *Principles of Colloid and Surface Chemistry, revised and expanded*. CRC press.
97. Hulst, H. C., & van de Hulst, H. C. (1981). *Light scattering by small particles*. Courier Corporation.
98. Lim, J., Yeap, S. P., Che, H. X., & Low, S. C. (2013). Characterization of magnetic nanoparticle by dynamic light scattering. *Nanoscale research letters*, *8*(1), 381.
99. Jahns, C. (2014). *Friction Reduction by using Nano-Fluids in Drilling* (Master's thesis, Institutt for petroleumsteknologi og anvendt geofysikk).
100. Riveland, F. A. (2013). *Investigation of nanoparticles for enhanced filtration properties of drilling fluid* (Master's thesis, Institutt for petroleumsteknologi og anvendt geofysikk).
101. 140solutions.com, (2016) *140 solutions for petroleum testing*, Anton Paar GmbH.
102. Eckelt, A. *Flow curve (*2016, 13 Jan) ; Available from: http://www.wee-solve.de/en/flow-curve.html
103. HOUEL, A., (2016), *USER MANUAL INSTRUCTIONS PHYSICA MCR501 ANTON PAAR*, ISIS
104. Viscopedia.com. *Viscometry measuring principles*. 2016]; Available from: http://www.viscopedia.com/methods/measuring-principles.

105. Eckelt, A. (2016 13 Jan). *Oscillatory tests* 2016 13 Jan. 2016]; Available from: http://www.wee-solve.de/en/oscillatory-tests.html
106. Germany, A. P. (2006). Rheoplus Software Volume 1-Installation & Introduction. *Ostfildern, Germany, Anton Paar Germany GmbH. Printed in Austria*, *1*, 31.
107. Company, F.I., *Model 21150 (2010), Differential Sticking Tester*. Houston, Texas, U.S.A.
108. Versteeg, H. K., & Malalasekera, W. (2007). *An introduction to computational fluid dynamics: the finite volume method*. Pearson education.
109. Baker, T. J. (2005). Mesh generation: Art or science?. *Progress in aerospace sciences*, *41*(1), 29-63.
110. FLUENT, A., (2013), *15-Theory Guide, ANSYS.* Inc., Canonsburg, PA.
111. Saffman, P. G. T. (1965). The lift on a small sphere in a slow shear flow. *Journal of fluid mechanics*, *22*(2), 385-400.
112. Cundall, P. A., & Strack, O. D. (1979). A discrete numerical model for granular assemblies. *geotechnique*, *29*(1), 47-65.
113. Zhang, P. (2012). *NUMERICAL SIMULATION OF PARTICLE-LADEN FLOWS IN CURVED PIPES* (Doctoral dissertation, Michigan State University).
114. van Buijtenen, M. S., Deen, N. G., Heinrich, S., Antonyuk, S., & Kuipers, J. A. (2009). Discrete Particle Simulation Study on the Influence of the Restitution Coefficient on Spout Fluidized-Bed Dynamics. *Chemical Engineering & Technology: Industrial Chemistry-Plant Equipment-Process Engineering-Biotechnology*, *32*(3), 454-462.
115. Shah, S. N., Shanker, N. H., & Ogugbue, C. C. (2010, April). Future challenges of drilling fluids and their rheological measurements. In *AADE fluids conference and exhibition, Houston, Texas*. sn.
116. Lee, J., Tehrani, A., Young, S., & Nguyen, C. (2014, June). Viscoelasticity and Drilling Fluid Performance. In *ASME 2014 33rd International Conference on Ocean, Offshore and Arctic Engineering* (pp. V005T11A015-V005T11A015). American Society of Mechanical Engineers.
117. Stenstrøm, H. (2015). *Nano silica treated water based drilling fluid formulation and analysis in various polymers and salts systems* (Master's thesis, University of Stavanger, Norway).
118. Belayneh, M., & Aadnøy, B. S. (2016, June). Effect of nano-silicon dioxide (SiO2) on polymer/salt treated bentonite drilling fluid systems. In *ASME 2016 35th International Conference on Ocean, Offshore and Arctic Engineering* (pp. V008T11A027-V008T11A027). American Society of Mechanical Engineers.
119. Parizad, A., Shahbazi, K., & Tanha, A. A. (2018). SiO2 nanoparticle and KCl salt effects on filtration and thixotropical behavior of polymeric water based drilling fluid: With zeta potential and size analysis. *Results in Physics*, *9*, 1656-1665.
120. Yue, H., Monreal-Bernal, A., Fernández-Blázquez, J. P., Llorca, J., & Vilatela, J. J. (2015). Macroscopic CNT fibres inducing non-epitaxial nucleation and orientation of semicrystalline polymers. *Scientific reports*, *5*, 16729.

121. Sun, J., Xu, Z., Li, W., & Shen, X. (2017). Effect of nano-SiO2 on the early hydration of alite-sulphoaluminate cement. *Nanomaterials*, *7*(5), 102.
122. Sadegh, H., Shahryari-ghoshekandi, R., Agarwal, S., Tyagi, I., Asif, M., & Gupta, V. K. (2015). Microwave-assisted removal of malachite green by carboxylate functionalized multi-walled carbon nanotubes: Kinetics and equilibrium study. *Journal of Molecular Liquids*, *206*, 151-158.
123. Stamatin, I., Morozan, A., Dumitru, A., Ciupina, V., Prodan, G., Niewolski, J., & Figiel, H. (2007). The synthesis of multi-walled carbon nanotubes (MWNTs) by catalytic pyrolysis of the phenol-formaldehyde resins. *Physica E: Low-dimensional Systems and Nanostructures*, *37*(1-2), 44-48.
124. Zhuang, S., Xu, X., Feng, B., Hu, J., Pang, Y., Zhou, G., ... & Zhou, Y. (2014). Correction to photogenerated carriers transfer in dye–graphene–SnO2 composites for highly efficient visible-light photocatalysis. *ACS applied materials & interfaces*, *6*(9), 6990-6990.
125. Liang, J., Liu, J., Yuan, X., Dong, H., Zeng, G., Wu, H., ... & Yu, Z. (2015). Facile synthesis of alumina-decorated multi-walled carbon nanotubes for simultaneous adsorption of cadmium ion and trichloroethylene. *Chemical Engineering Journal*, *273*, 101-110.
126. Kawasaki, S., Matsuoka, Y., Yokomae, T., Nojima, Y., Okino, F., Touhara, H., & Kataura, H. (2005). XRD and TEM study of high pressure treated single-walled carbon nanotubes and C60-peapods. *Carbon*, *43*(1), 37-45.
127. Viswanathan, B., Murugesan, S., Ariharan, A., & Lakhi, K. S. (2013). Hetero atom substituted carbon—potential hydrogen storage materials. *Advanced porous materials*, *1*(1), 122-128.
128. Pal, S., Ghorai, S., Das, C., Samrat, S., Ghosh, A., & Panda, A. B. (2012). Carboxymethyl tamarind-g-poly (acrylamide)/silica: a high performance hybrid nanocomposite for adsorption of methylene blue dye. *Industrial & Engineering Chemistry Research*, *51*(48), 15546-15556.
129. Thakur, S., Pandey, S., & Arotiba, O. A. (2016). Development of a sodium alginate-based organic/inorganic superabsorbent composite hydrogel for adsorption of methylene blue. *Carbohydrate polymers*, *153*, 34-46.
130. Mittal, H., Maity, A., & Ray, S. S. (2015). Synthesis of co-polymer-grafted gum karaya and silica hybrid organic–inorganic hydrogel nanocomposite for the highly effective removal of methylene blue. *Chemical Engineering Journal*, *279*, 166-179.
131. Thakur, S., Pandey, S., & Arotiba, O. A. (2017). Sol-gel derived xanthan gum/silica nanocomposite—a highly efficient cationic dyes adsorbent in aqueous system. *International journal of biological macromolecules*, *103*, 596-604.
132. Van Le, T., Le, M. L. P., Van Tran, M., Nguyen, N. M. T., Luu, A. T., & Nguyen, H. T. (2015). Fabrication of Cathode Materials Based on Limn2o4/Cnt and Lini0. 5mn1. 5o4/Cnt Nanocomposites for Lithium–Ion Batteries Application. *Materials Research*, *18*(5), 1044-1052.
133. O'reilly, J. M., & Mosher, R. A. (1983). Functional groups in carbon black by FTIR spectroscopy. *Carbon*, *21*(1), 47-51.

134. Vuković, G., Marinković, A., Obradović, M., Radmilović, V., Čolić, M., Aleksić, R., & Uskoković, P. S. (2009). Synthesis, characterization and cytotoxicity of surface amino-functionalized water-dispersible multi-walled carbon nanotubes. *Applied Surface Science*, *255*(18), 8067-8075.
135. Zappielo, C. D., Nanicuacua, D. M., dos Santos, W. N., da Silva, D. L., Dall'Antônia, L. H., Oliveira, F. M. D., ... & Tarley, C. R. (2016). Solid phase extraction to on-line preconcentrate trace cadmium using chemically modified nano-carbon black with 3-mercaptopropyltrimethoxysilane. *Journal of the Brazilian Chemical Society*, *27*(10), 1715-1726.
136. DeBruijn, G., Skeates, C., Greenaway, R., Harrison, D., Parris, M., James, S., ... & Wutherich, K. (2008). High-pressure, high-temperature technologies. *Oilfield Review*, *20*(3), 46-60.
137. Sahoo, N. G., Rana, S., Cho, J. W., Li, L., & Chan, S. H. (2010). Polymer nanocomposites based on functionalized carbon nanotubes. *Progress in polymer science*, *35*(7), 837-867.
138. Ismail, A. R., Sulaiman, W., Rosli, W., Jaafar, M. Z., Ismail, I., & Sabu Hera, E. (2016). Nanoparticles performance as fluid loss additives in water based drilling fluids. In *Materials Science Forum* (Vol. 864, pp. 189-193). Trans Tech Publications.
139. Laird, D. A. (1997). Bonding between polyacrylamide and clay mineral surfaces. *Soil science*, *162*(11), 826-832.
140. Akhtarmanesh, S., Shahrabi, M. A., & Atashnezhad, A. (2013). Improvement of wellbore stability in shale using nanoparticles. *Journal of Petroleum Science and Engineering*, *112*, 290-295.
141. Trépanier, C., & Pelton, A. R. (2006). Effect of temperature and pH on the corrosion resistance of passivated nitinol and stainless steel. *Proc. SMST*, 361-366.
142. Muslim, Z. R., & Abbas, A. A. (2015). The effect of ph and temperature on corrosion rate stainless steel 316l used as biomaterial. *Int. J. Basic Appl. Sci*, *4*, 17-20.
143. Vuppu, A. K., & Jepson, W. P. (1994, January). The effect of temperature in sweet corrosion of horizontal multiphase carbon steel pipelines. In *SPE Asia pacific oil and gas conference*. Society of Petroleum Engineers.
144. Khadom, A. A., Yaro, A. S., Kadum, A. A. H., AlTaie, A. S., & Musa, A. Y. (2009). The effect of temperature and acid concentration on corrosion of low carbon steel in hydrochloric acid media. *American Journal of Applied Sciences*, *6*(7), 1403-1409.
145. Prasetia, A. E., Salazar, A. T. N., & Toralde, J. S. S. (2010). Corrosion control in geothermal aerated fluids drilling projects in Asia Pacific. In *Proceedings of the World Geothermal Congress*.
146. Asmara, Y. P., Ismail, M. F., Chui, L. G., & Halimi, J. (2016, February). Predicting Effects of Corrosion Erosion of High Strength Steel Pipelines Elbow on CO2-Acetic Acid (HAc) Solution. In *IOP Conference Series: Materials Science and Engineering* (Vol. 114, No. 1, p. 012128). IOP Publishing.
147. Levy, A. V. (1995). *Solid particle erosion and erosion-corrosion of materials*. Asm International.

148. Postlethwaite, J., & Nesic, S. (1993). Erosion in disturbed liquid/particle pipe flow: effects of flow geometry and particle surface roughness. *Corrosion*, *49*(10), 850-857.
149. Salama, M. M. (2000). An alternative to API 14E erosional velocity limits for sand laden fluids. *TRANSACTIONS-AMERICAN SOCIETY OF MECHANICAL ENGINEERS JOURNAL OF ENERGY RESOURCES TECHNOLOGY*, *122*(2), 71-77.
150. Weirick, L. J. (1982). *Effects of oxygen, salt, and pH level on corrosion rate of drill-stem steel* (No. SAND-82-1616). Sandia National Labs., Albuquerque, NM (USA).
151. Clark, H. M. (1991). On the impact rate and impact energy of particles in a slurry pot erosion tester. *Wear*, *147*(1), 165-183.
152. De Bree, S. E. M., Rosenbrand, W. F., & De Gee, A. W. J. (1982, August). On the erosion resistance in water-sand mixtures of steels for application in slurry pipelines. In *8th International Conference on Hydraulic Transport of Solids in Pipes, BHRA Fluid Eng., Johannesburg, South Africa*.
153. Elkholy, A. (1983). Prediction of abrasion wear for slurry pump materials. *Wear*, *84*(1), 39-49.
154. Lynn, R. S., Wong, K. K., & Clark, H. M. (1991). On the particle size effect in slurry erosion. *Wear*, *149*(1-2), 55-71.
155. Sinha, S. L., Dewangan, S. K., & Sharma, A. (2017). A review on particulate slurry erosive wear of industrial materials: In context with pipeline transportation of mineral− slurry. *Particulate Science and Technology*, *35*(1), 103-118.
156. Gandhi, B. K., & Borse, S. V. (2004). Nominal particle size of multi-sized particulate slurries for evaluation of erosion wear and effect of fine particles. *Wear*, *257*(1-2), 73-79.
157. Roco, M. C., Nair, P., & Addie, G. R. (1987). Test approach for dense slurry erosion. *ASTM Spec. Tech. Publ*, *964*, 185-210.
158. Tuzson, J. J. (1984). Laboratory slurry erosion tests and pump wear rate calculations. *Journal of fluids engineering*, *106*(2), 135-140.
159. Deng, T., Chaudhry, A. R., Patel, M., Hutchings, I., & Bradley, M. S. A. (2005). Effect of particle concentration on erosion rate of mild steel bends in a pneumatic conveyor. *Wear*, *258*(1-4), 480-487.
160. Gu, S., Zhang, Y., & Yan, B. (2013). Solvent-free ionic molybdenum disulfide (MoS2) nanofluids with self-healing lubricating behaviors. *Materials Letters*, *97*, 169-172.
161. Ismail, A. F., Anuar, A., Rashmi, W., & Yusaf, T. (2014). Corrosion effects of CNT-nanofluids on different metals. *WIT Transactions on Engineering Sciences*, *87*, 139-146.
162. Fotowat, S., Askar, S., Ismail, M., & Fartaj, A. (2017). A study on corrosion effects of a water based nanofluid for enhanced thermal energy applications. *Sustainable Energy Technologies and Assessments*, *24*, 39-44.
163. Al-Yasiri, M. S., & Al-Sallami, W. T. (2015). How the drilling fluids can be made more efficient by using nanomaterials. *American Journal of Nano research and applications*, *3*(3), 41-45.
164. Holland, F., & Bragg, R. (1995). *Fluid flow for chemical and process engineers*. Elsevier.

165. Hussaini, S. M., & Azar, J. J. (1983). Experimental study of drilled cuttings transport using common drilling muds. *Society of Petroleum Engineers Journal*, *23*(01), 11-20.
166. Haider, A., & Levenspiel, O. (1989). Drag coefficient and terminal velocity of spherical and nonspherical particles. *Powder technology*, *58*(1), 63-70.

Appendix A

Fann Viscometer Data and Parameters for NPs-based Drilling Fluids (without polymer)

Table A-1 Rheological Data of Single Type NPs based Drilling Fluids

rpm	Viscometer reading					
	1g CB	1g CNT	1g Al_2O_3	1g SiO_2	Base mud	1g Gr
600	17	13	20	18	15	16
300	13	9	16	13	11	12
200	11	8	14	12	9	11
100	9	7	12	10	7	9
6	6	6	9	7	5	6
3	6	5	9	7	5	6
AV	8.5	6.5	10	9	7.5	8
PV	4	4	4	5	4	4
YP	4.599	2.555	6.132	4.088	3.577	4.088
10 sec	11	6	15	10	7	11
10 min	20	14	32	20	17	21

Table A-2 Rheological Data of CB-SiO_2 NPs based Drilling Fluids

rpm	Viscometer Reading				
	1g CB	1g CB-SiO_2	2g CB-SiO_2	1g SiO_2	1.5g CB-0.5g SiO_2
600	17	18	18	18	15
300	13	13	13	13	12
200	11	12	12	12	10
100	9	11	10	10	8
6	6	6	6	7	5
3	6	6	6	7	5
AV	8.5	9	9	9	7.5
PV	4	5	5	5	3
YP	4.599	4.088	4.088	4.088	4.599
10 sec	11	12	11	10	8
10 min	20	21	17	20	16

Table A-3 Rheological Data of Al_2O_3-CNT NPs based Drilling Fluids

rpm	Viscometer Reading		
	1g CNT	1g Al_2O_3	1g Al_2O_3-CNT
600	13	20	18
300	9	16	14
200	8	14	12
100	7	12	10
6	6	9	6
3	5	9	6
AV	6.5	10	9
PV	4	4	4
YP	2.555	6.132	5.11
10 sec	6	15	12
10 min	14	32	25

Table A-4 Rheological Data of Al_2O_3-SiO_2 NPs based Drilling Fluids

rpm	Viscometer Reading					
	2g Al_2O_3-SiO_2	1g Al_2O_3-SiO_2	1g Al_2O_3	1g SiO_2	2g Al_2O_3	2g SiO_2
600	25	19	20	18	36	17
300	20	14	16	13	32	13
200	19	13	14	12	20	11
100	18	10	12	10	18	9
6	14	7	9	7	17	6
3	14	7	9	7	16	6
AV	12.5	9.5	10	9	18	8.5
PV	5	5	4	5	4	4
YP	7.665	4.599	6.132	4.088	14.308	4.599
10 sec	20	12	15	10	25	10
10 min	33	23	32	20	45	17

Appendix B

Fann Viscometer Data and Parameters for NPs-based Drilling Fluids (with polymer)

Table B-1 Rheological Data of polymer-based Drilling Fluids

rpm	Viscometer reading			
	CMC	XG	AG	CS
600	29	45	15	12
300	20	38	12	9
200	17	34	10	8
100	12	29	9	6
6	7	19	7	4
3	7	18	7	4
AV	14.5	22.5	7.5	6
PV	9	7	3	3
YP	5.621	15.841	4.599	3.066
10 sec	11	17	8	4
10 min	36	37	14	15

Table B-2 Rheological Data of NPs XG-based Drilling Fluids

rpm	Viscometer reading				
	SiO_2 XG	Al_2O_3 XG	CNT XG	Gr XG	CB XG
600	50	70	50	53	58
300	42	59	41	42	48
200	39	53	38	39	44
100	33	46	33	34	36
6	21	31	21	25	25
3	19	5	20	23	24
AV	25	35	25	26.5	29
PV	8	11	9	11	10
YP	17.374	24.528	16.352	15.841	19.418
10 sec	21	30	23	28	32
10 min	30	51	33	43	46

Appendix C

Corrosion and Erosion-Corrosion Data

Table C-1 Effect of Temperature on Corrosion Rate

Temperature (°C)	Weight 1	Weight 2	Time (hr)	Corrosion Rate (mm/y)
20	1.9313	1.9307	47	0.0907
45	1.9529	1.952	49	0.1305
70	1.9133	1.9118	48	0.222
95	1.9328	1.93	48	0.4144

Table C-2 Effect of Pressure on Corrosion Rate

Pressure (bar)	Weight 1	Weight 2	Time (hr)	Corrosion Rate (mm/y)
50	1.9313	1.9307	47	0.0907
100	1.959	1.9583	48	0.104
150	1.9486	1.9477	47	0.136
200	1.9452	1.9442	45	0.1579

Table C-3 Effect of Rotation Speed on Corrosion Rate

Rotation Speed (rpm)	Weight 1	Weight 2	Time (hr)	Corrosion Rate (mm/y)
0	1.9597	1.9594	48	0.0444
200	1.9635	1.963	48	0.074
400	1.9627	1.9621	47	0.0907
500	1.9602	1.9593	46	0.139
600	1.9616	1.9601	49	0.2175

Table C-4 Effect of Salinity Concentration on Corrosion Rate

Salinity%	Weight 1	Weight 2	Time (hr)	Corrosion Rate (mm/y)
Tab Water	1.9627	1.9621	47	0.0907
3.50%	1.9622	1.9618	47	0.0605
5%	1.9589	1.9586	47	0.0453
10%	1.9577	1.9575	47	0.0302

Table C-5 Effect of Cuttings Size on Erosion-corrosion rate

Cutting Size (mm)	Weight 1	Weight 2	Time (hr)	Erosion-Corrosion Rate (mm/y)
0.841	1.945	1.9427	47	0.3477
1.7	1.909	1.9062	46.5	0.4278
3.3	1.9546	1.9511	48	0.518

Table C-6 Effect of Cuttings Concentration on Erosion-corrosion rate

Cutting Concentration	Weight 1	Weight 2	Time (hr)	Erosion-Corrosion Rate (mm/y)
1%	1.8866	1.8836	47	0.45
3%	1.8921	1.8891	48	0.44
5%	1.945	1.9427	47	0.3477
10%	1.8354	1.8332	47	0.3325
15%	1.961	1.9589	48	0.3108